Title
Mechanical Behavior and Thermal Stability of Acid-Base Phosphate Cements and Composites Fabricated at Ambient Temperature

Author
Colorado, Henry A.

Publication Date
2013

Peer reviewed|Thesis/dissertation

UNIVERSITY OF CALIFORNIA

Los Angeles

Mechanical Behavior and Thermal Stability of Acid-Base Phosphate Cements and Composites Fabricated at Ambient Temperature

A dissertation submitted in partial satisfaction of the

requirements for the degree Doctor of Philosophy in Materials Science and Engineering

by

Henry Alonso Colorado Lopera

2013

ABSTRACT OF THE DISSERTATION

Mechanical Behavior and Thermal Stability of Acid-Base Phosphate Cements and Composites Fabricated at Ambient Temperature

by

Henry Alonso Colorado Lopera

Doctor of Philosophy in Materials Science and Engineering

University of California, Los Angeles, 2013

Professor Jenn-Ming Yang, Chair

This dissertation presents the study of the mechanical behavior and thermal stability of acid-base phosphate cements (PCs) and composites fabricated at ambient temperature. These materials are also known as chemically bonded phosphate ceramics (CBPCs). Among other advantages of using PCs when compared with traditional cements are the better mechanical properties (compressive and flexural strength), lower density, ultra-fast (controllable) setting time, controllable pH, and an environmentally benign process. Several PCs based on wollastonite and calcium and alumino phosphates after thermal exposure up to 1000°C have been investigated.

First, the thermo-mechanical and chemical stability of wollastonite-based PC (Wo-PC) exposed to temperatures up to 1000°C in air environment were studied. The effects of processing conditions on the curing and shrinkage of the wollastonite-based PC were studied. The chemical

reactions and phase transformations during the fabrication and during the thermal exposure are analyzed in detail using scanning electron microscopy (SEM), X-ray diffraction (XRD), and thermo-gravimetric analysis (TGA Then, the thermo-mechanical and chemical stability of glass, carbon and basalt fiber reinforced Wo-PC composites, were studied using SEM, XRD, TGA. The flexural strength and Weibull statistics were analyzed. A significant strength degradation in the composites were found after the thermal exposure at elevated temperatures due to the interdifusion and chemical reactions across the fibers and the matrix at temperatures over 600°C.

To overcome this barrier, we have developed a new PC based on calcium and alumino-phosphates (Ca-Al PCs). The Ca-Al PCs were studied in detail using SEM, XRD, TGA, curing, shrinkage, Weibull statistics, and compression tests. Our study has confirmed that this new composite material is chemically and mechanically stable at temperatures up to 1000°C. Moreover, the compression strength increases after exposure to 1000°C. This is a significant result since phosphates typically show strength degradation at temperatures over 500°C.

In addition, other PCs materials were developed during this research with their current and potential applications. These include a new PC based on fly ash (Fly ash-PC) as raw material; and PC-based on boron (B-PC), which can be used in shielding neutron irradiation and infrastructure for nuclear facilities.

The dissertation of Henry Alonso Colorado Lopera is approved.

Nasr M. Ghoniem

Jiann-Wen Ju

Richard B. Kaner

Benjamin M. Wu

Jenn-Ming Yang, Committee Chair

University of California, Los Angeles

2013

To mi Family

Table of Contents

List of Figures

List of Tables

List of Acronyms

PC: Acid-Base Phosphate Cement

CBPC: Chemically bonded phosphates ceramics

SEM: Scanning electron microscopy

XRD: X-ray difraction

Wo: Wollastonite powder ($CaSiO_3$)

EDS: Energy dispersive spectroscopy

A0.0: Acid formulation with 0.0wt% borax

A2.9: Acid formulation with 2.9wt% borax

A5.0 (RefA): Acid formulation with 5.0wt% borax

TM: Thinky mixer

UD: unidirectional (fibers)

Acknowledgments

I want to thank my advisor, Professor Jenn-Ming Yang from UCLA for supervising my work. Thanks to his sincere care and guidance, understanding, motivation and support during the time I worked on this thesis. I am also grateful for the resolute financial support that he has provided me through research assistantships and conference travel.

Also, I want to thank to Professor H. Thomas Hahn from UCLA for supervising my work and for inviting me to work on this project, for his guidance, and financial support. This research has been possible because he invited me to work in his group on this project until his retirement.

I thank to Dr Clem Hiel from Composites Support and Solutions Incorporated (CSSI) for his advice and support. I am also grateful for the significant financial support that he has provided throughout this thesis. I also thank the personnel at CSSI for their generous support.

I also want to extend my appreciation to Professor Vijay Gupta's motivation and his advice in several areas of my research. He motivated me to work intensively and to optimize my experience at UCLA.

I am also grateful to Professor H. Pat Gillis, Professor Suneel Kodambaka, Professor Ioanna Kakoulli, and Dr Sergey Prikhodko for their advice in my academic journey.

Special thanks to my committee, Professor Nasr ghoniem, Professor Richard Kaner, Professor Jiann-Wen Woody Ju, and Professor Benjamin M. Wu, for useful comments and insightful questions about the research presented in this thesis.

I would also like to thank my main research collaborators who influenced my work: Dr Sanjay Dhage, Dr Zhe Wang, Dr John Z. Guo (from the Multifunctional Composites Laboratory lead by Professor H. Thomas Hahn), Juanri Tanjaya, Andrew Wong, Christophe Daniel, Jonathan Quan, Dr Wei Yuan, Dr Linhua Zou, John Kim, Vishrut Mehta (from the Hybrid & Multi-Phase Materials Laboratory lead by Professor Jenn-Ming Yang).

Thanks to Dr Dileep Singh from Argonne National Laboratory for his support and advice. Thanks for introducing me to the fascinating topics that fueled my research work in new materials and ceramics. Also thanks to Prof Carlos Castano and to his student Jason Pleitt for the collaboration and help on the nuclear tests at Missouri University of Science and Technology.

Finally, I want to thank my family for their resolute support, motivation and patience. Thanks to my parents Alicia and Julian for their constant support and motivation. Thanks to my wife Paula and to my daughter Sophia for their support during these years for making it all worthwhile.

This work was supported by the University of California Los Angeles; Composites Support and Solutions Inc.; NIST-ATP Program through a grant to Composites and Solutions Inc. (Program Monitor Dr. Felix H. Wu); Universidad de Antioquia-Colombia, and by the Fulbrigth-Laspau-Colciencias fellowship (Manager Liza Mallozi Tapiero).

If I neglected to mention you above, I would like to thank you very much.

Biographical Sketch

Henry A. Colorado completed his BS and MS in Mechanical Engineering in 2005 at the Universidad Nacional de Colombia, Medellin-Colombia, conducting research in dynamic behaviour of metals and thin layared materials. From 2005 to 2007 worked as a Lecturer of Manufacturing Processes and Applied Materials Laboratory at the Universidad de Antioquia, Colombia. Thereafter, he completed a MS in Materials Science at UCLA in 2010 while working in the science and manufacturing of ceramic matrix composites. Henry has received training in materials under extreme conditions at Idaho and Oak Ridge National laboratories. He spent five months in Argonne National Laboratory working in the synthesis of ceramics for nuclear waste stream stabilization and encapsulation. He also worked for Composites Support and Solutions Inc., at San Pedro- California, in structural composite materials.

1 Introduction

This thesis is about the study and development of acid-base phosphate cement (PCs) composites. The thesis is focused in structural and thermal applications, and therefore, cement-based composites were fabricated with different fibers. Because of their characteristics, PCs have properties from both cements and ceramics, and therefore are open to many applications in infrastructure. Among other advantages of using PCs instead of cements are the better mechanical properties (compressive and flexural strength), lower density, ultra-fast (controllable) setting time, and an environmentally benign process. In addition, these phosphate materials have a high acidity in the beginning of the reaction followed by a fast evolution to a neutral pH. The neutral pH is very convenient for composites since there is no corrosion in the reinforcement. On the contrary, traditional cements have high alkalinity during and after the reaction, which precludes the use of inexpensive E-glass fibers.

In contrast to traditional cements, PCs can be made complete at room temperature, which is not only inexpensive but also environmentally friendly. In Portland cement, the clinker (product of sintering limestone and alumino-silicate clay) is obtained at a very high temperature (about 1450ºC). In order to make the process inexpensive, mineral coal is used as fuel, which produces CO_2. Similarly, in traditional ceramics, sintering or thermal diffusion is conducted at high temperature. These methods not only involve high temperatures, but they are also expensive. Unlike the manufacturing processes for traditional cements and ceramics, PCs are fabricated at low temperature (typically less than 200°C) by acid-base reactions. The PCs evaluated in this project, the Wollastonite-based PC (Wo-PC), the Al-Ca based PC (Al-Ca-PC), and other metal oxides-based PC, were completely fabricated in a process conducted at room temperature.

A phosphoric acid formulation and metal-oxide powder (as the alkaline material) react to form the cement. Initially, the metal ions from the surface of the oxide particles are dissolved into the acidic liquid, in time the concentration of metal cations increases; the reaction of these with the phosphate anions form a calcium phosphate. The pH increases simultaneously as reaction progresses to a neutral value. In particular, when wollastonite is used (Ca^{+2} is the metal cation) in combination with phosphoric acid (PO_4^{-2} is one of the anions), calcium phosphate is obtained ($CaHPO_4.2H_2O$).

Besides these advantages, traditional cements are the most used engineering material because the cost is incredible low. Phosphate Cements cannot completely replace cements mainly because of the cost factor; however, for high performance applications such as high strength, high temperatures and extreme environments, PCs have the advantage.

This research involves materials science, manufacturing and some applications of PC composites under temperatures up to 1000°C. This thesis also discusses the development of new engineering materials, for structural and thermal applications. Thermo-mechanical tests were amply used and the fabrication process shown was optimized after the mechanical testing of many samples. This led to a material more chemically and mechanically stable at different temperatures.

Chapter 2 gives an overview of the PCs, specifically for Wo-PCs at room temperature. Chapter 3 summarizes the materials and experimental methods used in this research. Chapter 4 is the study of Wo-PC exposed to temperatures up to 1000°C in air environment. Chapter 5 is the study of glass, carbon, basalt, and silicon carbide fibers exposed to temperatures up to 1000°C in air environment. Similarly, in Chapter 6, the same study was conducted for the fiber reinforced Wo-PC composites, which were fabricated by pultrusion. Chapter 7 is a new PC matrix with high

reliability to work up to 1000°C in air environment. Finally, Chapter 8 is a general overview of other PC materials developed during this project with their current and potential applications.

2 Acid-Base Phosphate Cements (PCs)

2.1 Acid-base phosphate cements

Conventional ceramics usually require temperatures over 1000°C during a part of the manufacturing process, which in general is not only undesirable because it increases cost, but also has a negative environmental impact. Sintered ceramics have been used for thousands of years by humans and even today are the subject of a very intense research field. However, sintering results in a lot of wasted energy and the process is expensive at large manufacturing scales. The solution is chemical bonding, like in Portland cement (although making this cement requires a lot of energy during the complete process), which allows this product to be inexpensive in high volume production. Ceramics are expensive compared to cement, but they have in general higher mechanical strength, corrosion resistance, and temperature stability [1]. There are several emerging materials which have properties between Portland cement and ceramics: acid-base phosphate cements (PCs), which have been developed intensively during the last decade to fill the gap between cements and ceramics.

It is well established that between 900 and 1100 kg of CO_2 is emitted for every 1000 kg of Portland cement produced in the U.S. The quantity depends on the fuel type, raw ingredients used and the energy efficiency of the cement plant [2]. This research will present PCs as a potential substitute for high strength cements, and as an alternative to ceramic based material for use in structural applications, which is environmentally benign and can be fabricated at ambient temperature. In PCs ([3]-[7]) the bonding takes place in a chemical reaction at low temperatures, as opposed to fusion or sintering at elevated temperatures, in traditional ceramics and cements. The bonding in such CBCs is a mixture of ionic, covalent, and van der Waals bonding, with the

ionic and covalent dominating. In traditional cement hydration products, van der Waals and hydrogen bonding dominate [5].

The PCs are formed by acid-base reactions between an acid phosphate (such as that of potassium, ammonium or aluminum) and a metal oxide (such as that of magnesium, calcium, or zinc). Comprehensive and complete reviews are available about the different types of PCs ([1],[3] and [5]) in which is explained the metal oxide an acid-phosphate solution reaction to form cations, how these cations react with the phosphate anions to form a phosphate gel which crystallizes and consolidates into a ceramic; the pH and solubility role in obtaining a ceramic, and how the PC is produced by controlling the solubility of the oxide in the acid-phosphate solution [1]. A complete overview of the principles of the wider field of acid-based cements [8] and it is highly recommended before going into the details of the models to explain the kinetics of formation [9]-[11].

There are many developed CBCs for very diverse applications, including PCs as dental material [12] and for bone tissue engineering [13], capable of shielding gamma and neutron radiation [14], for nuclear waste solidification and encapsulation [15], for electronic materials applications [16]. There are also CBCs used as tooling for advanced composites [17], coatings on nanotubes and nanowires applications [18] and as an alternative to high temperature composites processing [19]. On the other hand, CBC with fillers and reinforcements have been made before, some of these are: CBC-wood composites [20], CBC-glass fibers reinforcements [3] and CBC-fly ash [1]. The PCs presented in this research are the result of mixing wollastonite powder ($CaSiO_3$) and a phosphoric acid (H_3PO_4) formulation to produce calcium phosphates (brushite $CaHPO_4 \cdot 2H2O$, monetite ($CaHPO_4$) and calcium dihydrogenphosphate monohydrate ($Ca(H_2PO_4)2 \cdot H_2O$)) and

silica for molar ratios between 1 and 1.66 [21]. These PC phases are well known as biomaterials [22]-[24]. The reaction of PC is exothermic and extremely fast, producing air bubbles that are very difficult to remove because of the high viscosity of the paste. In order to reduce the reactivity of the acid, dilute acid is required to make composites.

In ceramics and cements, the density has an important role in the mechanical response of the material. For Wo-PC it has been found that the density of the PC can be controlled by changing the mixing parameters, [25]. Figure 1 was made with density data for the Wo-PC samples as made. This image illustrates the advantage of Wollastonite-based PCs compared to Portland cement concrete. It has been observed in PCs that density typically varies from 1.9 to 2.4 g/cm^3. This produces a variation in the compressive strength typically from 60 to 130 MPa. Similarly, Portland cement concrete has a density that typically ranges from 3 to 3.5 g/cm^3 which produces a variation in the compressive strength typically from 30 to 40 MPa. When these values are plotted as compressive strength over the density, we see that Wo-PCs, and in general other PCs (it is possible to obtain similar values), have superior advantages for applications that require high strength and low density, in addition to relative ease of fabrication. Therefore, PCs fill a gap between cements and ceramics which is very useful in areas such as infrastructure.

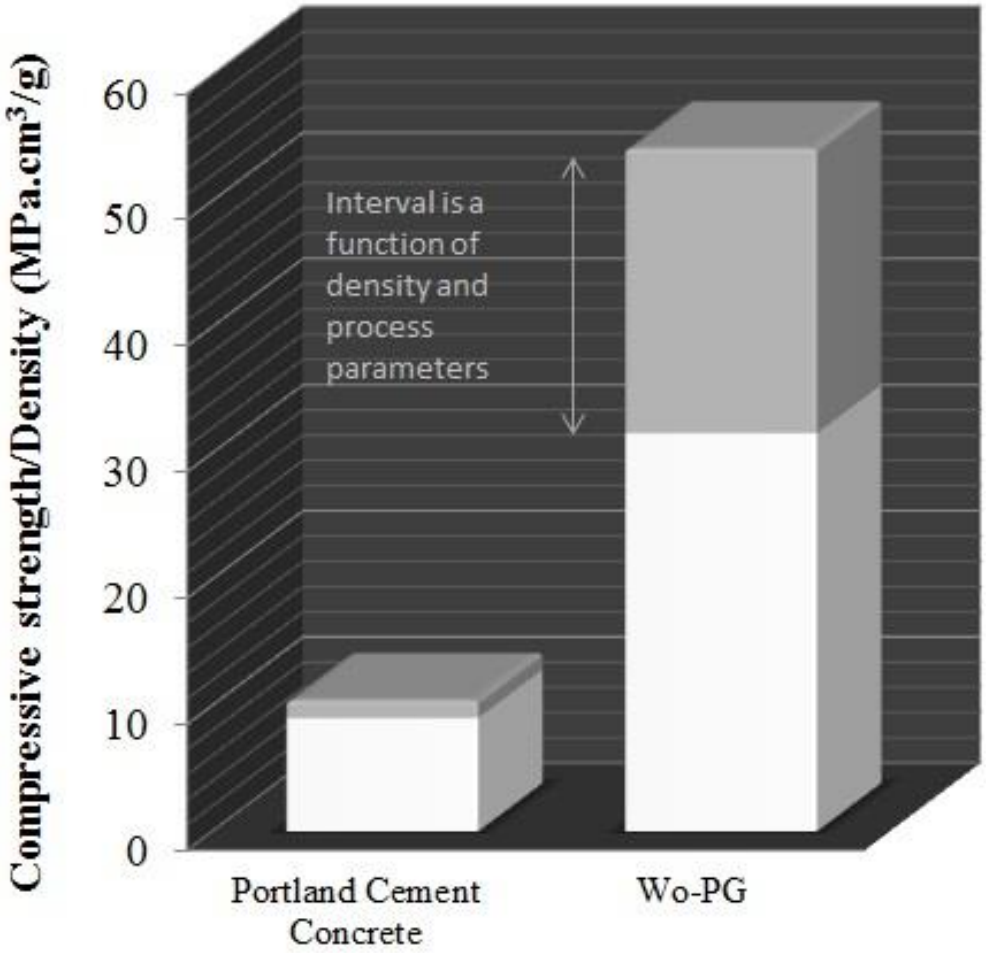

Figure 1 Comparison of the ratio compressive strength over the density for Portland cement concrete and Wollastonite-based PCs.

Thus, we have a general idea of the material and properties of the PC. Next sections will show in detail the phosphoric acid, wollastonite, and the reaction between them.

2.2 PC formation: phosphoric acid-metal oxide reaction

Several byproducts of the reaction of phosphoric acid, water and divalent cation M^+ are described in the literature. These include the phosphoric acid dissociation (equations 11-3) and the hydroxyl ions from the dissociation of water (equation 6). A summary of this reactions are shown in equations 8 to 11 [26].

$$M^{2+} + H_2PO_4^- \xleftrightarrow{K_{M^+}} MH_2PO_4^+ \quad (8)$$

$$\left(K_{M^+} = \frac{a_{MH_2PO_4^+}}{a_{M^{2+}} \cdot a_{H_2PO_4^-}}\right)$$

$$M^{2+} + HPO_4^{2-} \xleftrightarrow{K_{M^0}} MHPO_4^0 \quad (9)$$

$$\left(K_{M^0} = \frac{a_{MHPO_4^0}}{a_{M^{2+}} \cdot a_{HPO_4^{2-}}}\right)$$

$$M^{2+} + PO_4^{3-} \xleftrightarrow{K_{M^-}} MPO_4^- \quad (10)$$

$$\left(K_{M^-} = \frac{a_{MPO_4^-}}{a_{M^{2+}} \cdot a_{PO_4^{3-}}}\right)$$

$$M^{2+} + OH^- \xleftrightarrow{K_{OH^-}} MOH^+ \quad (11)$$

$$\left(K_{OH^-} = \frac{a_{MOH^+}}{a_{M^{2+}} \cdot a_{OH^-}}\right)$$

In general, equations 8 to 11 can be applied for the dissolution of all metal oxides and their formation of dissolved cations. When an oxide is dissolved in an acidic media, the solubility of the oxide controls the reaction [3]. Almost all oxides exhibit a low solubility (excepting group I in the periodic table) in aqueous media. Since the low solubility is the best condition to form a PC, there are many potential new phosphate materials to be made with this technique, and therefore the composition can be easily adjusted to new applications.

The model for the PC formation proposed by Wagh [3] is based on acid-base reactions leading in a geopolymerization like-process, represented in Figure 2. The process can be divided in the following steps:

(a) Dissociation leading. The dissolution process is firstly characterized by a ionization process (or dissociation). When oxide is stirred in water this decomposes into cations and anions, which occurs because of the collisions between the oxide molecules and the polar molecules of water. See Figure 2a.

(b) Aquosol formation. After the dissociation, a screening step occurs, in which the two charged ions resulting from this dissociation are kept separate by the water molecules. These screened and stable ions are known “aquosols” in the conventional sol-gel process. See Figure 2b.

(c) Acid–base reaction. The sols react with the aqueous phosphate anions to form the hydrophosphate salts, while the protons and oxygen react to form water. See Figure 2c.

(d) Percolation and gel formation. When the oxide powder is stirred in water more aquosols are formed in the solution and they start connecting to each other. This leads to the formation of a gel weakly connecting salt molecules. See Figure 2d.

(e) Saturation and crystallization of the gel into a ceramic. As the reaction continues, more and more reaction products are introduced into the gel. At some point, the slurry becomes too viscous. The gel now crystallizes around the unreacted core (residual metal-oxides) into a crystal lattice that grows into a ceramic. See Figure 2e.

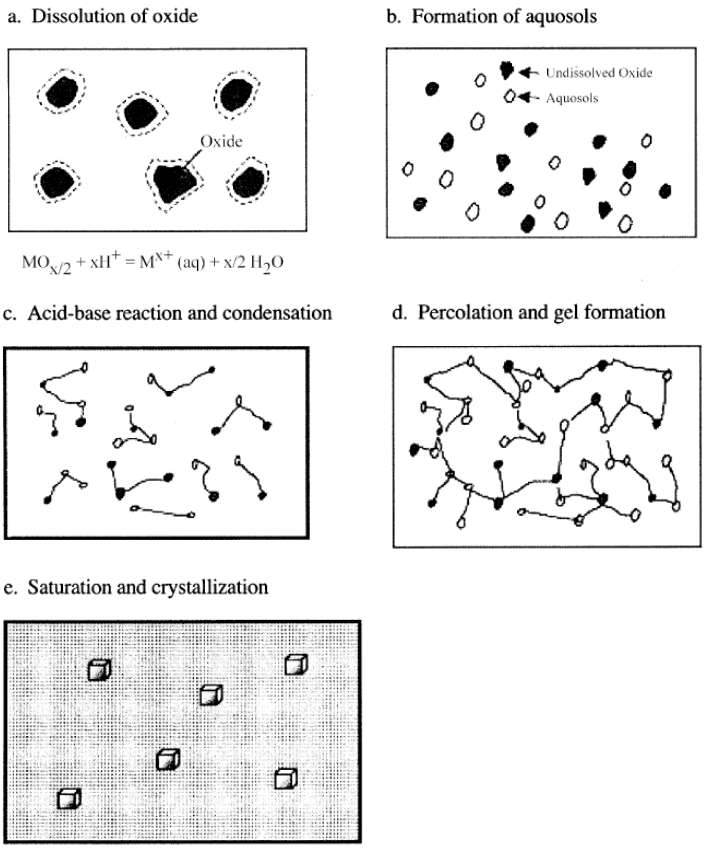

Figure 2 Schematic representation of PC formation [3].

2.3 Phosphoric acid

Phosphoric acid (also known as orthophosphoric acid) is a mineral inorganic acid with formula H_3PO_4. It is a polyprotonic acid, which dissociates stepwise as described in equations 1 to 3.

$$H_3PO_{4(aq)} \leftrightarrow H_2PO_4^-{}_{(aq)} + H^+ \quad (1)$$

$$H_2PO_4^-{}_{(aq)} \leftrightarrow HPO_4^{2-}{}_{(aq)} + H^+ \quad (2)$$

$$HPO_4^{2-}{}_{(aq)} \leftrightarrow PO_4^{3-}{}_{(aq)} + H^+ \quad (3)$$

The abundance of the different phosphate species as a function of pH (Figure 3) has been calculated using equations 4 and 5 (see details at [27] and [28]).

$$\begin{aligned} K_{a1} &= 10^{-2.16} \\ K_{a2} &= 10^{-7.21} \\ K_{a3} &= 10^{-12.32} \end{aligned} \tag{4}$$

$$\begin{aligned} A_{PO_4^{3-}} &= \frac{1}{\frac{[H^+]^3}{K_{a1}K_{a2}K_{a3}} + \frac{[H^+]^2}{K_{a2}K_{a3}} + \frac{[H^+]}{K_{a3}} + 1} * 100 \\ A_{H_3PO_4} &= \frac{[H^+]^3}{K_{a1}K_{a2}K_{a3}} * A_{PO_4^{3-}} \\ A_{H_2PO_4^-} &= \frac{[H^+]^2}{K_{a2}K_{a3}} * A_{PO_4^{3-}} \\ A_{HPO_4^{2-}} &= \frac{[H^+]}{K_{a3}} * A_{PO_4^{3-}} \end{aligned} \tag{5}$$

Where K is the dissociation constant defined as the product of the activities (more details are found at [26]-[32]); a $[H^+]$ is the proton concentration and A_i is the abundance of the species i as a percentage of the total phosphate concentration.

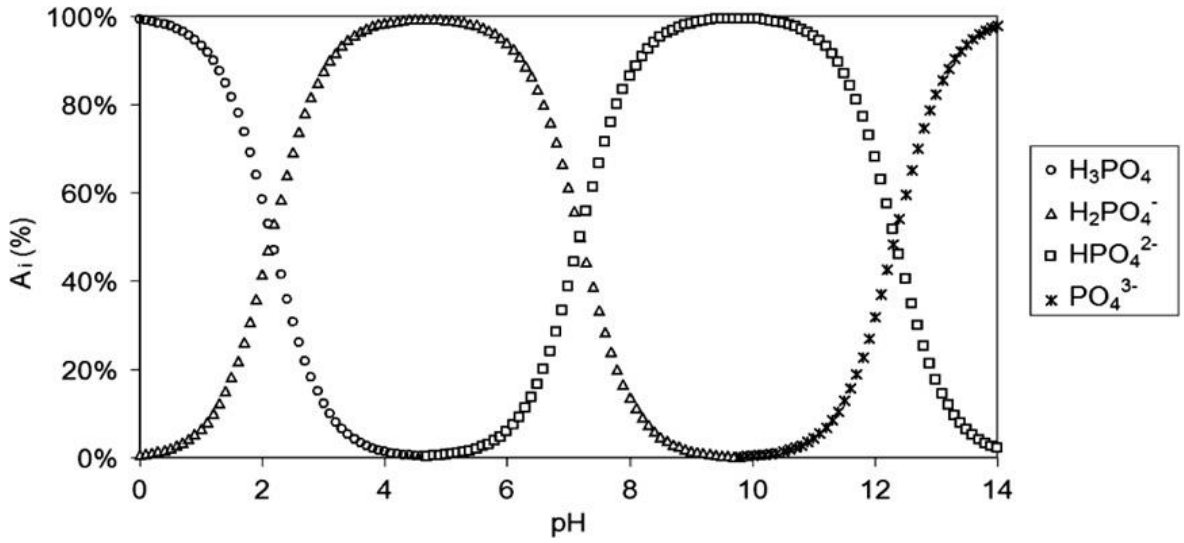

Figure 3 The abundance of the different phosphate species as a function of the pH; [28].

In addition, water also dissociates as a function of temperature [33] as shown in equation 6.

$$H_2O \leftrightarrow OH^- + H^+ \quad (6)$$

2.4 Phosphoric acid and wollastonite reaction

A case study of Section 2.6 is the reaction of phosphoric acid and wollastonite, which is a significant part of this thesis. Research has been conducted on this system before; [3], [26], [34] and [35].

Mosselmans [26] has studied the reaction of $CaSiO_3$ with H_3PO_4 leading to the formation of a Wollastonite-based PC. All byproducts and chemical reaction kinetics are well studied at ambient temperatures. Some thermal data was obtained to quantify the weight loss up to 1000°C, but the phase evolution was not characterized. Figure 4 [26] shows a nice schematic representation of the species in fully reacted mixtures for different molar H_3PO_4 to $CaSiO_3$ ratios (at a reaction temperature of 25°C and a molar H_2O to "P" ratio of 6.65): W (wollastonite), B (brushite), S (amorphous silica), M (monetite) and C (calcium dihydrogenphosphate mono hydrate).

Just as reference, in the thesis work conducted here, it molar ratios were estimated: r=P/Ca=0.9, $=H_3PO_4/CaSiO_{3=}$0.8, and H_2O/P=2.6. In general, our data confirms the diagram shown in Figure 4, although very weak monetite phase was detected in the XRD.

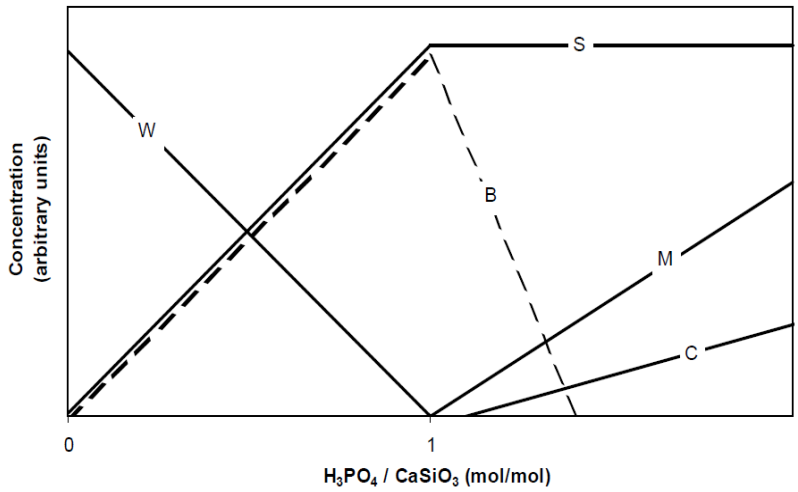

Figure 4 a) Schematic representation of the species present in fully reacted mixtures.

On the other hand, the influence of the reaction temperature on the reaction time has been also reported [26]. It was found that as temperature decreases, the reaction time increases and the heat flow decreases as well, which can be used to control the setting time during the manufacturing process. This is the primary reason why for the manufacturing of samples the raw materials (wollastonite and acid) are kept cold in a refrigerator.

In addition, Alshaaer [34] has studied the fabrication of Wollastonite-based PC at low temperatures. This study quantifies the mechanical properties after exposure at different temperatures and the phase identification was conducted up to intermediate temperatures for the Brushite to Monetite transformation. The effect of moisture and drying at low temperatures (less than 200°C) was studied and it showed a significant effect on the mechanical properties. Some samples were exposed up to temperatures of 1000°C but not much explanation was given to those materials. Shrinkage after 1000°C was about 23%. Bending strength was less than 6MPa below 800°C and about 11MPa after 1000°C exposure for dried samples. Compressive strength was less than 60MPa below 800°C and less han 80MPa after 1000°C exposure for dried samples. Based on the

Alshaaer [34] results, in this thesis, it has been implemented a slow drying process for three days as explained in Chapter 2.

Finally, very little research has been done on PC as a ceramic matrix for structural composites. Only few data is available mostly E-glass fibers; [3], [34] and [35].

2.5 References

[1] Jeong SY and Wagh AS. Chemical bonding phosphate ceramics: cementing the gap between ceramics, cements, and polymers. USA, Argonne National Laboratory report, 2002.

[2] Environmental Protection Agency AP 42 - Compilation of Air Pollutant Emission Factors, Volume I Stationary Point and Area Sources, Arunington, DC, 2005.

[3] Wagh AS. Chemical bonded phosphate ceramics, USA, Elsevier, 2004.

[4] Henry A. Colorado, Clem, Hiel, Jenn-M. Yang, H. Thomas Hahn. Wollastonite-based chemically bonded phosphate ceramic composites. Metal, ceramic and polymeric composites for various uses. 2011. ISBN 979-953-307-135-9. InTech, DOI: 10.5772/17120.

[5] Della M. Roy. New Strong Cement Materials: Chemically Bonded Ceramics. Science 1987; 235: 651-658.

[6] Colorado, H. A., C. Hiel, and H. T. Hahn. "Influence of Particle Size Distribution of Wollastonite on the Mechanical Properties of PCs (Chemically Bonded Phosphate Ceramics)." Processing and Properties of Advanced Ceramics and Composites III (2010): 85-98.

[7] Colorado, H. A., C. Hiel, and H. T. Hahn. "Processing-structure-property relations of chemically bonded phosphate ceramic composites." Bulletin of Materials Science 34.4 (2011): 785-792.

[8] Wilson AD and Nicholson JW. Acid based cements: their biomedical and industrial applications. Cambridge, England, Cambridge University Press, 1993.

[9] Wagh AS and Jeong SY. Chemically bonded phosphate ceramics: I, a dissolution model of formation. J. Am. Ceram. Soc. 2003; 86 (11): 1838-44.

[10] Wagh AS and Jeong SY. Chemically bonded phosphate ceramics: II, warm-temperature process for alumina ceramics. J. Am. Ceram. Soc. 2003; 86 (11): 1845-1849.

[11] Wagh AS and Jeong SY. Chemically bonded phosphate ceramics: III, reduction mechanism and its application to iron phosphate ceramics. J. Am. Soc. 2003; 86 (11) 1850-1855.

[12] Chow L and Eanes E. Octacalcium phosphate. Monographs in oral science, vol 18, Karger, Switzerland, 2001.

[13] Barinov S and Komlev V. Calcium Phosphate based bioceramics for bone tissue engineering. Trans Tech Publications Ltd, Switzerland, 2008.

[14] Chattopadhyay S. Evaluation of chemically bonded phosphate ceramics for mercury stabilization of a mixed synthetic waste. National Risk Management Research Lab. Cincinnati, Ohio, 2003.

[15] Singh D, Jeong SY, Dwyer K and Abesadze T. Ceramicrete: a novel ceramic packaging system for spent-fuel transport and storage. Argonne National Laboratory, Proceedings of Waste Management 2K Conference, Tucson, AZ, 2000.
[16] Young JF and Dimitry S. Electrical properties of chemical bonded ceramic insulators. J. Am. Ceram. Soc. 1990, 73 (9): 2775-2778.
[17] Miller L and Wise S. Chemical bonded ceramic tooling for advanced composites. Materials and Manufacturing Processes, Volume 5, Issue 2 1990, 229-252.
[18] Gomathi A, Vivekchand S, Govindaraj A and Rao C. Chemically bonded ceramic oxide coatings on carbon nanotubes and inorganic nanowires. Adv. Mater. 2005; 17: 2757-2761.
[19] Gulgun MA, Johnson B and Kriven W. Chemical bonded ceramics as an alternative to high temperature composite processing. Mat. Res. Soc. Symp. Proc. Vol. 346. Materials Research Society, 1994.
[20] Laufenberg T, Aro M, Wagh A, Winandy J, Donahue P, Weitner S and Aue J. Phosphate-bonded ceramic-wood composites. Ninth International Conference on Inorganic bonded composite materials, Vancouver, 2004.
[21] Mosselmans G, Monique B, Willem R, Wastiels J, Leermakers M, Rahier H, Brughmans S, and Van Mele B. Thermal hardening and structure of a phosphorous containing cementitious model material: phosphoric acid-wollastonite. Journal of Thermal Analysis and Calorimetry 2007; 88 (3): 723-729.
[22] Grover LM, Gbureck U, Young AM, Wright AJ, Barralet JE. Temperature dependent setting kinetics and mechanical properties of beta-TCP-pyrophosphoric acid bone cement. Journal of Materials Chemistry 2005, 15: 4955-4962.
[23] Brown W and Chow L. Chemical properties of bone mineral. Annu. Rev. Mater. Sci. 1976; (6): 213-235.
[24] Albee FH and Morrison HF. Studies in bone growth: triple calcium phosphate as a stimulus of osteogenesis. Ann. Surg. 1920; (71): 32–38.
[25] Colorado, H. A., C. Hiel, and H. T. Hahn. "Pultrusion of glass and carbon fibers reinforced Chemically Bonded Phosphate Ceramics." Journal of Composites Materials (2010).
[26] G. Mosselmans. Inorganic phosphorus based materials, produced at low temperature in an acid environment: mechanism, kinetics, molecular structure and thermomechanical properties. Doctoral thesis VUB ; March 2006
[27] K. Takehara, Y. Ide, T. Nakatazato, N. Yora, Journal of Electroanalytical Chemistry 293 (1990) 285.
[28] De Silva Muñoz, Leonardo, Alain Bergel, and Régine Basséguy. "Role of the reversible electrochemical deprotonation of phosphate species in anaerobic biocorrosion of steels." Corrosion Science 49.10 (2007): 3988-4004.
[29] Childs, C. W. "Equilibriums in dilute aqueous solutions of orthophosphates."The Journal of physical chemistry 73.9 (1969): 2956-2960.
[30] Elmore, K. L., et al. "Dissociation of Phosphoric Acid Solutions at 25° 1." The Journal of Physical Chemistry 69.10 (1965): 3520-3525.
[31] Pourbais M., “Atlas of Electrochemical Equilibria in Aqueous Solutions”, National Association of Corrosion Engineers, Texas U.S.A. (1974)

[32] Zemaitis J.F.Jr., Clark D.M., Rafal M., Scrivner N.C., “Handbook of Aqueous Electrolyte Thermodynamics”, DIPPR, New York (1986)
[33] Smith R.M., Martell A.E., “Critical Stability Constants: Inorganic Complexes”, Vol.4, Plenium Press, New York (1976).
[34] Alsaaer, M. Optimization of properties of Inorganic Phosphate Cement (IPC) for construction and high-temperature applications. Diss. PhD thesis, Vrije Universiteit Brussel (http://wwwtw. vub. ac. be/memc/website/index. htm), 2006.
[35] Colorado, H. A., Hiel C., Hahn H. T. and Yang J. M.. "Wollastonite-Based Chemically Bonded Phosphate Ceramic Composites." Intech (2011)

3 Materials and experimental methods

3. 1 Materials

3.1.1 Wollastonite

General information

Wollastonite is used in this research as a calcium source to create phosphates. Wollastonite is the mineral name of mono-calcium silicate ($CaSiO_3$) with triclinic or monoclinic structure [14]. Color is as different as white, cream, light yellow, pink, gray, green and brown [15]. Its specific gravity ranges from 2.9 to 3.1. Pure wollastonite melts at 1540°C, although the fluid temperature for commercially produced wollastonite may be 1380°C (NYCO Minerals Inc, 2012). Wollastonite is unique among nonmetallic industrial minerals for its combination of white color, acicular (needle-like) crystal shape, alkaline pH (typically more than 10), low cost and thermal stability. Because of its acicular shape (the aspect ratio is usually between 10 and 20) it is very effective as reinforcement and it is widely used as filler for plastics [16] and paints [17]. Because of its effectiveness in suppressing plastic flow, it is used as protection against surface damage [18]. Also, since it has been shown that wollastonite is bioactive, it has been used in several bio-engineering applications, [19] and [20]. In addition, due to its excellent thermal stability, wollastonite is used as flame retardant for polymers [21]; (see also Chapter 3 for specific Wollastonite used in this research and more applications, [1]).

Wollastonite is the result of the reaction between calcite and silica with the loss of carbon dioxide as shown in equation 7.

$$CaCO_3 + SiO_2 \rightarrow CaSiO_3 + CO_2 \quad (7)$$

Figure 5 shows the structure of wollastonite in its triclinic structure. The surface and its reaction with dissociated water was simulated [22]. Figure 5a shows the side view of relaxed surface

structure of wollastonite {100}. Structure is constituited of two chains repetition where the atoms are near to but not at position. Surface structure is very difficult to determine experimentally. Figure 5b shows the 3-dimmensional view. Figure 5c shows the $Ca^{2+}/2H^{+}$ exchange reaction on the wollastonite surface; and Figure 5d shows the simulation results of this reaction.

Manufactures data

Natural Wollastonite powder, calcium silicate $CaSiO_3$, from Minera Nyco (see Table 1 and 2) was used in this research. Different sizes were investigated (Chapter 4), however, almost all research was conducted with the M200 type (see Table 2 from manufacturer, [1]).

Table 1 Chemical composition of Wollastonite powder.

Composition	CaO	SiO_2	Fe_2O_3	Al_2O_3	MnO	MgO	TiO_2	K_2O	Impurities
Percentage	46.25	52.00	0.25	0.40	0.025	0.50	0.025	0.15	$\leq$0.4

The median particle size was determined with a cilas granulometer, the surface area was determined with an ASAP 2405 (Micromeritics), and the moisture content was determined with a Karl Fischer instrument. Other properties provided for the manufacturer for M200 Wollastonite powder are shown in Table 3. Figure 6 shows SEM images of Wollastonite.

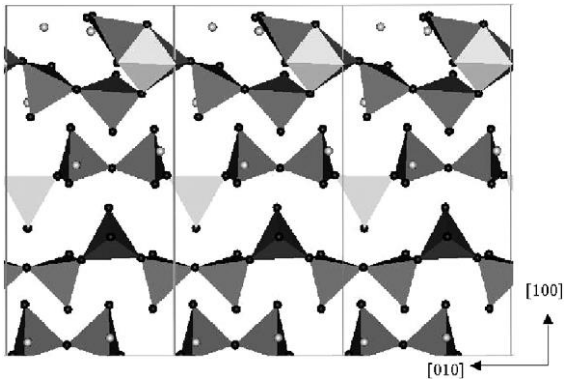

a)

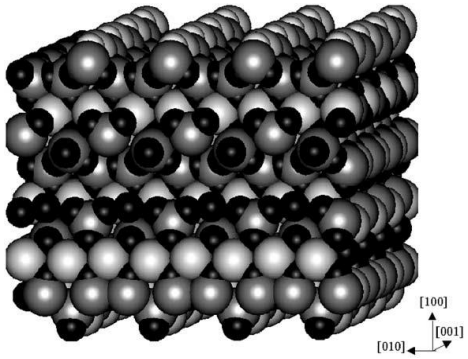

b)

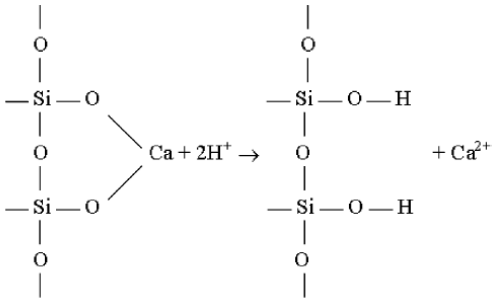

c)

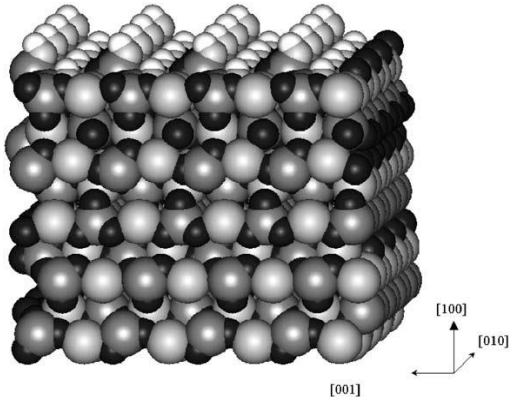

d)

Figure 5 a) Side view of relaxed surface structure of wollastonite {100} showing silicon as grey tetrahedron, oxygen as dark circle and calcium as light circle; b) 3D view of relaxed {100} wollastonite, the top layer oxygen is shown as white and other oxygen as black, calcium as large light grey ball, and silicon as large grey ball; c) schematic diagram of the $Ca2^{+}/2H^{+}$ exchange reaction on the wollastonite surface; d) Perspective view of hydroxylated {100} wollastonite showing oxygen of hydroxyl as light grey, hydrogen as white, bulk oxygen as black, calcium as light grey ball and silicon as grey ball.

Table 2 Properties of wollastonite powders as received

Powder reference	Median particle size (μm)	Surface Area (m^2/g) (BET)	Moisture (%)
M200	15	1.1	0.05
M400	8	1.6	0.20
M1250	3.5	2.9	0.25

Table 3 Properties of M200 wollastonite powder [1]

Appearance	White	Water Solubility (g/100cc)	0.0095
Morphology	Acicular	Density (lbs./gu.ft.)	181
Molecular Weight	116	Bulking Value (gal./lbs.)	0.0413
Specific Gravity	2.9	Mohs Hardness	4.5
Refractive Index	1.63	Coefficient of Expansion (mm/mm/°C)	$6.5x10^{-6}$
Ph (10% Slurry)	9.9	Melting Point (°C) - Theoretical	1540
		Melting Point (°C) -By ASTM D1857	1410

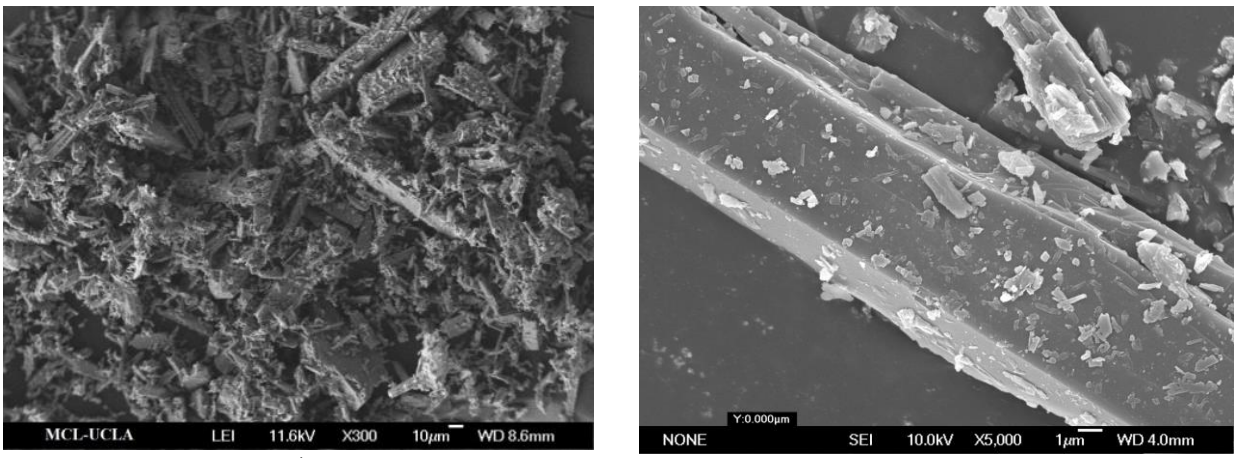

a) b)

Figure 6 SEM of M200 wollastonite powder at different magnification.

Wollastonite is a mineral with a triclinic structure. It is usually white and may contain small amounts of iron, magnesium, and manganese substituting for calcium. There are many industrial applications for wollastonite. These include reinforcements for structural ceramics products like bricks and pipes; filler for paint with improved resistance to the environment; filler for plastics.

3.1.2 Fly Ash

Fly ash class F from Diversified Minerals Inc was used in this research. The composition of Fly ash class F is shown in Table 4. Figure 7 shows SEM images of fly ash.

Table 4 Chemical composition range of Fly ash class F

Composition	CaO	SiO_2	Fe_2O_3	Al_2O_3
Percentage	5-22	59-63	2-5	11-15

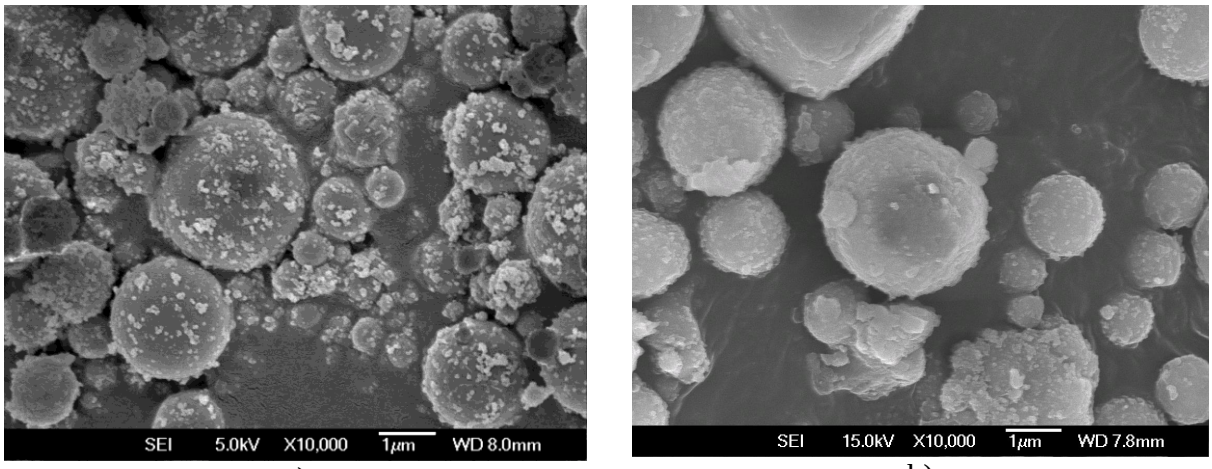

a) b)

Figure 7 Fly ash class powder at different magnification.

Fly ash is one of the residues generated in combustion. It is a pozzolan that reacts with available lime in cement providing more cementitious compounds and is a direct replacement for cement.

3.1.3 Fibers

Glass fibers Flexstrand 225 from Fiber Glass Industries Inc. [2], Carbon fibers A511 from Toho Tenax [3], Basalt fibers BCF13-1200KV12 from Kammemy Vek [4], and SiC fibers Hi-Nicalon form COI Ceramics Inc. [5], were used in this research. Table 5 summarizes the main data provided by the manufacturers. In case data was not supplied by them, a reference is included.

Glass and basalt fibers have similar compositions. Table 6 summarizes typical compositions for the fibers used. SiC fibers have a composition [5] of “Si” 62wt.%, “C” 37.0 wt.% and “O” 0.5wt.%. Carbon fibers have a composition of “C” > 98.0wt.%, [3].

Table 5 Properties of the glass, carbon, basalt and SiC fibers used in this research.

Fiber type	**E-glass**	**Basalt**	**Carbon**	**SiC**
Tensile strength of single filaments [MPa]	3100-3800 [6]	4000-4300	4205-4620	3450-3600
Tensile modulus of single filaments [PCa]	72-76	87-92	236-239	270
Fiber diameter (µm)	23.5	10-22	7.1	14
Density [g/cm^3]	2.5-2.6	2.67	1.77	2.74
Type of sizing	1334 polyvinyl ester (PVE)	Silane (0.4wt%)	Solution based on polyurethane	Polyvinyl Alcohol (PVA)
Softening point [°C]	840 [7]	960 [7]	-	-
Thermal conductivity, W/(m.°K)	0.034-0.04	0.031-0.038	10	7.7 at 25°C 10.1 at 500°C
Coefficient of linear expansion [10^{-6}/°C]	6.0	8.0	-0.1 [3] Long.: 1.6-2.1, [8] Transv.: 5-10, [8]	3.8 (200°C) 5.8 (1000°C), [9]

Table 6 Typical compositions for E-glass [6] and basalt fibers [10].

Component (wt%)	SiO_2	Al_2O_3	CaO	MgO	MnO	TiO_2	Na_2O	K_2O	Fe_2O_3	FeO	P_2O_5
Glass fiber	59.0	12.1	22.6	3.4	-	1.5	0.9	-	0.2	-	-
Basalt fiber	53.6	17.4	8.5	4.1	0.1	1.1	2.6	1.6	4.7	4.4	0.2

3.1.4 Phosphoric acid formulation

Three formulations of phosphoric acid (H_3PO_4) were used in this research, see Table 7. The main formulation used in this thesis is 5.0wt% of borax. Only in Chapter 4 other formulations were used (2.9wt% and 0.0wt% of borax). These formulations are protected by a patent from Composites Support Inc.

Table 7 Borax additions in the acid formulation

Compound	**0.0 wt% Borax**	**2.9 wt% Borax**	**5.0 wt% Borax (main formulation used)**
Simplified name	**A0.0**	**A2.9**	**A5.0**
Borax (sodium borate), (%)	0.0	2.9	5
Water, (%)	11	10.7	15
H_3PO_4, (%)	75.8	73.6	68.2
Zinc Oxide, (%)	6.6	6.4	5.9
Aluminum oxide, (%)	6.6	6.4	5.9
TOTAL	100	100	100

3. 2 Experimental methods

3.2.1 Matrix manufacturing

For wollastonite-based PC the manufacturing was conducted by mixing an aqueous phosphoric acid formulation and natural wollastonite powder in a 1.2 ratio liquid/powder. Both the wollastonite powder and the phosphoric acid formulation were maintained at 6˚C in a closed container (to prevent water absorption) for 1 hour in order to increase the pot life of the resin and keep the viscosity low for more than 1h.

The mixing process of wollastonite powder and phosphoric acid formulation was first done by hand (for about 10s), see Figure 8a. Then, it was conducted in a Planetary Centrifugal Mixer (Thinky Mixer AR-250, TM) for more than 1min, see Figure 8b and c.

Next, the mixture was poured into Teflon molds (see Figure 8d) of different sizes depending on the sample type. For testing the ceramic matrix, cylindrical samples were fabricated and tested in compression mode. For composites samples, ceramic matrix with unidirectional fibers, rectangular rods were fabricated and tested in bending mode. A polymeric mold release was

always used to prevent damage in the ceramic during the sample mold release. To stabilize the weight of the sample, a drying process (to remove unbounded water) was conducted carefully in order to avoid crack growing or thermal stresses. The drying process was performed at 50 ˚C for 24 hours, followed by 105˚C for 24 hours. Finally, the sample was dried at 200˚C for 24 hours.

a)

b)

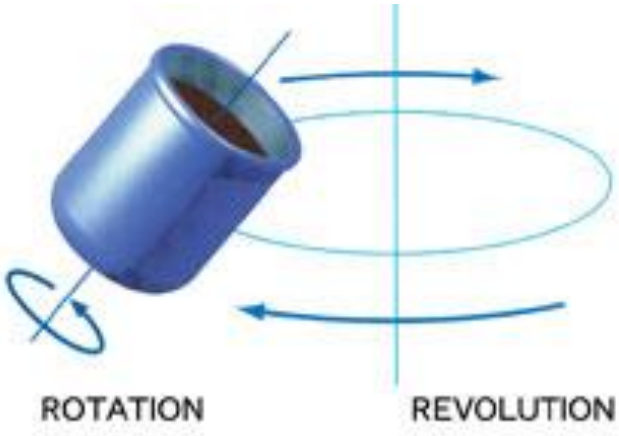

c)

d)

Figure 8 pre-mixing of wollastonite powder and the acid by hand; b) Thinky mixer AR-250, c) planetary mixing principle, d) b) pouring the resin into a mold after the mixing was conducted..

Figure 9 shows a simplified flow chart of the process. Mixing times were changed in some experiments (see each chapter for details), but in general the most common mixing time was 2min, enough to remove bubbles and guarantee an homogeneous mixing.

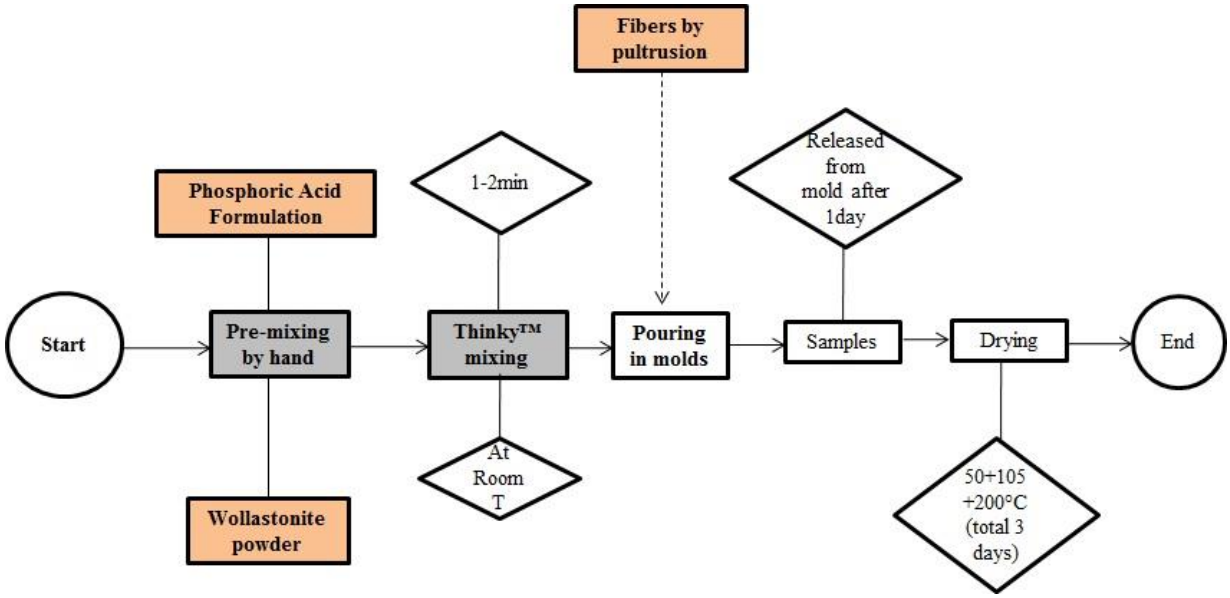

Figure 9 Simplified flow charts of the processes.

Several mixing (such as resonant acoustic and blade mixing) and processing techniques (such as vacuum at 0.01MPa) were used to optimize [11] the process shown in Figure 9. This was done in order to remove the bubbles and to produce high compression/bending strength, taking into account factors such as the cost and the green processing.

3.2.2 Composites manufacturing

Composites were fabricated by pultrusion. Pultrusion is a continuous process for the manufacture of composite materials with constant cross-section, see Figure 10a. Reinforced fibers are pulled through a resin, followed by a heated die, where the PC solidifies. The pultrusion process used in this research for the Wo-PC reinforced with glass fiber is shown in Figure 10b. The die-

temperature was 110˚C (230˚F) and the pull speed was 30.5 cm/min (1 ft/min). Pultruded bars for both graphite and glass fibers are presented in Figure 10c.

All samples were fabricated with about 15 volume % of fibers and the fibers used were glass, carbon and basalt. All samples were dried 1 day at 50°C, 1 day at 100°C and 1 day at 200°C in order to remove the water completely. Glass fibers Textrand 225 from Fiber Glass Industries, Graphite fibers Tenax(R)-A 511, and Basalt fibers BCF13-1200KV12 Int from Kammemy Vek were used in this research. In order to plot the Weibull distributions, twenty samples were tested for each temperature and composition and then tested in three point bending tests. The thermal treatment followed in this experiment is the thermal exposure described in the next section.

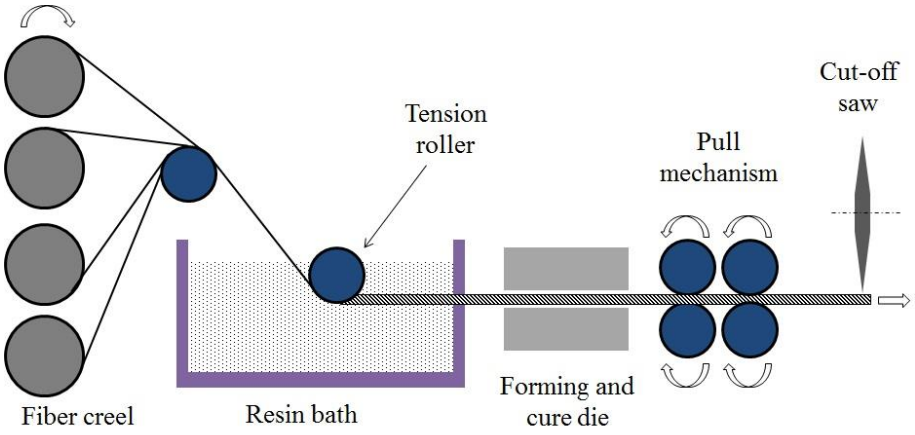

a)

b)

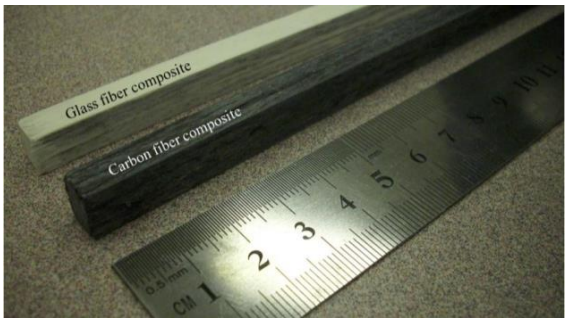

c)

Figure 10 a) diagram of the pultrusion process, b) pultrusion die during manufacturing of PCs reinforced with glass fibers, a) and pultruded bars of PCs reinforced with glass fibers (white) and with carbon fibers (black).

3.2.3 Thermal treatments

In addition to the drying process, the PC matrix, the fibers and the composite, were studied after thermal exposure at different temperatures. Progressive thermal exposure tests were conducted at temperatures of 100°C, 200°C, 300°C, 400°C, 500°C, 600°C, 900°C, 800°C, 900°C, and 1000°C. Each thermal step took 1 hour. Additional tests were conducted for some compositions tested 1000°C for 2, 12 and 24 h.

3.2.4 Scanning Electron Microscopy

To see the microstructure, sample sections were initially ground using silicon carbide paper grits ANSI 240, 400 and 1200. Then they were polished with alumina powders of 1, 0.3 and 0.05μm grain size progressively. After polishing, samples were dried in a furnace at 100˚C for 24 hours and observed in an optical microscope. For SEM examination, samples were mounted on an aluminum stub and sputtered in a Hummer 6.2 system (15mA AC for 30 sec) creating approximately a 1nm thick film of Au. The SEM used was a JEOL JSM 6700R in high vacuum mode. Elemental distribution x-ray maps were collected on the SEM with an energy-dispersive X-ray spectroscopy analyzer (SEM-EDS). The images were collected on the polished and gold-coated samples, with a counting time of 51.2 ms/pixel. In case of fibers, each fiber (at least 20) was measure in the SEM in order to know the diameter to be used in the mechanical characterization. For the fiber size distribution, fibers were put into resin and then polished to measure the diameter and also analyze their structure.

3.2.5 X-ray diffraction

Samples were ground for X-Ray Diffraction (XRD) experiments, which were conducted in an X'Pert PRO (Cu Kα radiation, λ=1.5406 Å) equipment, at 45KV and scanning between 10º and 70º.

3.2.6 Thermo-gravimetric analysis

Thermo gravimetric Analysis (TGA) was performed in Perkin Elmer Instruments Pyris Diamond TG/DTA equipment. The temperature ramp was 10ºC/min from room temperature up to 1000ºC, with previous equilibration at 50ºC for 10min. All experiments were conducted in air atmosphere in an alumina pan with air at 100mL/min. Some experiments were conducted in an argon atmosphere at 100mL/min to help in the analysis.

3.2.7 Density

Density tests were conducted over PCs with fly ash as filler. All samples were tested after a drying process (50˚C for 1 day, followed by 100˚C for 1 day) in a Metter Toledo^{TM} balance, by means of the buoyancy method. Six samples for each composition were tested. The dry weight (Wd), submerged weight (Ws), and saturated weight (Wss) were measured. The following parameters were calculated:

Bulk volume: Vb = Wss – Ws; Apparent volume: Vapp = Wd – Ws; Open-pore volume: Vop = Wss – Wd; % porosity = (Vop/Vb) x 100 %; Bulk Density: Db = Wd/ (Wss - Ws); and Apparent Density: Da = Wd/(Wd – Ws). In these calculations the density of water was taken to be 1.0 g/cm^3.

Only in Chapter 7, for the curing samples obtained in the gel timer, density was calculated by the weight/volume ratio of the samples.

3.2.8 Curing tests

Two types of curing experiments were conducted. One aims to measure the temperature changes during the setting process of the cement. The other test, aims to measure the pot life in a very empirical but useful method for industry. In this case, a gel-timer was used.

Temperature-based method

For all cure samples, 24g of the acid solution and 20g of powder (wollastonite + fly ash) were mixed at room temperature in the TM for 15 sec in a container with a hole to allow resulting gases to escape. Three factors were considered in determining this short mixing time:

- some wollastonite powders are very reactive due to their grain sizes. Therefore a short time was selected
- the small amount of total precursor (44g) requires short mixing time; and
- at room temperature it is easier to see the effect of using different powders , additives and processing methods on the setting time.

Curing curves were then obtained by measuring the temperature change with time for different filler content. Both mixing and curing were conducted in TM containers. The mixing was performed in 125ml Polypropylene jars while the curing was performed in 24ml Polypropylene jars. A thermocouple was set at the bottom of the container, as shown in Figure 11a. The same containers (used for mixing and for curing) were used following the same parameters and experimental conditions for all samples.

Gel-timer method

The setting time was also studied in a Gardco Standard Gel Timer (110V) apparatus, Figure 11b. A commercial aluminum foil-made container was used in all cases, which shows the low acid

strength of the formulation used in this research. Different sample amounts and conditions were used. Details will be explained in Chapter 4 and 7.

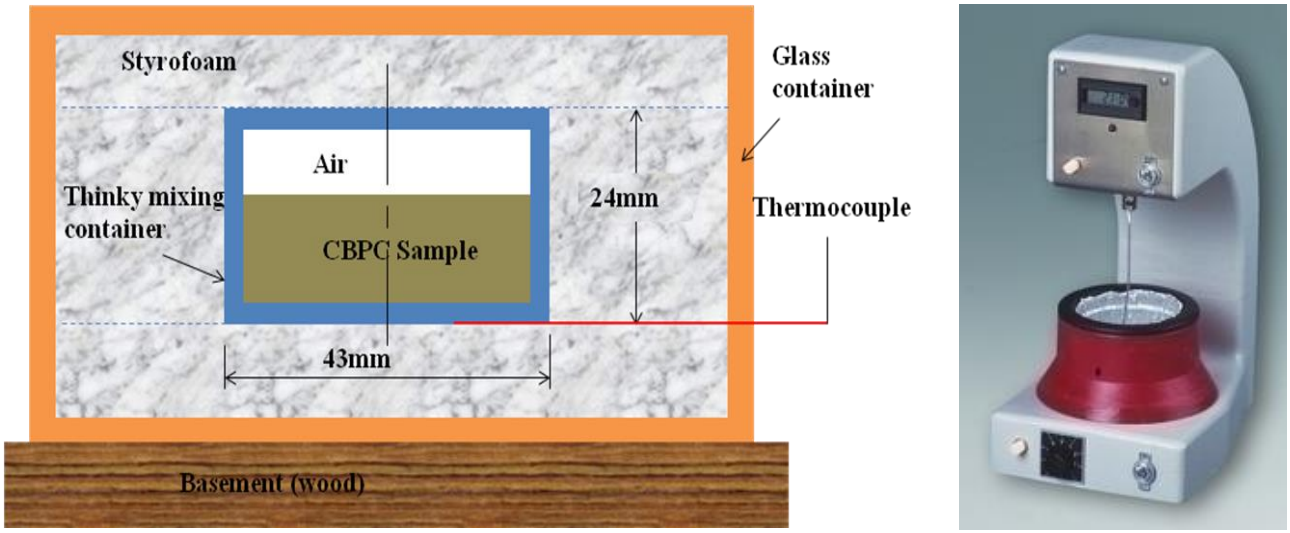

a) b)

Figure 11 a) Experimental set up for the curing experiments. All tests were conducted at room temperature in a closed (to humidity) plastic container, with a thermocouple inserted into a hole and then sealed with tape; b)

3.2.9 Mechanical tests

For each type of composite and thermal treatment, at least twenty samples were tested in bending tests in order to plot Weibull distributions. These tests were performed on an Instron 4411 at a crosshead speed of 2.5 mm/min in the case of macro samples (PC matrix and composites). Samples were cut from pultruded rectangular bars, with dimensions 9.0x12.7x200mm^3. The span length was 127mm. This same parameters and machine was also used to test the PC matrix in compression. For compression tests, samples were poured in a Teflon mold and cylinders were obtained after solidification.

In the case of the individual fiber, a single fiber was mounted on a cardboard frame by applying instant glue to both ends. The gage length was 50mm. For each type of fiber and thermal

treatment, twenty samples were tested by tensile tests in order to plot Weibull distributions. These tests were performed on an Instron 5940 at a crosshead speed of 5.0 mm/min. Fiber diameter was measured on each sample after testing in a scanning electron microscope. All samples and compositions fabricated in this thesis have been studied under the Weibull statistics found elsewhere, [12] and [13]. More details regarding the specific test are given in each chapter.

3.3 References

[1] NYCO MINERALS INC. New York, USA. Technical Data Sheets. http://www.nycominerals.com/

[2] Fiber Glass Industries, Inc., fiber glass manufacturer. New York, USA. Website: http://fiberglassindustries.com.

[3] Toho Tenax America Inc, carbon fiber manufacturer. Tennessee, USA. Website: http://www.tohotenaxamerica.com/contfil.php

[4] Kamenny Vek, basalt fiber manufacturer. Moscow, Russia. Website: http://www.basfiber.com/

[5] COI Ceramics, Inc., SiC fiber manufacturer. San Diego, USA. Website: http://www.coiceramics.com/index.html.

[6] Frederick T. Wallenberger, James C. Watson, and Hong Li. Glass Fibers. 2001 ASM International. ASM Handbook, Vol. 21: Composites (#06781G): 27-34.

[7] Militký, Jiří, Vladimír Kovačič, and Vladimír Bajzík. "Mechanical properties of basalt filaments." FIBRES & TEXTILES in Eastern Europe 15.5-6 (2007): 64-65.

[8] Pradere, C., and C. Sauder. "Transverse and longitudinal coefficient of thermal expansion of carbon fibers at high temperatures (300–2500K)." Carbon 46.14 (2008): 1874-1884.

[9] Andersson, C. H., and R. Warren. "Silicon carbide fibres and their potential for use in composite materials. Part 1." Composites 15.1 (1984): 16-24.

[10] Černý, M., et al. "Comparison of mechanical properties and structural changes of continuous basalt and glass fibres at elevated temperatures." Ceramics–Silikáty 51.2 (2007): 82-88.

[11] Colorado, H. A., C. Hiel, and H. T. Hahn. "Processing-structure-property relations of chemically bonded phosphate ceramic composites." Bulletin of Materials Science 34.4 (2011): 785-792.

[12] Zok, Frank W., Xiuyen Chen, and Christian H. Weber. "Tensile strength of SiC fibers." Journal of the American Ceramic Society 78.7 (1995): 1965-1968.

[13] Hertzberg, Richard W. Deformation and fracture mechanics of engineering materials. Vol. 89. New York: Wiley, 1996.

[14] Daniel Maxim L., McConnell E.E.: A Review of the Toxicology and Epidemiology of Wollastonite. Inhalation Toxicology, 17(9): 451-466 (2005).

[15] Wilbourn J.D., McGregor D.B., Partensky C., Rice J.M.: IARC reevaluates silica and related substances. Environmental Health Perspectives 1997; 105(7): 756–158.

[16] Luyt A.S., Dramićanin M.D., Antić Ž., Djoković V.: Morphology, mechanical and thermal properties of composites of polypropylene and nanostructured wollastonite filler. Polymer Testing, 28(3): 348-356 (2009).
[17] Rothon R.N.: Particulate filler for polymers. Rapra Review Reports, (2001).
[18] Misra R.D.K., Hadal R., Duncan S.J.: Surface damage behavior during scratch deformation of mineral reinforced polymer composites. Acta Materialia, 52(14): 4363–4376 (2004).
[19] Makarand R., Nabi Saheb D., Jyoti J., Ramesh B.: Preparation, characterization and in vitro biocompatibility evaluation of poly(butylene terephthalate)/wollastonite composites. Biomaterials, 22(15): 1591–1597 (2001).
[20] Xuanyong L., Chuanxian D., Paul K.C.: Mechanism of apatite formation on wollastonite coatings in simulated body fluids. Biomaterials, 25(10): 1755-1761 (2004).
[21] Hamdani-Devarennes S., Pommier A., Longuet C., Lopez-Cuesta J.M., Ganachaud F.: Calcium and aluminium-based fillers as flame-retardant additives in silicone matrices II. Analyses on composite residues from an industrial-based pyrolysis test. Polymer Degradation and Stability, 96(9): 1562–1572 (2011).
[22] Kundu, T. K., K. Hanumantha Rao, and S. C. Parker. "Atomistic simulation of the surface structure of wollastonite and adsorption phenomena relevant to flotation." International Journal of Mineral Processing 72.1 (2003): 111-127.

4 Acid-base phosphate cements fabricated with wollastonite powder

4.1 Introduction

In this research, acid-base phosphate cements fabricated with wollastonite powder (Wo-PC) and phosphoric acid (H_3PO_4) was used, which, when mixed in a ratio of 100/120 sets in to a solid material. wollastonite is a natural calcium meta-silicate which is mostly used as filler in resins and plastics, ceramics, metallurgy, biomaterials, and other industrial applications [2].

The mixing of wollastonite with phosphoric acid produces calcium phosphates (brushite ($CaHPO_4 \cdot 2H_2O$), monetite ($CaHPO_4$) and calcium dihydrogenphosphate monohydrate ($Ca(H_2PO_4)2 \cdot H_2O$)) and silica for molar ratios (P/Ca) between 1 and 1.66, [2]. We found that with the phosphoric acid formulations of liquid to wollastonite with a ratio of 1.2 results in a neutral product, with a pH of 7.0. This is particularly interesting when they are compared with Portland cement for which pH is in excess of 12, which does not allow the use of E-glass fibers as a reinforcement.

This Chapter will present the material science of the Wo-PC, its compressive strength analyzed with Weibull statistics, and the effects of particle size distribution on mechanical properties. Curing and compression tests were performed for PCs made with wollastonite powder of different sizes. The mechanism of weight loss is presented. The emphasis of this Chapter is the thermo-mechanical behavior study of these materials at temperatures up to 1000°C. The microstructure in all cases was analyzed and the chemical reactions are included.

4.2 Experimental

The manufacturing of PC samples was conducted by mixing an aqueous phosphoric acid formulation (later presented) and natural wollastonite powder (from Minera Nyco; see Table 1 and 2) in a 1.2 liquid/powder ratio. The pH of the PC after curing was 7.0. The mixing process of

wollastonite powder and phosphoric acid formulation was firstly done by hand (for about 10s). Then, it was conducted in a Planetary Centrifugal Mixer (Thinky Mixer AR-250, TM). For curing test samples, both the wollastonite powder and the phosphoric acid formulation were maintained at room temperature. For compression samples, both the wollastonite powder and the phosphoric acid formulation were maintained at 6 ˚C in a closed container (to prevent water absorption) for 1 hour in order to increase the pot life of the resin and keep the viscosity low for more than 1h. Figure 8a shows the pre-hand mixing. Figure 8b shows the pouring of the resin into Teflon molds. The resin as shown has a very low viscosity (similar to water) ideal for impregnating the mold or making composites.

Table 8 Chemical composition of wollastonite powder.

Composition	CaO	SiO_2	Fe_2O_3	Al_2O_3	MnO	MgO	TiO_2	K_2O
Percentage	46.25	52.00	0.25	0.40	0.025	0.50	0.025	0.15

The median particle size was determined with a cilas granulometer, the surface area was determined with an ASAP 2405 (Micromeritics), and the moisture content was determined with a Karl Fischer instrument. These properties are presented in Table 2. In all cases pH (10% slurry) was 9.9.

Table 9 Properties of wollastonite powders as received

Powder reference	Median particle size (μm)	Surface Area (m^2/g) (BET)	Moisture (%)
M200	15	1.1	0.05
M400	8	1.6	0.20
M1250	3.5	2.9	0.25

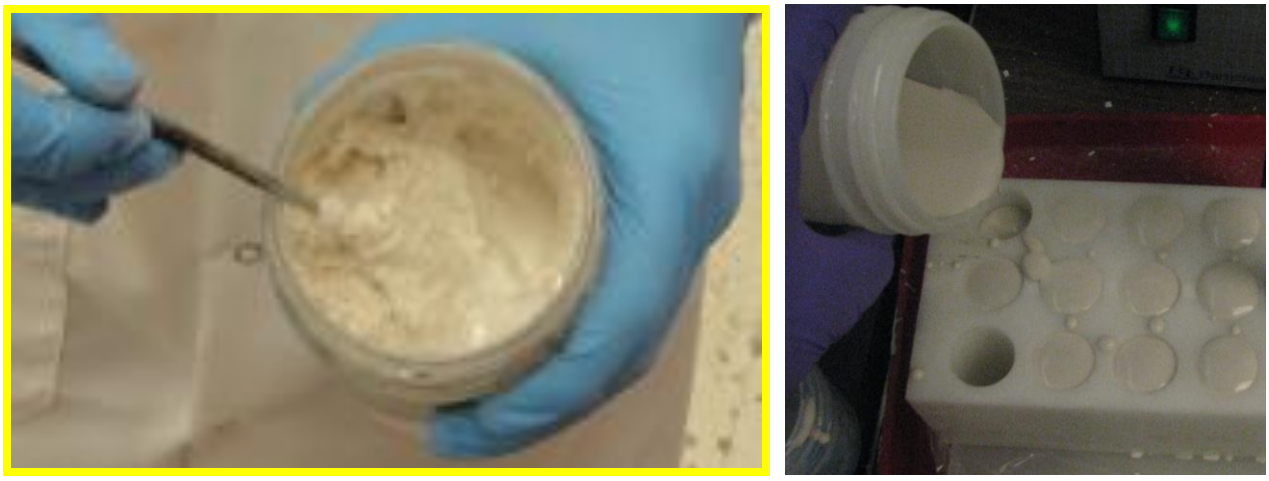

a) b)

Figure 12 pre-hand mixing of wollastonite powder and the acid; b) pouring the resin into a mold after the mixing was conducted in the Thinky mixer apparatus.

A linear shrinkage test was performed following the ASTM C326-09 standard for drying and firing shrinkages of ceramic whiteware clays. Test specimens were bars of 19mm in diameter by 127 mm in length. Shrinkage reference lines were made with a knife at zero and 102 mm. The drying process was performed at 50 ˚C for 24 hours, followed by 105 ˚C for 24 hours. In addition to the aforementioned procedure, added drying time for 24 hours at 200˚C was employed. After all annealing times, the samples were cooled in the oven until it reached room temperature.

Finally, density tests were conducted over PC samples made with M200, M400, and M1250 wollastonite powders after a drying process (50˚C for 1 day, followed by 105˚C for 1 day, followed by 205˚C for 1 day) in a Metter Toledo^{TM} balance, by means of the buoyancy method.

4.3 Wo-PC formation, microstrucure, and phase transformations upon diver temperature exposure

As discussed in Chaper 2, the dissolution reactions and ionic concentrations <$Ca^{2+(}$aq)> are given in equations 1 and 2, [3] and [4]. Figure 13 shows the ionic concentration (from equations 1b and 2b) for

calcium (from wollastonite) as a function of pH. As the pH increases, the concentration of Ca^{2+} decreases. As dicussed in Chapter 3, the pH is the driven force for of the PC formation, since they are materials formed by the acid-based reaction. Therefore, at the very early stage of mixing, when the calcium ions just start to dissolve into the liquid, the pH is 1, and we expect the dissolution rate to be very high. As time is going on, there are more ions in the liquid and therefore the pH increases, which decreases the dissolution of new ions rate as well.

$$CaSiO_3 + 2H^+ = Ca^{2+}(aq) + H_2SiO_3 \quad \text{(in the pH range 0-10)} \quad (1a)$$

$$\log\langle Ca^{2+}(aq)\rangle = 1.315 - pH \quad (1b)$$

$$CaSiO_3 + H^+ = Ca^{2+}(aq) + H_2SiO_3^- \quad \text{(in the pH range 10-11.45)} \quad (2a)$$

$$\log\langle Ca^{2+}(aq)\rangle = -3.61 - pH \quad (2b)$$

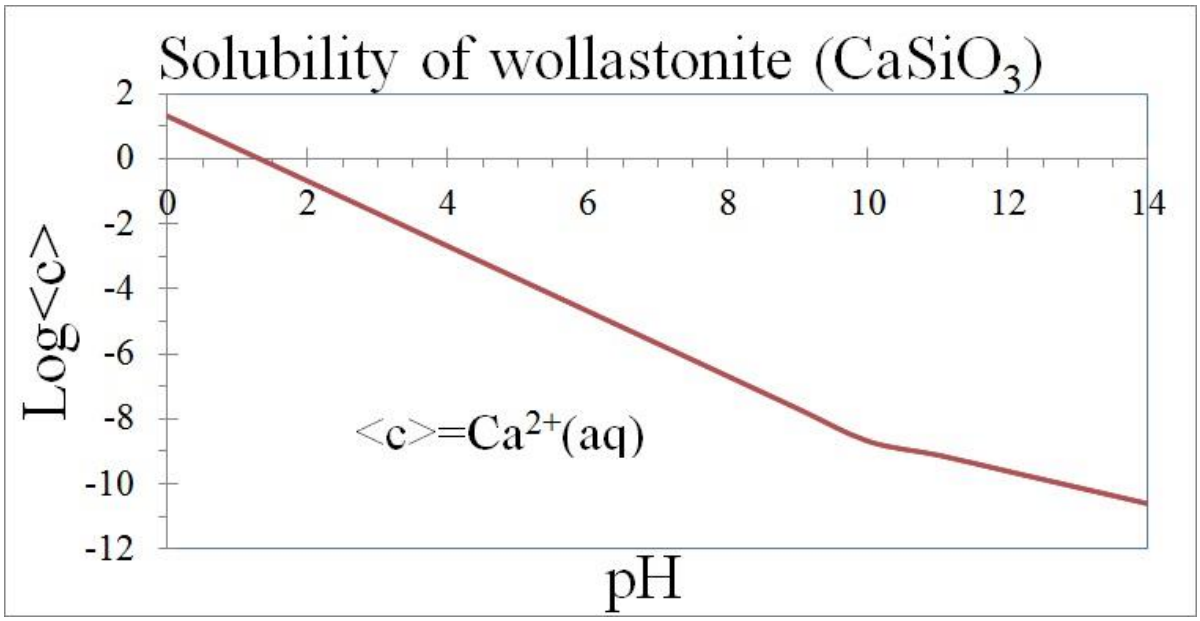

Figure 13 Solubility curve for calcium (from wollastonite) as a function of pH.

This dissolution is an endothermic reaction, and this is seen in the PCs as a slight decrease in the temperature while the mixing is conducted, [4] and [5]; when liquid is saturated, there is no more calcium

released into the liquid. Simultaneously, calcium phosphate starts to grow in a strong exothermic reaction. Residual wollastonite, silica grains, and impurities serve as nucleation points.

Figure 14 shows the XRD data for the wollastonite-based PC under different temperatures. This ceramic material is a composite itself, a multi-phase material, as shown by the spectrum taken after the drying process of 200°C. The phases in the material as made are residual wollastonite ($CaSiO_3$), quartz (SiO_2), brushite ($CaHPO_4.\ 2H_2O$) and monetite ($CaHPO_4$). The main phases by quantity are wollastonite and brushite. In addition, amorphous calcium phosphate and amorphous silica are present. Equations 3 and 4 describe the process.

$$CaSiO_3 + H_3PO_4 + H_2O = SiO_2 + CaHPO_4.\ 2H_2O \quad (3)$$

$$2CaHPO_4.2H_2O \ \rightarrow \ 2CaHPO_4 \ + 4H_2O\uparrow \quad (4)$$

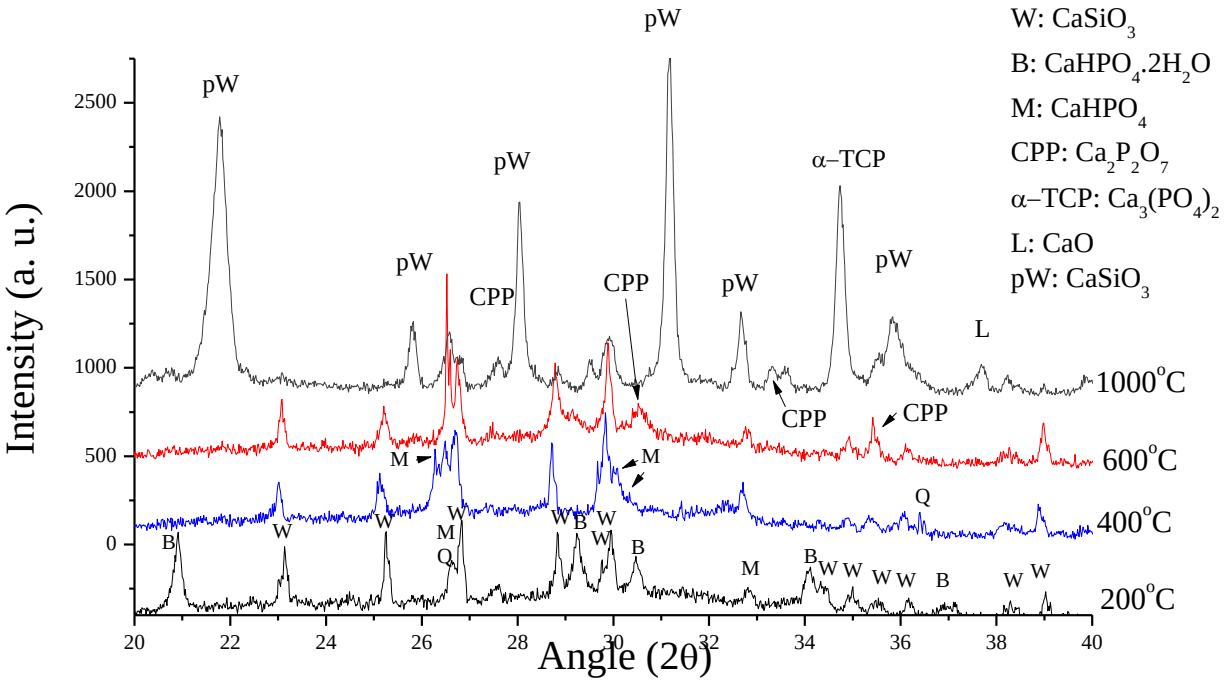

Figure 14 XRD data for the wollastonite based-PC under different temperatures.

Figure 15a shows that weight loss at 1000°C for the Wo-PC is 18%. The DTA data shows two exothermic peaks, A at 130 °C and B at 183 °C corresponding to the release of unbonded and bonded (to brushite) water respectively. It also shows the corresponding shrinkage associated with this water release, which is significant. Peaks C and D have been associated to the CPP and TCP transformations, respectively. Figure 15b shows the weight loss at 1000°C for wollastonite, which is 0.3%. Thus, wollastonite does not lose weight (no-shrinkable phase) when compared to the PC matrix and therefore the shrinkages is due to the phosphates. The transformation at 670°C is associated with small amounts of silica in the raw powder.

In addition to XRD, phases were identified experimentally with SEM-EDAX. Figure 16 shows X-ray maps for the cross section of PCs, all over the same region of the secondary electron image (SEI) of Figure 16a. The composition distribution of calcium, silicon, and phosphorous is shown in Figure 16b, c, and d, respectively. Carbon and oxygen distributions were also obtained but are not presented because they were almost constant over the entire image. Figure 16b shows evidence of some wollastonite ($CaSiO_3$) grains which transformed into silica (by giving up calcium) and some which did not transform. Figure 16c shows silica glass as well as wollastonite grains. Figure 16d shows the calcium phosphate matrix. Numbers 1, 2 and 3 correspond to silica, wollastonite, and calcium phosphates respectively.

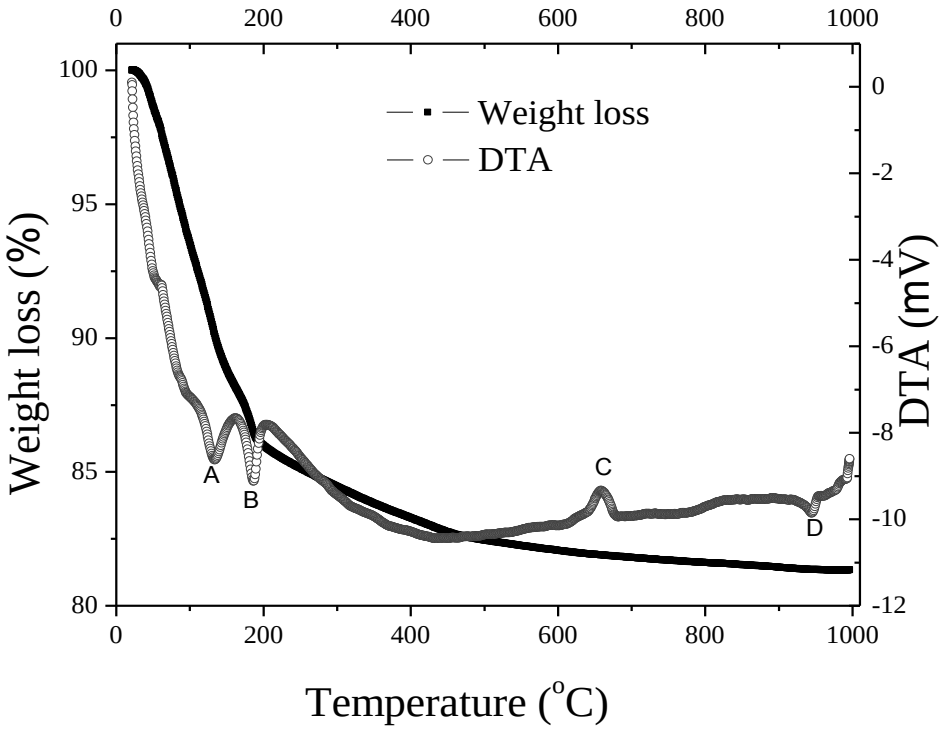

a)

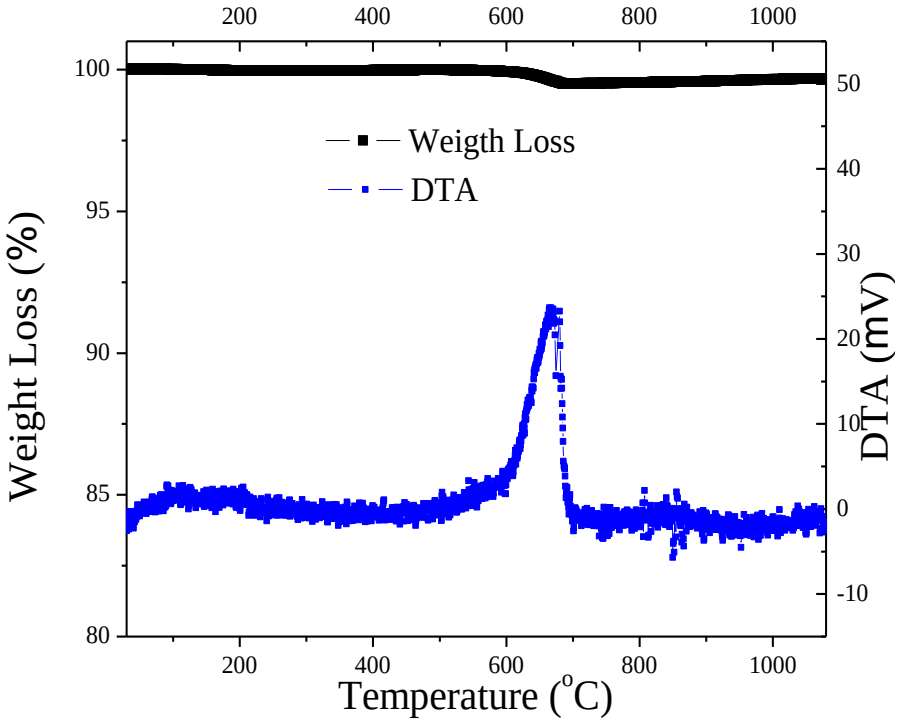

b)

Figure 15 TGA and DTA data for a) wollastonite-based PC, b) wollastonite powder

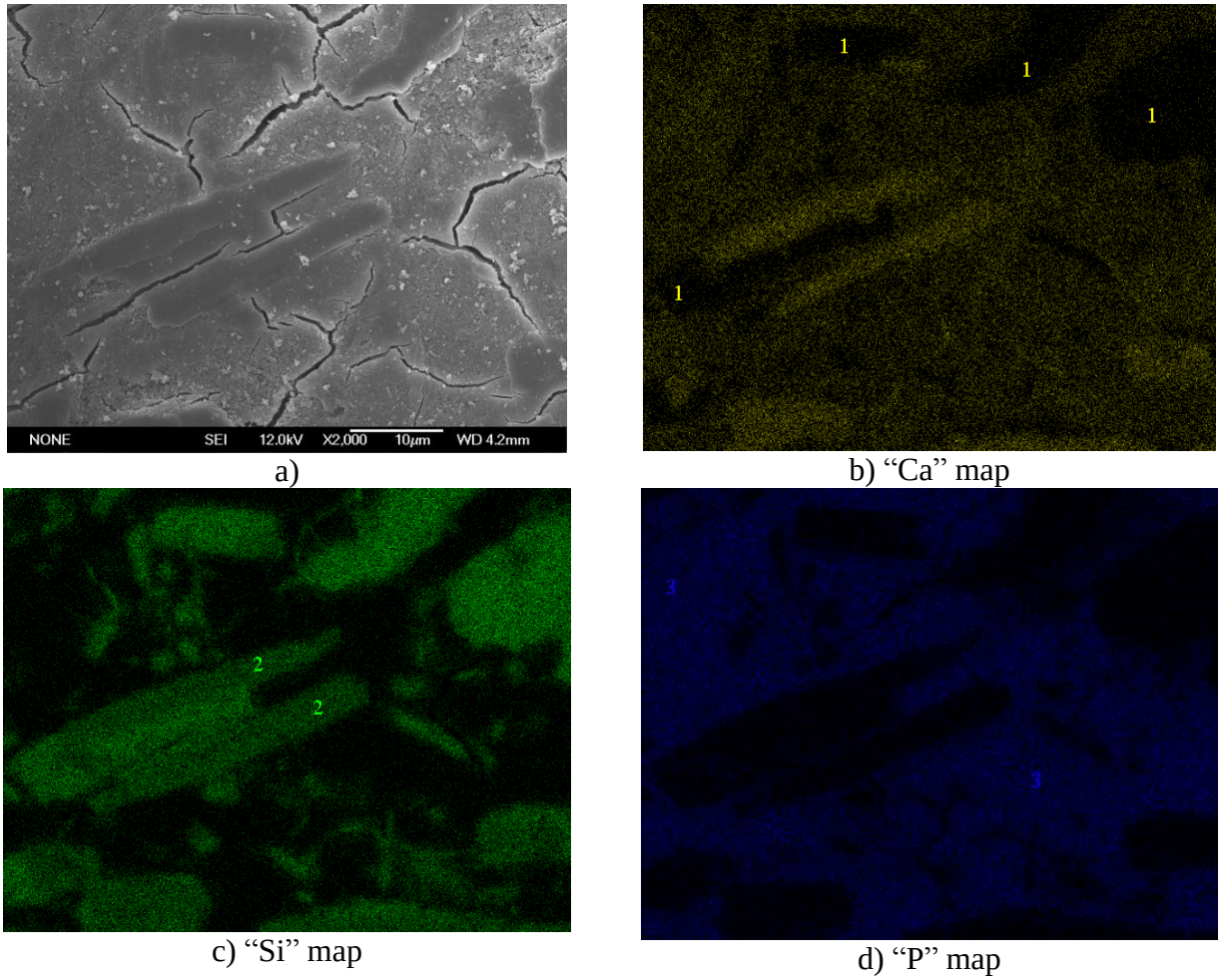

a) b) "Ca" map

c) "Si" map d) "P" map

Figure 16 X-ray maps for the Wo-PC, a) topographical image; and b) Ca, c) "Si" and d) "P" concentration images. Numbers 1, 2, and 3 correspond to silica, wollastonite, and calcium phosphates respectively.

4.8.1 PC formation mechanism

The formation mechanism reported before for PCs [6] and shown in Figure 2 is not the general case of the PC formation. This representation is valid only in the case where the oxide is dissolved completely in the acid followed by the gelation and polymerization process. As shown in Figure 16, in the Wo-PCs (in all following the PC methodology), and in all oxides tested in this thesis, residual oxide grains were always found in the final solid material. A generalized representation of PC formation is shown in Figure 17. In this representation, the residual grains

from the oxide raw material used, consolidated into a composite material at the end of the formation process. Figure 17a shows the first instant of the premixed oxide powder and acidic liquid. Then, metal ions are dissolved into the acidic formulation as shown in Figure 17b. Thereafter, metal aquasols formation starts, Figure 17c. Then, polymerization starts and continues up to a gel point (Figure 17d and e). Finally, the gel crystallizes in a solid phosphate material. Thus, the final material is a PC matrix with residual oxide particles working as reinforcement. Figure 17 is a very simplified representation of the PC formation. For instance, typically PC matrix contains grains, micro-pores and phosphate phases grown by nucleation (most likely precipitation at the residual grains-acid interface) independent of the polymerization obtained phases. In the next section, a more detailed representation for the system wollastonite-phosphoric acid is shown.

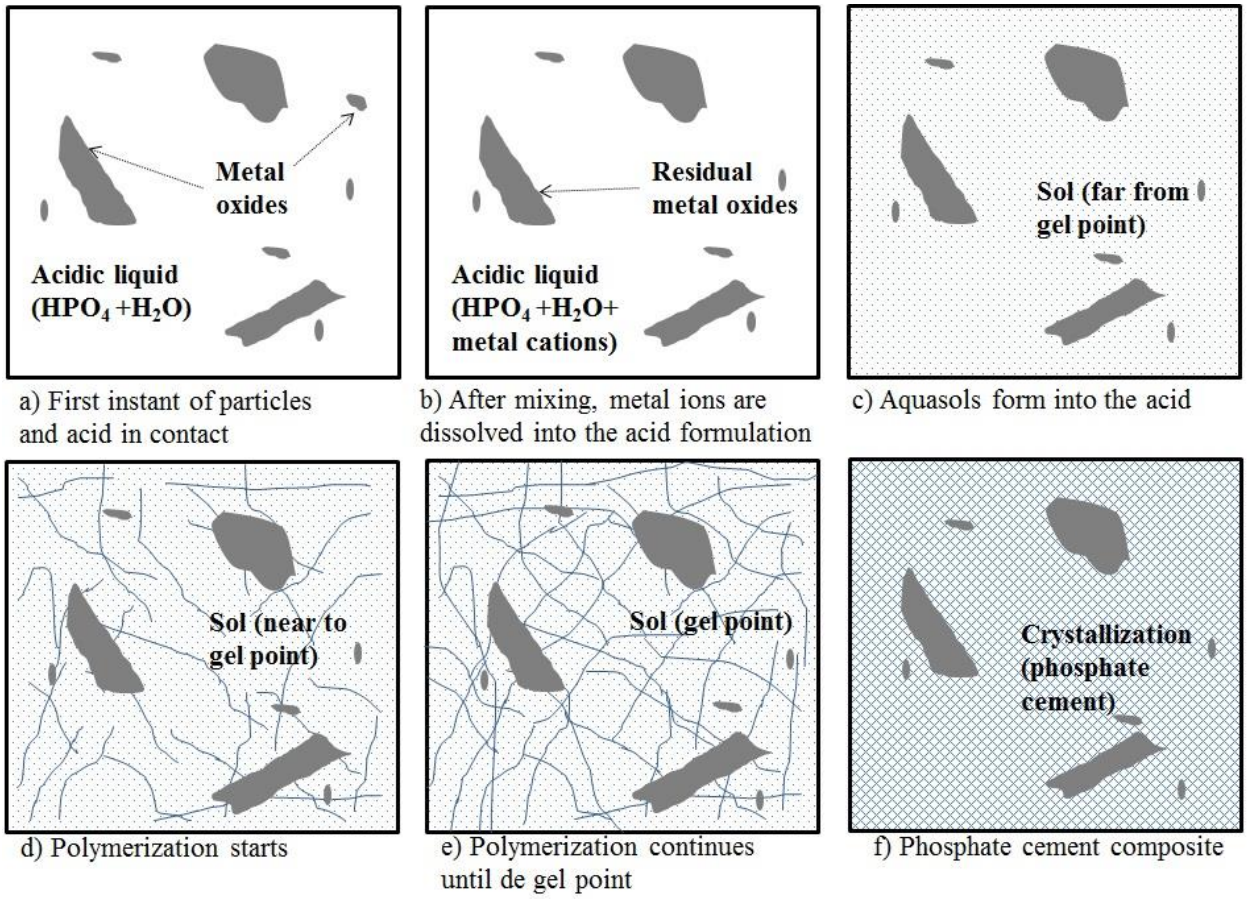

a) First instant of particles and acid in contact

b) After mixing, metal ions are dissolved into the acid formulation

c) Aquasols form into the acid

d) Polymerization starts

e) Polymerization continues until de gel point

f) Phosphate cement composite

Figure 17 Representation of the proposed Wo-PC formation.

4.8.2 Wo-PC formation mechanism

The first instant of the contact between the acidic formulation and wollastonite grains is shown in Figure 18a. Air bubbles, from air trapped in the powder, are release during the mixing process. If carbon is present as an impurity can be as calcium carbonate $CaCO_3$ (impurities are ≤0.4 as shown in Table 1), which can form CO_2 and calcium hydroxide ($CaCO_3 + H_2O \rightarrow Ca(OH)_2 + CO_2$). Immediately wollastonite is in contact with the acid, calcium ions start dissolving into the acidic formulation. The mixing when is conducted vigorously releases almost all bubbles into the air. For illustration proposes, residual bubbles content have been exaggerated in this representation.

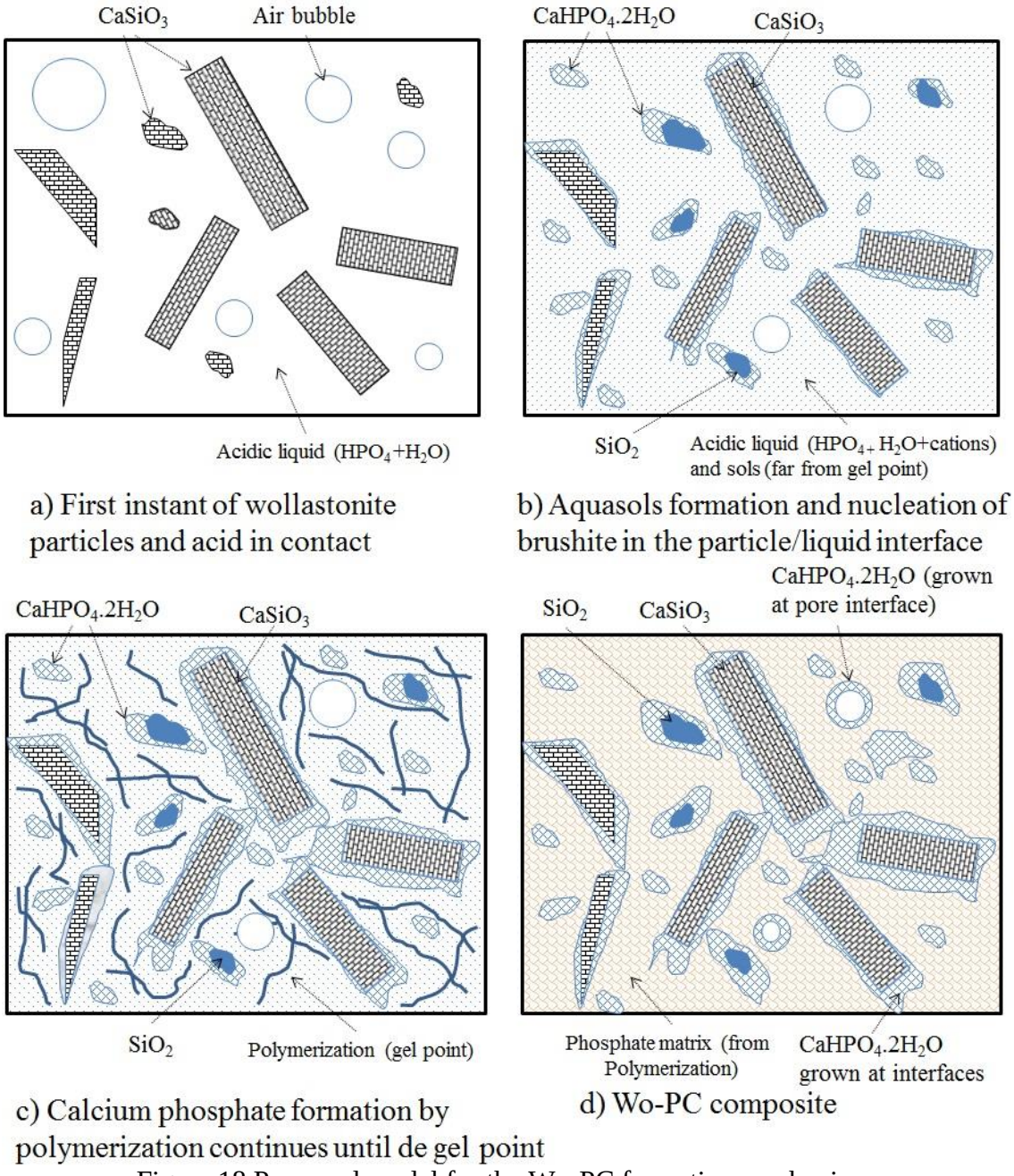

Figure 18 Proposed model for the Wo-PC formation mechanism.

At the beginning of the reaction, only brushite is formed, and silica is generated as a residual byproduct of the calcium ions released from the exterior of the wollastonite grains. Figure 18b shows an early stage of the solid formation. The dissolution of calcium ions into the acidic liquid

allows the growing of phosphate crystals mainly at the interfaces. At the same time, aquasols are formed in the liquid. As time is going on, polymerization starts and chains grow. The gel point representation is shown in Figure 18c. Thereafter, a continuous calcium-phosphate ceramic matrix is formed as shown in Figure 18d. This matrix is a mixture of brushite and calcium amorphous phosphates. Since these calcium phosphates are the dominant acid-base product, and serves as the main binding phases.

Then a shrinkage process starts, see Figure 19, which is depending of the exposure temperature and humidity. The shrinkage is mainly due to the release of unbound water (initially mixed with the acid). Shrinkage induces a micro-cracking phenomenon, which is due to the loss of water, phases change (brushite to monetite) and the difference in the coefficient of thermal expansion. This phenomenon will be discussed in more detail later. If temperature is increased over 100°C, monetite starts to appear more intensively in the XRD as a consequence of brushite losing the structural water as was described in Chapter 3; [7].

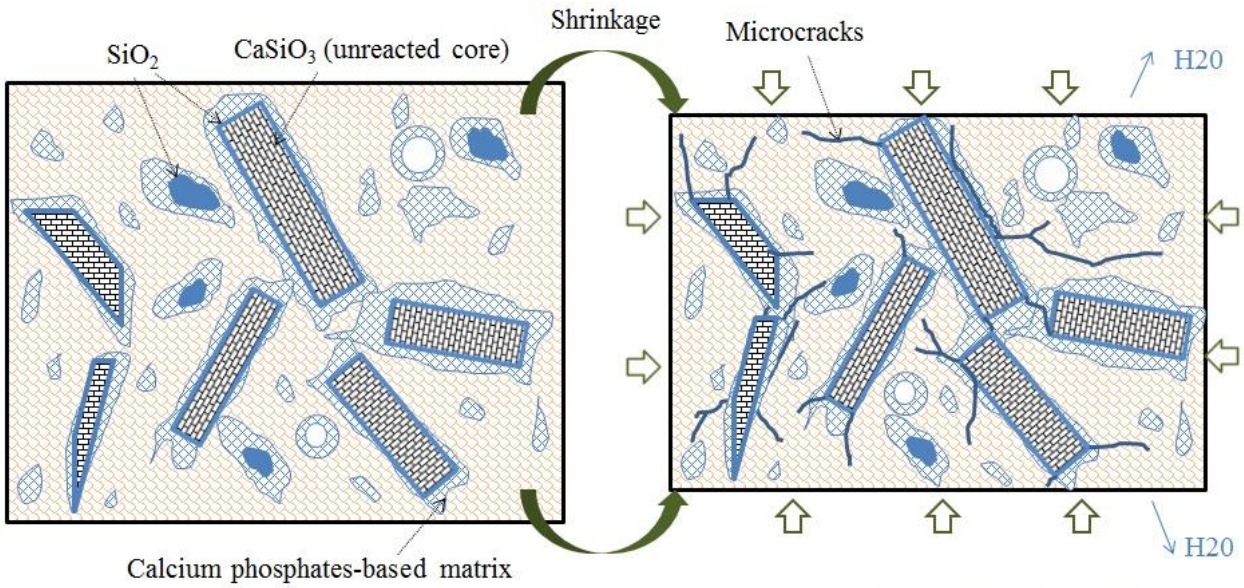

Figure 19 Proposed model for the Wo-PC formation mechanism.

4.8.2 Wo-PC exposed to different temperatures

As the exposure temperature increases, new crystalline phases start to appear in the XRD. After the exposure to 400°C for 1h, all brushite has transformed into monetite, see Figure 14. No new phases were found after the exposure to 600°C, however, silica softeninng is expected to appear there for which an important change in the mechanical behaviour can be expected. Samples exposed to 800°C for 1h showed calcium pyrophosphate ($Ca_2P_2O_7$ or CPP), which is known as a high temperature stable calcium phosphate phase, [8] and [9]. Equation 5 describes the reaction of calcium pyrophosphate as a dehydration of monetite in the gamma phase [9]. At 750°C, the gamma phase tranforms into the beta phase as shown in equation 6, however, it was not clearly observed in this PC, which could be due to the effect of other phases, which upon the activation energy driven by the temperature release ions that inhibited this transformation.

On the other hand the XRD for the sample exposed to 1000°C for 1h showed two new phases, tricalcium phosphate (α-$Ca_3(PO_4)_2$ or α-TCP) and pseudowollastonite. TCP is a a high temperature stable calcium phosphate phase; [10] and [11]. The formation of TCP has been reported [12] as the reaction of Lime (calcium oxide, CaO) and CPP as shown in equation 7. Lime is a material we found as part of the wollastonite but also can be a byproduct of the decomposition of calcium phosphates such as amorphous phases since the energy is too high to break the bonds at 1000ºC. Finally, pseudowollastonite is a high temperature form of $CaSiO_3$ [13], typically obtained at temperatures higher than 1125ºC at 1atm [14], and this temperature decreases if high pressure is applied [15]. As shown in the XRD of Figure 14, these phases appeared after the exposure to 1000°C, which is associated to the interdiffusion effect of ions coming from other phases as impurities into the residual wollastonite grains.

$$CaHPO_4 \rightarrow \gamma\text{-}Ca_2P_2O_7 + 2H_2O\uparrow \quad (5)$$

$$\gamma\text{-}Ca_2P_2O_7 \rightarrow \beta\text{-}Ca_2P_2O_7 \quad (6)$$

$$Ca_2P_2O_7 + CaO \rightarrow Ca_3(PO_4)_2 \quad (7)$$

Figure 20 shows EDS-SEM image for the Wo-PC. It can be seen that the Ca/P ratio in the matrix is less than 1 for most of the point, which mostly corresponds to the phosphate-based matrix. The microcraking is significant as represented in Figure 17d.

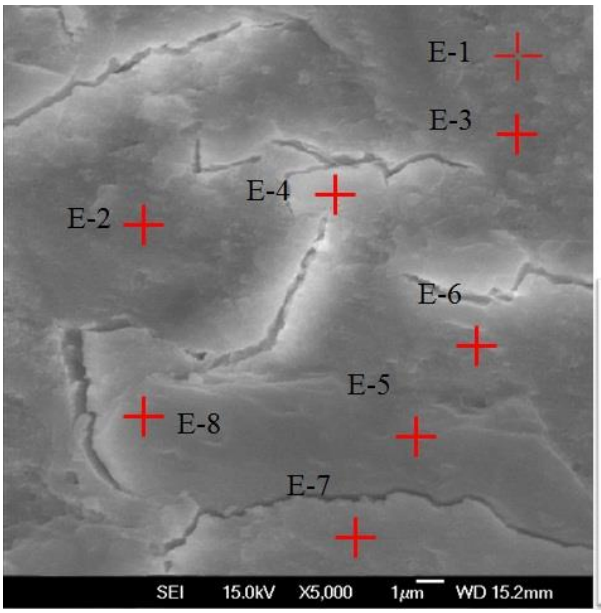

EDS Quantification of atomic percentages

Point	P	Ca	Si	Al	Ca/P	Ca/Si	Al/Ca
E1	11.85	4.24	0.00	18.95	0.36	NA	4.47
E2	11.12	4.87	4.39	6.29	0.44	1.11	1.29
E3	12.41	6.04	13.99	0.00	NA	0.43	0.00
E4	3.60	1.50	15.13	2.46	0.42	0.10	1.64
E5	1.75	0.74	20.81	0.74	0.42	0.04	1.00
E6	10.34	4.46	0.88	16.58	0.43	5.07	3.72
E7	10.94	8.49	8.88	1.00	0.78	0.96	0.12
E8	0.00	0.51	22.20	0.00	NA	0.02	0.00

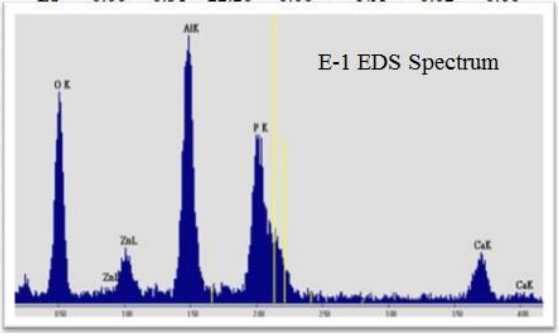

Figure 20 EDS-SEM for wollastonite-based PC.

Figure 20 shows other EDS-SEM image for other part of the PC including a residual wollastonite grain (points E-1 to E-4 and E-9) and brushite crystals (E-5 to E-8).

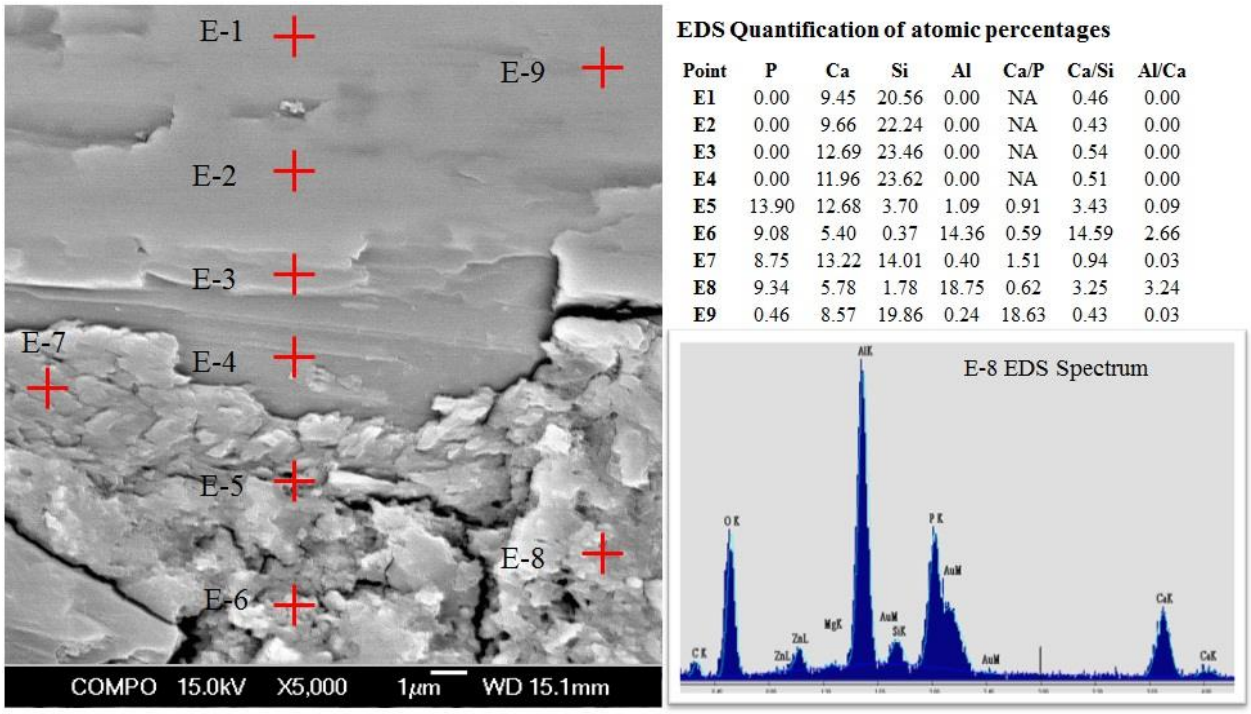

Figure 21 EDS-SEM for wollastonite-based PC.

4.4 Shrinkage and microcraking phenomena in the Wo-PC

Figure 22 shows SEM images of different phases and their relation to the micro-cracking phenomenon for a PC sample dried at 200°C with the procedure explained in Chapter 3. Figure 22a shows the shrinkage phenomenon leading to the micro-cracking in the Wo-PC is due to the shrinkage in the calcium phosphate-based matrix. The residual wollastonite grain does not show cracks. Interfacial cracks also appeared in the wollastonite/matrix interface as a result of the shrinkage. From TGA results shown in Figure 15a and b, the weight loss for this PC is about 5wt% 100°C, 13wt% at 200°C, and 18wt% at 1000°C. On the contrary, the weight loss for wollastonite powder is about 0wt% at 100°C, 0.1wt% at 200°C, and 0.3wt% at 1000°C. This data shows there are shrinkable and non-shrinkable phases in the PC, as confirmed by Figure 22a. Figure 22b shows the PC after etching (3sec etching in acetic acid 1% in water) in order to

show the calcium phosphates. The residual wollastonite grains remain as polished while the phosphate matrix is revealed by the corrosive reagent and brushite crystals are visible.

Figure 22c shows nucleation of brushite on a wollastonite grain. Figure 22b is a magnification of Figure 22c. These small nano-crystals and micro and nanoporous structures are typical in PCs and geopolymers. Figure 22e shows brushite crystals growing around a residual wollastonite grain. Figure 22f shows a representation of the Wo-PC obtained in the SEM images. The Wo-PC is a composite material with a phosphate-based matrix with silica and residual wollastonite grains. Microcracks are also shown. The silica and wollastonite grains act as reinforcement, blocking the crack propagation.

4.5 Variation in acid and its effects on the setting and mechanical behaviour

Three different formulations of acids were used to see the effect of minor additions of borax ($Na_2B_4O_7 \cdot 10H_2O$). Borax is a compound frequently used in the ceramic industry. The setting experiments were conducted mixing 20g of wollastonite with 24 g of acid as described for the curing experiment in Chapter 2. The main additives of the acidic formulation are the phosphoric acid (H_3PO_4) and water (both are close to 90wt%). Several additives including aluminum and zinc oxides, and borax, are also included in minor contents. Additives are mainly added to optimize the setting time by controlling the reactivity of the acid, with the aim of using the materials in large scale manufacturing. Adding water into the acid decreases the setting time of the PC. However, this addition also increases the reactivity because H_3PO_4 dissociates in aqueous solution, releasing the hydrogen ion H^+ and a conjugate base which reacts with the calcium cations. Also, H_3PO_4 is a polyprotonic acid which dissociates stepwise as shown in equation 8.

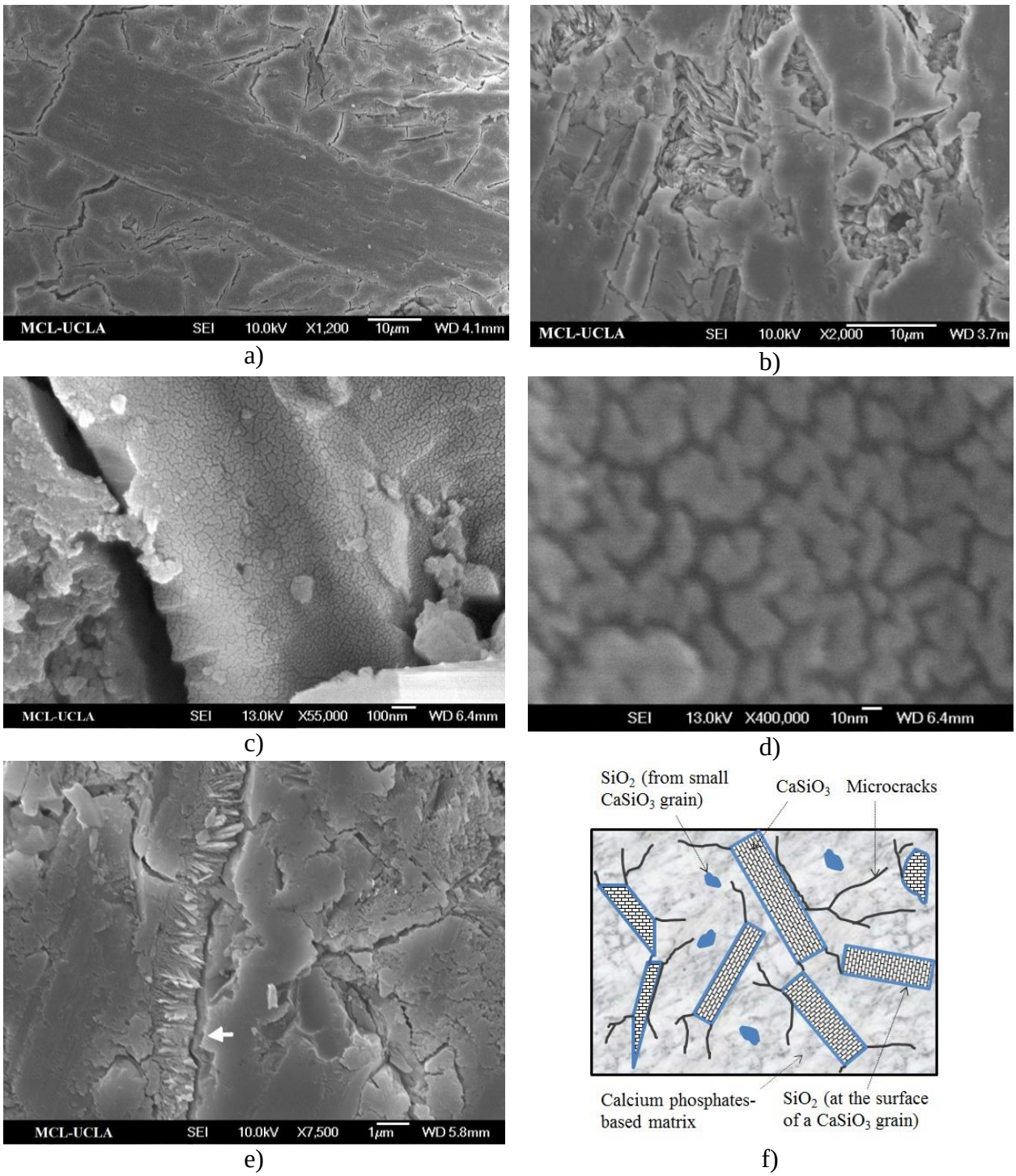

Figure 22 a) SEM images of Wo-PC; b) PC with residual wollastonite grains after 3sec etching time; c) PC after 10 sec etching time showing nucleation of brushite over a residual wollastonite grain; d) same image than c) at higher magnification showing small brushite nuclei; e) brushite crystals growing on a wollastonite grain; and f) schematic representation of the phases and cracks in the PC.

$$H_3PO_4 + H_2O \rightarrow H_2PO_4^- + H^+ \quad (8)$$

$$H_2PO_4^- \rightarrow HPO_4^{2-} + H^+ \quad (9)$$

$$HPO_4^{2-} \rightarrow PO_4^{3-} + H^+ \quad (10)$$

The acid used in all this research is named as the reference acid, 5.0wt% Borax, see Table 7. Formulations with 0.0 and 2.9 wt% borax were used only in this Chapter. Other simplified names used for these acids in the images are A0.0, A2.9 and A5.0.

Figure 23 shows curing curves for wollastonite-based PC made with the liquid formulation with different borax contents. In general, as borax content increases, the setting time increases and the heat release decreases. As water content increases, the setting time decreases and the heat released (temperature peak due to the exothermic reaction) increases as well. Therefore, there are two competing factors affecting the setting time: the water accelerates the setting meanwhile borax decelerates the setting. It has been found (Composites Support and Solutions Inc) that the acid containing 2.9wt% borax-10.7wt% water is the best combination. For mechanical properties, the water content is limited in order to control problems such as excess of voids, a weak reaction which leads to a weak material, and high shrinkage. For manufacturing of large parts, it has been determined that 100 minutes of setting time is required. Therefore, we have a way to control these properties. Considering the information presented above, it can be concluded those in terms of the reactivity (setting time + temperature peak), samples made with the acid with 2.9wt% of borax could produce a material with a higher compressive strength.

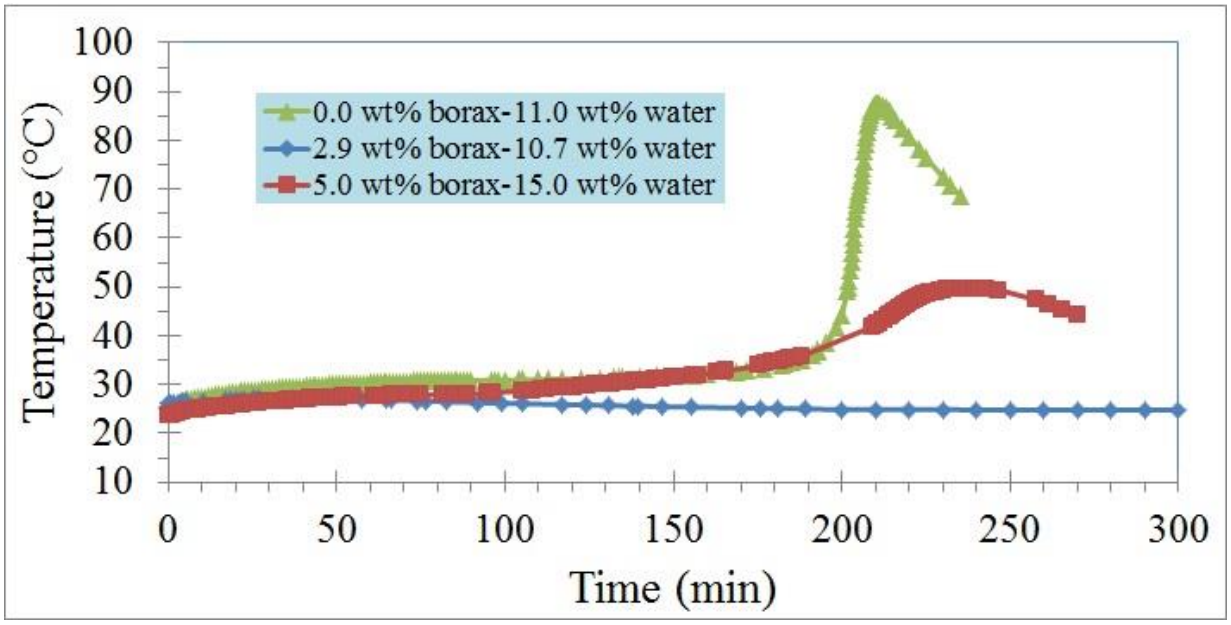

Figure 23 Curing curves for Wo-PCs made with three acidic formulations, acids with 0.0, 2.9 and 5.0wt% borax.

4.6 Compressive strength

Figure 24 summarizes the Weibull statistics for the wollastonite-based PCs made with three different liquids (see Table 7) after exposure to 200, 400, 600, 800, and 1000°C for 1h. All the fit equations are included in form of the temperature label, in which the slope corresponds to the Weibull modulus.

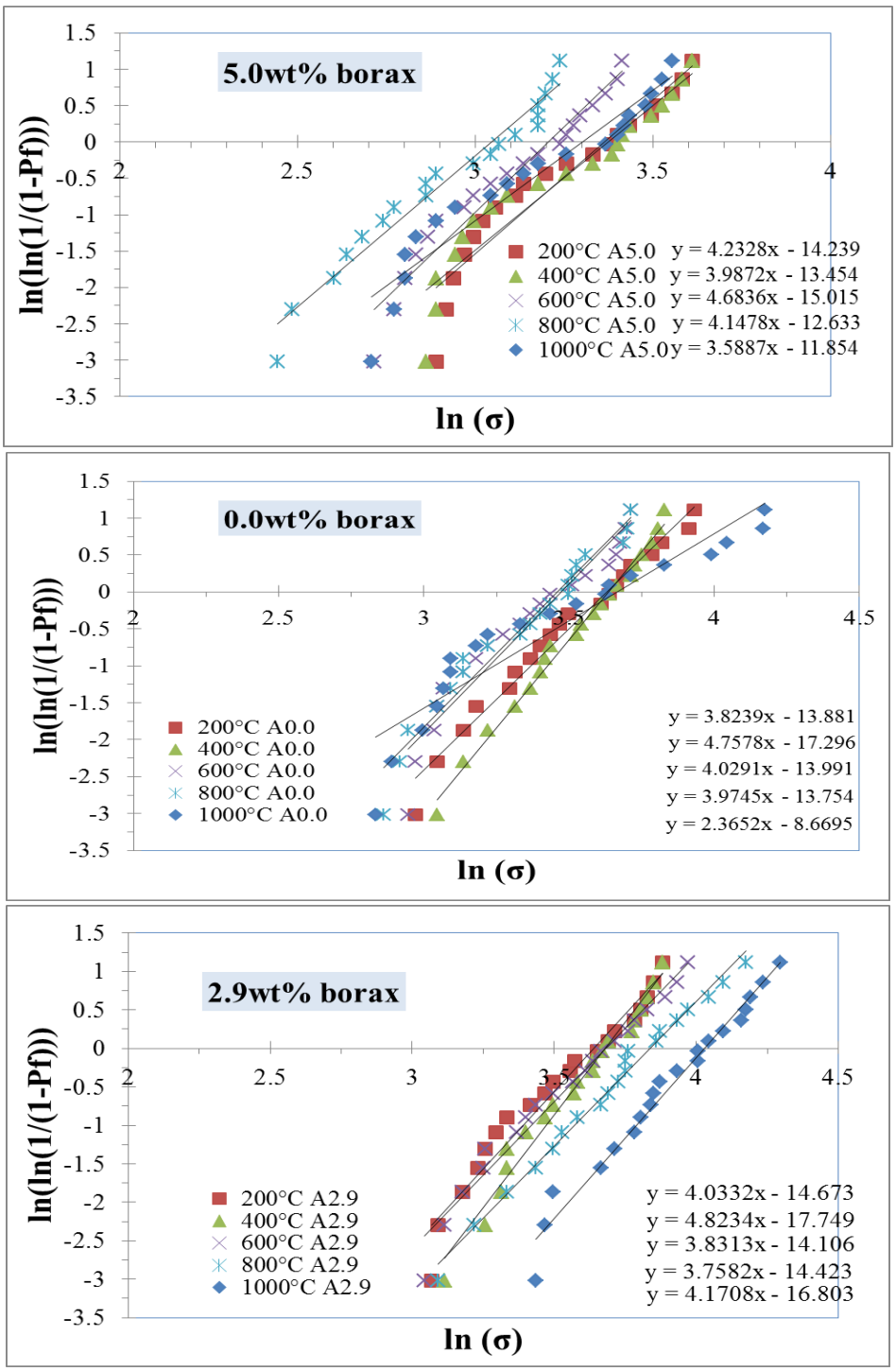

Figure 24 Weibull statistics for the compressive strength of samples made with different acid formulations.

Figure 25 shows the Weibull distributios for the 3 acidic formulations. Figure 25a shows that for samples made with the reference acid (2.9wt% borax-10.7wt% water), the best compressive

strength results are for samples exposed to 200 and 400°C; then followed by 1000°C, 600°C, and 800°C. The Weibull modulus is shown in Figure 25c, where the best result (the less variability, the highest the modulus) was found at 600°C and the worst one was at 1000°C. Figure 25b shows very similar results for samples made with the acid 0.0wt% borax, the best compressive values were obtained for samples after exposed to 200°C and 400°C; and for 1000°C in one portion of the curve. In this case the Weibull modulus was better at 400°C and the worst (of all results including all acids) was at 1000°C. Figure 25c shows that the better compressive strength values are for samples after exposure to 1000°C, followed by 800°C, 600°C, 400°C, and 200°C. In this case the Weibull modulus was not only high at 400°C (as for the acid 0.0wt% borax) but also it was competitive at 1000°C. Based on this data, the acid 2.9wt% borax produces more stable and reliable composites.

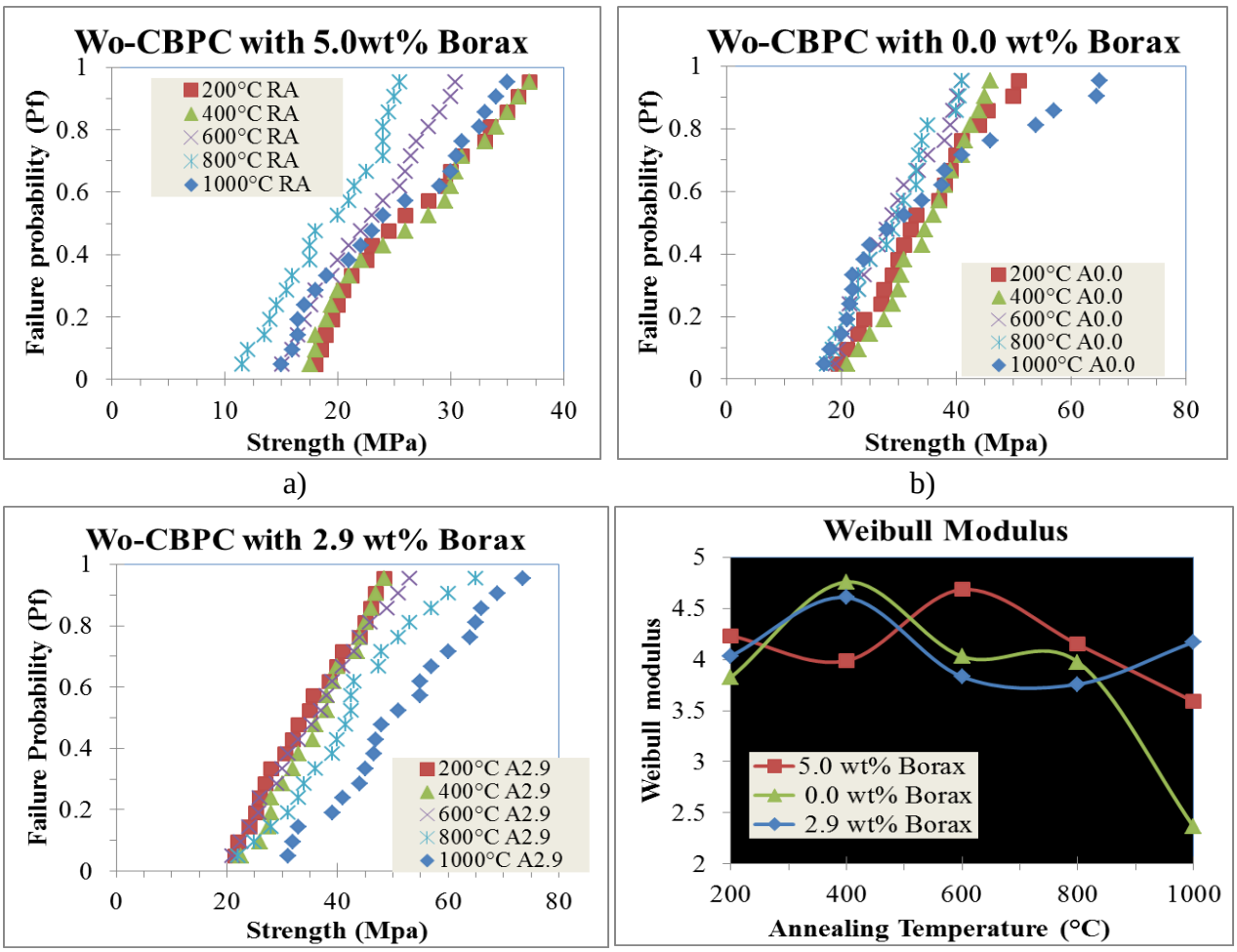

Figure 25 Weibull distribution and modulus for the compressive strength of samples made with different acid formulations.The reference acid (RA) has 5.0wt% of borax.

These significant results can be better observed by organizing the data by temperature as shown in Figure 26. In all cases, from the mechanical behavior point of view, the best acid formulation to make PC was the acid 2.9wt% borax and the worst one was the acid 5.0wt% borax.

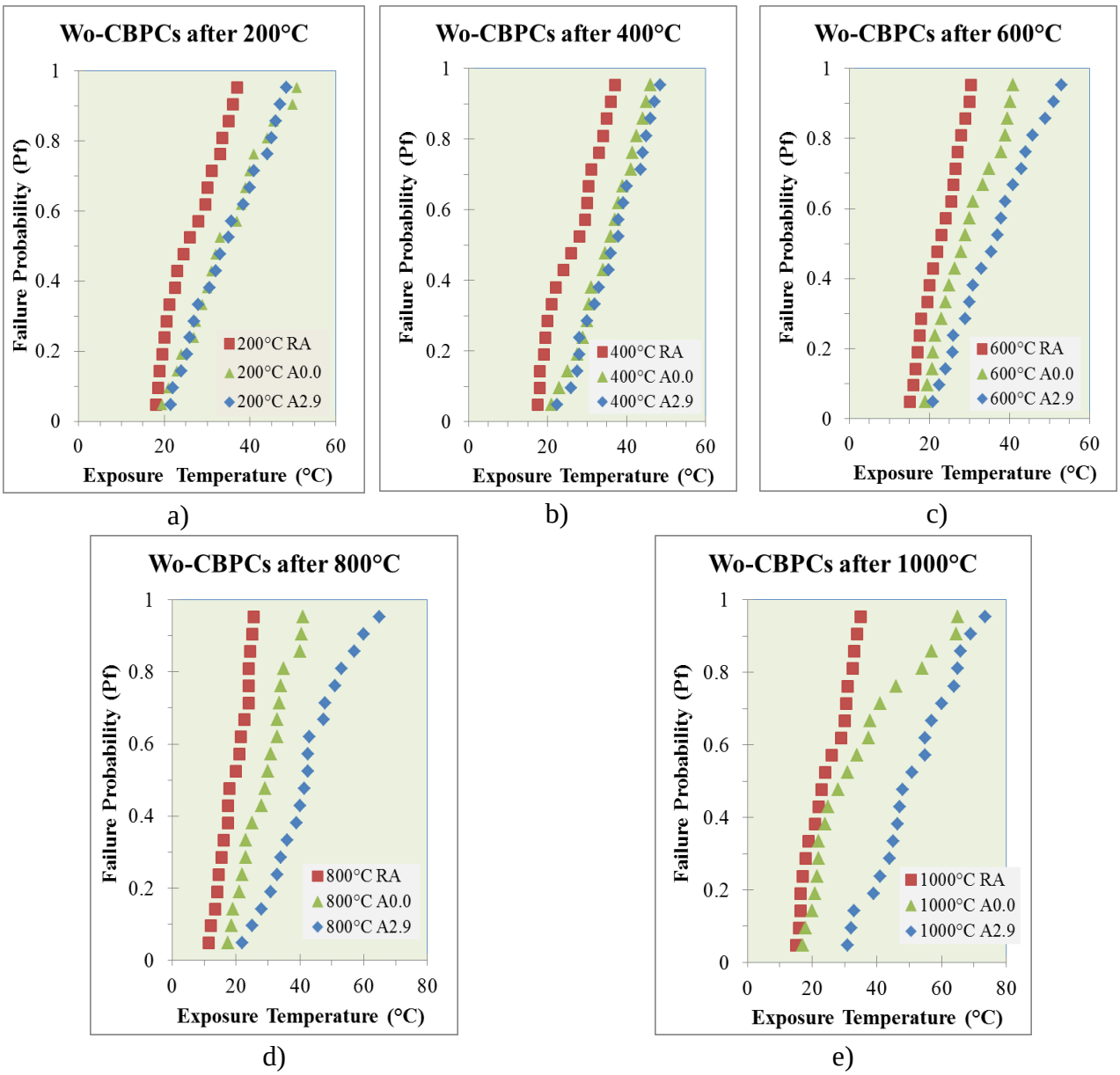

Figure 26 Weibull distribution for the compressive strength of samples fabricated with different acid formulations group by temperatures.

4.7 Other charaterization

Results from the linear longitudinal shrinkage test following the ASTM C326-09 standard are presented in Figure 27. Samples tested at 105 ˚C and 200˚C had macro cracks and some residual

bending deformation. Figure 27 also illustrates that the longitudinal shrinkage is lower than the diametrically shrinkage.

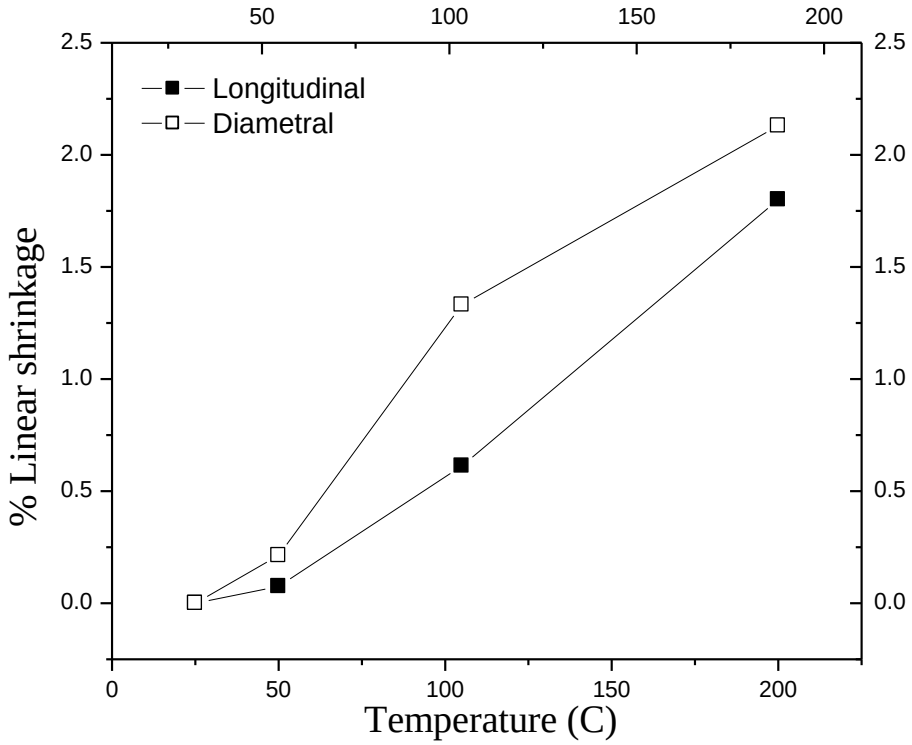

Figure 27 Drying and firing shrinkage test of PC made with M200 wollastonite powder two years old following the ASTM C326-09 for linear longitudinal test. In addition, diameter shrinkage was also obtained.

Figure 28a shows curing curves of PCs made with M200, M400 and M1250 wollastonite powders, all at room temperature. For the curing curve of the PC made with M200 wollastonite powder, the higher temperature values at the shorter times correspond to the heat generated for the mixing in the TM; the other powders do not show this effect because they react faster and get hotter than M200. The size effect on the curing is shown in Figure 28b, from peaks presented in Figure 28a. A first order exponential decay fit was performed.

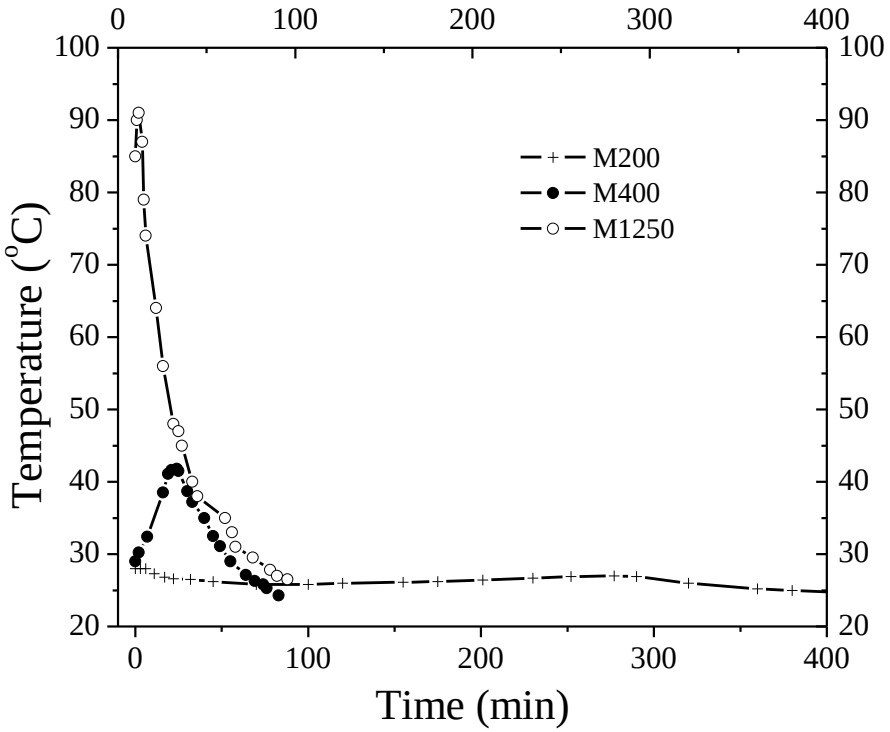

a)

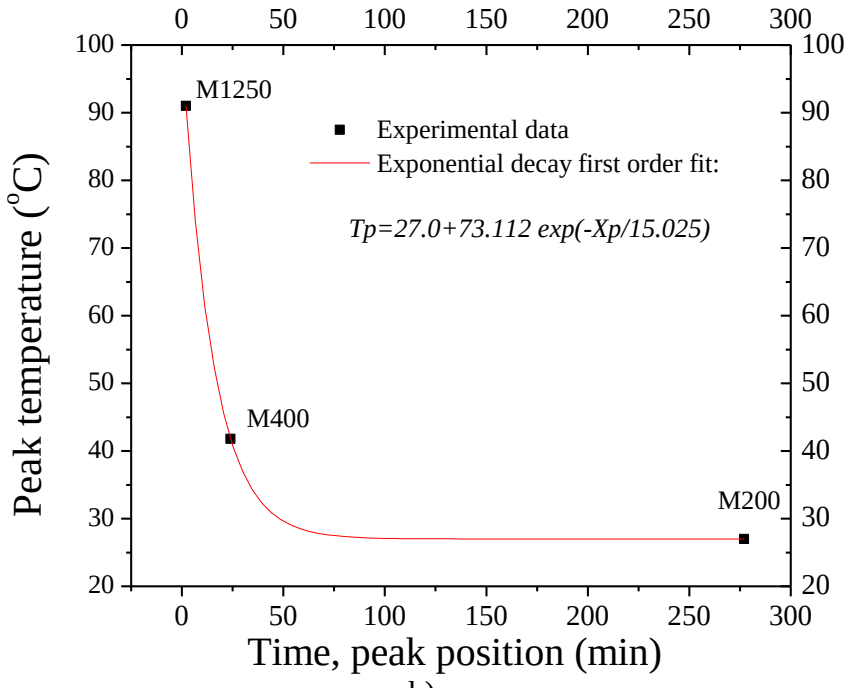

b)

Figure 28 a) Curing for different PCs materials at room temperature (one year old powders), b) Size effect of wollastonite powder on the PC setting taken from a).

Aging of wollastonite powder has also been examined. The reactivity of the powder (observed when is mixed with the aqueous phosphoric acid formulation) decreased with age even though samples were kept in a sealed plastic container. This is caused by moisture absorption (wollastonite is a hygroscopic material). Figure 29a shows the aging effects of M200 wollastonite powder in the curing of PCs. The difference between the two years and one week old samples is striking: the two years old sample has an increase in the peak position (time) around four times the corresponding peak for the one week old sample.

Figure 29b shows the aging effect on M200 wollastonite powder. The peak temperature decreases and the time associated with these peaks increases as the powder gets older. The reactivity decreases because the ambient humidity from air reduces the calcium action on the reaction.

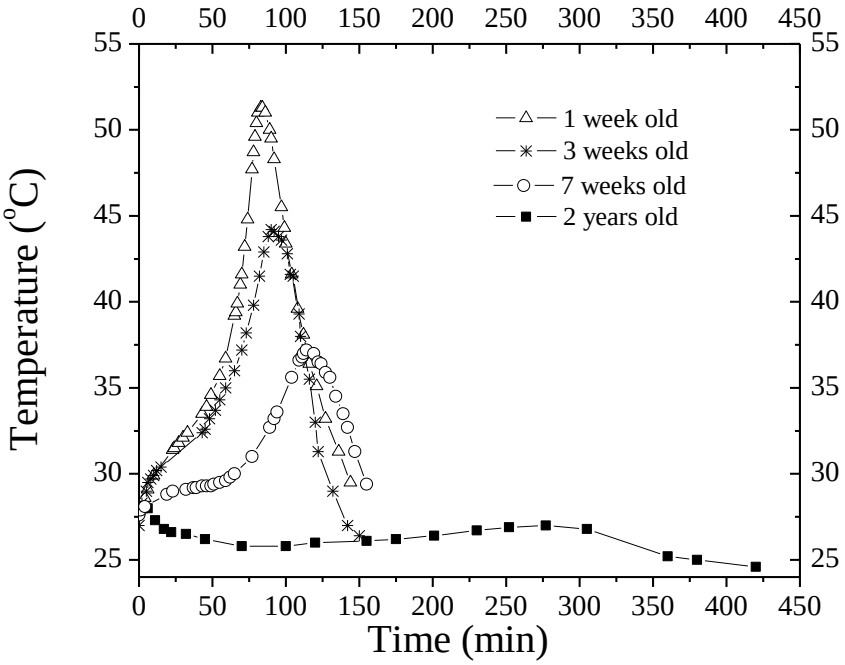

a)

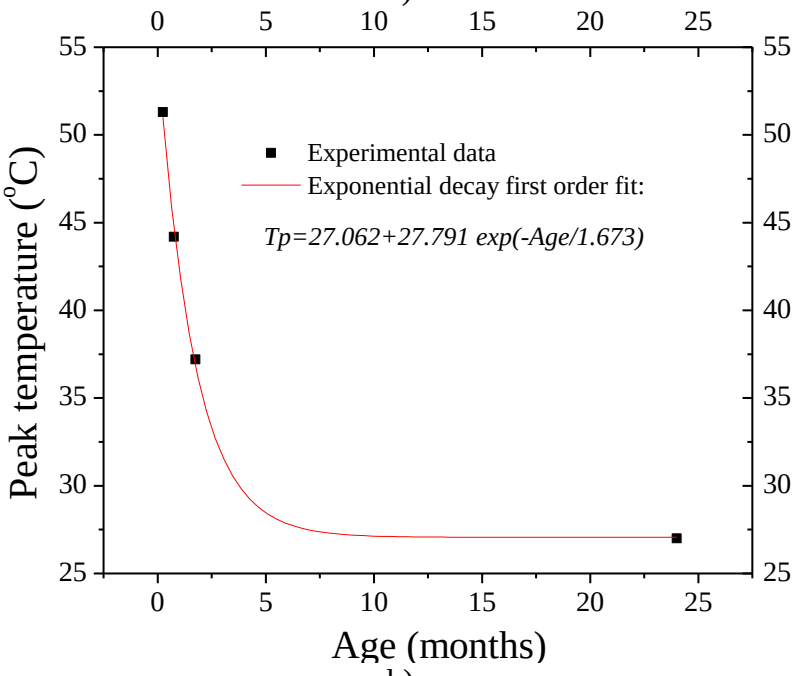

b)

Figure 29 a) curing curves for PC made with M200 aged at different times; b) exponential decay first order fit for peak positions points obtained from a).

Finally, curing tests for PC made with M1250 wollastonite powder after exposure to 300°C for 2h in air atmosphere are presented in

Figure **30**. This phenomenon can be associated with the known behavior of wollastonite in contact with water, in which there is [2] a rapid release of surface Ca^{2+} replacement by $2H^{+}$. Thus, under the air moisture, the wollastonite surface becomes more stable which decreases its reactivity.

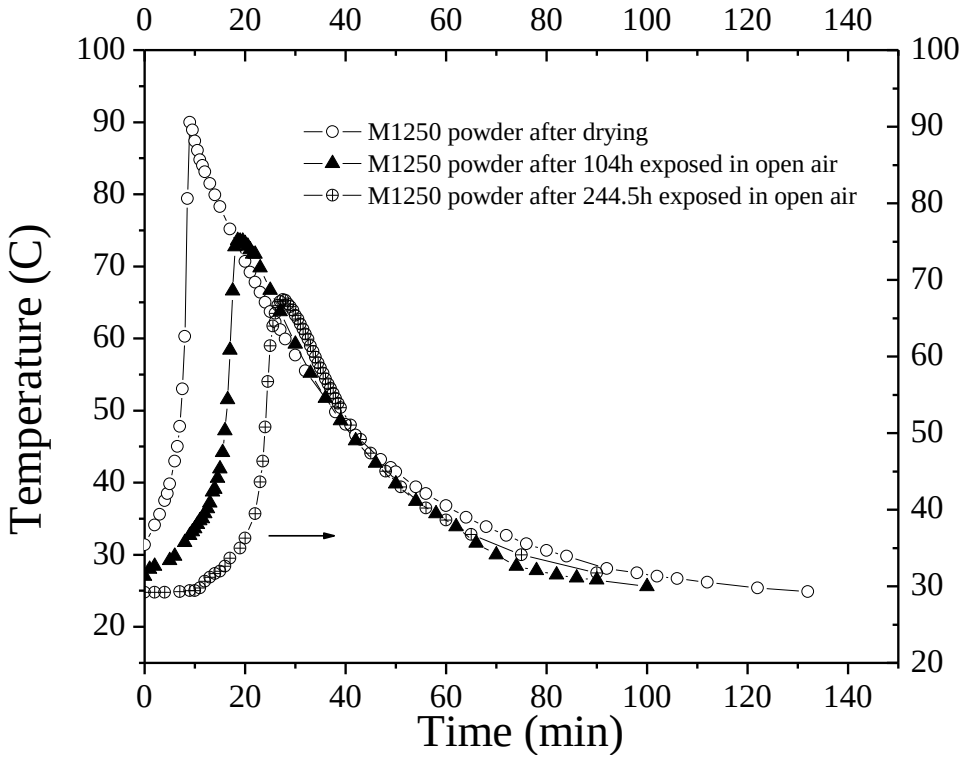

Figure 30 curing curves for PC made with M1250 after exposed to 300°C for 2 hours and then put it in an open container open to air.

The compressive strength for the PCs made with two years old M200, M400 and M1250 wollastonite powders as well as PC fabricated with one week old M200 wollastonite powder are presented in

Figure **31**.

The error bars are slightly higher for the small powders sizes, which can be caused by increased porosity due to the high reactivity. As expected, the highest values (not the mean) are observed for the small sizes. The manufacturing problem is minimized by cooling the raw materials at temperatures of around 3˚C as was done in this research; however, indications in

Figure **31** are that the M400 particle size distribution creates a maximum compressive strength. On the other hand, the compression strength for two year old PC made with M200 is 45% less than for the baseline material made with two week old M200. This effect can also be associated with the moisture effect on the wollastonite surface, which decreases its reactivity when it is mixed with the aqueous phosphoric acid formulation.

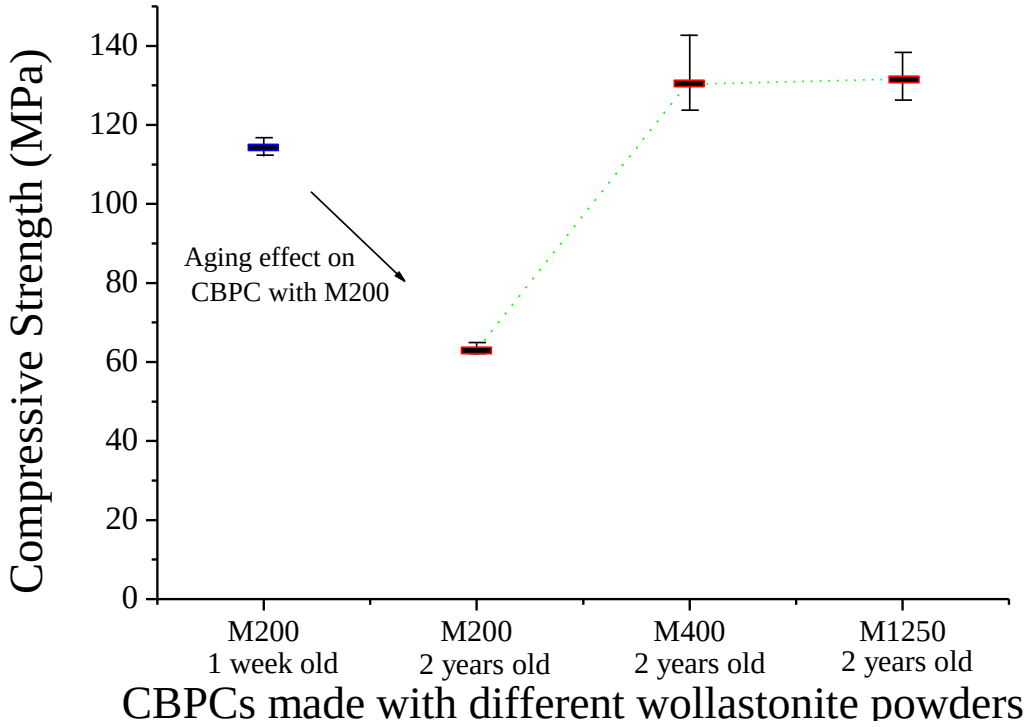

Figure 31 Compressive strength for PCs made with M200, M400 and M1250 wollastonite powders. The green dot line indicates powders with same age.

Density tests were performed over the two years old samples tested in compression for PCs made with M200, M400 and M1250 after the following drying process: 50˚C for 1 day, followed by 105˚C for 1 day, followed by 205˚C for 1 day. Results, presented in Table 10, show that as the mean of particle distribution decrease (from M200 to M1250), the density decreases. This result can have two causes:

- As the powder size decreases, more surface area allows for a more complete reaction (less unreacted wollastonite particles in the PCs). This means more calcium phosphate in the matrix, which is the more porous and micro-crack containing phase of the PC.
- Since reactivity is very fast for small powder sizes, it is more likely that internal voids could be introduced from poor impregnation in the mold since the paste was very viscous. This explains the higher variability in compression for PCs made with the small powders as compared to PC made with M200

  On the other hand, the density mean value of 2.19 g/cm^3 is particularly interesting when compared with Portland cement, for which it is 3.15 g/cm^3. Even lower density values have been reported for other PCs [4].

Table 10 Density values for different PCs after the drying process

Powder reference	M200	M400	M1250
Density (g/cm^3)	2.319	2.146	2.112
Volume (cm^3)	0.904	0.903	0.900

4.8 Discussion

All the chemical reactions involved in the formation of the wollastonite-based PC have been described and analyzed. Also, it has been presented the dissolution reactions of the acid and calcium ions in the acidic liquid, as well as the phases that appear as temperature is increased.

The SEM images revealed microcracking as shown in the proposed for the PC formation, see Figure 17. The explanation of the mechanisms regarding the micro-cracking induced by the thermal drying of water in the PCs fabrication has also presented in this thesis. It was established that the combination of shrinkable and non-shrinkable phases with low interfacial strength in the PCs produces shrinkage stresses. Since all materials involved are brittle (wollastonite, silica, brushite and calcium phosphates), microcracks develop in the matrix (calcium phosphates) and the residual grains/matrix interface.

The linear coefficient of thermal expansion (CTE) plays an important role in the microcraking phenomena. The CTE for wollastonite changes between 5.7 $x10^{-6}$ $°C^{-1}$ and 7.5 $x10^{-6}$ $°C^{-1}$ depending of the temperature range as shown in Table 11 ([20], [21], [22]).

Table 11 Coefficient of thermal expansion for wollastonite

Temperature range [°C]	25 to 200°C [20]	25 to 300°C [20]	25 to 400°C [20]	25 to 500°C [20]	25 to 600°C [20]	100 to 800°C [21]	100 to 1000°C [22]
Coefficient of thermal expansion [$°C^{-1}$]	5.7 $x10^{-6}$	6.3 $x10^{-6}$	6.7 $x10^{-6}$	7.0 $x10^{-6}$	7.5 $x10^{-6}$	6.5 $x10^{-6}$	6.1 $x10^{-6}$

The CTE for brushite is anisotropic. For the for the unit-cell edges “a”, “b” and “c” are $9.7x10^{-6}$, $3.82x10^{-5}$ and $5.54x10^{-5}$ $°C^{-1}$, respectively, and for the cell volume it is $9.7x10^{-5}$ $°C^{-1}$, [23]. These values are given for a temperature range between 4.2 and 470°C. Thus, the CTE for brushite is one order of magnitude bigger than the CTE for wollastonite. This clearly is a big issue when the Wo-PC is exposed to temperatures over 100°C. This difference in the CTE is contributing to the damage in the phosphate matrix, which is accelerated by the dehydration of brushite when transforms to monetite.

On the other hand, the effect of particle size distribution of wollastonite powders on PCs has been presented, and it was shown how the curing process is changed by exposing the wollastonite to air moisture, even though its water absorption contents did not show any significant change in both XRD and TGA tests.

From the curing tests it can be observed that manufacturing can become a significant issue when small powders are used, since they react very fast when compared with the M200 powder, there is only a very short time to fabricate actual parts. Wollastonite powders change the curing parameters with the exposure in air. Even though the curing peak position was shifted to a longer time, no new phases were detected in the XRD and no significant changes were detected at the TGA since weight loss was as low as the instrument limits of detection. We conclude that small changes in the wollastonite surface can produce high changes in the reactivity when wollastonite is mixed with the aqueous phosphoric acid formulation. Problems in detecting surface changes in wollastonite were also documented [18].

For the compression tests, it was observed that the error bars increased when the size decreased, while keeping the other manufacturing parameters constant (temperature, mixing time, etc.). The compression strength for PC made with two year old M200 shows a reduction of about 45% as compared to baseline PC fabricated with two week old powder.

Besides the variability and the problem of making samples at room temperature, the mean compressive strength results were about 100MPa when new powders is used. However, a higher strength (also lower variability) can be obtained by optimizing the cooling of the raw materials [7]. Moreover, Wo-PC is a good solution for firewalls, thermal and structural applications (see [24]-[27]).

Density tests show that the lowest values for the PCs occur with finer powders. This behavior was associated with more porous phases as well as with pores introduced during fabrication of the sample.

4.9 Conclusion

The formation mechanism of acid-base phosphate cements fabricated with wollastonite powder (Wo-PC) and phosphoric acid has been explained. The phase transformations leading the formation of the main binding phase (brushite) and the final microstructure of the cement containing residual wollastonie particles were presented. After the thermal exposure, significant changes in the mechanical behaviour and chemistry contributed to the deterioration of the Wo-PC. When Wo-PC is exposed to temperatures over 100°C, the difference in the CTE between brushite and wollastonite, and the brushite transforming to monetite, significantly deteriorate the microstructure of Wo-PC leading to a microcraking. Thus, the main thermally induced damage occurs for temperatures below 400°C. On the other hand, the aging of wollastonite has a significant impact in the mechanical behavior, reducing the compressive strength as low as 50% of the value obtained with new powder.

4.10 References

[1] T.K. Kundu, K. Hanumantha Rao, S.C. Parker. Atomistic simulation of the surface structure of Wollastonite and adsorption phenomena relevant to flotation. Int. J. Miner. Process. 72, 111 –127 (2003).

[2] Mosselmans G, Monique Biesemans, Willem R, Wastiels J, Leermakers M, Rahier H, Brughmans S, and Van Mele B 2007 Journal of Thermal Analysis and Calorimetry Vol. 88 3 723.

[3] Pourbaix, M. Atlas of electrochemical equilibria in aqueous solutions. Pergamon Press, New York, 1974.

[4] Wagh, Arun S. Chemically bonded phosphate ceramics: Twenty-first century materials with diverse applications. Elsevier Science, 2004.

[5] Colorado, H. A., Roopa Ganga, and Dileep Singh. "Chemically Bonded Phosphate Ceramics for Stabilization of High-Sodium Containing Waste Streams." Developments in Strategic Materials and Computational Design III (2013): 55-68.
[6] Wagh AS. Chemical bonded phosphate ceramics, USA, Elsevier, 2004.
[7] Dosen, Anja, and Rossman F. Giese. "Thermal decomposition of brushite, CaHPO4· 2H2O to monetite CaHPO4 and the formation of an amorphous phase." American Mineralogist 96.2-3 (2011): 368-373.
[8] El Kady, Abeer M., Khaled R. Mohamed, and Gehan T. El-Bassyouni. "Fabrication, characterization and bioactivity evaluation of calcium pyrophosphate/polymeric biocomposites." Ceramics International 35.7 (2009): 2933-2942.
[9] Wikholm, Nancy W., Ralph A. Beebe, and J. S. Kittelberger. "Kinetics of the conversion of monetite to calcium pyrophosphate." The Journal of Physical Chemistry 79.8 (1975): 853-856.
[10] Ryu, Hyun-Seung, et al. "An improvement in sintering property of< i> β</i>-tricalcium phosphate by addition of calcium pyrophosphate." Biomaterials 23.3 (2002): 909-914.
[11] Pattanayak, Deepak K., et al. "Synthesis and sintered properties evaluation of calcium phosphate ceramics." Materials Science and Engineering: C 27.4 (2007): 684-690.
[12] Safronova, T. V., et al. "Properties of calcium phosphate powder synthesized from calcium acetate and sodium hydrophosphate." Glass and Ceramics 68.3 (2011): 131-135.
[13] Yang, Hexiong, and Charles T. Prewitt. "On the crystal structure of pseudowollastonite (CaSiO 3)." American Mineralogist 84.5-6 (1999): 929-932.
[14] Aza, Piedad N., Francisco Guitián, and Salvador Aza. "Phase Diagram of Wollastonite-Tricalcium Phosphate." Journal of the American Ceramic Society78.6 (1995): 1653-1656.
[15] Essene, Eric. "High-pressure transformations in CaSiO 3." Contributions to Mineralogy and Petrology 45.3 (1974): 247-250.
[16] Colorado, H. A., C. Hiel, and H. T. Hahn. "Influence of Particle Size Distribution of Wollastonite on the Mechanical Properties of PCs (Chemically Bonded Phosphate Ceramics)." Processing and Properties of Advanced Ceramics and Composites III (2010): 85-98.
[17] Henry A. Colorado, Clem, Hiel, Jenn-M. Yang, H. Thomas Hahn. Wollastonite-based chemically bonded phosphate ceramic composites. Metal, ceramic and polymeric composites for various uses. 2011. ISBN 979-953-307-135-9.
[18] T.K. Kundu, K. Hanumantha Rao, S.C. Parker. Atomistic simulation of the surface structure of Wollastonite and adsorption phenomena relevant to flotation. Int. J. Miner. Process. 72, 111 –127 (2003).
[19] Colorado, H. A., C. Hiel, and H. T. Hahn. "Processing-structure-property relations of chemically bonded phosphate ceramic composites." Bulletin of Materials Science 34.4 (2011): 785-792.
[20] Weston, R. M., and P. S. Rogers. "Anisotropic thermal expansion characteristics of wollastonite." Mineral. Mag 40.314 (1976): 649-51.
[21] Whitmer M. T., 1969. Industrial Minerals, 19, 16-20.
[22] Rigby, G. R., G. H. B. Lovell, and A. T. Green. "The reversible thermal expansion and other properties of some calcium ferrous silicates." Trans. British Ceram. Soc 44 (1945): 37-52.

[23] Schofield, P. F., K. S. Knight, J. A. M. van Der Houwen, and E. Valsami-Jones. "The role of hydrogen bonding in the thermal expansion and dehydration of brushite, di-calcium phosphate dihydrate." Physics and chemistry of minerals31, no. 9 (2004): 606-624.

[24] Colorado, H. A., H. T. Hahn, and C. Hiel. "Pultruded glass fiber-and pultruded carbon fiber-reinforced chemically bonded phosphate ceramics." Journal of Composite Materials 45(23), (2011): 2391-2399.

[25] H. A. Colorado, C. Hiel and H. T. Hahn. Chemically Bonded Phosphate Ceramics composites reinforced with graphite nanoplatelets. Composites Part A. Composites: Part A 42 (2011): 376–384.

[26] Colorado, H. A., C. Hiel, H. T. Hahn, and J. M. Yang. "High Temperature Furnace Door Test for Wollastonite Based Chemically Bonded Phosphate Ceramics with Different Reinforcements." Processing and Properties of Advanced Ceramics and Composites IV, Volume 234 (2012): 269-274

[27] H. A. Colorado, C. Daniel, C. Hiel, H. T. Hahn, J. M. Yang. Mechanical Properties of Chemical Bonded Phosphate Ceramics with Fly Ash as Filler, in: S. Widjaja and D. Singh (Eds.), Advanced Processing and Manufacturing Technologies for Structural and Multifuctional Materials V, Wiley: Ceramic Engineering and Science Proceedings, Volume 32, Issue 8, 2011, New Jersey, (2011): 97-107.

5 Thermal stability of fibers up to 1000°C

5.1 Introduction

The increase in the requirements and applications for thermal and chemical stability of composites under high temperature and oxidation environments has stimulated the development of many ceramic and polymer matrix composites with fibers. However, under high temperature and oxidation exposure even ceramic fibers show significant decrease in their properties. It is known that the most common reinforcement used in composites is glass fiber. At temperatures of up to 650°C, the glass fiber degradation is the result of larger surface flaws present after heat treatment [1]. The tensile tests were mostly done using the fiber bundle test and only one temperature (450°C) was investigated with the single-fiber test. It is known that when glass fibers are exposed to fire directly or within a matrix, they eventually fail by thermally induced embrittlement and rupture [2].

The tensile strength of glass fibers decreases as temperature increases. This relationship has been attributed to several mechanisms [1] such as (1) the annealing of compressive residual stresses, (2) the re-orientation of a microstructure, (3) the formation of a surface layer with different properties to the fiber core, and (4) the development of surface flaws due to corrosion at high-temperature. Mechanisms (1) and (3) are not well accepted. Mechanisms (2) and (4) are the more commonly used. Thus, more research has to be conducted in order to explain this complex process; moreover, when glass fibers are surrounded by a ceramic matrix and exposed to oxidation, depending on the temperature, the inter-diffusion can be such a significant to destroy structurally the fiber. This phenomenon certainly makes the analysis more complex.

Carbon fibers are an important part of the materials used in composites for aerospace and aeronautics. They show variable [4] thermal, electric, and mechanical properties: elastic moduli

are between 30 and 900PCa and tensile strength can be as high as 6PCa. However, regarding its importance, very little data can be found in the literature about the carbon fiber behavior at high temperature. Carbon fiber oxidation behavior is known under diverse thermal conditions [3] and it has been found that the strength decreases with the temperature and the surface oxidation is very uniform. The mechanical strength of the fibers is directly proportional fiber size. Equations 1 and 2 show the chemical reactions that lead to the oxidation of the fiber. It is well known in composites that once the interfacial bond between the fiber surface and the matrix has been de-bonded by oxidation, a significant reduction in the mechanical properties of the composite is obtained. Therefore, it is very important to understand the mechanisms of that deterioration of single fibers in order to not only explain the composite behavior but also to find ways to decrease such oxidation.

$$C + O_2 = CO_2 \quad (1)$$

$$C + 0.5\ O_2 = CO \quad (2)$$

On the other hand, high temperature tensile tests [4] show that elastic modulus is quite constant at temperatures $\leq$ 1000°C and it decreases steeply at temperatures > 1000°C; which has been associated with an increase in anharmonic vibrations that could lead to plastic deformations and reduce the linear elastic behavior. It has been found [5] that in general, carbon fibers at high temperature show three different stress-strain behaviors depending upon the temperature and the fiber structure/texture:

- Pure elastic behavior at low temperatures
- Viscoelastic behavior at intermediate temperatures
- Viscoplastic behavior at high temperatures.

The coefficient of thermal expansion (CTE) of carbon fibers in the range of room temperature up to 2227°C has been reported [8]. The CTE longitudinal varies from $5x10^{-6}$ °C^{-1} to $10x10^{-6}$ °C^{-1} and the CTE longitudinal to the axis varies from $1.6x10^{-6}$ °C^{-1} to $2.1x10^{-6}$ °C^{-1}. These variations depend on the fiber's structural properties.

Basalt fibers are manufactured from basalt rocks, the most widespread volcanic stone in the earth's crust. Basalt fibers main problems [7] are due to the crystallization of some of the components of some structural parts (plagioclase, magnetite, pyroxene) and due to the non-homogeneity of melt, which limits it applications to temperatures below 800°C [7]. However, due to the relatively new use of these fibers in non-military applications (after 1995), there is a lack of data, and as a consequence; full understanding of the mechanisms involved in the deterioration due to the oxidation of the fibers at high temperatures needs much research. Due to the abundance of the raw materials, basalt rock has been used in wide variety of composites.

It has been found that basalt fibers in combination with a thermally stable matrix can work well in temperatures up to 550-600°C depending on the fiber type [10]. Also, this same research found that a significant loss of tensile modulus above 400°C occurs and the onset temperature of deterioration of mechanical properties has been proposed to be related to the detected crystallization.

Silicon carbide oxidation at different temperatures has been well documented [10]. Many byproducts can be obtained depending on the chemical reaction. Some of the possible reactions are summarized in equations 3-10. It was observed that oxidation of SiC between 900–1600°C resulted in a surface layer of SiO_2 that formed a protective film [11].

$$SiC + 4O \rightarrow SiO_2 + CO_2 \quad (3)$$

$$SiC + 2O \rightarrow SiO + CO \quad (4)$$

$$SiC + 3O \rightarrow SiO_2 + CO \quad (5)$$

$$SiC + 2O \rightarrow SiO_2 + C \quad (6)$$

$$SiC + 3O \rightarrow SiO + CO_2 \quad (7)$$

$$SiC + O \rightarrow SiO + C \quad (8)$$

$$SiC + 2O \rightarrow Si + CO_2 \quad (9)$$

$$SiC+O\rightarrow Si + CO \quad (10)$$

It has been previously reported that thermal treatments can reduce the Weibull moduls from around 4 to 2.5 [9], which was associated to a crystallization of the structure and the surface damage produced by the reaction between SiO_2 and C. Weibull analysis upon SiC fibers shows [13] that as the gage length increases, the tensile strength decreases significantly.

In this chapter, some of the most popular fibers for industry (E-glass, carbon, basalt and silicon carbide) have been studied under oxidation environments at different temperatures (200°C, 400°C, 600°C, 800°C, and 1000°C) and their properties have been compared before and after the thermal processes. Particularly, the most regular and affordable fiber of each type is analyzed. The thesis shows comparative results and it focuses on the mechanical behaviour. This is because since many studies have been conducted with the bundle fiber method for these fibers (which is easier to conduct because of the sample preparation) there is little data regarding Weibull parameters for single fibers. Results of single fiber are very different when they are compared to the bundle fiber results. Further motivation for this research is to develop in the future inexpensive methods to protect these fibers in extreme oxidation environments such as extreme pH environments, oxidation due to high temperature exposure and thermal shock.

5.2 Experimental Procedure

Glass fibers Flexstrand 225 from Fiber Glass Industries Inc. [2], Carbon fibers HTS40 from Toho Tenax [3], Basalt fibers BCF13-1200KV12 from Kammemy Vek [4], and SiC fibers Hi-Nicalon form COI Ceramics Inc. [5], were used in this research. Table 5 summarizes the main data provided by the manufacturers. In case data was not supplied by them, a reference is included. ASTM D2101 was followed in this research. Glass and basalt fibers have similar compositions. Table 6 summarizes typical compositions for the fibers used. SiC fibers have a composition [5] of "Si" 62wt.%, "C" 37.0 wt.% and "O" 0.5wt.%. Carbon fibers have a composition of "C" > 98.0wt.%, [3].

All samples were annealed for 1h at 200°C, 400°C, 600°C, 800°C, and 1000°C. In order to observe the cross section of the fibers using SEM (JEOL JSM 6700R), fibers were put into resin and then polished (after sputtered in a Hummer 6.2 system at conditions of 15mA AC for 30 sec to obtain a thin film of Au) until mirror finish using SiC papers and alumina of 1μm. At least 20 fibers at each thermal condition were measured in diameter in order to build up size distributions. Not all fibers types were characterized at all thermal treatments due to diverse problems such as fiber stability and handling. Over some temperatures ranges, some fibers either disappeared completely or deteriorated in such a way that it was not possible to prepare a sample for tensile tests.

Fibers were ground for X-Ray Diffraction (XRD) experiments, which were conducted in an X'Pert PRO (Cu Kα radiation, λ=1.5406 Å) equipment, at 45KV and scanning between 10º and 70º. A single fiber was mounted on a cardboard frame by applying instant glue to both ends. The gage length was 50mm. For each type of fiber and thermal treatment, twenty samples were tested by tensile tests in order to plot Weibull distributions. These tests were performed on an Instron

5940 at a crosshead speed of 5.0 mm/min. Fiber diameter was measured on each sample after testing in a scanning electron microscope. Thermo gravimetric Analysis (TGA) was performed in Perkin Elmer Instruments Pyris Diamond TG/DTA equipment. The temperature ramp was 10ºC/min from room temperature up to 1000ºC, with previous equilibration at 50ºC for 10min. All experiments were conducted in air atmosphere in an alumina pan with air at 100mL/min.

5.3 Results

Figure 32 shows SEM images of the fibers' surface at different temperatures. Figure 32shows glass fibers as received and after exposure to 600°C. After the 600°C oxidation treatment the fibers weaken such that even regular handling to prepare them for SEM has produced the cut shown in the image. Figure 32b shows carbon fibers as received and after 600°C oxidation. It can be observed how the fiber diameter reduction and both surface and core damage are significant. Figure 32c shows basalt fibers as received, after 600°C and after 1000°C oxidation. The progressive formation of an oxide layer as the temperature of the oxidation is increased can be observed. Figure 32d shows SiC fibers as received, after 600°C and after 1000°C oxidation. It can be observed that after 600°C the fibers appear to have no damage and in fact it seems even better that the as received fiber, which can be due to a possible cleaning of the fiber surface. At 1000°C fibers in general show small deterioration; however, some of them, like the one shown in the image, show some internal and surface damages.

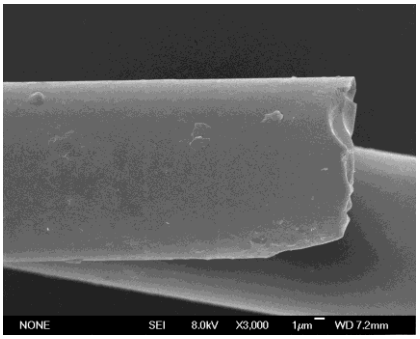

a) Glass fibers as received

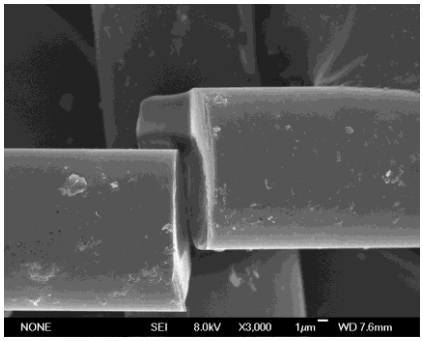

Glass fibers exposed to 600°C

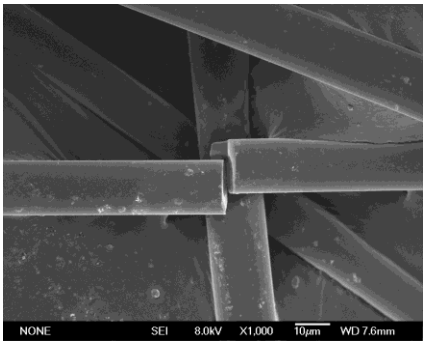

Glass fibers exposed to 600°C

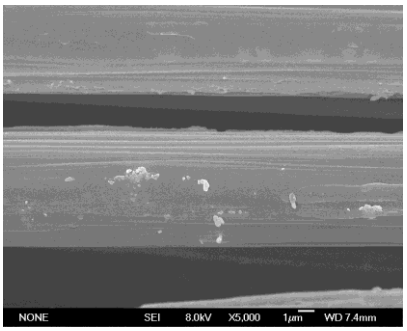

b) Carbon fibers as received

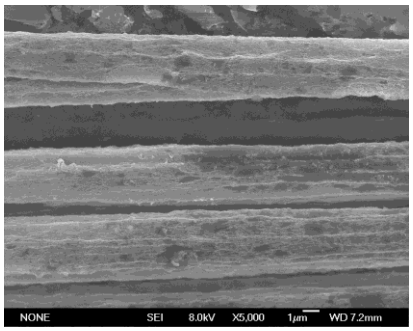

Carbon fibers exposed to 600°C

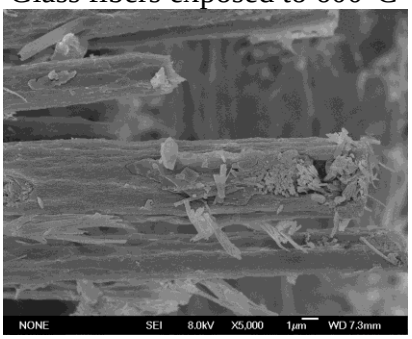

Carbon fibers exposed to 600°C

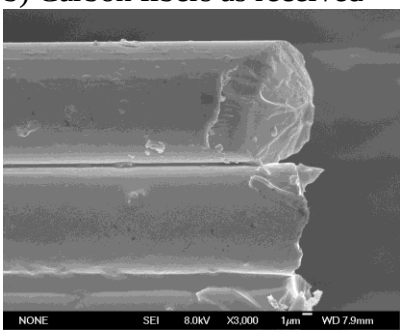

c) Basalt fibers as received

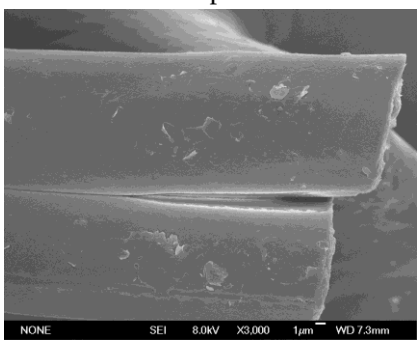

Basalt fib. exposed to 600°C

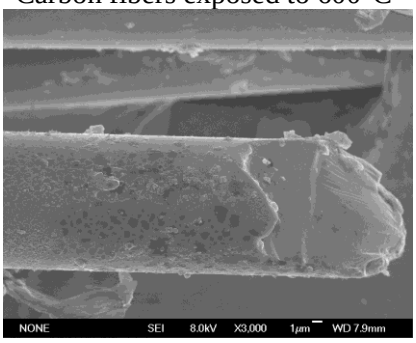

Basalt fib. exposed to 1000°C

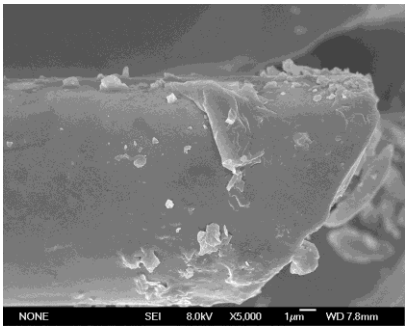

d) SiC fibers as received

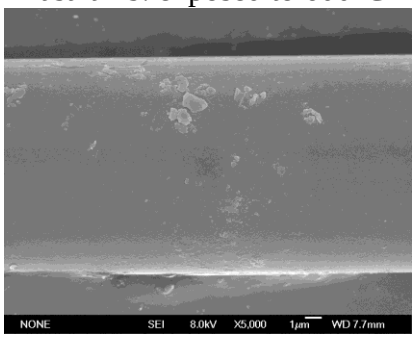

SiC fibers exposed to 600°C

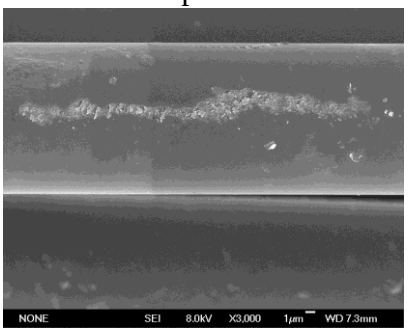

SiC fibers exposed to 1000°C

Figure 32 SEM images for the fibers at different temperatures.

Figure 33 shows the cross section view for the fibers exposed to 400°C oxidation. For glass, carbon, basalt and SiC fibers the shown magnification was always used for the same fiber at all temperatures in order to measure the diameter in the SEM.

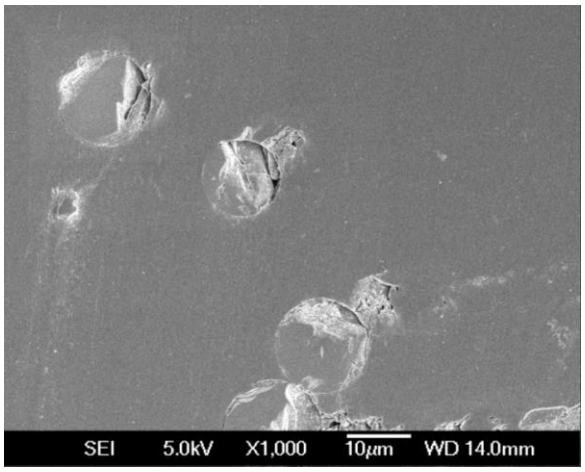

Glass fiber exposed to 400°C

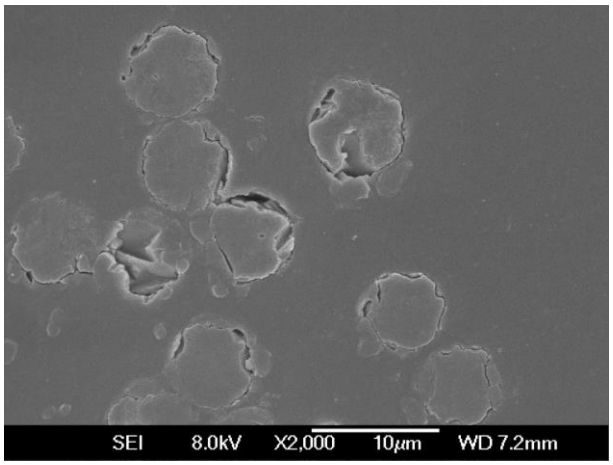

b) Carbon fiber exposed to 400°C

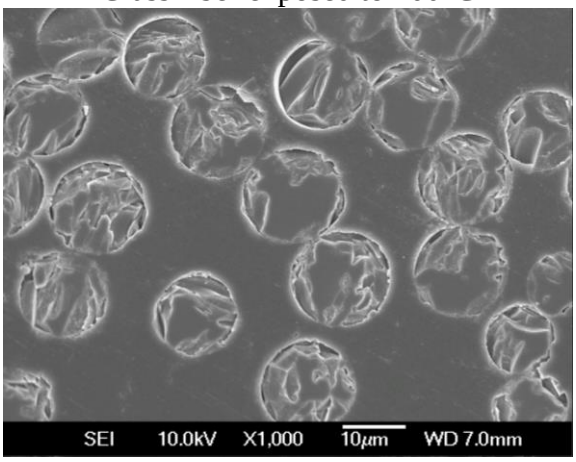

c) Basalt fiber exposed to 400°C

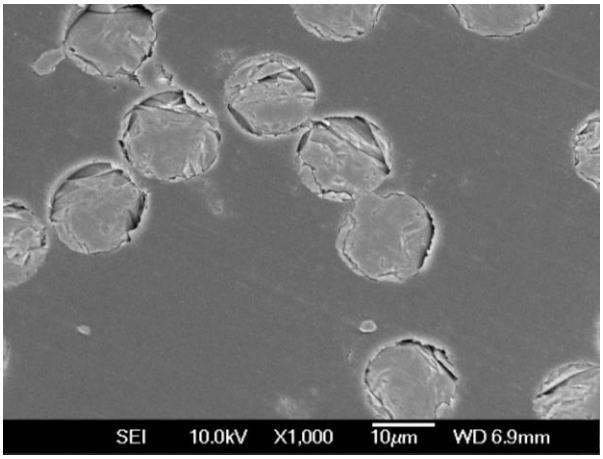

d) SiC exposed to 400°C

Figure 33 SEM cross section images for the fibers exposed to 400°C.

Figure 34 shows different diameter distributions for the fibers. In general it can be observed that as the temperature of the thermal oxidation treatment increase, the variability of the size decreases as well, which is due to a very different phenomena as we will see below with the other characterization. For glass and basalt fibers at 800 and 1000ºC this variability has

decreased. Carbon fibers also decreased this variability after the exposure to 400°C. SiC fibers also decreased this variability in diameter.

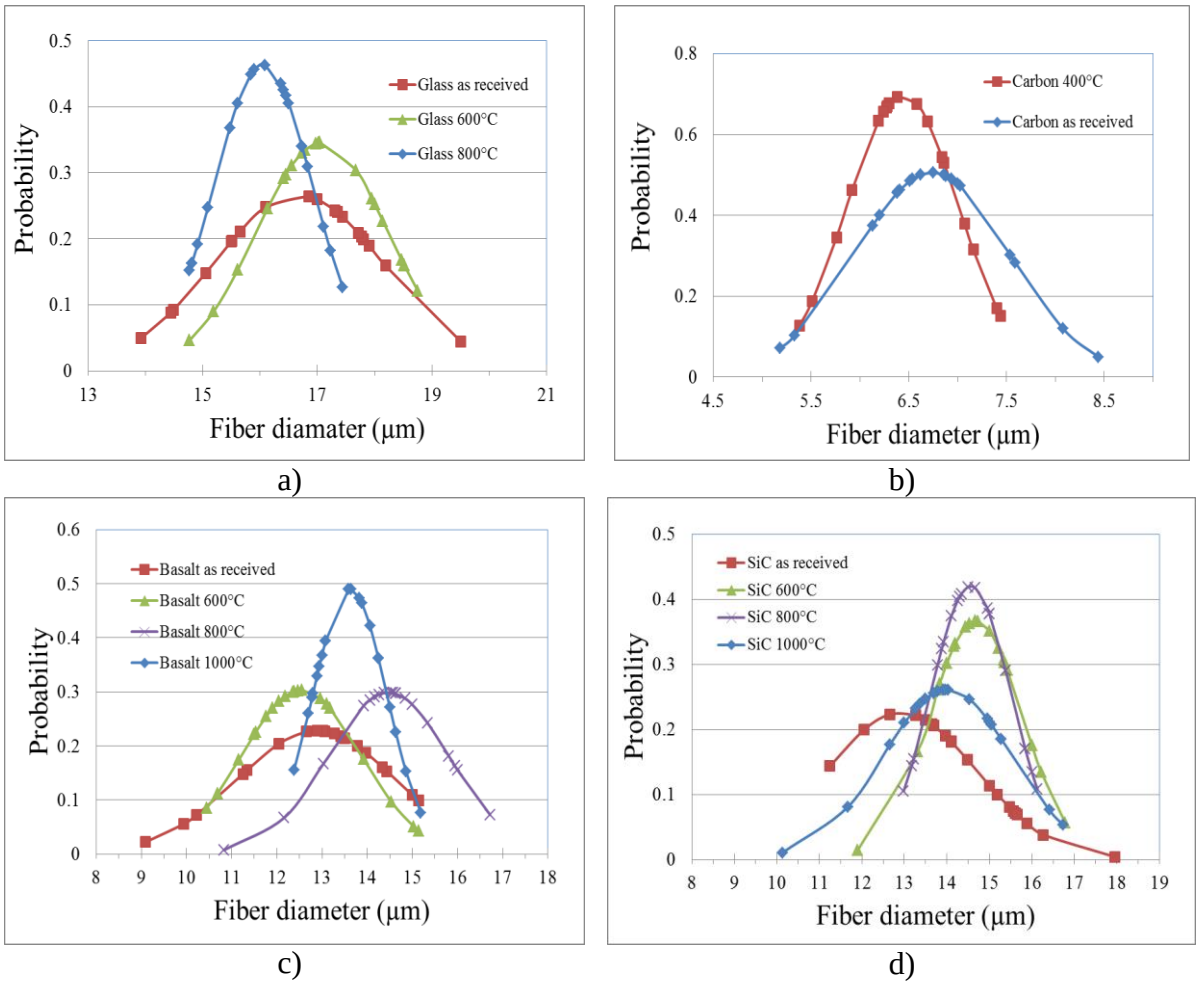

Figure 34 Diameter distribution of fibers for a) glass, b) carbon, c) basalt and d) SiC fibers.

The mean and standard deviation of the fiber diameter for the fibers at different oxidation temperatures has been included at Table 12. These mean values were used to calculate the tensile strength of the fibers.

Table 12 Main parameters obtained from the diameter measured for the fibers at the SEM.

Condition	Glass		Carbon		Basalt		SiC	
	Mean	SD	Mean	SD	Mean	SD	Mean	SD
As-received	16.671	1.497	6.740	0.789	12.876	1.747	14.466	1.570
400°C	16.811	1.241	6.438	0.573	12.702	1.233	14.523	1.673
600°C	17.083	1.317	-	-	12.544	1.153	14.679	1.088
800°C	16.054	0.862	-	-	14.472	1.336	14.563	0.950
1000°C	-	-	-	-	13.617	0.815	14.010	1.528

Figure 35 shows XRD for fibers after exposed to different temperatures in an oxidation environment. It was found that glass fiber even though is melted when it is exposed to 600ºC and then solidified, never became crystalline and its spectrum do not change, see Figure 35a.

On the other hand, carbon fiber was only tested until 400ºC because at 600°C it is almost all oxidized as CO_2 or CO (see Figure 35b). The XRD spectra at 400°C and bellow are nearly the same and just show fiber remains as amorphous. For basalt fibers, Figure 35c, after the exposure to 600°C the fiber became chemically unstable since it starts changing from amorphous to crystalline. This effect is reinforced after the exposure to 1000°C. Finally, SiC fibers show the same XRD pattern during all conducted oxidation treatments.

The phases generated during this crystallization are complex structures. Plagioclase, Magnetite and Pyroxene are by products that have been detected during the manufacturing. Silicate-Fe and Clinoferrosilicate showed the highest intensity.

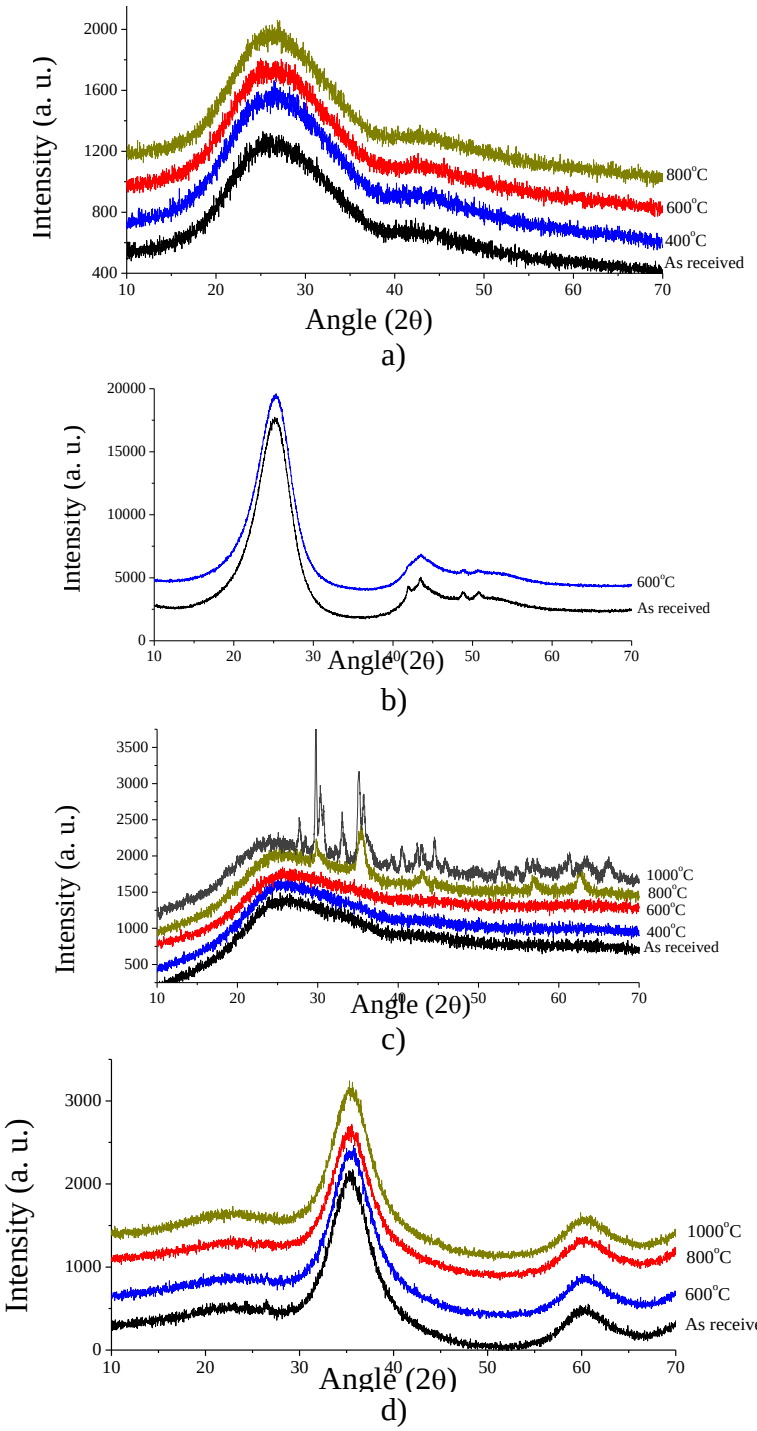

Figure 35 XRD for a) glass, b) carbon, c) basalt and d) SiC fibers exposed to different air oxidation treatments.

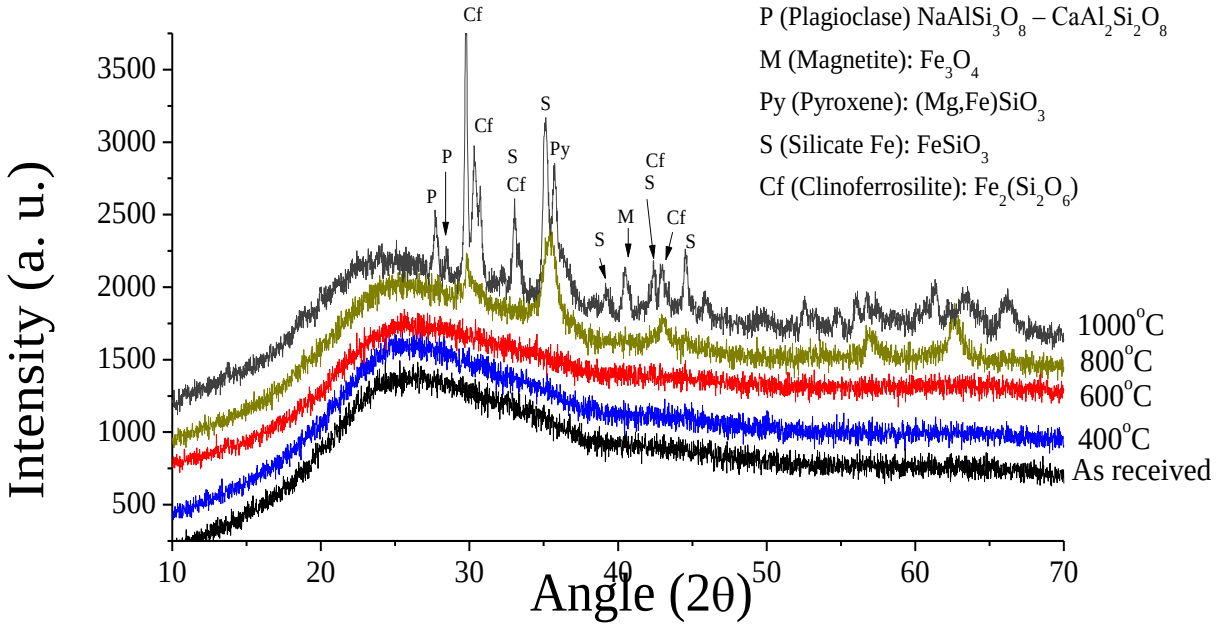

Figure 36 XRD details for the crystallization of basalt fibers exposed to the oxidation at high temperature.

Figure 37 shows the TGA data for different fibers from room temperature to 1000°C in air atmosphere. Figure 37a shows that glass fibers have very low weight loss over the full range of only just about 2%. The wide heat flow curve is due to the softening and further melting of the fibers which occurs almost over the full range but most significantly after 600°C and has a peak at 834°C due to an oxide formation. Figure 37b shows that carbon fibers have very significant transformations at 600°C. After 700°C the carbon is completely gone either as CO or CO_2, although this process started at about 400°C. Figure 37c shows that basalt fibers have very low weight loss over the full range of only just about 2.5%. It can be seen that there are several complex transformations that mildly correspond to the changes already presented in the discussion of the XRD. Figure 37d shows the results for SiC under air oxidation, which weight loss over the full temperature range is about 13%. Finally, all weight loss data have been summarized in Figure 37e. It can be observed that glass and basalt fibers have very similar

weight loss data. SiC fibers have more significant weight loss, and carbon fibers are completely disappeared as a consequence of the oxidation. Finally, there is a heat flow increase at the starting temperatures, more significant for glass, basalt and SiC fibers. This rise in the heat flow is associated with the crystallization of the polymeric sizing (see Table 5) that is impregnated over the fiber surface.

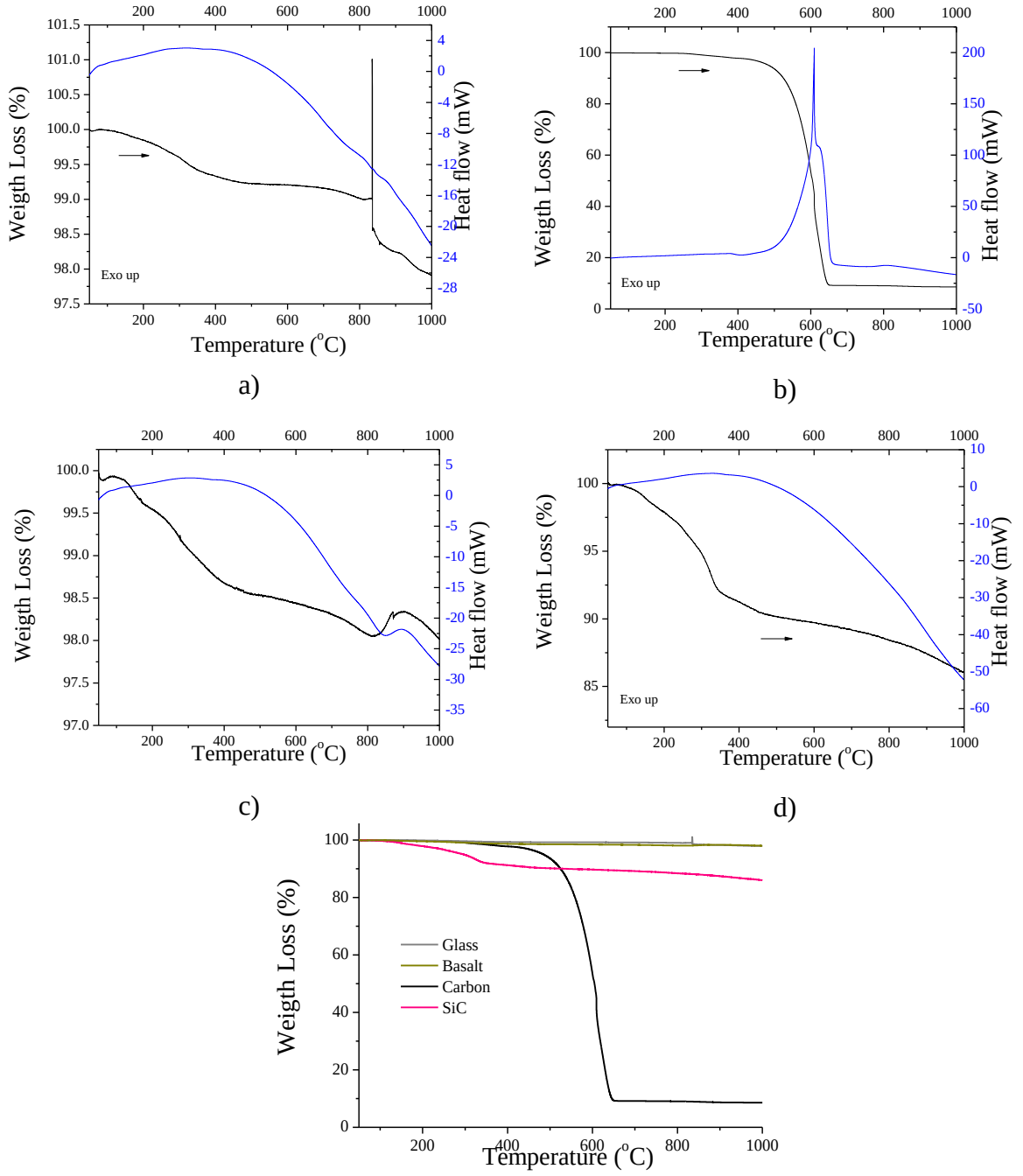

Figure 37 TGA in air atmosphere for a) glass, b) carbon, c) basalt and d) SiC fibers, e) weight loss in air atmosphere for all samples.

Figure 38 shows the Weibull probability (survival probability) for the glass, carbon, basalt and SiC fibers after the oxidation at different temperatures. Higher temperatures for the glass, carbon

and basalt fibers produced high deterioration in the fibers to the point that it was not able to make a sample for the tensile tests.

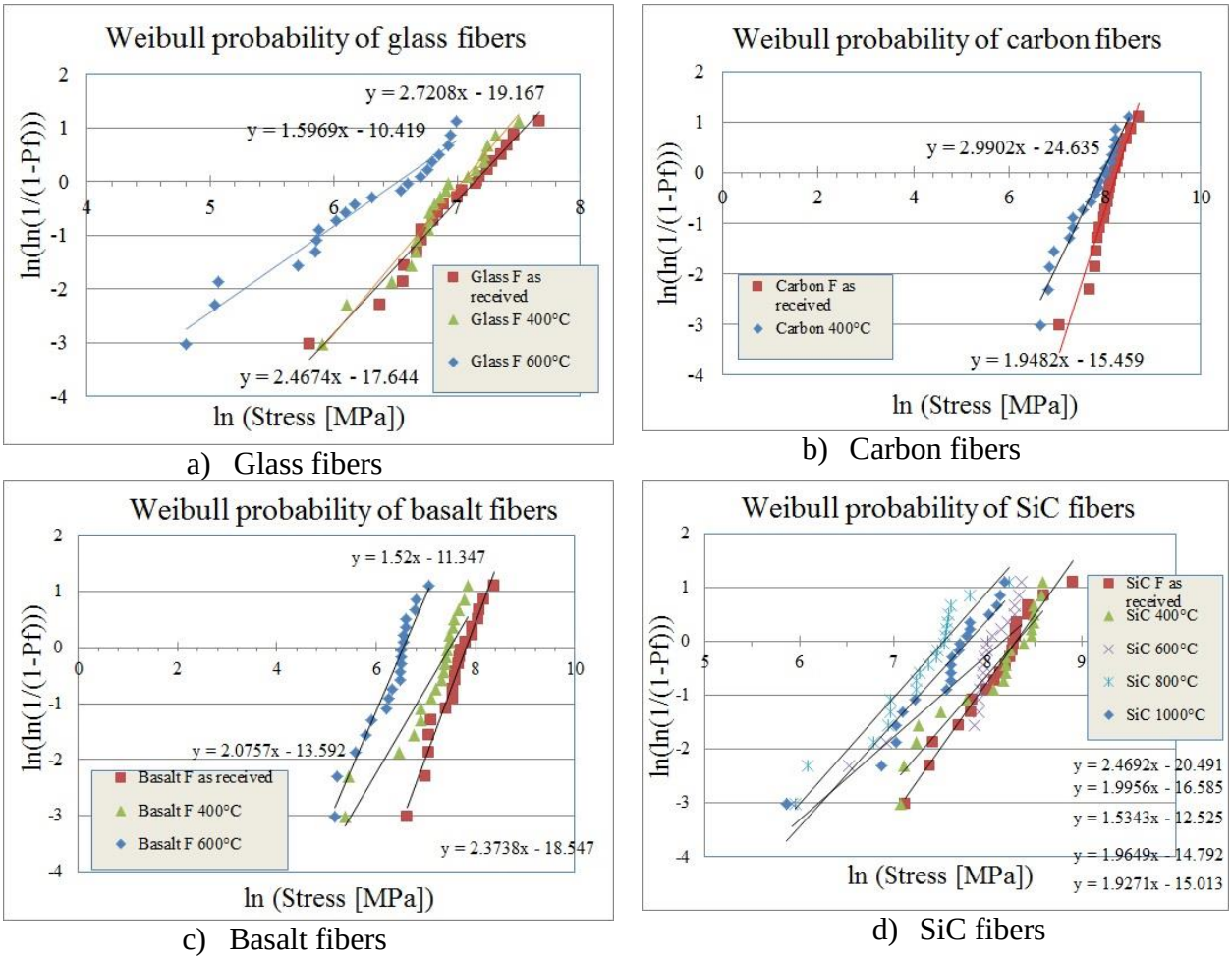

a) Glass fibers

b) Carbon fibers

c) Basalt fibers

d) SiC fibers

Figure 38 Weibull probability for tensile strength of a) glass, b) carbon, c) basalt and d) SiC fibers.

Figure 39 shows the Weibull distribution for glass fibers after exposed to air oxidation at different temperatures for 1h. Fibers as received and after exposed to 400°C do not show any significant difference from the tensile strength point of view. After the exposure to 600°C, a strong deterioration due to softening and localized melting occurs, as shown in the corresponding curve. For higher temperatures it was not possible to conduct any tensile experiments since the

weakening of the fiber made sample preparation impractical. It is important to note how variable the strength of these fibers is even in the as received condition, which is of about 1 order of magnitude.

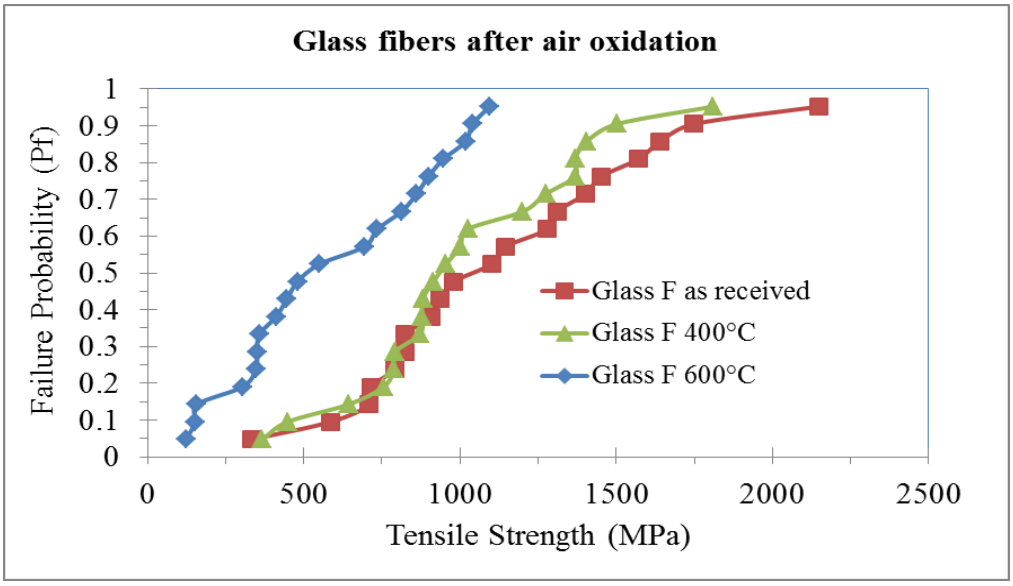

Figure 39 Weibull distribution for glass fibers.

Figure 40 shows the Weibull distribution for carbon fibers as received and after exposure to air oxidation at 400°C. At 600°C treatment a strong deterioration due to oxidation occurs (formation of CO or CO_2). This effect on the tensile properties is observed in the corresponding curve. For higher temperatures, it was not possible to conduct any tensile experiments since the fibers were completely oxidized and converted in gas byproducts. It is important to note how variable the strength of these fibers is even in the as received condition, which is near to 1 order of magnitude.

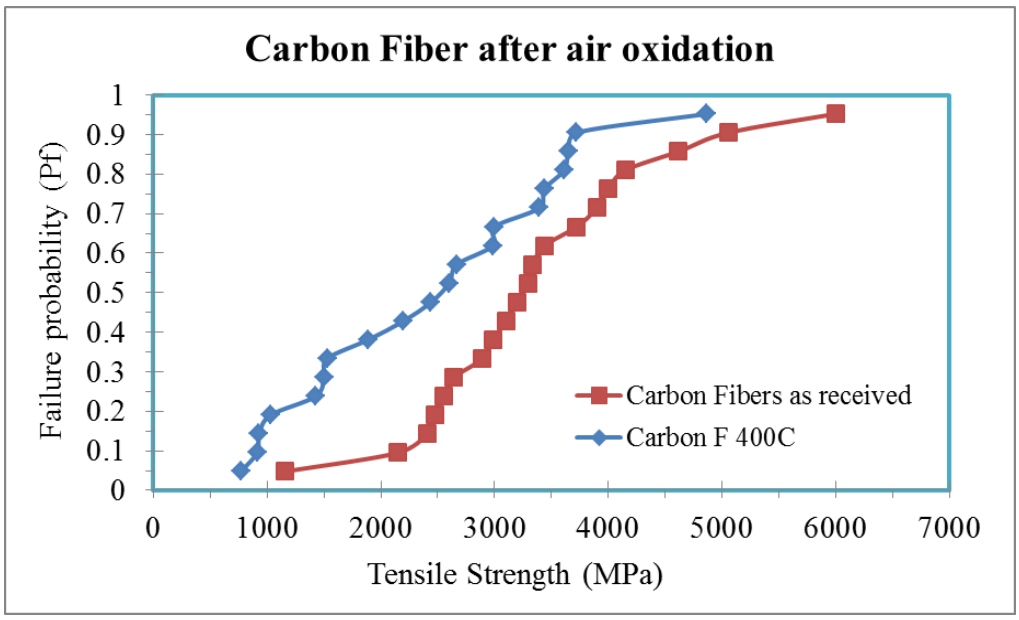

Figure 40 Weibull distribution for basalt fibers.

Figure 41 shows the Weibull distribution for basalt fibers after exposure to air oxidation at different temperatures for 1h. Fibers as received and exposed to 400°C do show a significant difference in the tensile strength. For fibers with the 600°C treatment there is a huge reduction in the tensile values, although the variability has been substantially decreased. At temperatures near 800°C and above, it has not been possible to conduct any tensile experiments due to the weakening of the fiber.

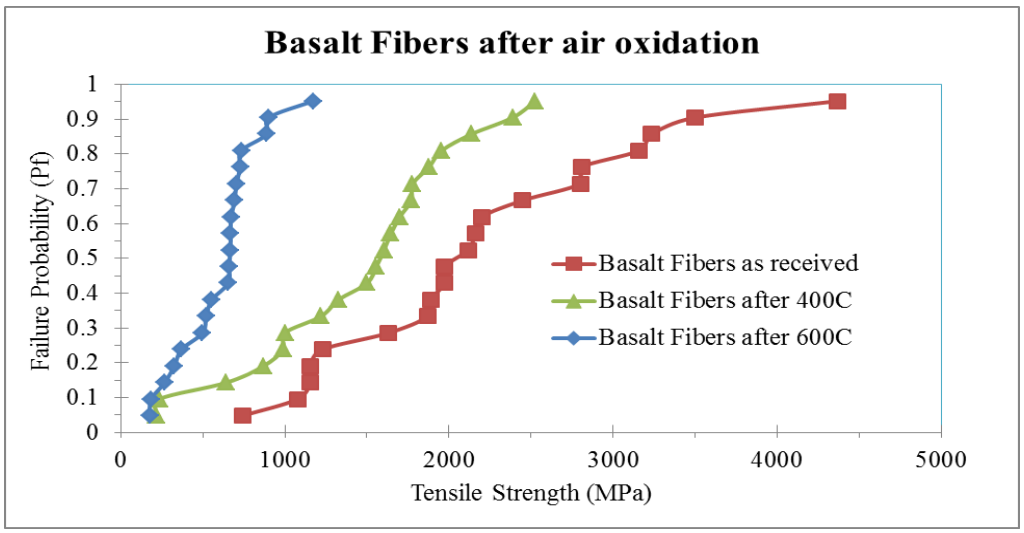

Figure 41 Weibull distribution for basalt fibers.

Figure 42 shows the Weibull distribution for SiC fibers after exposure to air oxidation at different temperatures for 1h. Fibers as received and exposed to 400°C do show a difference in the tensile strength. For fibers with the 600, 800 and 1000°C treatments there is a significant reduction in the tensile values and a reduction in the variability as well.

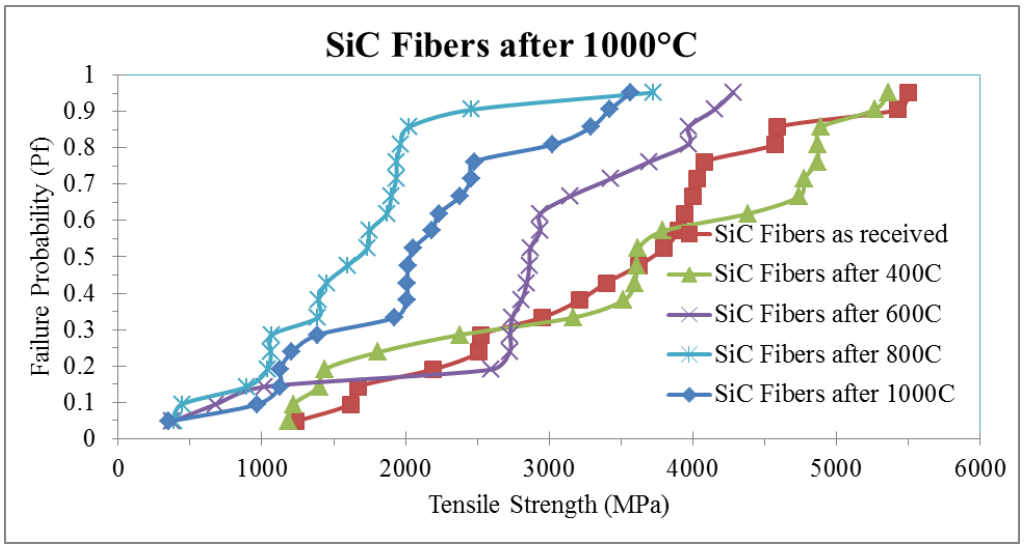

Figure 42 Weibull distribution for SiC fibers.

Figure 43 shows the Weibull modulus for the Weibull distributions of the fibers presented above. This data is directly related to the variability in the tensile strength values. The values are low when they are compared to the same bulk materials or engineering ceramics.

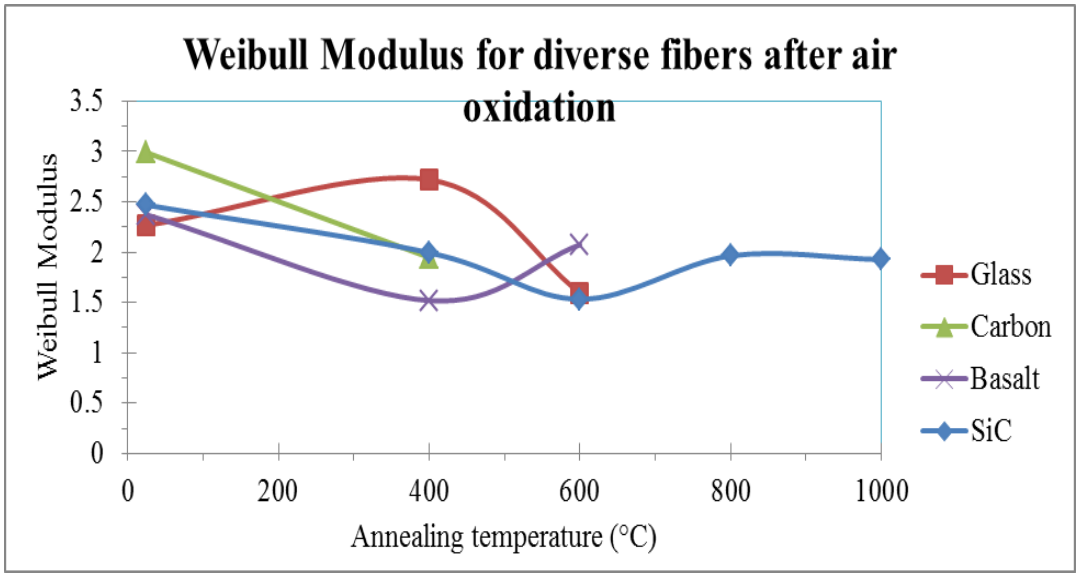

Figure 43 Weibull modulus for diverse fibers.

Figure 44 shows a summary of the mean tensile strength for the values presented before in the different Weibull distributions. In general it is observed that all fibers are deteriorated by the oxidation from exposure to air, even SiC exposed to 400°C.

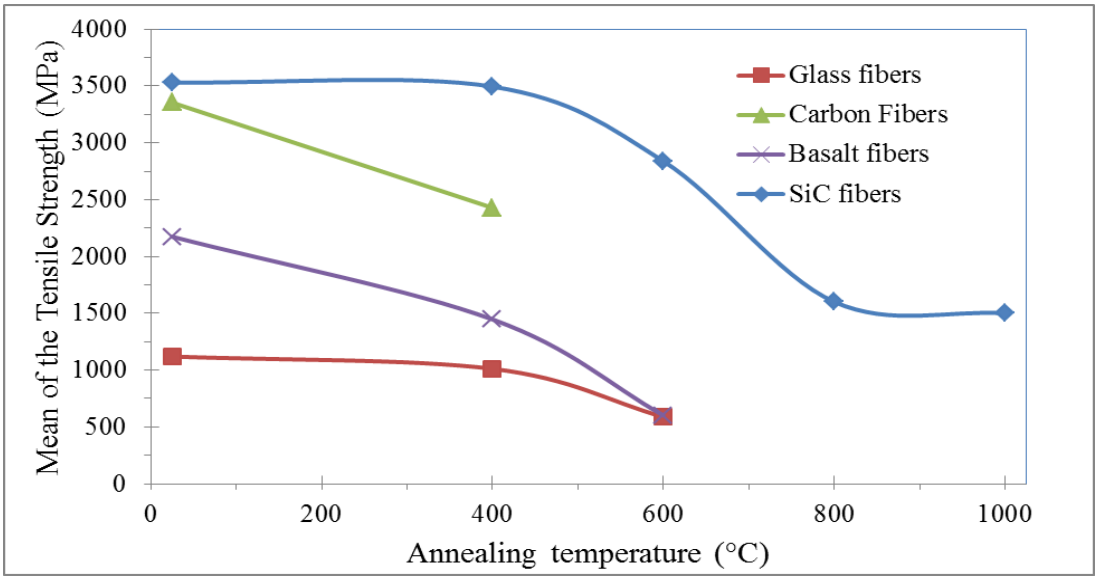

Figure 44 Mean tensile strength values taken from the Weibull distributions presented before.

5.4 Analysis

It has been found in this research that fibers ultimate strength has a higher variability than the data reported by manufacturers, see Table 5. This data from manufacturers typically is not well reported since it does not include details of the tensile testing procedures, such as the number of tested samples, the test type (single fiber or bundle fiber), crosshead speed and diameter measurement procedure. All these factors have a significant impact on results.

In the case of glass fibers, it was found that strength for fibers in the as received condition varies from 333 to 2149MPa with a corresponding low Weibull modulus of 2.5, which is understandable given the size variability is very high. Few defects, like cracks (see Figure 45) in the as-received fibers, were found. These defects are the main reason why the mean strength is 1120MPa, lower than the 1750MPa value reported, although this one [19] has same problem of incomplete reported data regarding the samples length.

After the exposure to 400 and 600°C for 1h, the Weibull modulus was 2.7 and 1.6 respectively. Reported results [1] show that for fibers as received and exposed to 450°C for 15 and 30min, this parameter was between 8.6 and 9.3. This explains why the strength variability reported from manufacturers is lower. However, it seems there is an error in the formula, which could increase the values artificially.

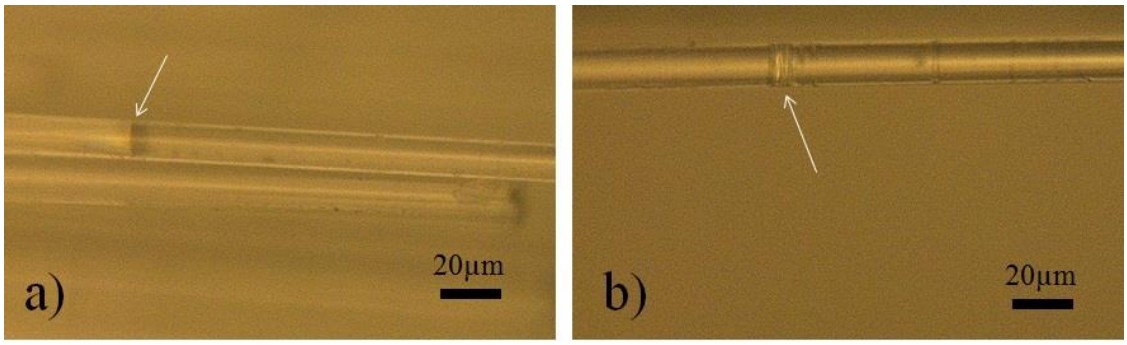

Figure 45 Optical images from glass fibers.

In the case of carbon fiber, the Weibull modulus obtained for fibers as-received was 3.0 and 1.95 and after the exposure to 400°C for 1h, and the strength varies from 1154 to 6000MPa. In-situ high temperature tensile tests [5] show values between 5.1 and 6.5 in experiments conducted at room temperatures up to 2000°C.

For basalt fibers, it was found that strength for fibers in the as received condition varies from 744 to 4370MPa. The Weibull moduli obtained for fibers as-received were 2.4, 1.5 and 2.1, after the exposure to 25, 400 and 600°C respectively. Other researchers [7] have analyzed the effect of the type of Weibull analysis upon their basalt fiber composition and values have been found near to 3 for the modulus, which is close to the reported value here. This variability can also be attributed to the variation of the chemical compositions of the commercial basalt fibers [10].

For SiC fibers it was found that the tensile strength varies from 1235 to 7374MPa. The Weibull moduli obtained for fibers as-received were 2.5, 2.0, 2.0 and 1.9, after the exposure to 25, 400, 600, 800 and 1000°C respectively. The literature reports a large scatter of modulus from fiber to fiber with a tendency to increase with decreasing fiber diameter [9]. Two-parameter Weibull analysis shows typical values for the Weibull moduli of 2.6 and 5.4. On the other hand, Weibull analysis over SiC fibers extracted from the composite [13] indicate that the strength distribution of the SiC fibers cannot be described solely in terms of a single flaw population, characterized by the two-parameter Weibull function (4.3 and 18 Weibull moduli were found). Although in this research fibers were used as received, it will be convenient to see the effect on the parameter when such a model is used.

5.5 Conclusion

Glass, carbon, basalt and SiC fibers have been oxidized in air for 1h at 200°C, 400°C, 600°C, 800°C, and 1000°C. In all fibers the tensile strength was significantly affected by the temperature. Carbon fiber is completely destroyed after exposure to 600°C in air environment, only white ash remains. If temperature is increased this ash completely disappears. Basalt fibers exposed to 600°C are very weak and at 800°C they partially melt and weaken to the point for which it is not possible to do tensile tests. At 1000°C the glass fibers completely melt. On the contrary, SiC fibers do not melt, however, after the exposure to 1000°C their tensile properties are significantly decreased (more than 50%). In general it was found that all fibers were affected by oxidation. Other important result obtained was the lack of information supplied from the manufacturers regarding details of the tensile tests conducted for the fibers. It is well known the high significance of the sample length and diameter on test results.

5.6 Future work

Although four different types of fibers were tested in this project under different oxidation temperatures for 1h and results showed a huge variability for all of them, only one brand and type of each was tested. Therefore, it would be good to do the same experiment for the best fiber of each type. It will be useful to know the data when a two Weibull parameter model is used.

Also, it will be useful to conduct the same set of experiments for the same fibers in a non-oxidation environment such as in an argon atmosphere.

5.7 References

[1] Feih, S., et al. "Strength degradation of glass fibers at high temperatures."Journal of materials science 44.2 (2009): 392-400.

[2] Kandare, Everson, et al. "Fiber-reinforced epoxy composites exposed to high temperature environments. Part II: modeling mechanical property degradation."Journal of Composite Materials 45.14 (2011): 1511-1521.

[3] Yin, Y., et al. "The oxidation behaviour of carbon fibres." Journal of materials science 29.8 (1994): 2250-2254.

[4] Sauder, Cédric, Jacques Lamon, and René Pailler. "Thermomechanical properties of carbon fibres at high temperatures (up to 2000 C)." Composites science and technology 62.4 (2002): 499-504.

[5] Sauder, Cédric, Jacques Lamon, and René Pailler. "The tensile behavior of carbon fibers at high temperatures up to 2400 C." Carbon 42.4 (2004): 715-725.

[6] Pradere, C., and C. Sauder. "Transverse and longitudinal coefficient of thermal expansion of carbon fibers at high temperatures (300–2500K)." Carbon 46.14 (2008): 1874-1884.

[7] Militky, Jiri, and Vladimir Kovacic. "Ultimate mechanical properties of basalt filaments." Textile research journal 66.4 (1996): 225-229.

[8] Militký, Jiří, Vladimír Kovačič, and Vladimír Bajzík. "Mechanical properties of basalt filaments." FIBRES & TEXTILES in Eastern Europe 15.5-6 (2007): 64-65.

[9] Černý, M., et al. "Comparison of mechanical properties and structural changes of continuous basalt and glass fibres at elevated temperatures." Ceramics–Silikáty 51.2 (2007): 82-88.

[10] Varadachari, Chandrika, Ritabrata Bhowmick, and Kunal Ghosh. "Thermodynamics and Oxidation Behaviour of Crystalline Silicon Carbide (3C) with Atomic Oxygen and Ozone." ISRN Thermodynamics 2012 (2012).

[11] Jorgensen, Paul J., Milton E. Wadsworth, and Ivan B. Cutler. "Oxidation of silicon carbide." Journal of the American Ceramic Society 42.12 (2006): 613-616.
[12] Andersson, C. H., and R. Warren. "Silicon carbide fibres and their potential for use in composite materials. Part 1." Composites 15.1 (1984): 16-24.
[13] Zok, Frank W., Xiuyen Chen, and Christian H. Weber. "Tensile strength of SiC fibers." Journal of the American Ceramic Society 78.7 (1995): 1965-1968.
[14] Fiber Glass Industries, Inc., fiber glass manufacturer. New York, USA. Website: http://fiberglassindustries.com.
[15] Toho Tenax America Inc, carbon fiber manufacturer. Tennessee, USA. Website: http://www.tohotenaxamerica.com/contfil.php
[16] Kamenny Vek, basalt fiber manufacturer. Moscow, Russia. Website: http://www.basfiber.com/
[17] COI Ceramics, Inc., SiC fiber manufacturer. San Diego, USA. Website: http://www.coiceramics.com/index.html.
[18] Frederick T. Wallenberger, James C. Watson, and Hong Li. Glass Fibers. 2001 ASM International. ASM Handbook, Vol. 21: Composites (#06781G): 27-34.
[19] Chawla, Krishan K. Composite materials: science and engineering. Springer, 1998.

6 Pultruded acid-base phosphate cement composites fabricated from wollastonite powders

6.1 Introduction

Besides the presented advantages of PCs as castable cementitious materials, they are known for their good compressive properties and relatively poor tensile strength. Composite reinforcements (such as fibers or particles) improve tensile properties enough that the material can be used in structural applications in tension. In particular, the pultrusion process to fabricate fiber reinforced composites has several advantages: increased mechanical strength (fiber is processed under tension); high fiber content; highly automated processing; high production; low cost; and fine tolerances. PC reinforced with particles and fibers ([1]-[4]) has been produced before, showing the feasibility of PC as a building material. In this Chapter are shown unidirectional (UD) fiber reinforced chemically bonded phosphate ceramic composited fabricated from wollastonite powders (Wo-PCs) by pultrusion. These composites were produced as the result of mixing calcium silicate (wollastonite, $CaSiO_3$) and phosphoric acid (H_3PO_4) to produce calcium phosphates (i. e. brushite or monetite), silica, sometimes quartz, and depending on the reactivity, some remaining wollastonite powder (chemical reactions as well as phase identification can be reviewed in [5], [6] and [7]). Then, fibers were incorporated by pultrusion. E-glass, carbon and basalt fiber were used, whose manufacturers and properties have been presented in Chapter 3.

6.2 Manufacturing

Figure 10 shows fiber reinforced PCs fabricated by pultrusion. All samples were fabricated with about 15 volume % of fibers and the fibers used were glass, carbon and basalt. All samples were dried 1 day at 50°C, 1 day at 100°C and 1 day at 200°C in order to remove the water completely. Glass fibers Textrand 225 from Fiber Glass Industries, Graphite fibers Tenax-A 511, Basalt fibers BCF13-1200KV12 Int from Kammemy Vek, and SiC fibers from Nicalon were used in

this research. In order to plot the Weibull distributions, twenty samples were tested for each temperature and composition and then tested in three point bending tests. The thermal treatment followed in this experiment is the thermal processing described in the previous chapters.

a) b)

Figure 46 a) pultrusion die during manufacturing of PCs reinforced with unidirectional glass fibers, b) and pultruded bars of PCs reinforced with glass fibers (white) and with carbon fibers (black).

The pultrusion process for the PCs reinforced with glass fiber is presented in Figure 10a. The die-temperature was 110˚C (230˚F) and the pull speed was 30.5 cm/min (1 ft/min). Pultruded bars for both graphite and glass fibers are presented in Figure 10b.

On the other hand, in the handmade process, a Teflon fluoropolymer mold was used to avoid adhesion of the PC. Samples were released after 48 hours and then dried following the process detailed above.

6.3 Pultruded composites

6.3.1 Wo-PC matrix glass fibers composites

The Weibull distribution of pultruded glass fiber reinforced Wo-PC composites at different exposure temperatures is shown in Figure 47. For all samples, the thermal exposure time was 1h. As temperature is increased, the curves move toward low bending strength values and the variability is reduced as well.

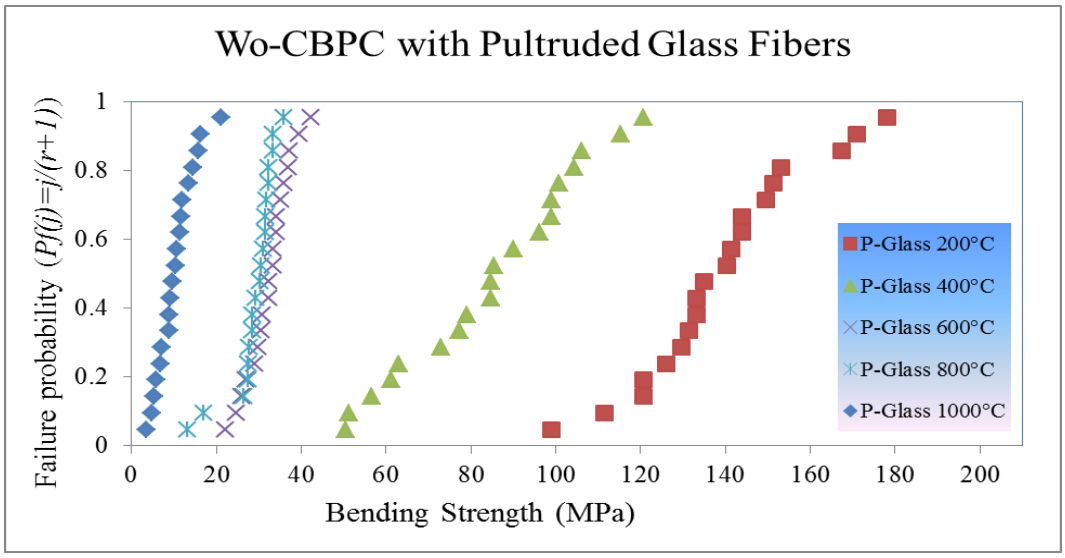

Figure 47 Weibull distribution of Wo-PC with different pultruded fibers.

Figure 48 shows the Weibull modulus for the composite of Figure 47, which measure the variability of the data and the number increase when the variability (flaws length distribution) . All fit curves are also included in Figure 48. Modulus in general decreases as temperature increases, however, there is an increase at 600°C.

This curve is explained by analyzing the microsctructure shown in optical microscopy at Figure 49. As temperature is increased, the matrix and fiber is significantly damaged. Figure 50 shows SEM images, which reveals clearly the structural damage in both the fiber and the ceramic

matrix, as temperature increases. Figure 50a, b, c, d, e and f show cross section view images of the composite as made, 200°C, 400°C, 600°C, 800°C, and 1000°C respectively.

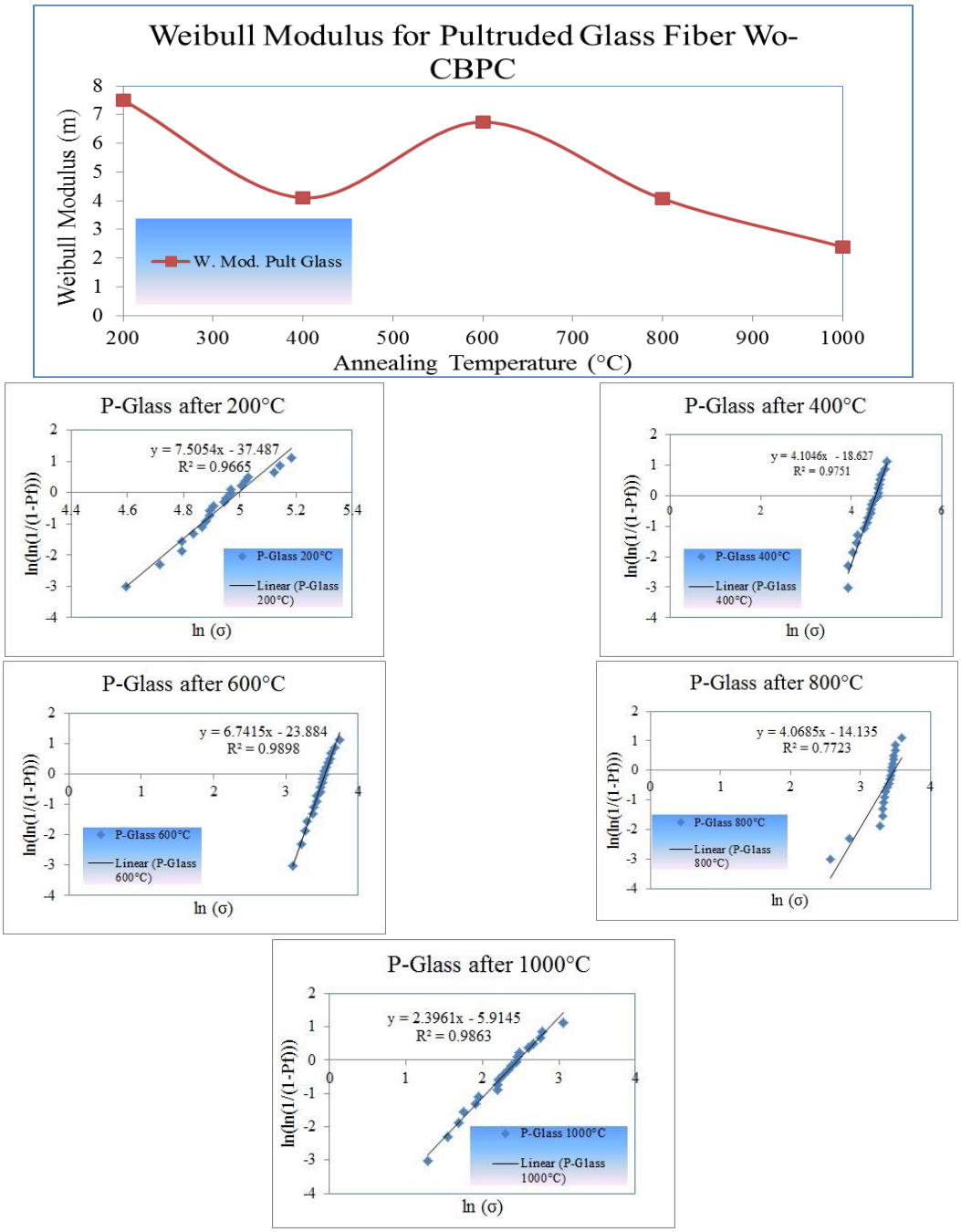

Figure 48 Weibull modulus as a function of the thermal exposure temperature and its corresponding curves fit for the pultruded glass fiber reinforced Wo-PC composites.

Figure 50a shows the composite as made. Wollastonite grains are between fibers, which anticipates a very complex inter-relation even at room temperatures, where the particle size blocks the resine impregnation during the manufactiring. However, in our particular case for the M200 powder, the impregnation is good as shown in this picture.

At 400°C, Figure 50c, the fiber does not show much deterioration. However, at 600°C, Figure 50d, fiber borders are damaged and partial melting is observed. Tests were conducted every 100°C, but no significant difference between the intervals 300°C-400°C, 500°C-600°C, 700°C-800°C, and 900°C-1000°C was found.

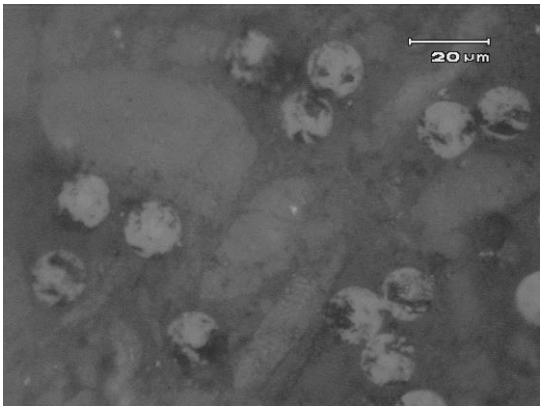

a) As made

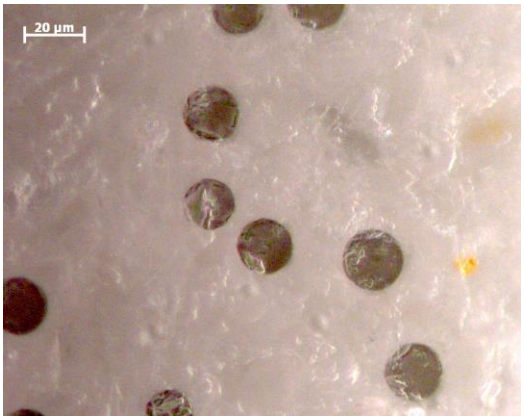

b) 200°C

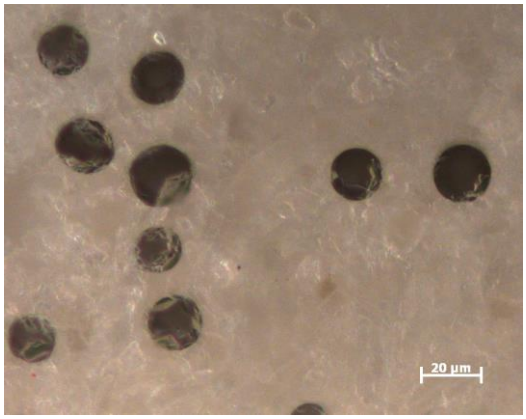

c) 400°C

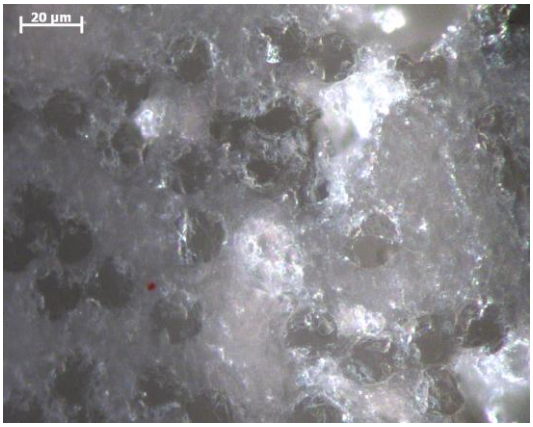

d) 600°C

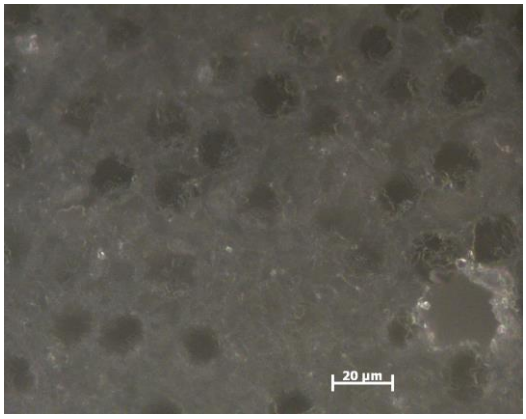

e) 800°C

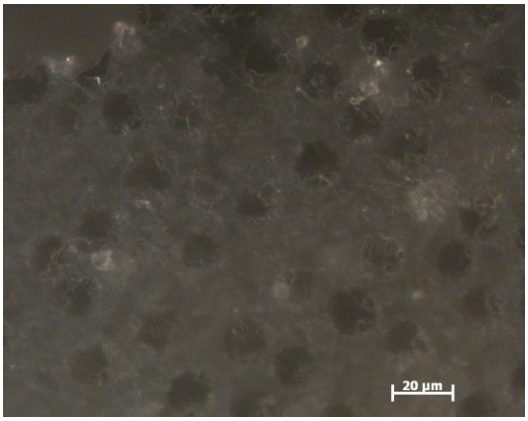

f) 1000°C

Figure 49 Optical microscopy images of the glass fiber-reinforced composite at different thermal exposure temperatures.

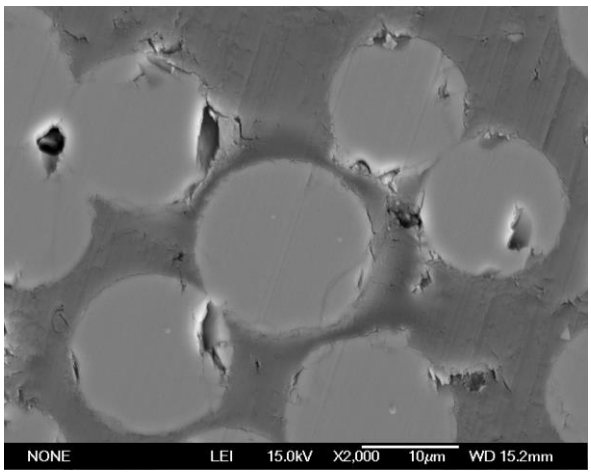

a) As made

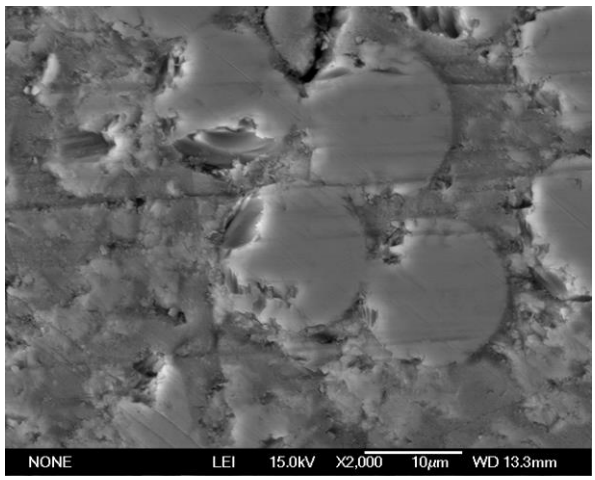

b) 200°C

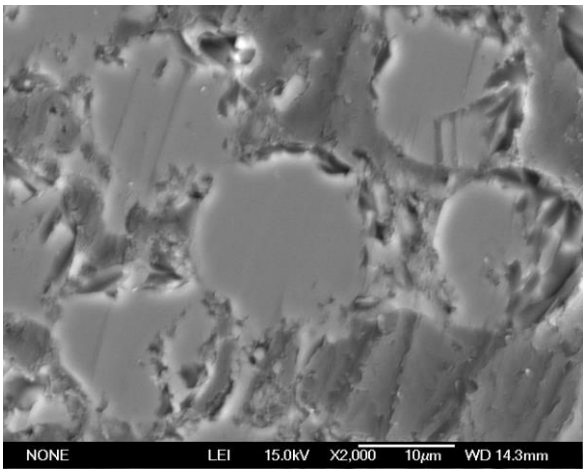

c) 400°C

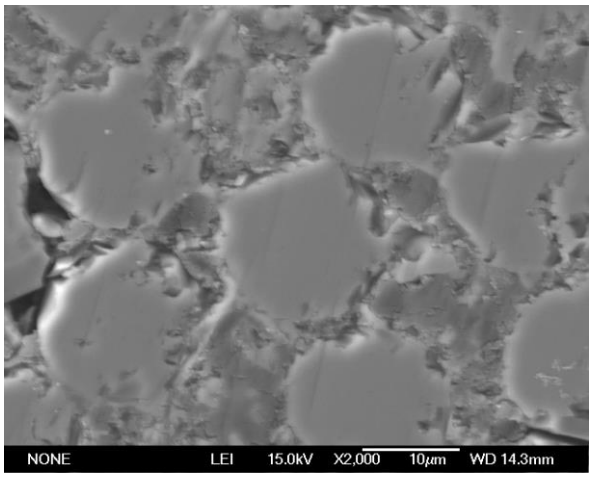

d) 600°C

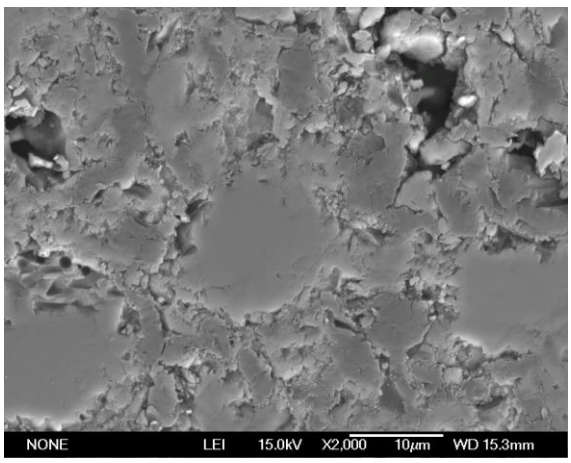

e) 800°C

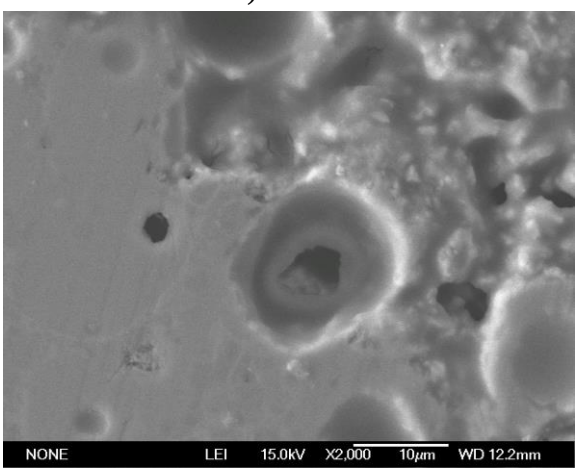

f) 1000°C

Figure 50 Cross section images of the glass fiber-reinforced composite at different exposure temperatures.

At 800°C, Figure 50e, it is hard to recognize the fiber since the porosity of the matrix had increased. This is because the matrix also has several components that have already reacted and became unstable as explained in Chapter 4. At 1000°C, (Figure 50f) the fiber is completely melted and holes appeared in the fiber's area. The melting or partial softening of the fibers and silica phase in the composite impregnates some micro defects, like flaws from the matrix, which reduce the flaw number and in some cases decreases the variability in the strength values. This causes an increase in the Weibull modulus.

Figure 51 shows SEM-EDS data for the pultruded glass fiber reinforced Wo-PC after exposure at 200°C for 1h. X-ray compositional lines and the quantification of selected atoms are included. The complete data is included in an Annex section. As shown in these lines (A and B), some elements such as "Zn", "Fe", "Mg" and "C" are not only almost undetectable (in some cases not detected) but also almost constant through the line. Then, elements such as "Si", "Ca", "O", "P" and in some cases "Al" play a significant role in controlling the chemistry and final properties of the ceramic composite.

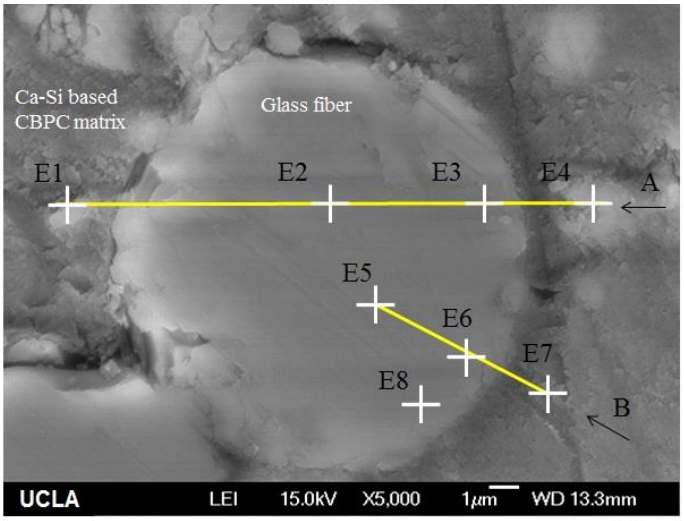

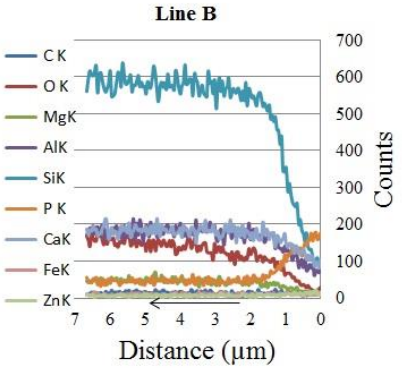

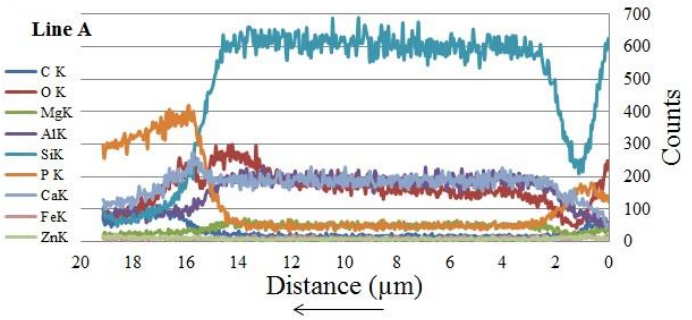

EDS Quantification of atomic percentages

Point	P	Ca	Si	Al	Ca/P	Ca/Si	Al/Ca
E1	8.77	4.60	0.95	2.01	0.52	4.84	0.44
E2	0.00	10.86	30.71	8.79	NA	0.35	0.81
E3	0.00	11.41	31.07	8.49	NA	0.37	0.74
E4	4.13	3.66	10.86	1.27	0.89	0.34	0.35
E5	0.51	9.08	23.86	7.06	17.80	0.38	0.78
E6	0.59	9.80	24.75	7.25	16.61	0.40	0.74
E7	11.23	11.72	5.38	5.24	1.04	2.18	0.45
E8	0.54	8.88	22.94	6.69	16.44	0.39	0.75

Figure 51 EDS-SEM for cross section of the glass fiber-reinforced composite after exposed to 200°C for 1h. Arrows near the lines indicate where the scan started.

Line A in Figure 51 shows that at the borders of the fiber there is a soft attenuation, which is expected according to the interdiffusion expected from “Ca” ions and other species. At spot E1, the “Si” content increases continously until reaching a near stable concentration though all the fiber diameter. Then, “Si” content decreases at the matrix but increases again near the spot E4. Also, on the left side, “Ca” and “Al” have similar concentrations. Inside the fiber, both concentrations increase and are very similar to each other in contents. However, in the matrix-fiber interface, the “Ca” has a small peak while “Al” has a soft transition from lower to higher concentration. This is associated to a local accumulation of calcium ions extracted from a wollastonite residual grain. The fiber acts as a natural block for the diffision of these ions into the

matrix. On the other side of the fiber, the “Ca” and “Al” contents drop to almost zero. On the other hand, the concentration of “P” is also high in the left side and then, there is an abrupt change in the slope of the curve. Along this line and inside the fiber, the “P” content is near to zero, and then increases again near E4. Therefore we identified the two spots at the end of the lines in E1 as brushite ($CaHPO_4.2H_2O$) and in E4 as a combination of brushite and silica (not residual wollastonite since “Ca” is near to zero).

The EDS quantification for the atomic percentages shows that there is not diffusion of “P” ions diffusing into the fiber. All elements detected are not included, but they will be discussed at the end of this chapter. Line B has a more simple analysis because it starts in a matrix area without a high concentration of “Si”, which means not silica or residual wollastonite is nearby and therefore that part of the matrix is a more homogeneous Ca-Si phosphate matrix. EDS data shows the spot E5 has minor (but not zero) “P” contents, which is due to a “P” diffusion through a microcrack or other deffect in the fiber.

Figure 52a shows SEM-EDS for the pultruded glass fiber reinforced Wo-PC after exposed at 400°C for 1h. A typical spectrum is also shown for the spot E1. Both morphology and X-ray compositional lines are similar as presented in Figure 51. The atomic composition shows that “Ca” is reduced progressively as we move toward the interface matrix-fiber (from E1 to E3). Also, E3 and E4 spots show that matrix has a near homogeneus “Ca” distribution. “P” was found inside the fiber, which shows that “P” penetrates the fiber interdifussion start to occur at temperatures as low as 400°C. “Ca/P” distribution counts better this interdiffusion. Also, Ca/Al distribution is very homogeneous when it is compared to sample exposed to 200°C, Figure 51, which is significant to show that at this temperature there is enogh energy to produce ion flux.

Figure 52b shows SEM-EDS for the pultruded glass fiber reinforced Wo-PC exposed to 600°C for 1h. In this case the morphology of the fibers change a lot when is compared to the previous images, which is in agreement with the previous shown data for the single glass fiber characterization including imaging, thermal and for the Weibull statistics presented above as well. It corresponds to a partial fiber glass decomposition as shown by the TGA data presented before, which is more notorious at the interface. The X-ray compositional map shows that "Si" and other elements content are still homogeneous in most part of the fiber, however at the interfaces the variation is random. Quartz and amorphous silica, byproducts of wollastonite, are also affected at this temperature. Quartz melts at more than 1600°C when pure, however in this material as we saw in Chapter 4, the thermal properties of some phases (such as wollastonite transforming into pseudo-wollastonite below the expected temperature) are affected by the interdiffusion in these complex composite materials.

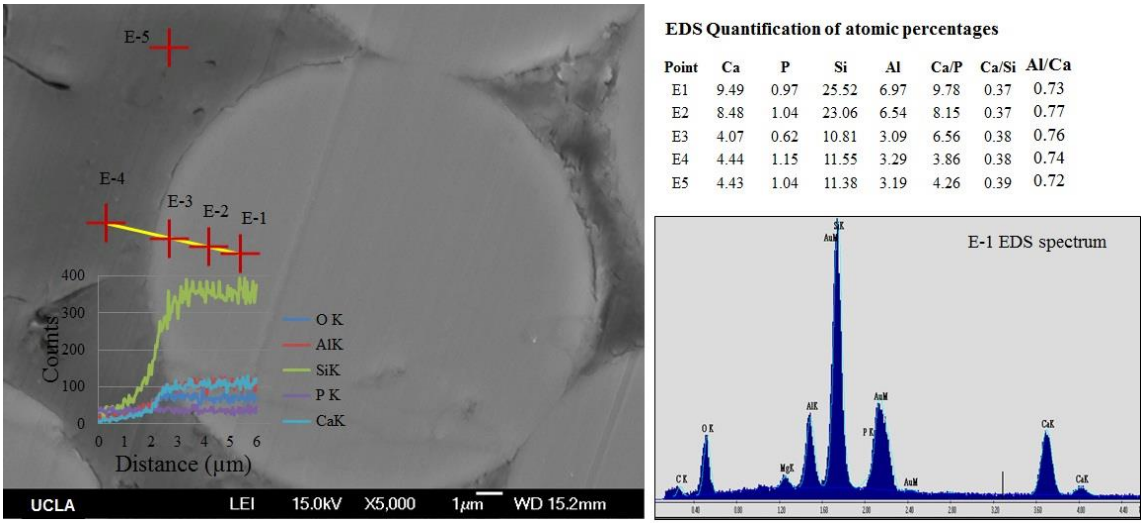

EDS Quantification of atomic percentages

Point	Ca	P	Si	Al	Ca/P	Ca/Si	Al/Ca
E1	9.49	0.97	25.52	6.97	9.78	0.37	0.73
E2	8.48	1.04	23.06	6.54	8.15	0.37	0.77
E3	4.07	0.62	10.81	3.09	6.56	0.38	0.76
E4	4.44	1.15	11.55	3.29	3.86	0.38	0.74
E5	4.43	1.04	11.38	3.19	4.26	0.39	0.72

a) 400°C

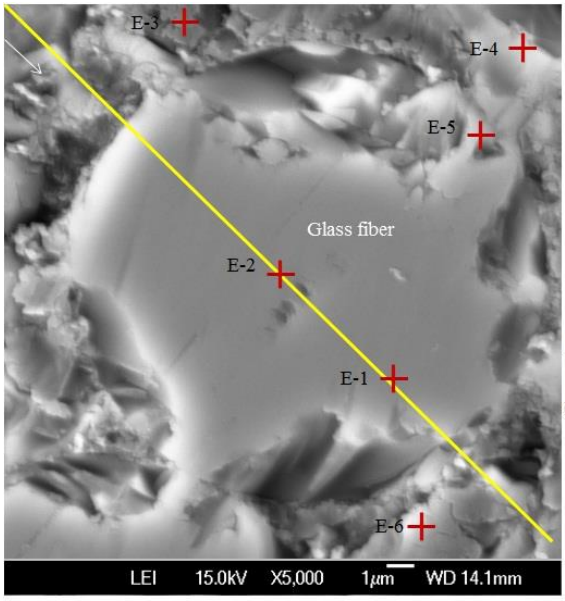

EDS Quantification of atomic percentages

Point	Ca	P	Si	Al	Ca/P	Ca/Si	Al/Ca
E1	9.57	0.92	25.81	7.19	10.40	0.37	0.75
E2	9.86	0	26.97	7.67	-	0.37	0.78
E3	0.95	0	1.41	0.76	-	0.67	0.80
E4	5.16	12.12	0.92	3.96	0.43	5.61	0.77
E5	9.8	2.6	21.76	6.75	3.77	0.45	0.69
E6	0.25	0.9	3.15	0.16	0.28	0.08	0.64

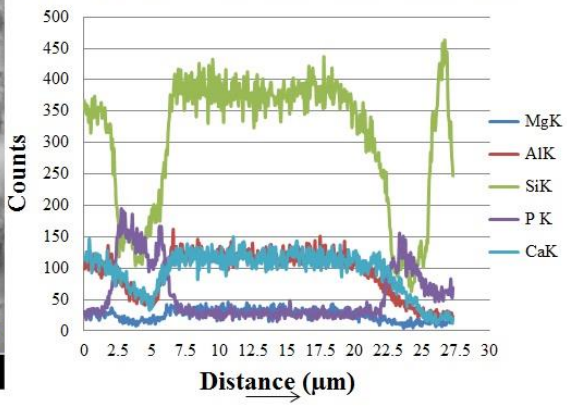

b) 600°C

Figure 52 EDS-SEM for cross section of the glass fiber-reinforced composite exposed for 1 to a) 400°C, and b) at 600°C. Arrows near the lines indicate where the scan started.

Since for this glass fiber composite 600°C is a critical temperature, X-ray compositional maps are shown in Figure 53a. Details about the quantitative EDS atomic percentages are shown in Figure 53b which have been used to identify the different materials in the maps.

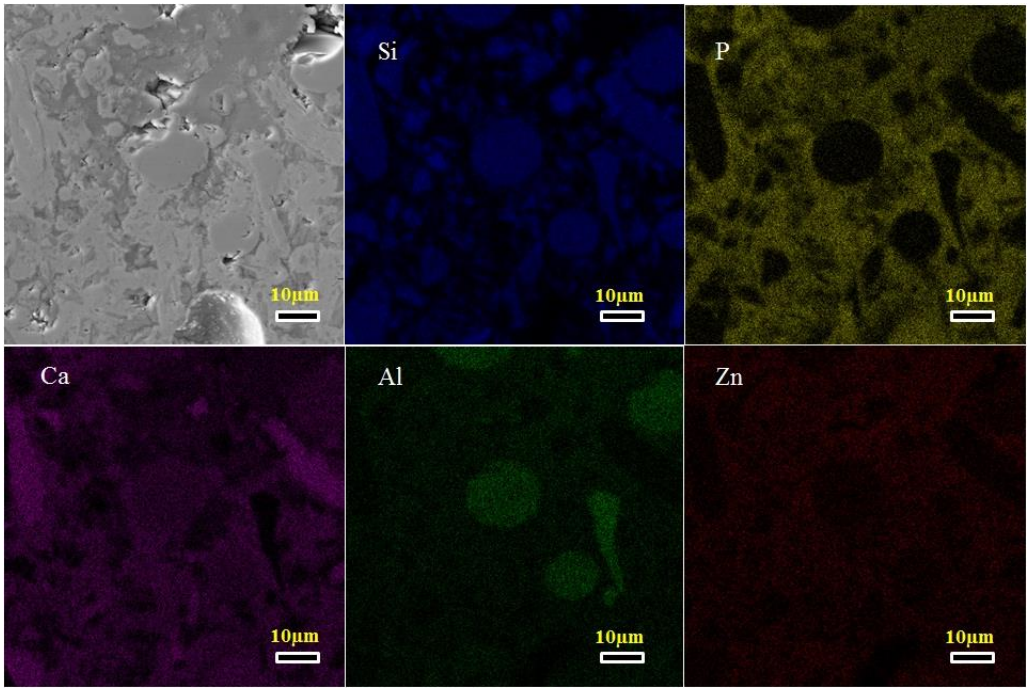

a)

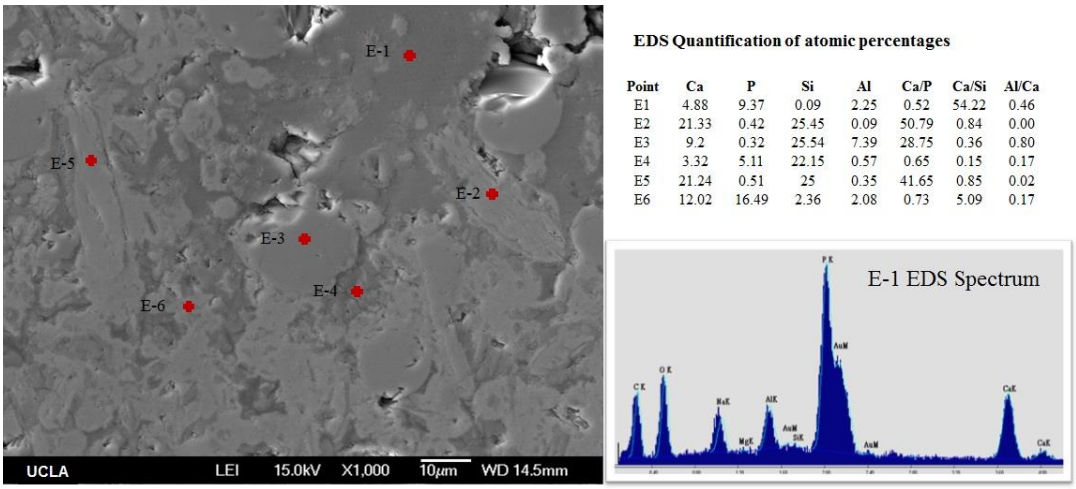

EDS Quantification of atomic percentages

Point	Ca	P	Si	Al	Ca/P	Ca/Si	Al/Ca
E1	4.88	9.37	0.09	2.25	0.52	54.22	0.46
E2	21.33	0.42	25.45	0.09	50.79	0.84	0.00
E3	9.2	0.32	25.54	7.39	28.75	0.36	0.80
E4	3.32	5.11	22.15	0.57	0.65	0.15	0.17
E5	21.24	0.51	25	0.35	41.65	0.85	0.02
E6	12.02	16.49	2.36	2.08	0.73	5.09	0.17

b)

Figure 53 EDS-SEM X-ray maps for cross section of the glass fiber-reinforced composite exposed to 600°C for 1h.

In Figure 53a maps reveal diverse information. “Si” has about the same intensity in both particles and fibers. “P”, “Ca”, “Al” and “Zn” are very homogeneous in the matrix. “Ca”-map shows that only few residuals grains are almost fully transformed from wollastonite to silica. Also, it is

shown that “Al” is the best way to detect glass fibers as they clearly have the highest concentration in the composite. In the “Al” and “Si” maps, a crystal like wedge is seen near the fibers. Since this particle only appears in these maps, it is suggested to be a type of alumino-silicate mineral such as Sillimanite (Al_2SiO_5).

Figure 54a shows SEM-EDS for the pultruded glass fiber reinforced Wo-PC exposed to 800°C for 1h. The fiber borders were not identified because they are completely diffused into the matrix, which shows its decomposition. E1 and E2 spots have very similar composition which shows that the fiber core is preserved.

Figure 54b shows SEM-EDS for the pultruded glass fiber reinforced Wo-PC exposed to 1000°C for 1h. In the place of the fiber we have a hole. The damage is notorious.

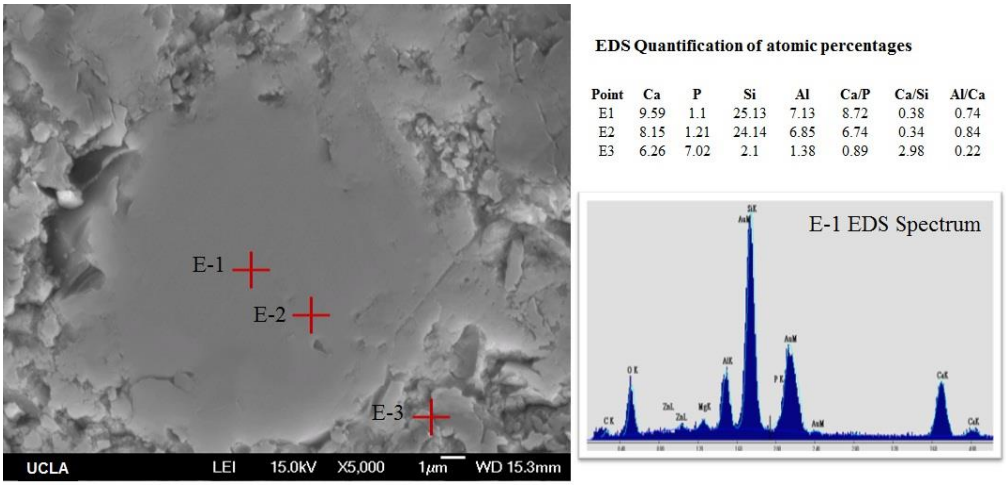

a) 800°C

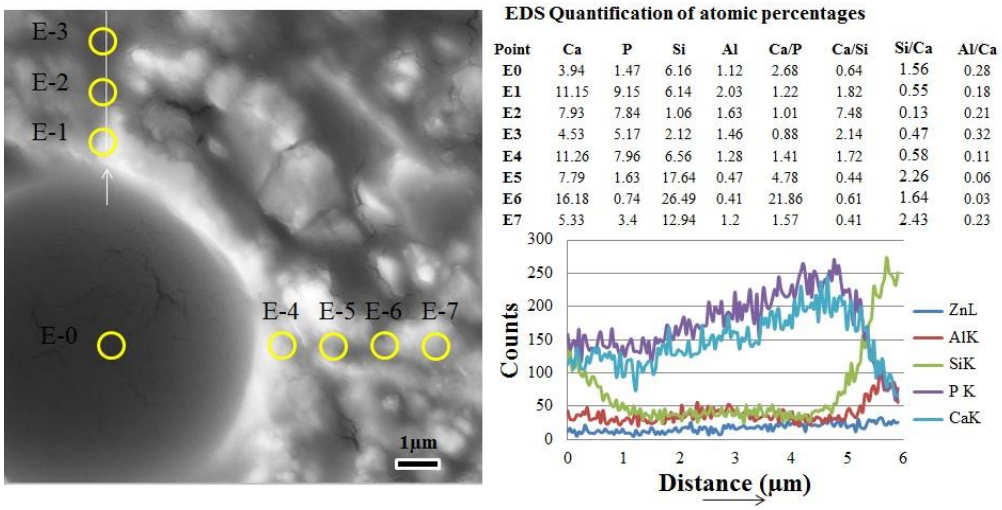

b) 1000°C

Figure 54 EDS-SEM for cross section of the glass fiber-reinforced composite exposed for 1h to a) 800°C, and b) 1000°C.

6.3.2 Wo-PC matrix carbon fibers composites

The Weibull distribution of pultruded carbon fiber reinforced Wo-PC composites at different exposure temperatures is shown in Figure 55. For all samples, the thermal treatment time was 1h. As occurred for glass fibers, as temperature is increased, the curves move toward low bending strength values, and the variability is reduced as well.

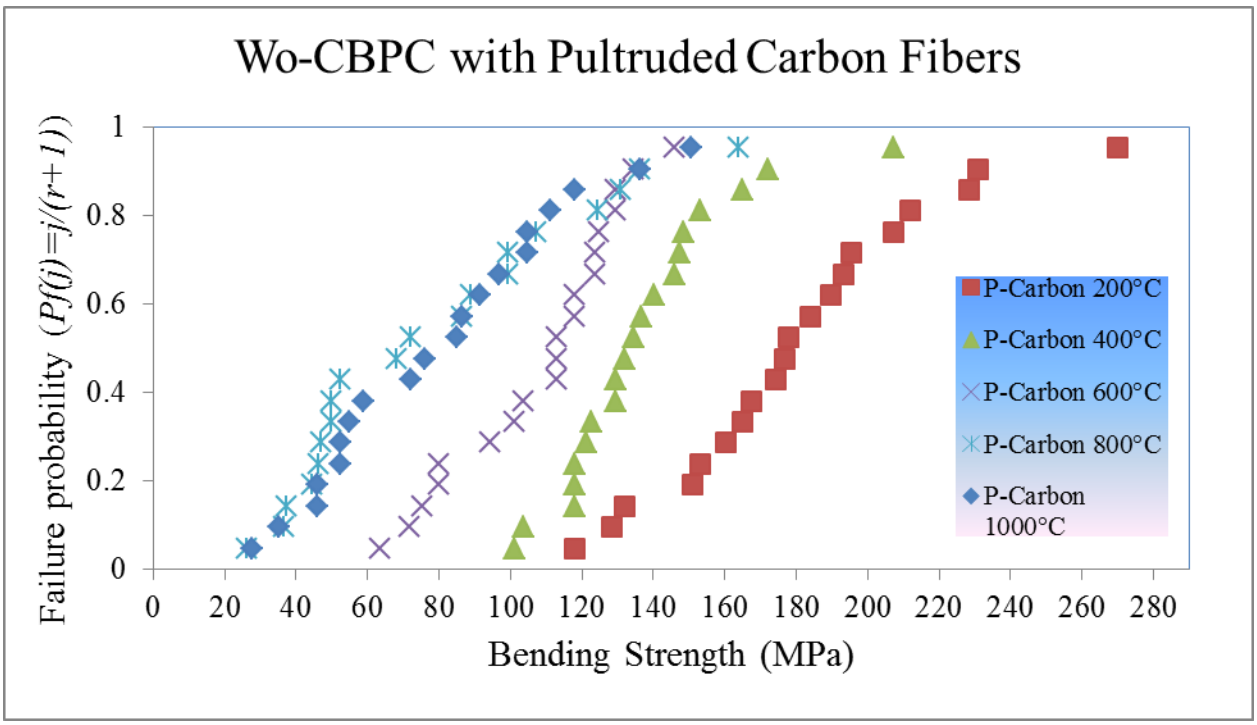

Figure 55 Weibull distribution of Wo-PC with different pultruded carbon fibers.

Figure 56 shows the Weibull modulus for the composite of Figure 55 . All fit curves are also included. As for the previous glass fiber composites, the modulus also has increased, at 400°C. This curve is explained by analyzing the microsctructure shown in Figure 58, the fiber stability in the ceramic matrix as temperature increases. Figure 58a, b, c, d, e and f show cross section view images of the composite at room temperature, 200°C, 400°C, 600°C, 800°C, and 1000°C respectively. Figure 58a shows the composite as made.

Figure 57 shows the deterioration of the PC-carbon fiber composites as the temperature is increased. After the exposure to 600ºC, the fiber has been completely oxidized and converted into air byproducts as explained in Chapter 5 (basically CO_2 and CO).

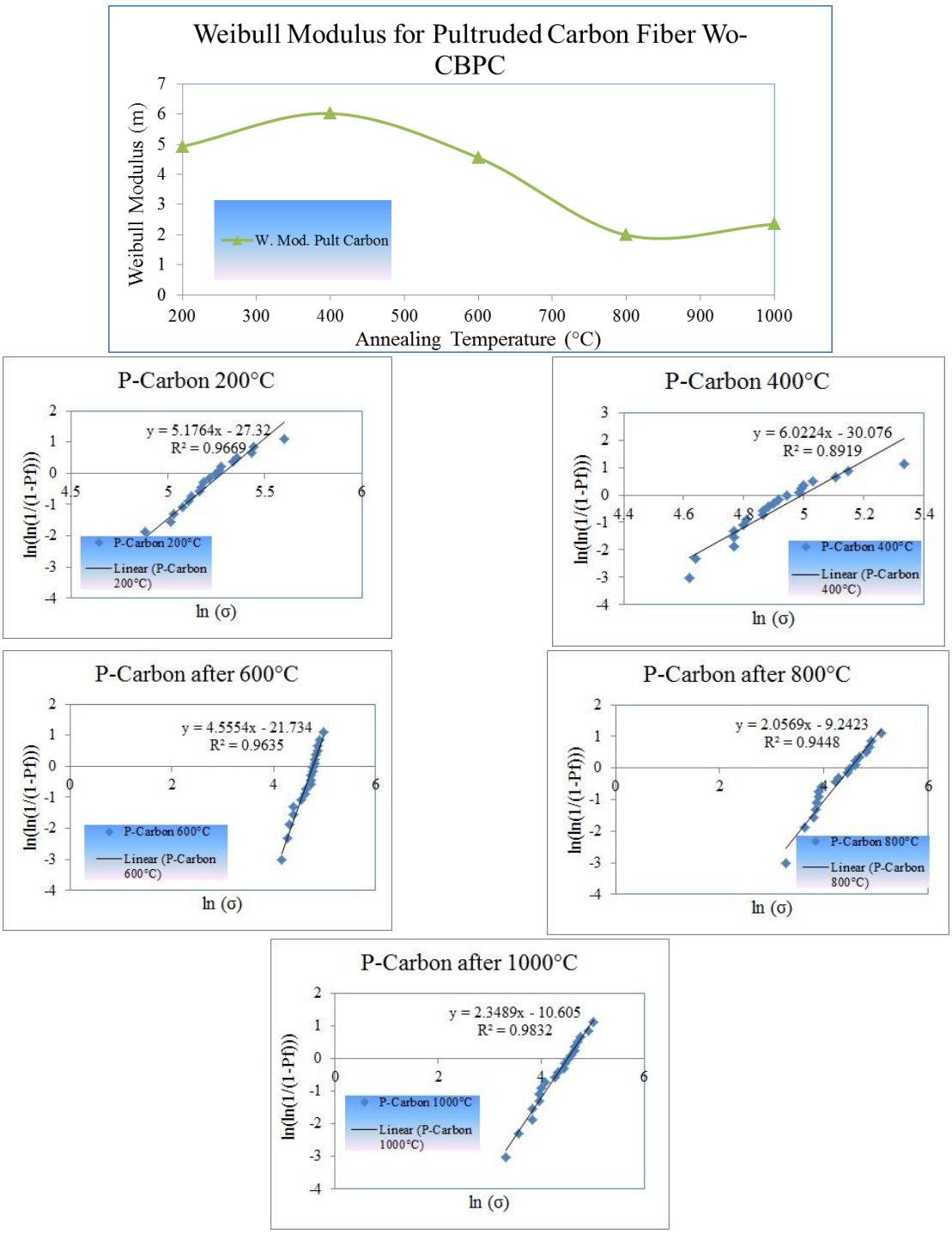

Figure 56 Weibull modulus as a function of the exposure temperature and its corresponding curves fit for the pultruded carbon fiber reinforced Wo-PC composites.

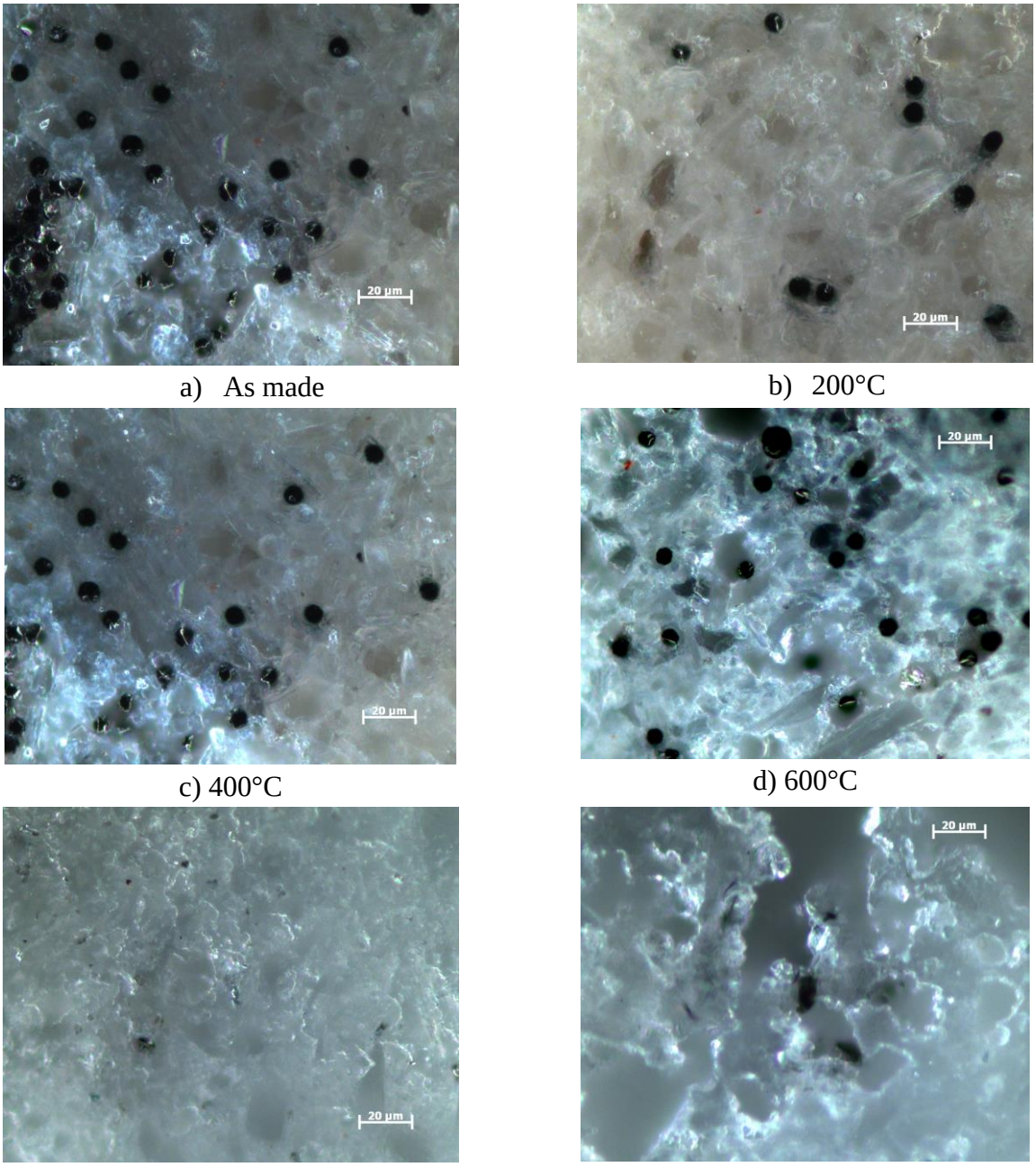

a) As made b) 200°C

c) 400°C d) 600°C

e) 800°C f) 1000°C

Figure 57 Optical microscopy images of the carbon fiber-reinforced composite at different exposure temperatures.

It is observed that as the exposure temperature is increased, the fiber degradation starts mostly at the interface, Figure 58a and b. At 600°C, the degradation of the carbon fibers is significant. At

800°C, most of the fiber is oxidized. At 1000°C, the holes that remain in the PC are the only sign of evidence of the lost fiber.

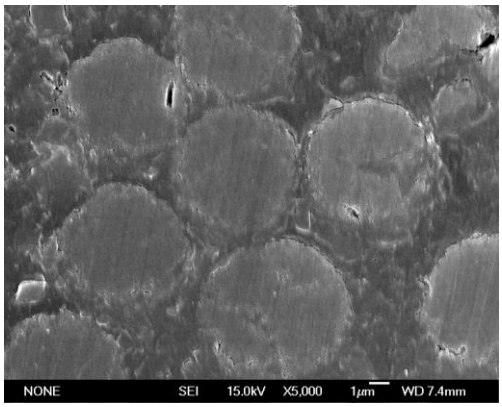

a) 200°C

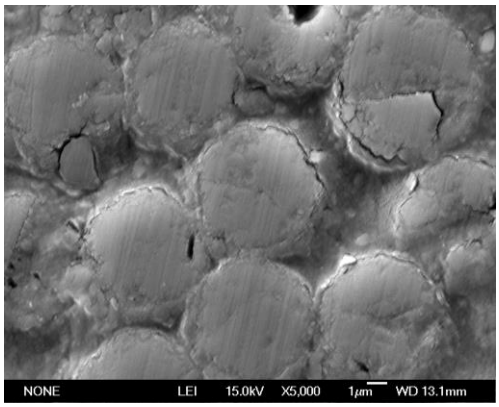

b) 400°C

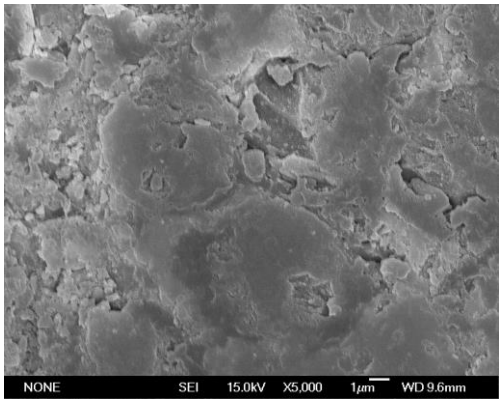

c) 600°C

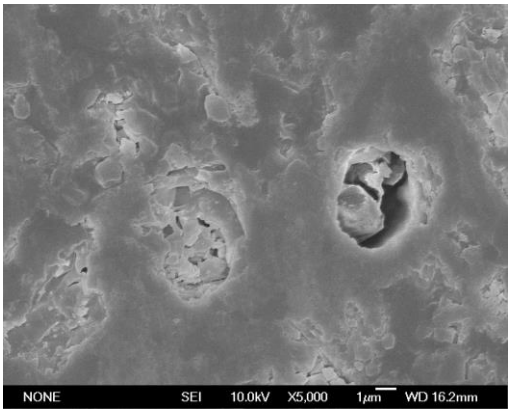

d) 800°C

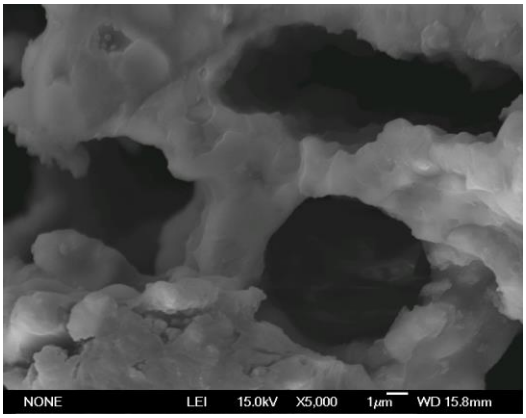

d) 1000°C

Figure 58 Cross section images of the carbon fiber-reinforced composite at different exposure temperatures.

Figure 59a shows the carbon fiber-reinforced composite exposed to 400°C for 1h. It is seen that both interface and the interior of the fiber do not seem significantly affected in the structure. Quantitative EDS atomic percentages show that “C” is very constant inside the fiber. “C/O” is more varied inside the fiber, which shows an heterogeneous oxidation process.

Figure 60a shows carbon fiber-reinforced composite exposed to 600°C for 1h. Some structural damages start to appear. Quantitative EDS atomic percentages show that “C” concentration is still homgeneous inside the fiber. The concentration of “C/O” shows a significant oxidation of the fiber when is compared with results at 400°C for 1h.

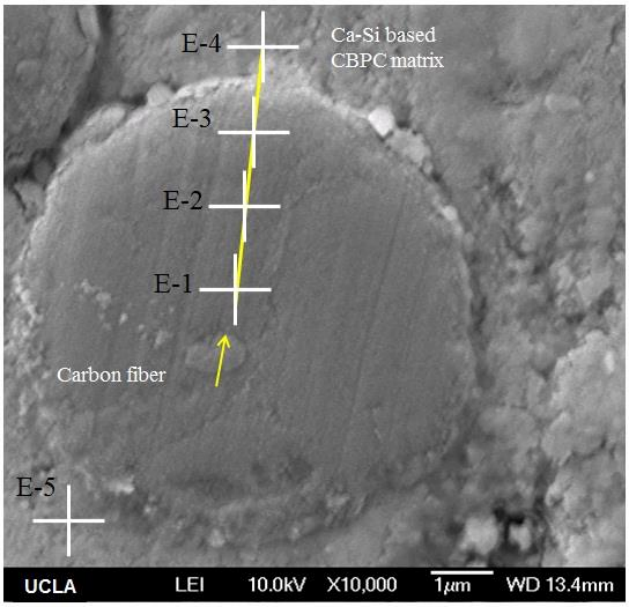

EDS Quantification of atomic percentages

Point	Ca	P	Si	C	O	Ca/P	Ca/Si	Ca/C	C/O
E1	0.13	0.87	0.15	93.18	1.62	0.15	0.87	0.00	57.52
E2	0.12	0.68	0.15	93.96	1.26	0.18	0.80	0.00	74.57
E3	0.23	0.66	0	93.87	2.26	0.35	-	0.00	41.54
E4	4.53	9.28	0.81	56.81	18.57	0.49	5.59	0.08	3.06
E5	2.08	4.34	25.98	25	33.46	0.48	0.08	0.08	0.75

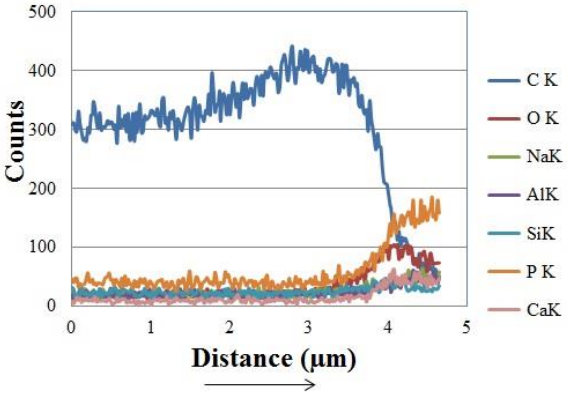

a)

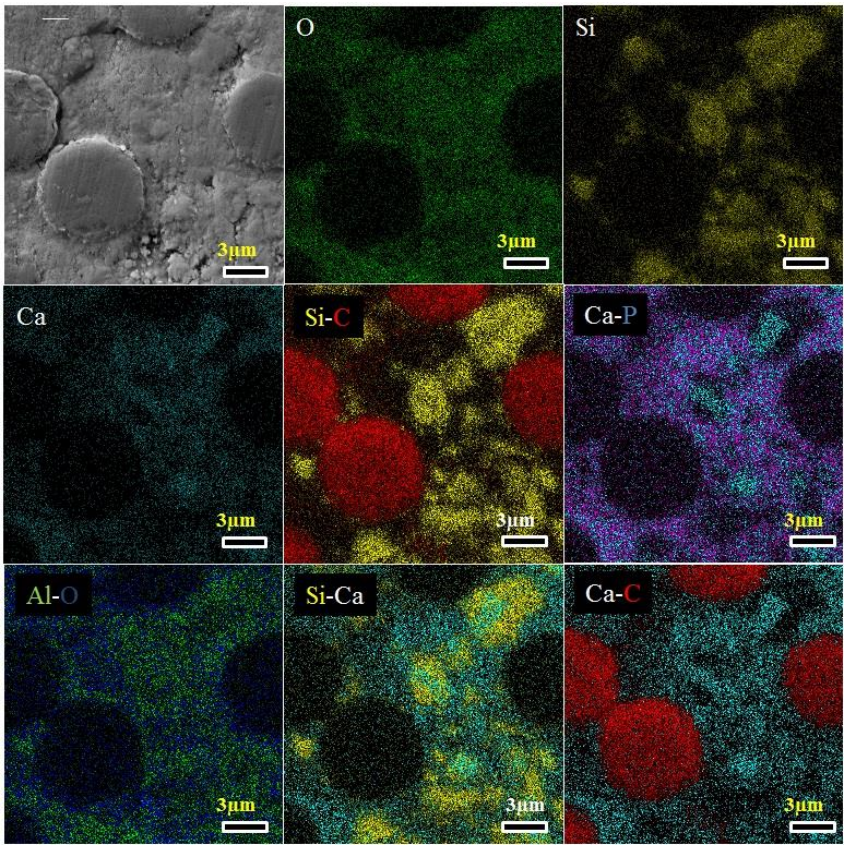

b)

Figure 59 a) SEM image and EDS-SEM X-ray maps for carbon fiber-reinforced composite exposed to 400°C for 1h.

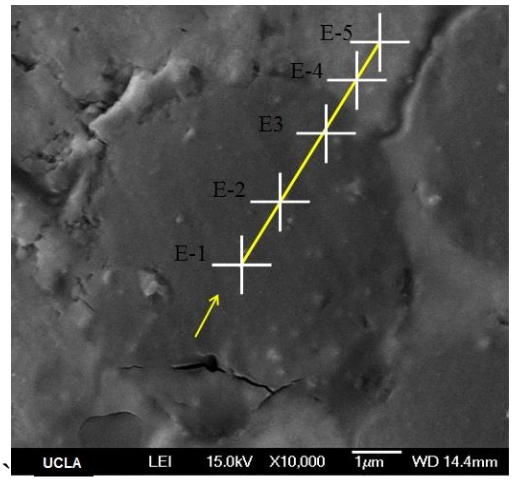

EDS Quantification of atomic percentages

Point	Ca	P	Si	C	O	Ca/P	Ca/Si	Ca/C	C/O
E1	0.12	0.31	0.12	93.71	0.95	0.39	1.00	0.00	98.64
E2	0.11	0.28	0.09	93.14	2.22	0.39	1.22	0.00	41.95
E3	0.22	0.51	0.18	93.64	2.02	0.43	1.22	0.00	46.36
E4	0.91	1.57	0.52	86.54	5.03	0.58	1.75	0.01	17.20
E5	4.32	7.42	1.62	57.4	19.71	0.58	2.67	0.08	2.91

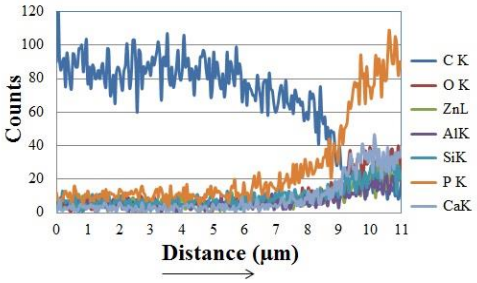

a)

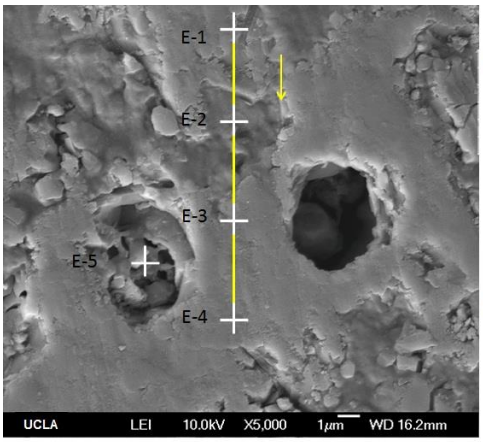

EDS Quantification of atomic percentages

Point	Ca	P	Si	C	O	Ca/P	Ca/Si	Ca/C	C/O
E1	19.86	9.26	5.72	49.07	11.02	2.14	3.47	0.40	4.45
E2	7.75	4.69	26.22	27.8	27.8	1.65	0.30	0.28	1.00
E3	32.92	20.84	4.68	15.59	20.13	1.58	7.03	2.11	0.77
E4	30.54	20.87	1.41	17.83	24.16	1.46	21.66	1.71	0.74
E5	9.33	5.49	21.17	22.94	37.51	1.70	0.44	0.41	0.61

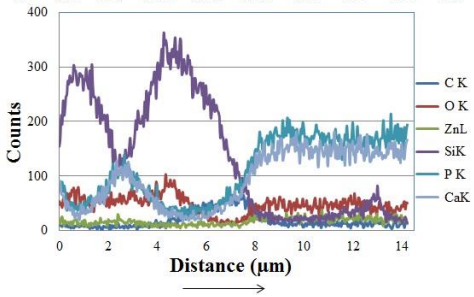

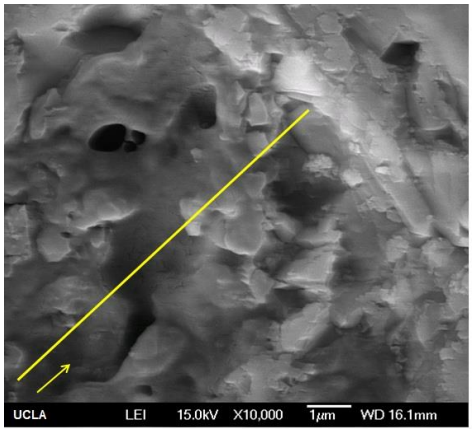

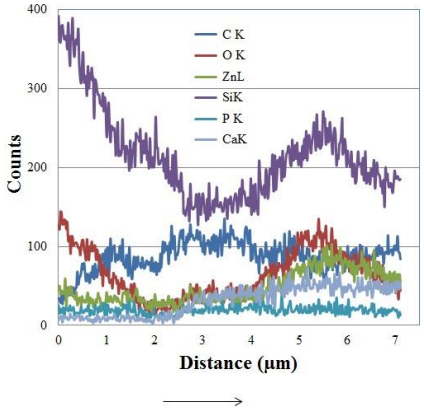

b)

Figure 60 EDS-SEM for cross section of the carbon fiber-reinforced composite exposed for 1h to a) 600°C, and b) 800°C.

Figure 61 shows carbon fiber-reinforced composite exposed to 1000°C for 1h. As shown by the holes feibers used to occupy, they are completely oxidated into CO_2 and CO. At this time the PC matrix is also very affected by the heat and as expained in a chapter before, matrix have gone under several transformations which affect their structural and chemical stability. Quantitative EDS atomic percentages show that both "C" and "C/O" are relatively homogeneously distributed. Although in this sample having smooth or continious surface is a challenge, it is seen in the x-ray maps that "Ca", "Si", and "P" diffused out of the fiber and appeared consistently in the matrix.

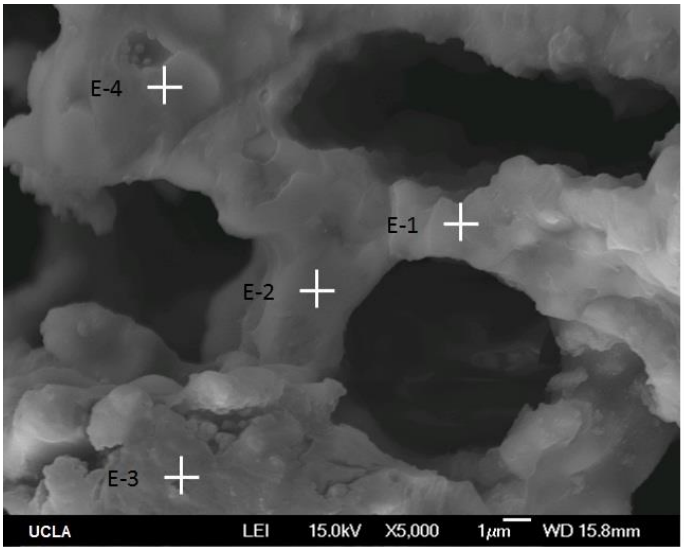

EDS Quantification of atomic percentages

Point	Ca	P	Si	C	O	Ca/P	Ca/Si	Ca/C	C/O
E1	9.82	6.87	18.67	15.87	47.87	1.43	0.53	0.62	0.33
E2	31.62	19.36	2.31	15.13	30.98	1.63	13.69	2.09	0.49
E3	29.86	21.45	2.69	14.84	29.68	1.39	11.10	2.01	0.50
E4	1.74	4.08	30.84	15.95	43.13	0.43	0.06	0.11	0.37

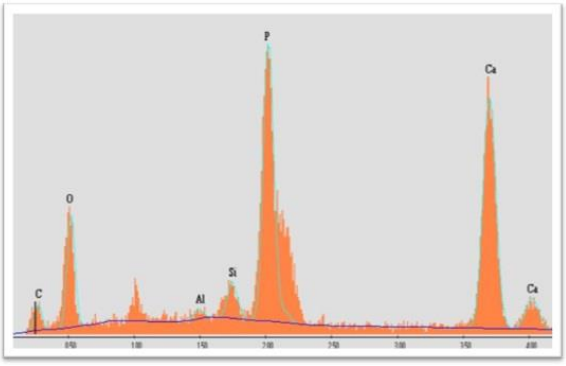

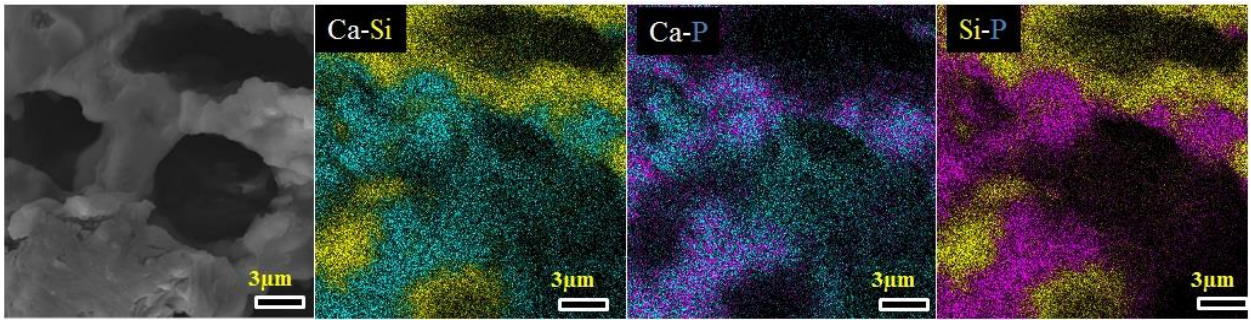

Figure 61 EDS-SEM X-ray maps for cross section of the carbon fiber-reinforced exposed to 1000°C for 1h.

6.3.3 Wo-PC matrix basalt fibers composites

The Weibull distribution of pultruded basalt fiber reinforced Wo-PC composites at different exposure temperatures is shown in Figure 62. For all samples, the thermal process was conducted for1h. As occurred for glass and basalt fibers, the temperature increase moved the curves toward the low bending strength values and reduced the variability as well.

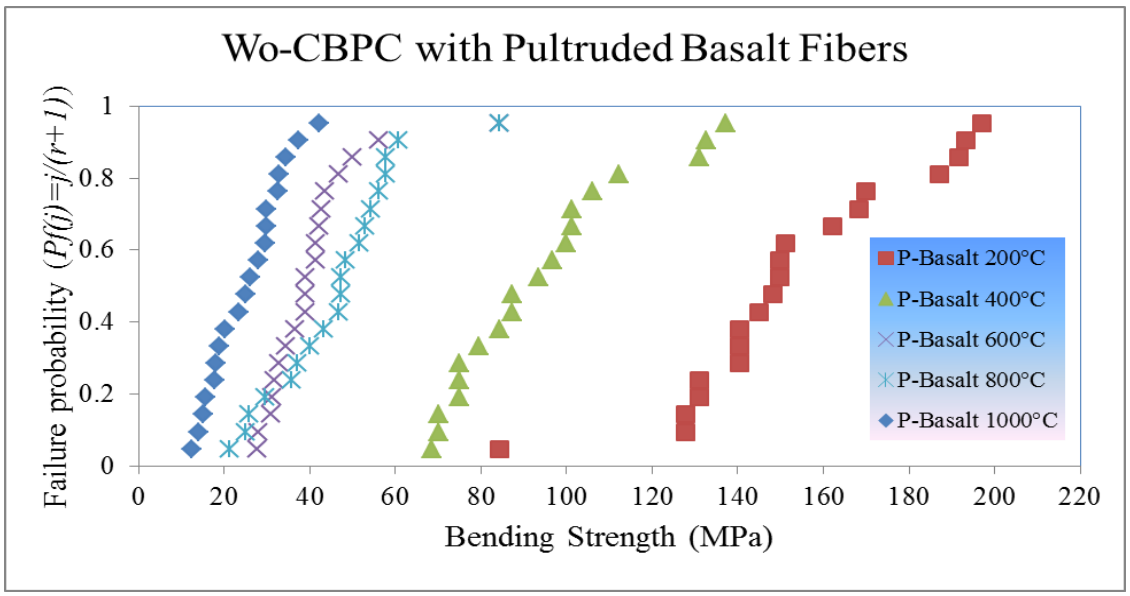

Figure 62 Weibull distribution of Wo-PC with different pultruded basalt fibers.

Figure 63 shows the Weibull modulus for the composite of Figure 62. All fit curves are included. It is shown than as temperature increases, the modulus increases in a monotonic function. This curve is explained with the microsctructure shown in Figure 64, the fiber stability in the ceramic matrix as temperature increases.

Figure 64a, b, c, d, e and f show cross section images of the composite at room temperature, 200°C, 400°C, 600°C, 800°C, and 1000°C respectively. Figure 21a shows the composite as made. It is observed that as the exposure temperature is increased, fibers show changes in color.

At 800°C, fiber turns darker as an effect of the oxidation. At 1000°C, the color of the fiber became ligher and some melting is observed. This melting dissolves some of the components into the PC matrix, such as the red compound, which is moslty FeO.

Figure 65a, b, c, d, e and f are SEM images of the composite at room temperature, and after exposed to 200°C, 400°C, 600°C, 800°C, and 1000°C respectively. Figure 65a shows the composite as made. It is observed that even after the exposure to 1000°C, some fibers remain without much structural damage in the core while others show very significant degradation. This behaviour evidence an heterogenous oxidation-degradation of the fiber due to the variability in the matrix composition surrounding the fiber.

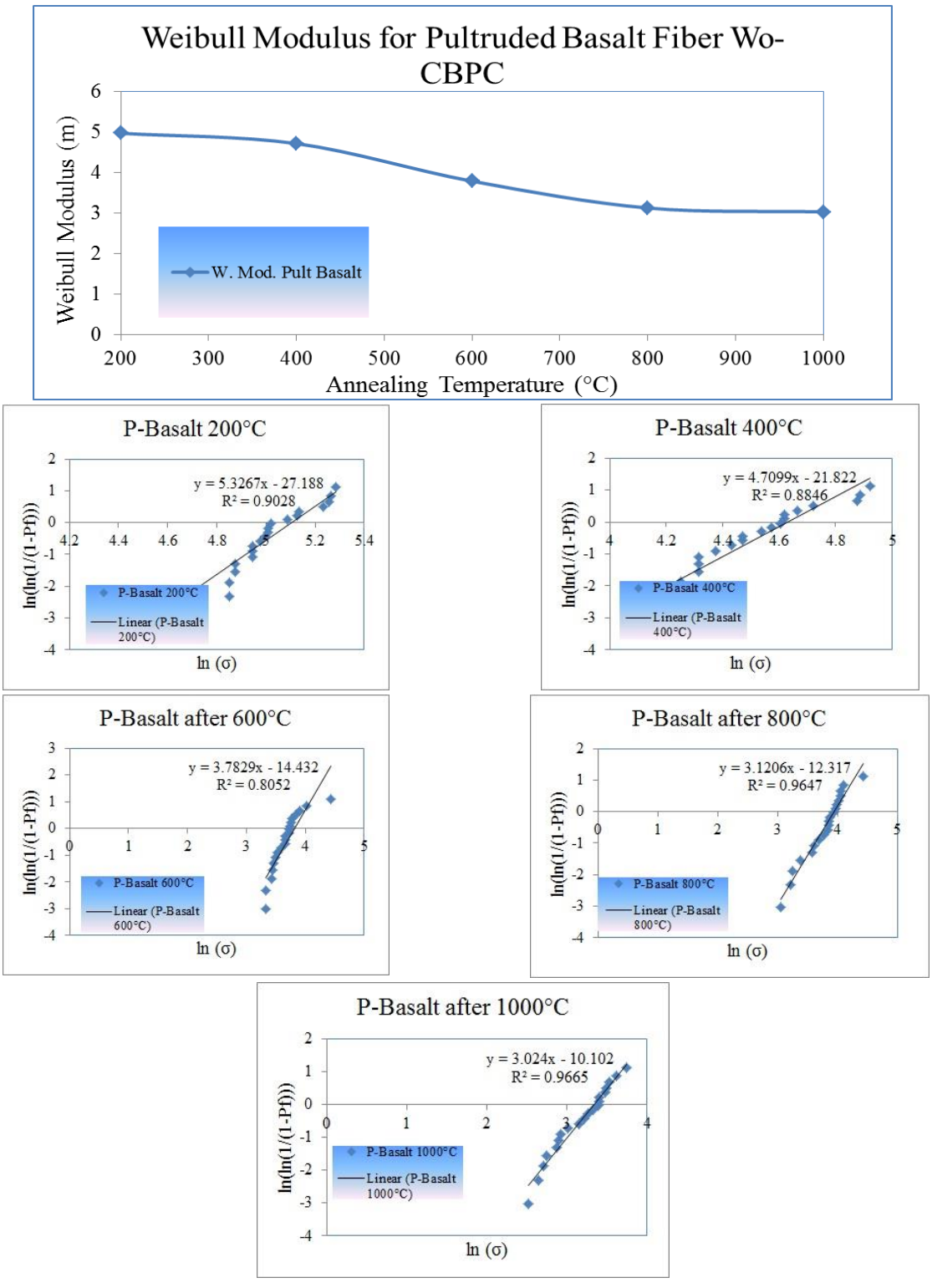

Figure 63 Weibull modulus as a function of the exposure temperature and its corresponding curves fit for the pultruded basalt fiber reinforced Wo-PC composites.

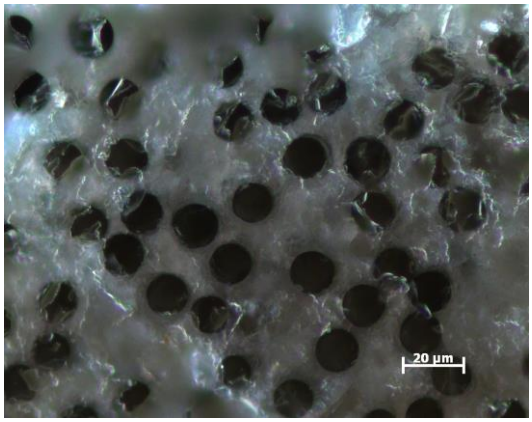

a) As made

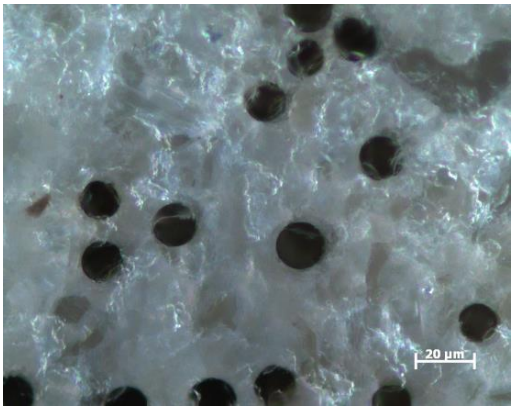

b) 200°C

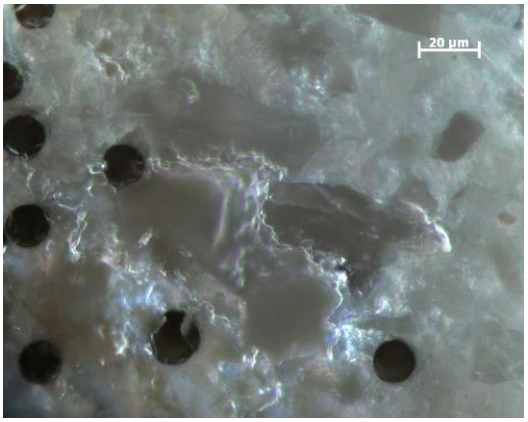

c) 400°C

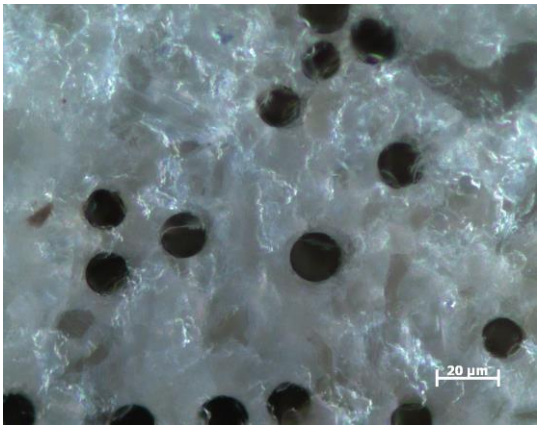

d) 600°C

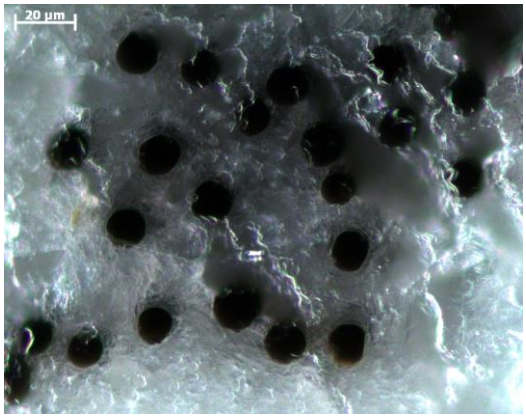

e) 800°C

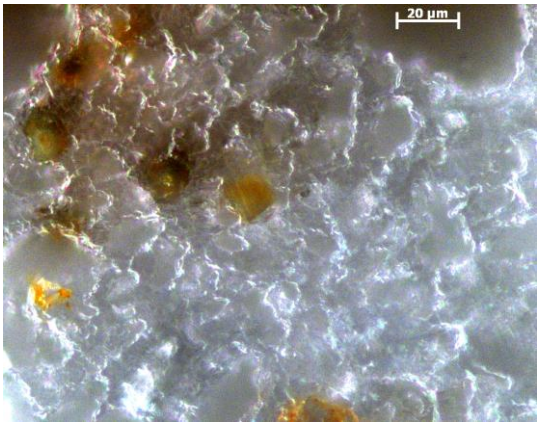

f) 1000°C

Figure 64 Optical microscopy images of the basalt fiber-reinforced composite exposed to different temperatures.

Figure 66a shows basalt fiber-reinforced composite exposed to 400°C for 1h. The EDS-line shows that inside the fiber first “Si” and second “Al” dominates the composition. In the matrix,

first “P” and then “Ca” dominate. The quantification of the atomic percentages shows that “P” content increases as we move outside the fiber. Also, inside the fiber the “Fe”, “Si” and “Ca” atomic percentages are almost constant, which indicated that the fiber composition did not change significantly.

However, “P” content coming from the matrix was detected at about 2μm of the fiber/matrix interface. Figure 66b shows EDS maps for the composite exposed to 400°C for 1h. From these maps, basalt fiber is qualitatively identified by its higher “Al” content when compared to the matrix.

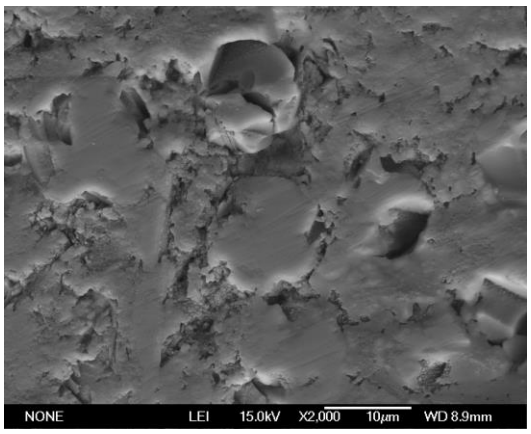

a) 200°C

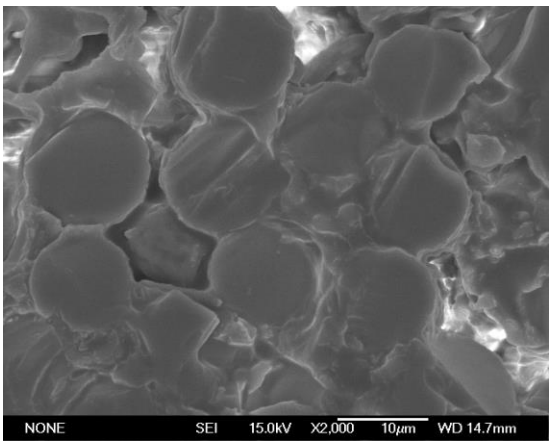

b) 400°C

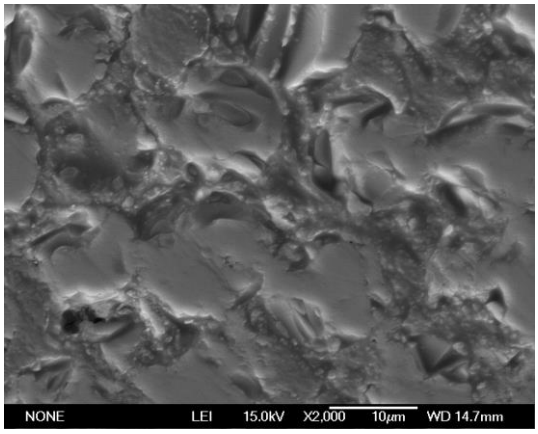

c) 600°C

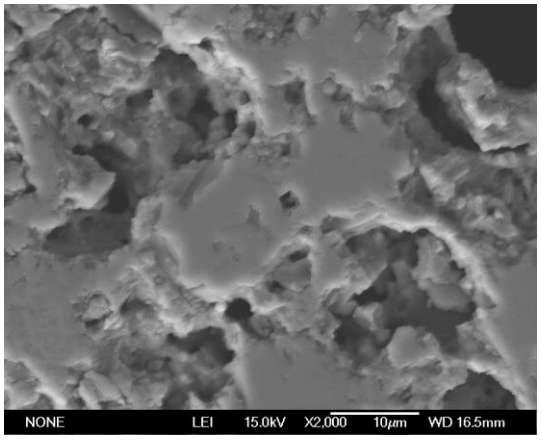

d) 800°C

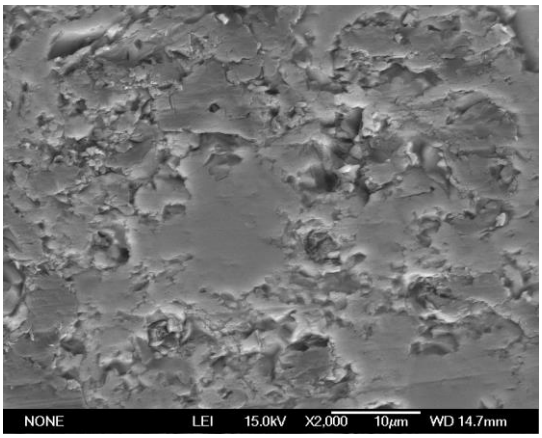

e) 1000°C

Figure 65 Cross section view images of the basalt fiber-reinforced composite exposed to different temperatures.

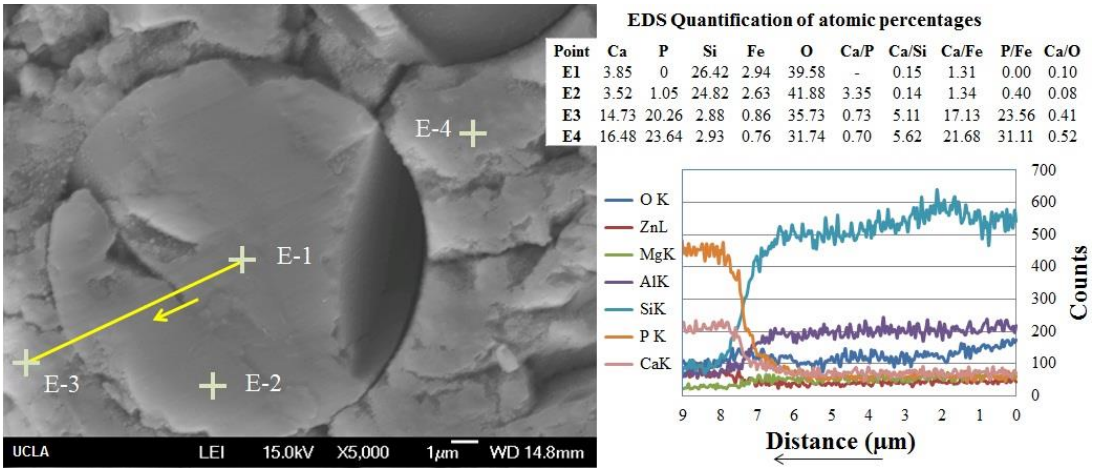

a)

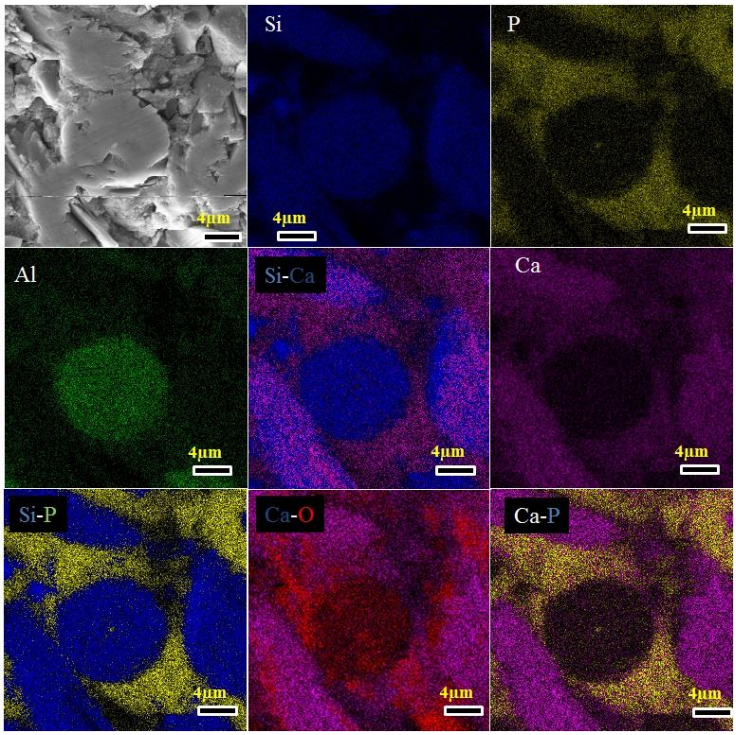

b)

Figure 66 a) SEM image and EDS-SEM X-ray maps for basalt fiber-reinforced composite exposed to 400°C for 1h.

Figure 67a shows the basalt fiber-reinforced composite exposed to 600°C for 1h. The EDS-line shows the compositional profile of elements in a region including two basalt fibers. The "Si" content decreases near the interface and almost no "P" was detected in between the fibers. Also,

inside the fiber the “Fe”, “Si” and “Ca” atomic percentages are completely different (when compared with results at 400°C, which indicated a significant change in the fiber composition. This shows that basalt fibers are not stable chemically at this temperature in these oxidation environments. Figure 67b shows EDS-SEM for the same composite exposed to 800°C. There is damage in the matrix.

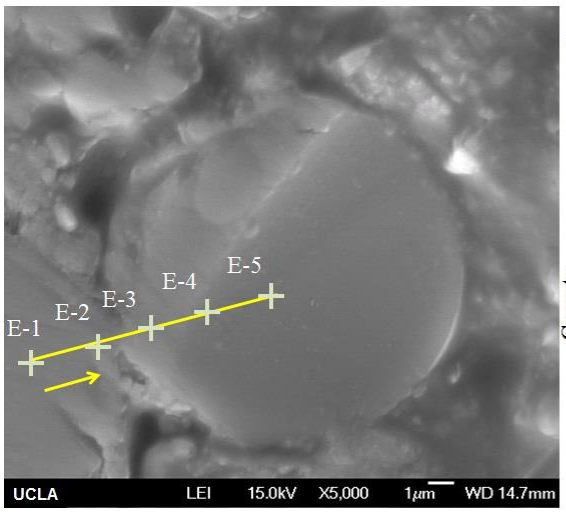

EDS Quantification of atomic percentages

Point	Ca	P	Si	Fe	O	Ca/P	Ca/Si	Ca/Fe	P/Fe	Ca/O
E1	4.14	1.68	22.82	3.24	26.58	2.46	0.18	1.28	0.52	0.16
E2	2.51	13.54	6.79	1.27	28.46	0.19	0.37	1.98	10.66	0.09
E3	2.45	5.3	5.52	1.71	12.93	0.46	0.44	1.43	3.10	0.19
E4	0.61	1.56	2.92	0.54	12.4	0.39	0.21	1.13	2.89	0.05
E5	1.83	1.58	14.88	1.83	33.6	1.16	0.12	1.00	0.86	0.05

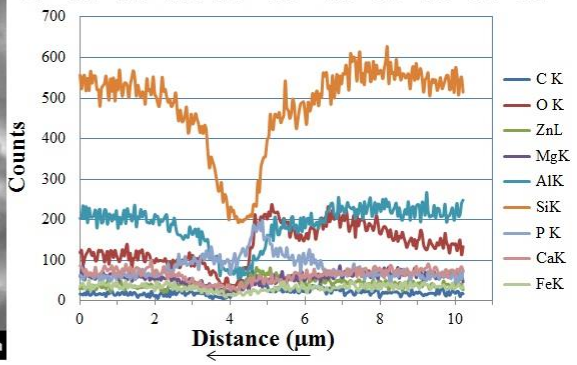

a)

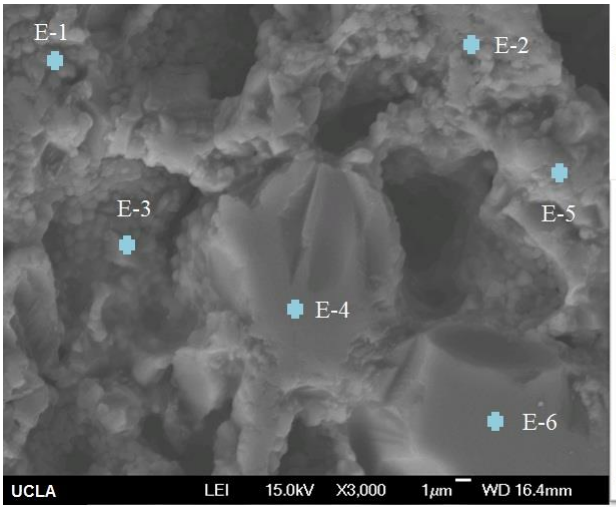

EDS Quantification of atomic percentages

Point	Ca	P	Si	Fe	O	Ca/P	Ca/Si	Ca/Fe	P/Fe	Ca/O
E1	14.18	17.3	11.44	0.96	20.05	0.82	1.24	14.77	18.02	0.71
E2	6.31	6.23	6.92	0.22	43.09	1.01	0.91	28.68	28.32	0.15
E3	10.82	18.28	8.33	0.96	23.39	0.59	1.30	11.27	19.04	0.46
E4	2.93	0.68	23.76	3.3	33.08	4.31	0.12	0.89	0.21	0.09
E5	0.66	1.33	24.43	0.69	49.27	0.50	0.03	0.96	1.93	0.01
E6	3.63	0.64	25.05	3.55	33.14	5.67	0.14	1.02	0.18	0.11

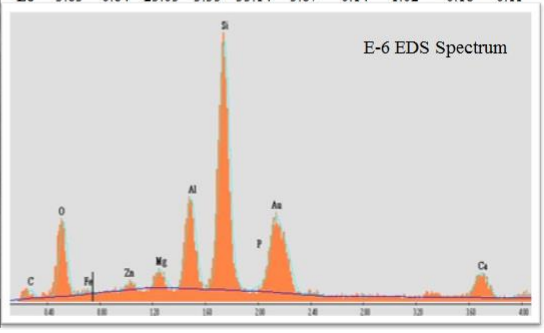

b)

Figure 67 EDS-SEM for cross section of the basalt fiber-reinforced composite exposed for 1h to a) 600°C, and b) 800°C.

Figure 68a shows other area of the composite exposed to 800°C. In this case, the damage is very low. This reveals the high variability in the composition between the matrix and the fiber. Figure 68b shows X-ray maps for the same area shown in Figure 68a.

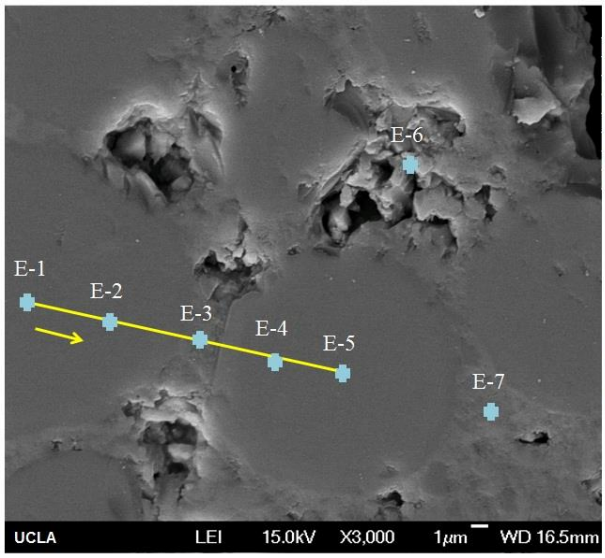

EDS Quantification of atomic percentages

Point	Ca	P	Si	Fe	O	Ca/P	Ca/Si	Ca/Fe	P/Fe	Ca/O
E1	3.34	0	23.31	2.68	31.11	-	0.14	1.25	0.00	0.11
E2	3.96	0	25.3	3.1	31.6	-	0.16	1.28	0.00	0.13
E3	6.8	11.37	15.97	0.79	33.6	0.60	0.43	8.61	14.39	0.20
E4	3.13	1.76	22.96	2.82	31.79	1.78	0.14	1.11	0.62	0.10
E5	3.68	1.07	24.2	2.96	32.21	3.44	0.15	1.24	0.36	0.11
E6	9.34	12.2	20.82	0.62	38.67	0.77	0.45	15.06	19.68	0.24
E7	12.66	16.88	4.46	0.45	27.9	0.75	2.84	28.13	37.51	0.45

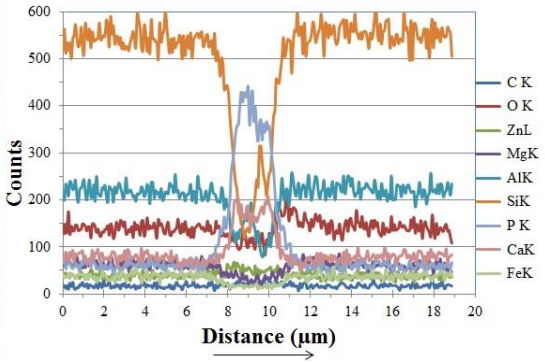

a)

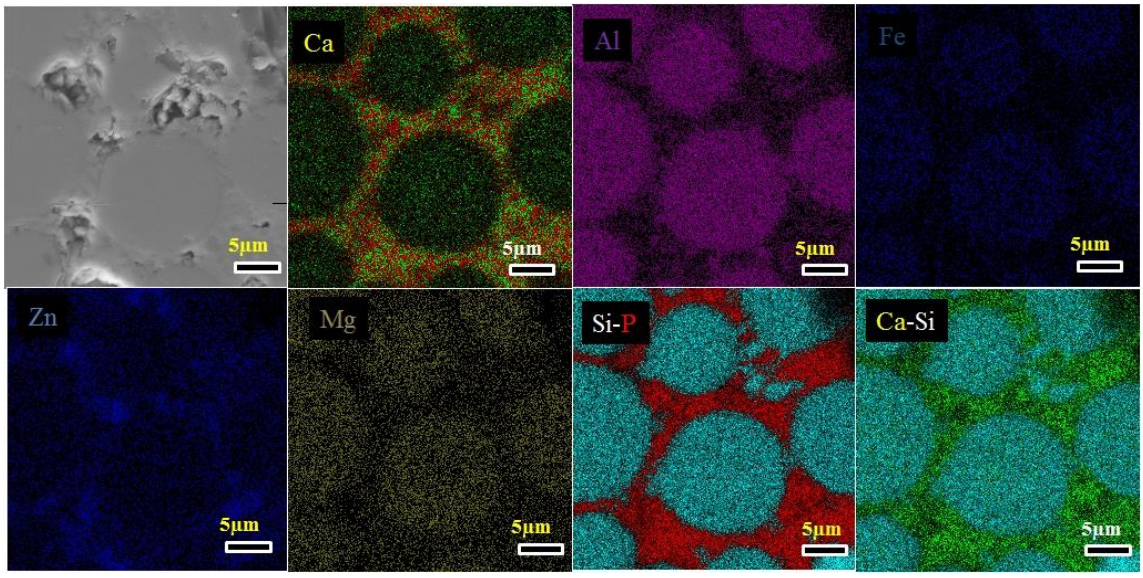

b)

Figure 68 EDS-SEM for cross section of the basalt fiber-reinforced composite exposed for 1h to 800°C, and b) X-ray maps for other area of the same sample.

Figure 69 shows SEM-EDS images for basalt fiber-reinforced composite exposed to 1000°C for 1h. Figure 69a shows a typical microstructure where fibers have been damaged by the oxidation. The points E3 and E4 were took over a residual basalt fiber as the high concentration of Fe indicates. The precipitates (point E3) are due to the crystallization of the fiber (see Chapter 5). Figure 69b shows the compositional profile of elements in a region with a basalt fiber. Although the fiber/matrix interface is completely deteriorated, the core of the fiber looks without significant structural problems. Figure 69c shows the X-ray maps for a place including Figure 69b. “Zn” and “Mg” distributions are very homogeneaous over the image.

6.3.4 Summary of pultruded fiber reinforced PC composites

Figure 70 shows the summary of bending strength results analized with Weibull statistics for Wo-PC pultruded composites exposed to different temperatures. In all exposure temperatures glass, basalt and carbon fibers composites have the lowest, intermedia and highest compressive strength values respectively. It is observed that after the exposure to 400°C the disperssion in the values increased a lot for carbon fibers, which is due to carbon oxidates until completely dissapear in the surface if the composite sample, but some fibers cores mantain the carbon for more time.

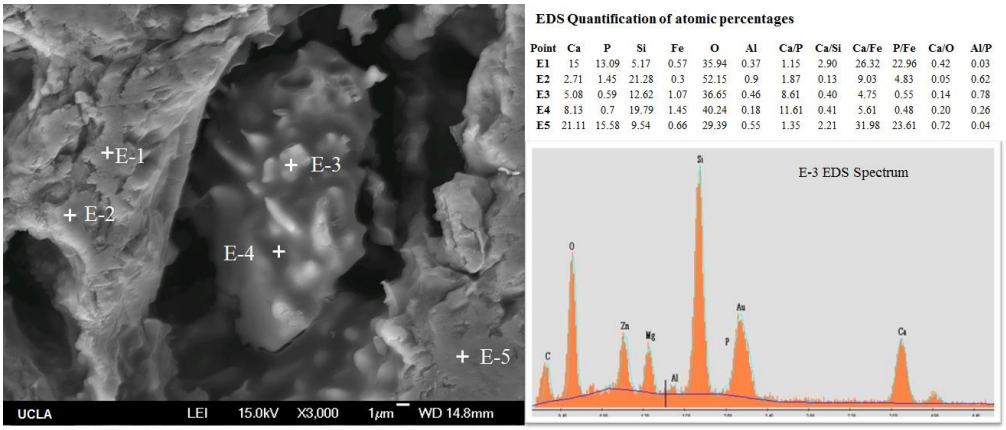

a)

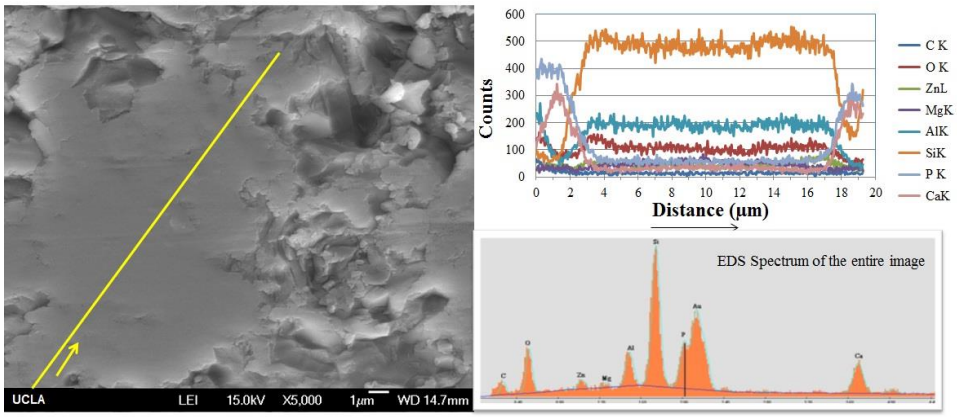

b)

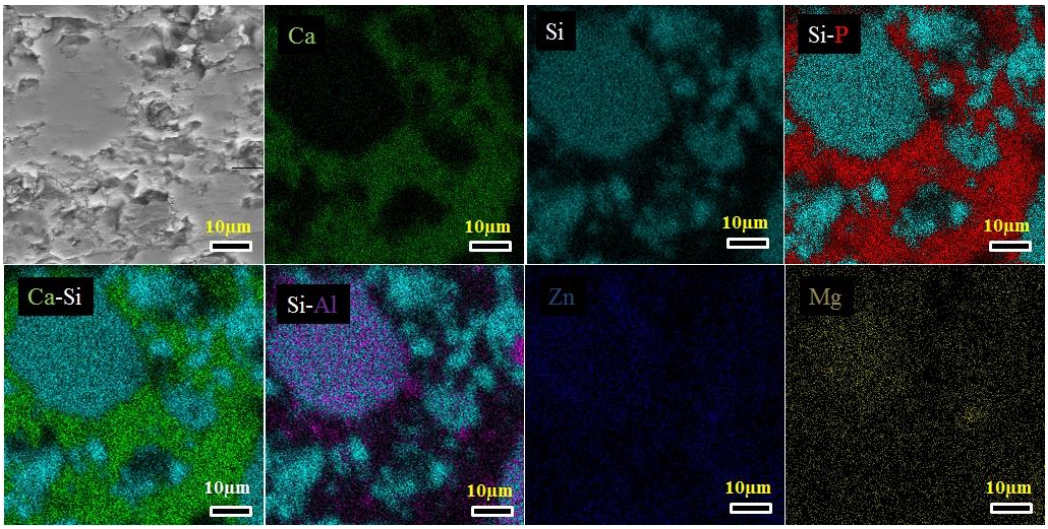

Figure 69 EDS-SEM for cross section of the basalt fiber-reinforced composite exposed to 1000°C for 1h, b) region showing a basalt fiber, and c) X-ray maps (region including b).

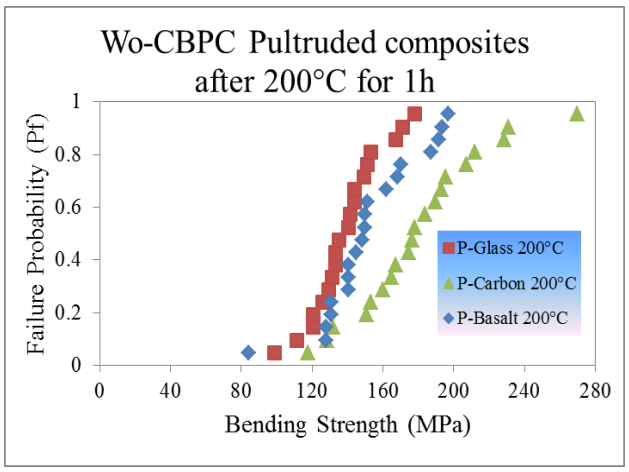

a)

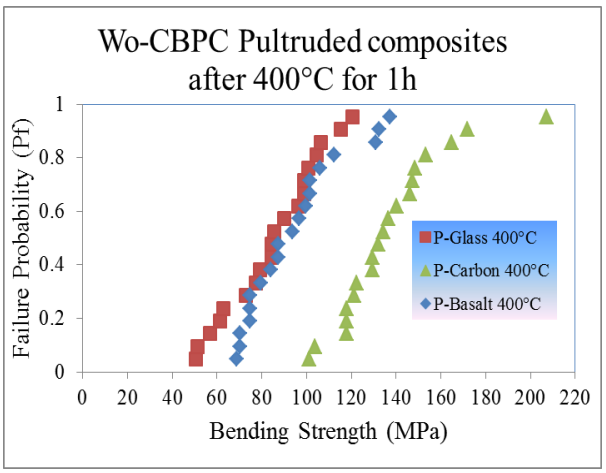

b)

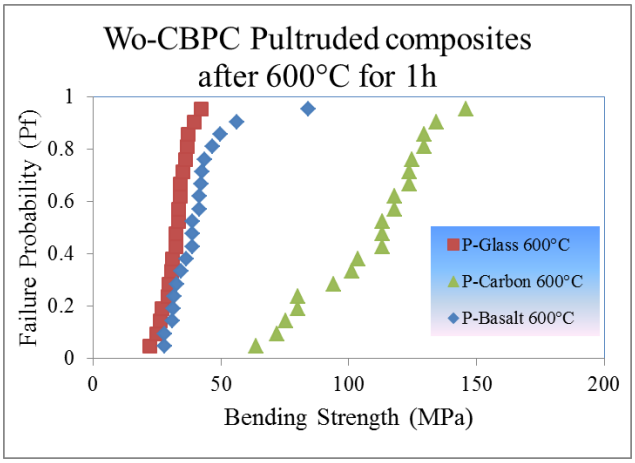

c)

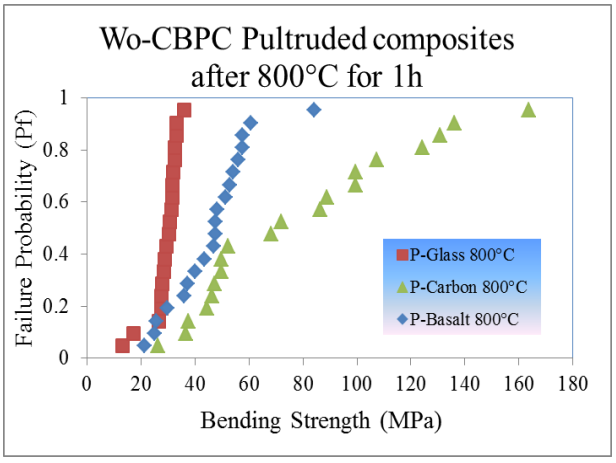

d)

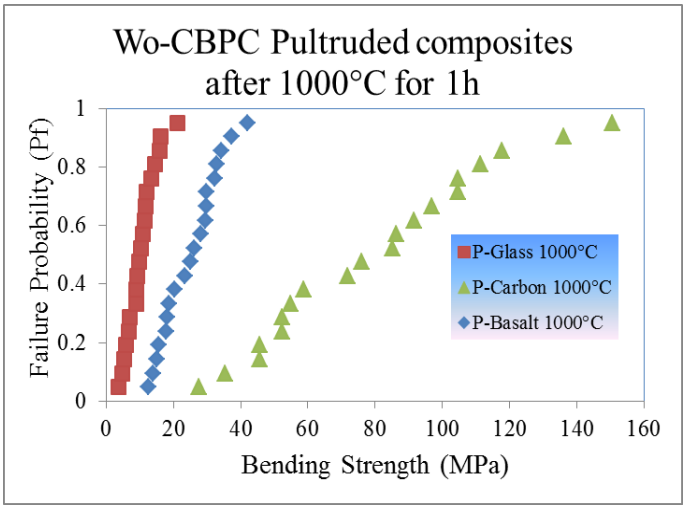

e)

Figure 70 Wo-PC pultruded composites at different temperatures

Figure 71 shows the summary of Weibull modulus for Wo-PC pultruded composites exposed to different temperatures. The variability of the Weibull parameter with temperature was discussed before. The most stable Weibull parameter is the one for basalt fiber composites. The highest modulus for the composite after the heat exposure, which is the better as this indicates less variability, are the modulus for glass fibers exposed to 200°C, carbon to 400°C, glass to 700°C and to 800°C, and basalt to 1000°C.

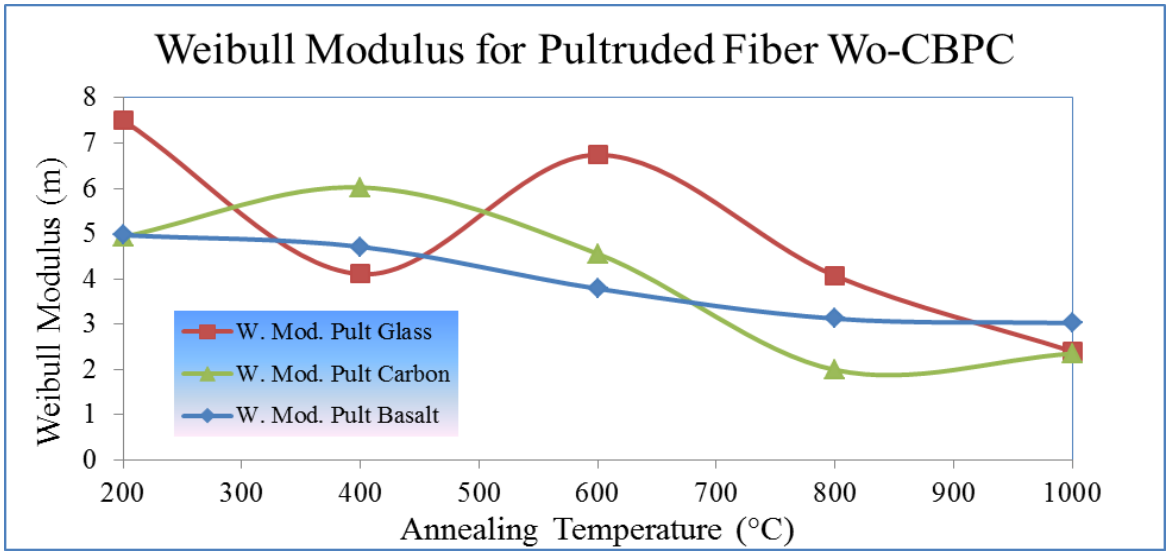

Figure 71 Weibull modulus for pultruded fiber Wo-PC

Figure 72 shows the mean values for the bending strength presented in the Weibull statistics. It is clear the effect of the deterioration in the strength at exposure temperatures over 200°C. As has been discussed before, this is due to a combined effect of the deterioration of the matrix and the fibers.

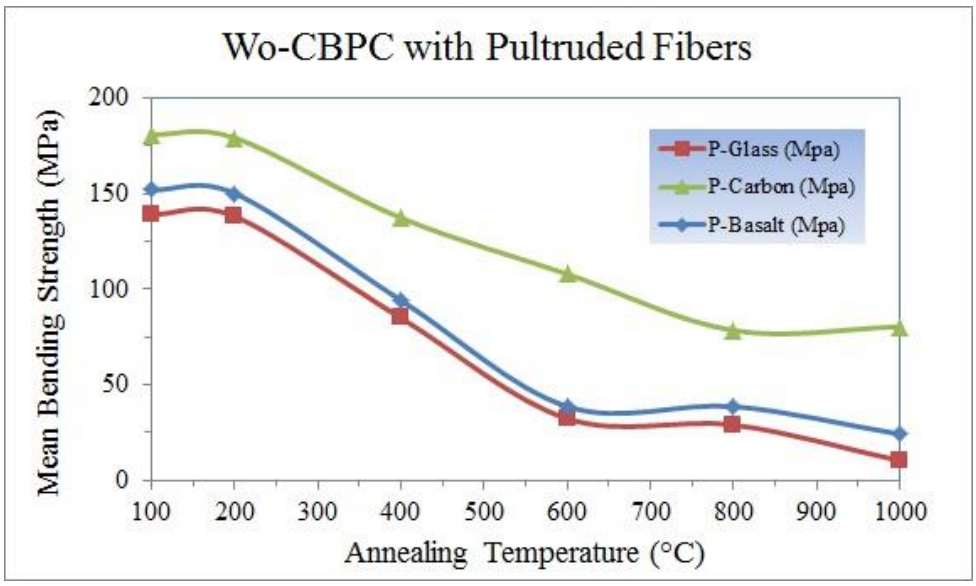

Figure 72 Bending strength values for Wo-PC

Figure 73 shows the normalized results shown in Figure 72. The best composite after the heat exposure is the pultruded carbon fiber-matrix Wo-PC composite. It was shown in Chapter 5 that carbon fibers are the most deteriorate fibers in our experiment. This is due to the oxidation and it is more significant when the fibers are directly exposed to the air. When fibers are surrounded by a ceramic matrix, the oxidation effects decrease. It is observed that the thicker the composite, the most protected the carbon fibers from oxidation.

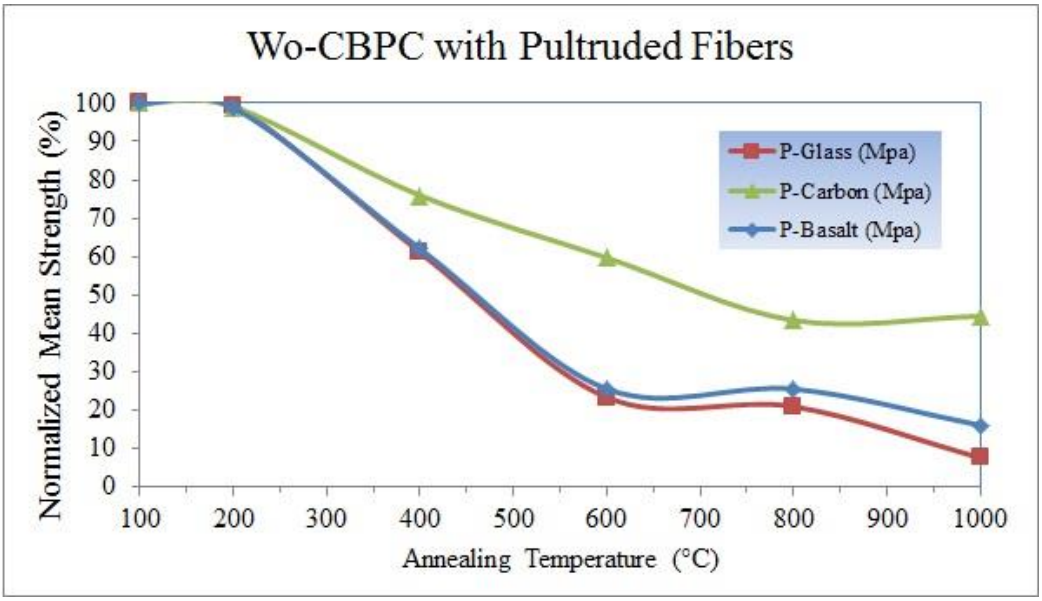

Figure 73 Normalized bending strength mean values for Wo-PC

6.4 Discussion

Figure 74 shows the amount of "Ca", "Si" and "P" atomic % as a function of the distance and temperature in the glass fiber. Each point corresponds to a mean value of 5 data. Figure 74a, b and c summarize the mean values for the atomic percentages of these elements. Data were took at 1 and 4µm from the fiber/matrix interface toward the center of the fiber. "Ca" and "Si" concentrations decrease as temperature increases which means they are diffusing out of the fiber. The main decrease in the concentration of "Ca" and "Si" occurs at 600 and 800ºC, which corresponds to the main transformations in the fiber, as presented in Chapter 5. On the other hand, as temperature increases, "P" concentration decreases, see Figure 74c. In addition, the matrix concentration was taken at 4µm from the fiber/matrix interface (which corresponds with the negative values in Figure 74 d, e and f). The line connecting the fiber and matrix data is schematic because the resolution in the EDAX is about 1µm. Matrix composition is challenging to characterize since it has multiple phases. Therefore, the composition in the matrix is took as a

additonal but not significant data. On the contrary, since fiber composition is homogeneous as received, they can be used to analyze the composition changes in the matrix as temperature increases. It is found for “Ca”, “Si” and “P” up to 600ºC that as temperature increases, the concentration slightly decreases as well, Figure 74g.

Up to 600ºC, “Ca” and “Si” concentration in the fiber decreased. “P” increased after the exposure to 800ºC which is due to the softening and partial melting of both the fiber and some matrix components (see Chapter 4). At exposure temperature of 1000ºC the error in the fiber data is expected to be large since the fiber was melt in areas. On the other hand, for the matrix, taking in to the account the error bars, it is observed that the concentration is realtively constant. However, at exposure temperatures higher than 600ºC, meanwhile in the fiber the “Ca”, “Si” and “P” concentrations decrease, in the matrix tends to increase, which is explained as interdifussion.

Figure 75 shows the amount of “Ca”, “Si” and “P” as a function of the distance and temperature in the basalt fiber. Figure 75a shows that “Ca” decreases in the fiber as temperature increases. Also, “Ca” is higher at 4µm than at 1µm although the error is large (Figure 75g). At exposure temperature of 1000ºC, “Ca” increases. This is associated to the melting of the fiber and several phases in the matrix (Ca-containing phases such as amorphous calcium phosphates and free-“Ca” phases such as silica) which drags “Ca” ions and particles into the deteriorated basalt fiber. Figure 75b shows that “Si” in general decreases as temperature increases. On the contrary, Figure 75c shows that “P” increases as temperature increases, which is a regular homogenization by diffusion. “P” is coming from the matrix. In Figure 75d, e and f, the matrix concentration was added. In general, it is observed that “Ca” and “P” decreases in the matrix as temeprature increases. On the contrary, for the matrix at 600 and 800ºC, “Si” content decreases.

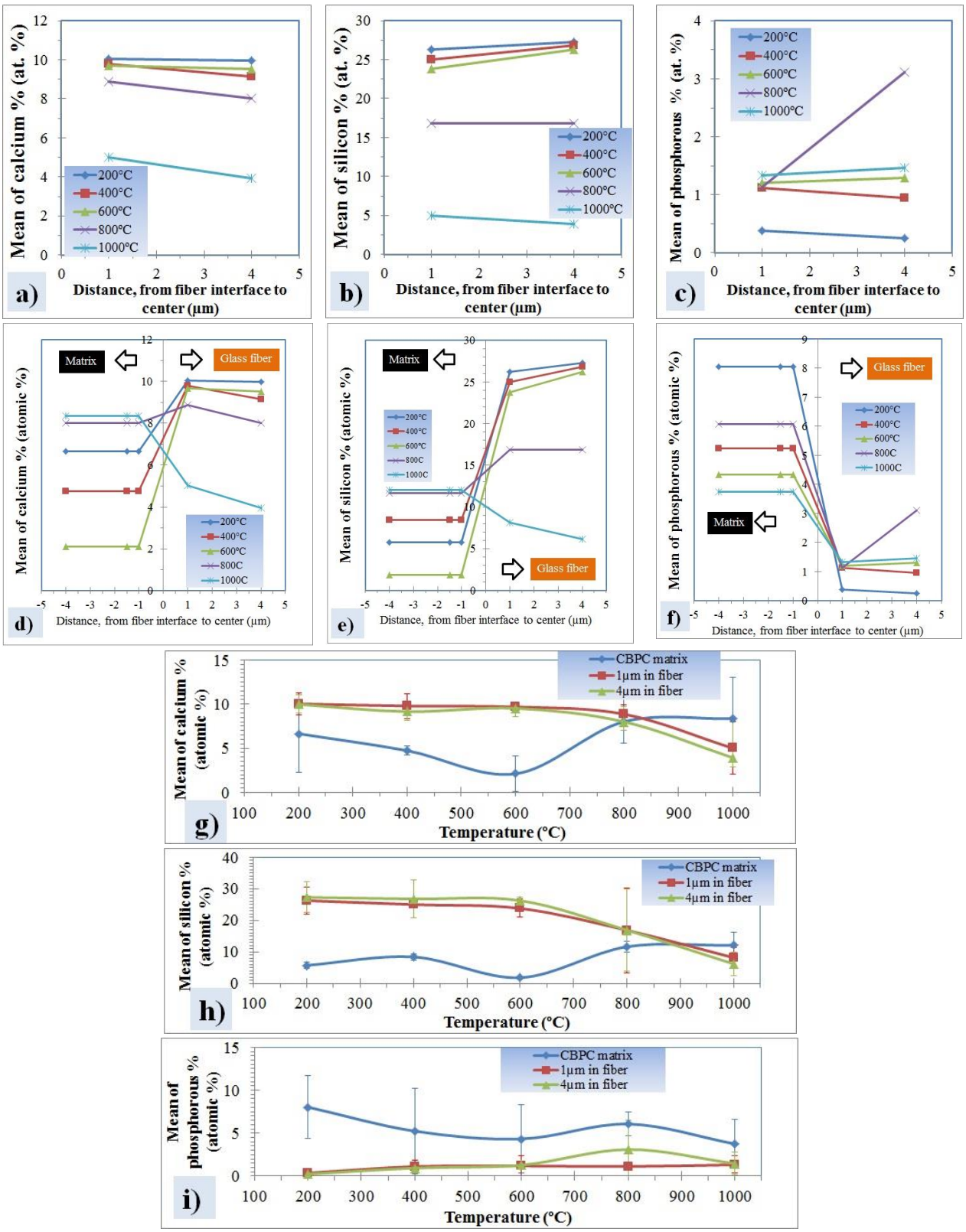

Figure 74 Amount of "Ca", "Si" and "P" as a function of the distance and temperature in the glass fiber.

The summary of the above results as a function of exposure temperature are shown in Figure 75g, h and i. In general, results show the effect of homogenization by diffusion. The interdifussion is so complex but it is seen that in general “Ca”, “Si” and “P” at high temperatures are going into the fiber, although “Ca” and “Si” are diffusing out as well. The fact that all three ions are increasing into the fiber area is explained as a consequence of the basalt fiber deterioration. As shown in Chapter 5, fiber loss a lot of weight (which generates porous, flags and other deffects) and also crystalizes forming “Ca” and “Si” crystalline phases.

Figure 76 shows the amount of calcium, silicon and phosphorous as a function of the distance and temperature in the carbon fiber. The results were obtained only up to 600ºC because over this temperature most of the carbon has been oxidized in gas byproducts as has been discussed in Chapter 5. Figure 76a, b and c, show that as temperature increases, “Ca”, “Si”, and “P” increases as well, which is due to the homogenization by diffusion. Since the carbon fiber does not contain these elements originally, it is a unidirectional diffusion flux, moreover, the carbon oxidation is mostly forming gas byproducts which do not stay in the matrix. Figure 76d, e and f show the matrix “Ca”, “Si” and “P” contents.

In general for all the three elemets the concentration decreases in the matrix as temperature increases (taking into the account the variability due to a multti-phase matrix composition). Finally, Figure 76g, h and i show the concentrations as function of temperature for Ca, Si, and P. The concentration is in general low, mainly due to a lack in thermal activation energy to move atoms through the inerface (matrix/fiber) because of low temperature.

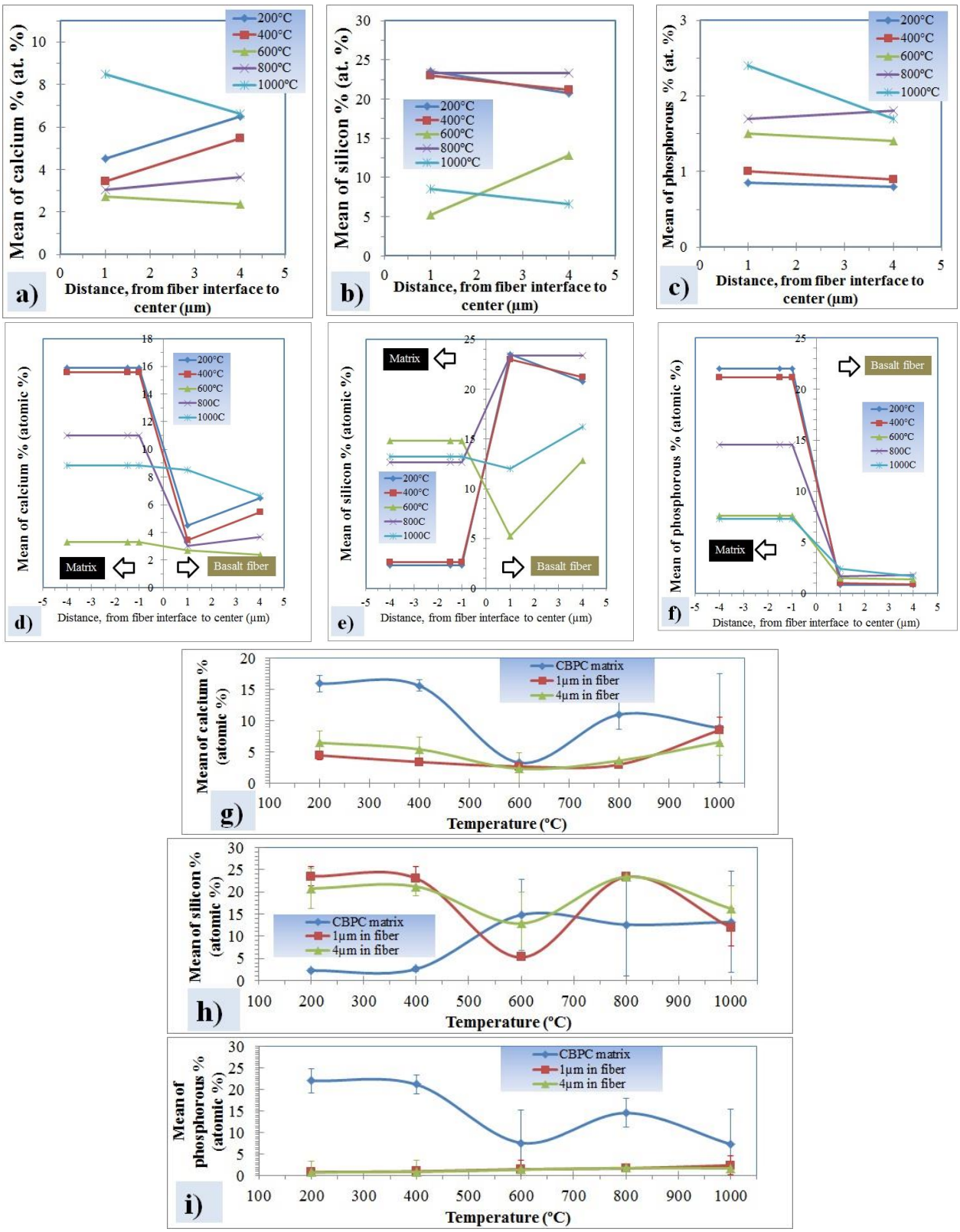

Figure 75 Amount of "Ca", "Si" and "P" as a function of the distance and temperature in the basalt fiber.

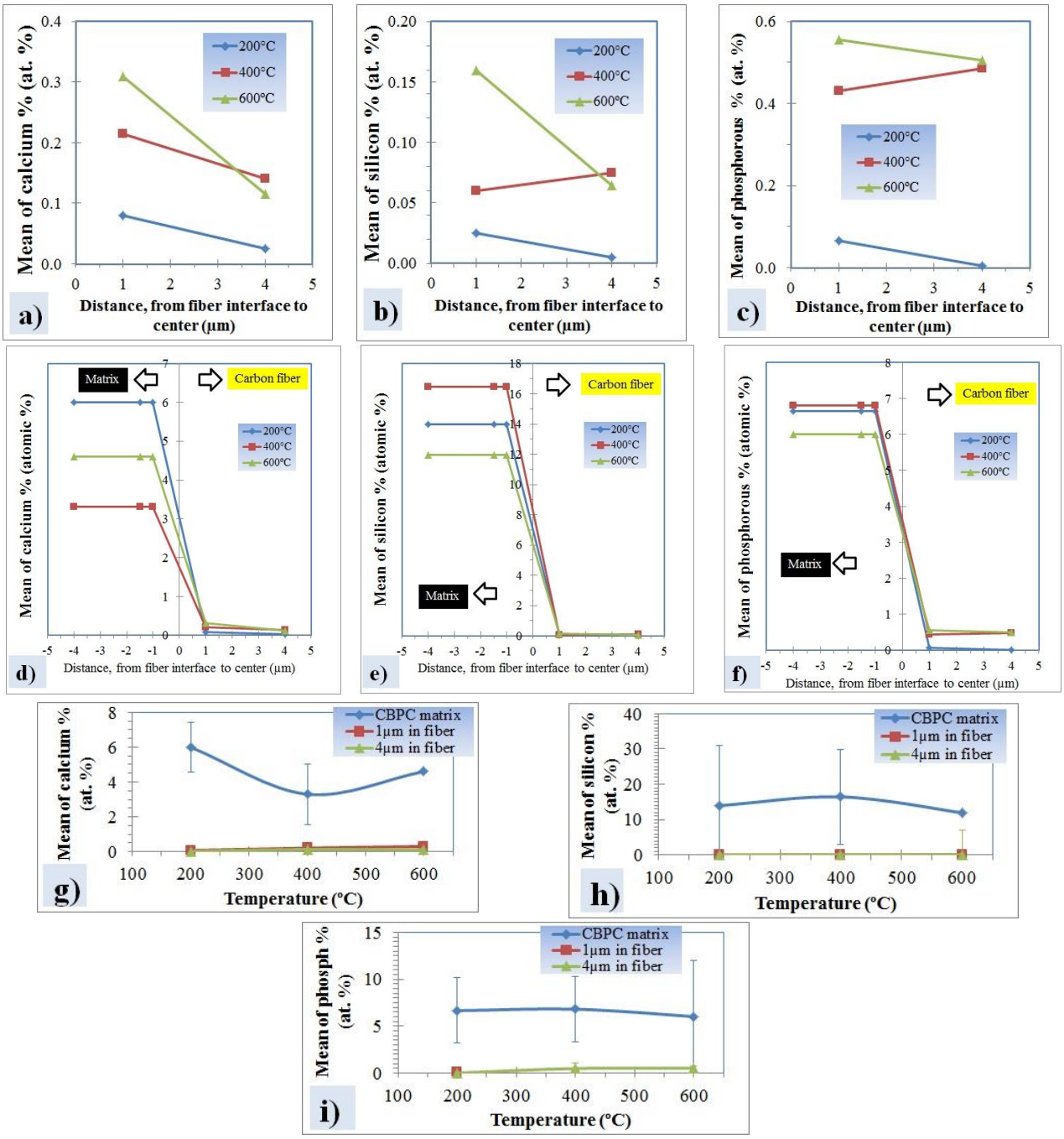

Figure 76 Amount of "Ca", "Si" and "P" as a function of the distance and temperature in the carbon fiber.

Figure 77 shows some general trends from the data presented before for composites exposed to temperatures ≥ 600°C. Figure 77a shows the way data was collected for the images presented

before. Figure 77b shows the general observation for interdiffusion. For glass fiber, mainly after the exposure to 600ºC, "P" is going into the fiber, while "Ca" and "Si" is leaving. For carbon fiber all three Ca, "P" and Si, are diffusing into the fiber, and "C" is lost as a byproduct of the oxidation in CO_2 and CO mainly (see Chapter 5). Figure 77c show a representation of the phenomena observed as temperature increases. This corresponds mainly to a homogenization treatment.

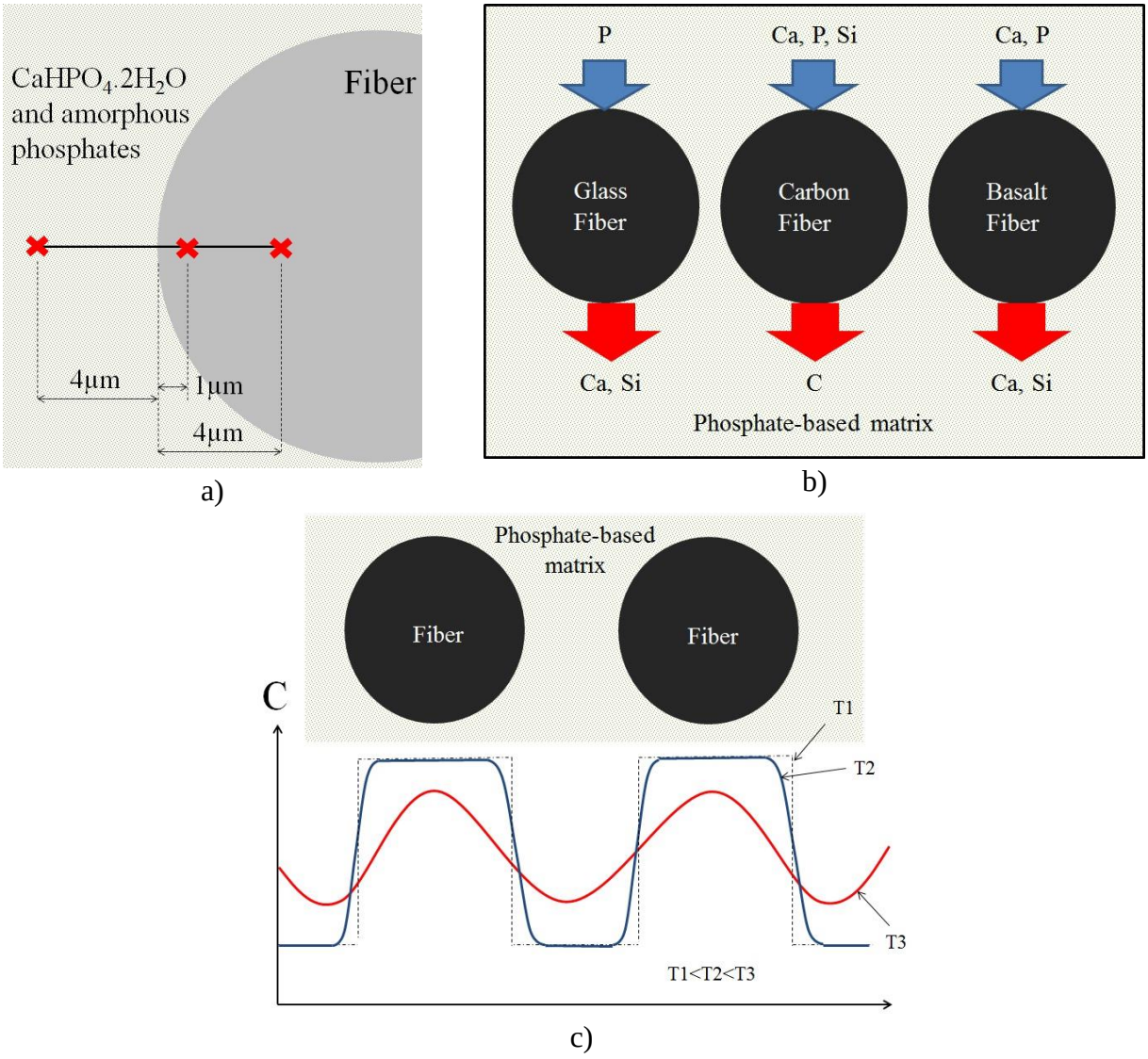

Figure 77 Diagram representing diffusion phenomena between the phosphate-based matrix and the fibers in the wollastonite-based PC at high temperature.

Therefore, in addition to the deterioration at high temperature of both the matrix (e.g. due to the low stability of some of its phases and shrinkage due to water release, see Chapter 4), and the fibers, the interdiffusion through the interface matrix/fiber is a serious source of structural damage for this composites.

Finally, the coefficient of thermal explansion (CTE) was expected to have a higher significant influence on the damage of the composite. The microcracking observed in Chapter 4 did not appear for the fiber reinforced composite. It was not found notorious evidence of damage due to the difference in the CTE between the fibers and the ceramic matrix.

6.5 Future work

The interdifussion at temperatures higher than 600ºC was found to be a significant problem to the thermo-mechanical stability of the fiber reinforced PC fabricated from wollastonite powder by pultrusion. This is a major problem not solved not only for PCs but also for geopolymers, engineering ceramics and cements. Therefore, one solution in this line will be a significant step in the direction of using cements and ceramics under high loads at 1000°C. To decrease the negative impact of this phenomenon, one possible solution will be to use fibers with very similar composition to the matrix. In the case of phosphates, there is not such a commercial fiber yet. The other solution is to use fibers with diffusion barriers, such ceramic coatings. Properties of this coatings eventually could be tailored for diffusion and adhesion properties, and in future could replace the polymeric sizing used in the fiber manufacturing.

In addition, a more detailed study including simulations and longer exposure times could be conducted and implemented as a methodology to understand the behaviour of cementitous materials at high temperature.

6.6 Conclusion

The Wo-PC composite with glass, carbon and basalt fibers exposed to temperatures up to 1000ºC. The deterioration in both the matrix and the fibers was shown by the SEM and is was quantified by three point bending tests. From these tests, Weibull distributions were built and the variability was quite large mainly due to such deterioration at high temperature. The interdifussion was shown by data obtained with EDAX mainly inside the fibers at fixed distances form the fiber/matrix interface and it was shown that this phenomena significantly contribute negatively to the structural and chemical stability. It was found that the carbon fiber composite had the best properties after the exposure to temperatures up to 1000ºC when compared to other fibers. For these fibers, the thicker the composite, the most protected the carbon fibers from oxidation, and therefore, the better reliability for the composite at high temperature.

6.7 References

[1]. Colorado, H. A., C. Hiel, and H. T. Hahn. "Chemically bonded phosphate ceramics composites reinforced with graphite nanoplatelets." Composites Part A: Applied Science and Manufacturing 42.4 (2011): 376-384.

[2]. Sugama T. and Taylor M. (1994). Interfacial and Mechanical Behavior of Fiber-Reinforced Calcium Phosphate Cement Composites. Cement & Concrete Composites 16: 93-106.

[3]. Sid A. Dimitry. (1991). Characterization of reinforced chemically bonded ceramics, Cement and Concrete Composites, Volume 13, Issue 4: 257-263.

[4]. Sean Wise, Kevan Jones, Claudio Herzfeld and David D. Double. (1998). Cropped steel fiber reinforced chemically bonded ceramic (CBC) composites, Mat. Res. Soc. Symp. Proc. Vol. 114, Materials Research Society.

[5]. Mosselmans G, Monique Biesemans, Willem R, Wastiels J, Leermakers M, Rahier H, Brughmans S, and Van Mele B. (2007). Journal of Thermal Analysis and Calorimetry Vol. 88 3 723.
[6]. Alshaaer Mazen. (2006). Optimization of properties of inorganic phosphate cement for construction and high temperature applications. PhD Thesis Vrije Universiteit.
[7]. H. A. Colorado, C. Hiel and H. T. Hahn. (2010). Influence of Particle Size Distribution of Wollastonite on the Mechanical Properties of PC's (Chemically Bonded Phosphate Ceramics). Materials Science & Technology, Conference and Exhibition. October 17-21 in Houston, Texas USA. Submitted for Journal publication in Ceramics Transactions.
[8]. Colorado, H. A., H. T. Hahn, and C. Hiel. "Pultruded glass fiber-and pultruded carbon fiber-reinforced chemically bonded phosphate ceramics." Journal of Composite Materials 45.23 (2011): 2391-2399.

7 Calcium-aluminum acid-base phosphate cements (Al-Ca PCs) for temperatures up to 1000°C

7.1 Introduction

Wollastonite-based PCs (Wo-PCs) and its composite as presented before are significantly deteriorated by the temperatures as low as 400ºC. This produces problems such as low thermal and chemical stability of some phases, shrinkage, micro and macro cracking, inhomogeneity of phase distribution. It is well known that fibers can help to decrease or delay significantly these problems in the composite. Based on this fact, we found successful commercial products that work relatively well under fire environments such as Intelli-Firewall, [1] and [2], made of Wo-PCs. However, PCs are functional materials suitable to be made of more stable phosphates which need to be investigated. New oxides could produce high temperature stable PCs. Therefore, there is a good opportunity to develop new PCs. The aim of this chapter is to develop a new composition that is stable at temperatures up to 1000°C. Since there are many commercial ceramic fibers with high performance at high temperatures, the aim in this chapter is only to produce a new matrix. However, a future work should be conducted in order to find the most appropriate ceramic fibers. Thus, upon the development of a composition stable at high temperature, similar characterization procedures on the fibers and the PC composite as presented in [1] can be followed to understand and optimize the composites.

The new PC presented in this chapter is based on two mineral powders reacting with the phosphoric acid: wollastonite, and alumina (Al_2O_3). Thus, it is a wollastonite-alumina based PC and we can refer to it as Ca-Al-PC because the metal ions that enable the acid base reaction. It can also be known as alumina-based PC just to remember alumina is the raw material that originates the microstructure stable at high temperature.

There have been different approaches to this problem before using traditional cements, most commonly using Portland Cement, the most widespread manmade material in the world. One approach has been the use of high performance concretes in the from calcium aluminate cements ([4]-[8]), CACs. As Portland cement (PC) and CAC are classified as hydraulic cement (cement that not only hardens by reacting with water but also forms a water-resistant product, ASTM C150). For PC, tricalcium (C_3S) and dicalcium silicates (C_2S) form mainly amorphous calcium silicate hydrate (C-S-H) and crystalline calcium hydroxide (CH upon contact with water). In CACs, monocalcium aluminate (CA) upon reaction with water forms calcium aluminate hydrates. However, both PC and CAC are not green cements. PC clinker is made by heating in a rotary kiln at high temperature using a homogeneous mixture of raw materials at about 1450 °C. On the other hand, for CACs, monocalcium aluminate is formed when the appropriate proportions of calcium carbonate and aluminum oxide are heated together until the mixture melts at about1390 °C. This requires high amount of energy and in order to make this process commercially competitive coal is used as a main heat source. In addition, these are alkaline materials. Typically the pH is more than 12, which limits the composites fabrication with some inexpensive fibers. Also, it is known that PC takes about 28 days to reach a good compressive strength (about 10MPa), and it is not very different for CACs [4]. In addition, these traditional cements' compressive strengths are reduced significantly when they are exposed to high temperatures above than 500°C. With all this, it is proposed in this Chapter a new PC material which can compete in terms of high performance and extreme environments with high performance cements.

7.2 Manufacturing

Al-Ca-PC samples were fabricated by mixing aqueous phosphoric acid with natural wollastonite and alumina powders. PCs with 0, 5, 10, 20 and 40wt% of alumina-α (with purity 99% from Buehler was added to the mixture in different concentrations. For all of the samples, the 1.2 ratio liquid (phosphoric acid formulation) to powders (wollastonite + alumina) was kept constant as shown in Table 13. In all cases, wollastonite and alumina powders were mixed by hand. Then, they were added to the acid and mixed in the Thinky mixing for 2min. In all cases the pH was 7 after the setting of the cement.

Table 13 Contents of the raw materials used for the fabrication of Al-Ca-PCs.

Raw materials	**PC-0wt% Al_2O_3**	**PC-5wt% Al_2O_3**	**PC-10wt% Al_2O_3**	**PC-20wt% Al_2O_3**	**PC-40wt% Al_2O_3**
	Weight (g)	Weight (g)	Weight (g)	Weight (g)	Weight (g)
Wollastonite (M200 from NYCO)	100	95	90	80	60
Alumina-α (from Buehler)	0	5	10	20	40
Phosphoric acid formulation	120	120	120	120	120

For sample manufacturing, a Teflon mold was used to make the samples for compression (diameter 12.7mm x length 25.4mm) and glass tubes with an interior diameter of 0.5in were used to make the samples (diameter 12.7mm x length 100mm) for weight loss experiments. For the structural stability of the composites, different exposure temperatures and times were conducted over the same sample followed by progressive exposure at temperatures of 100°C, 200°C, 300°C, 400°C, 500°C, 600°C, 900°C, 800°C, 900°C, and 1000°C. Each temperature step took 1 hour. After each heat exposure, samples were weighed, diameter and length were measured and

they were visually inspected for damages. Samples also were evaluated under other thermal conditions such as 1000°C for 2, 12 and 24h. For all thermal treatments, samples were characterized with the SEM, XRD and compression tests. In order to know the effect of water content in the acid, some samples were fabricated with an acid with different water content. The regular acid used in most of this thesis is referenced as Ref A.

Figure 78 shows results obtained with a gel timer device. Two different powders were tested in order to see the size effect on the curing time: 0.30, 0.5, 1.0 and 5.0 μm. All samples have very good pot life (more than 1h) taking into the account that this material need to be improved with additives (already well known) to control the setting properties. All tests were conducted at 25°C. Hence, a future product can use 5.0 μm size particles to reduce production costs. This research is focusing in the alumina grain size of 1.0 μm. Figure 78 also includes the mass effect of the sample in the setting time for the size 1.0 μm. It can be seen that as the alumina content increases in the PC (percentage is taken over the 100wt% powders, alumina + wollastonite, while the acid to powders ratio is kept in 1.2), the pot life is decreased. In the case of 40wt% of alumina, the setting time was 51min, which is a reasonable to make composites. On the other hand, the mean values for the density measurements are also included for each sample plotted in Figure 78 (red circles). Density is quite homogeneous, the mean was in between 1.8 and 2.1 g/cc, and the standard deviation had a maximum of 0.005g/cc.

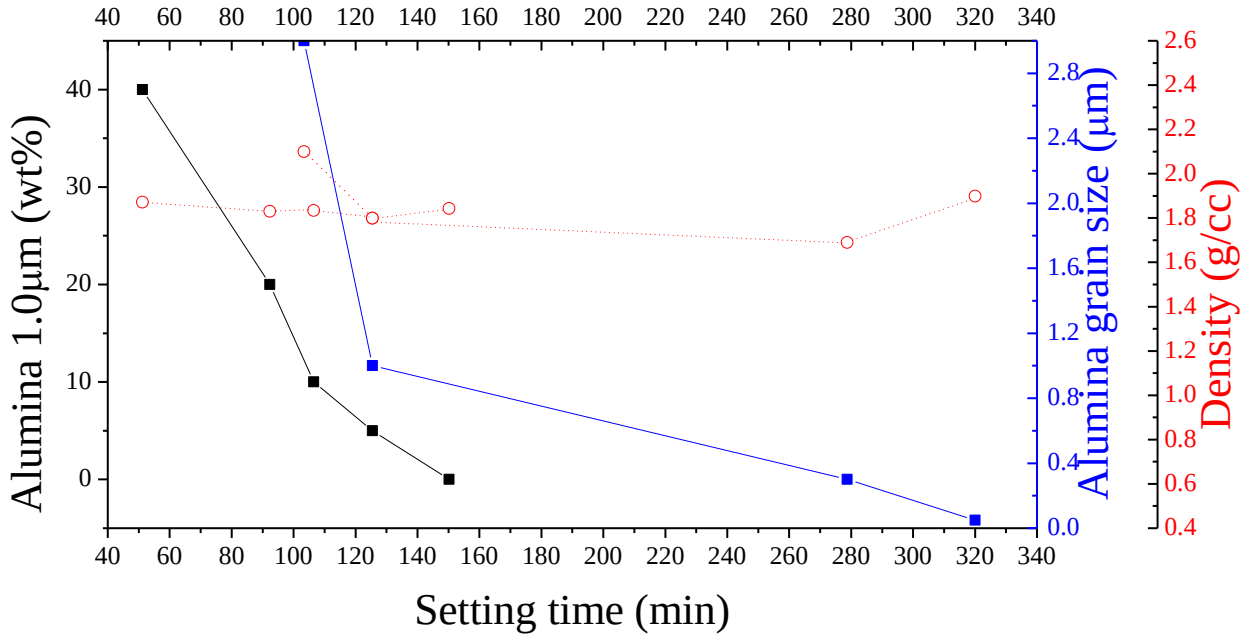

Figure 78 Setting time for alumina-based PCs as a function of the alumina content in the PC, the alumina grain size and the density.

7.3 Results

Figure 79 shows samples as made and after progressive thermal exposure. Although the test was followed by progressive thermal exposure at 10 different temperatures as described above, only the most significant images of sample damage are included. All samples as made have the same diameters and lengths and they have no cracks or bents. Figure 79a shows that after temperature is increased, the sample without alumina is significantly damaged by cracking. After the heat exposure to 1000°C for 1h, some samples showed cracks as big as the diameter of the sample. Figure 79b shows another view the entire sample length. It can be observed that as temperature increased the bending of the samples increases as well (due to the heat exposure). However, this bending effect decreases as the alumina content increases. Particularly, samples with 20 and 40wt% of alumina do not show bending while the worst sample was the one without alumina. Since they did not show macro cracking at all it suggests that a new binding phase is able to

connect all matrix as a result of the alumina added. Thus, alumina does not act as a filler and it is the main binding phase when 20 and 40wt% is added.

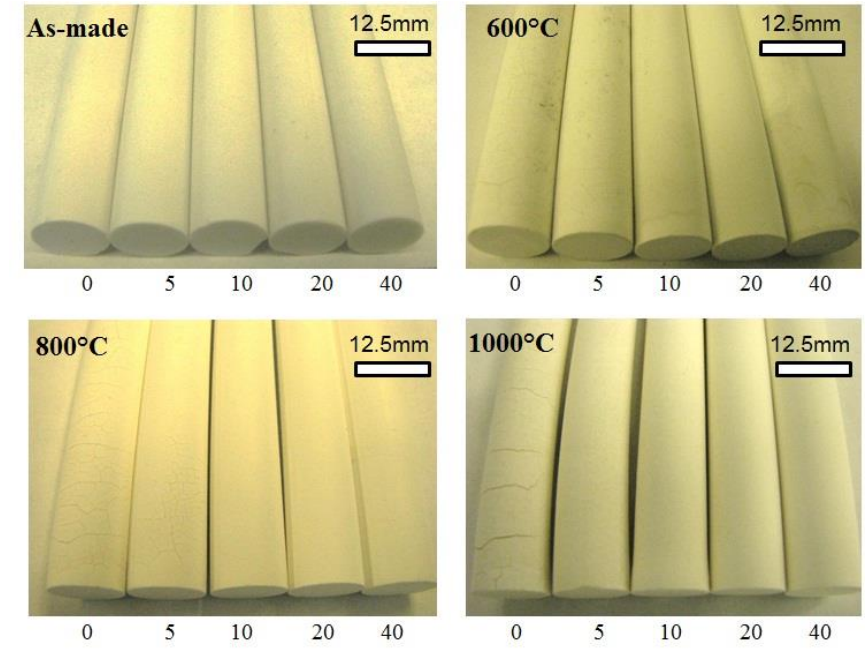

a)

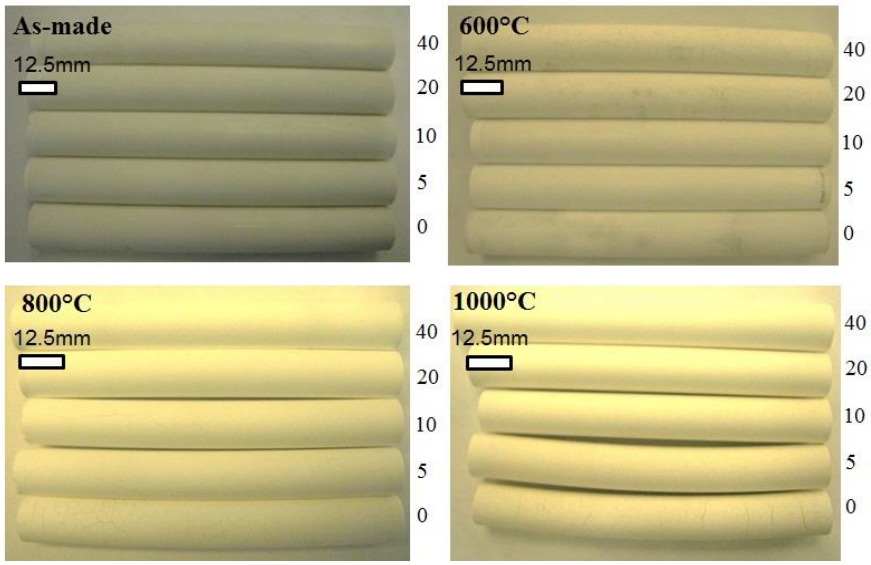

b)

Figure 79 Samples after different thermal exposure for 1h.

Figure 80a shows images of samples after all the thermal cycle is completed. Samples made with the powders and the different acid formulations (5.0, 0.0 and 2.9 wt% of borax) show that the increase in the alumina content in all cases enable the material to not bend, crack and even shrink. Figure 80b shows a magnification of samples fabricated with the regular acid, with 0% alumina (left) and with 20% alumina (right), which confirms the above described results.

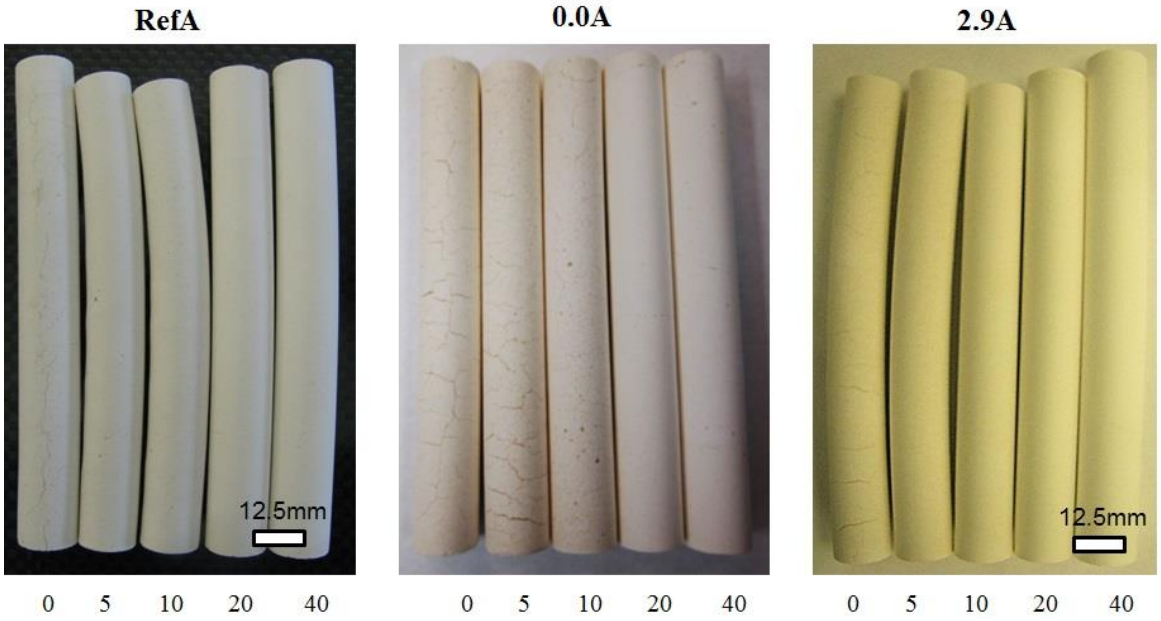

Figure 80 a) Samples after all the heat exposure treatments for 1h were finished, b) magnification for samples with 0% alumina (left) and with 20% alumina (right) fabricated with the reference acid.

Figure 81a and b shows the weight loss and diameter reduction for samples fabricated with the regular acid with the thermal exposure treatments. The length reduction was measured as well, but it is not

included because some samples bent during the thermal treatments and this increased a lot of error in the data (it was observed the same trend obtained for the diameter reduction). In general, the addition of alumina decreased the weight loss. The diameter reduction was the lowest for samples with 20 and 40wt% of alumina. Figure 81c and d shows the weight loss and diameter reduction for samples fabricated with the acid with 0.0 wt% of borax. In this case, on the contrary with results for the regular acid, the lowest weight loss has been obtained for the samples with 40wt% of alumina. As for regular acid, the diameter reduction were the lowest for samples with 20 and 40wt% of alumina. Figure 81e and f shows the weight loss and diameter reduction for samples fabricated with the acid with 2.9 wt% of borax. Similarly for the acid with 0.0 wt% of borax, the addition of alumina decreased the weight loss. Also, on the contrary with results for the regular acid, the lowest loss weigth has been obtained for the samples with 40wt% of alumina. The diameter reduction were the lowest for samples with 40wt% of alumina.

Figure 82 shows summary of results for the different acidic formulations per alumina content. For 0.0wt% of alumina added, similar weight loss was obtained for the three acidics formulations. These results show that Wo-PC has a insignificant changes in the weigth loss when water and borax is changed in the liquid formulation.

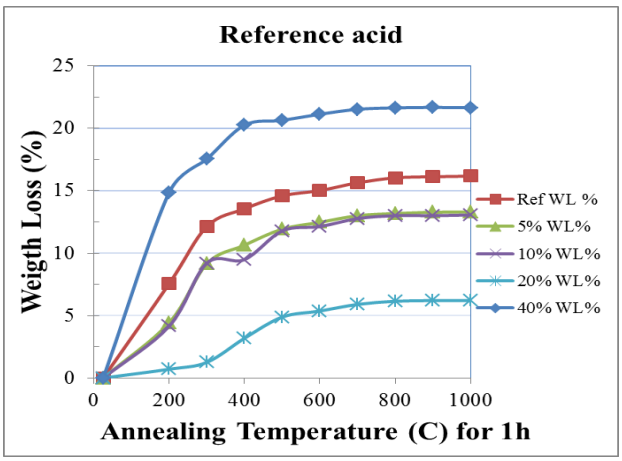

a

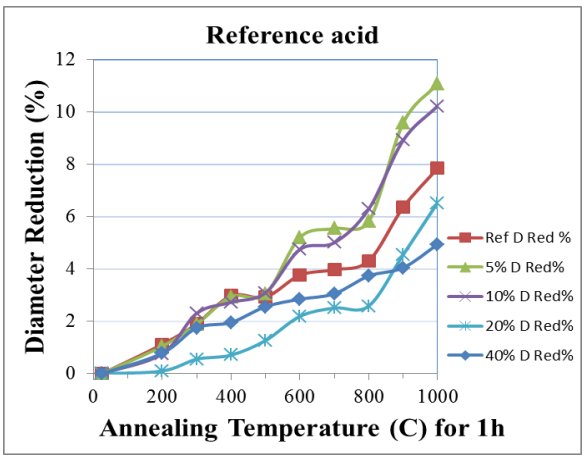

b

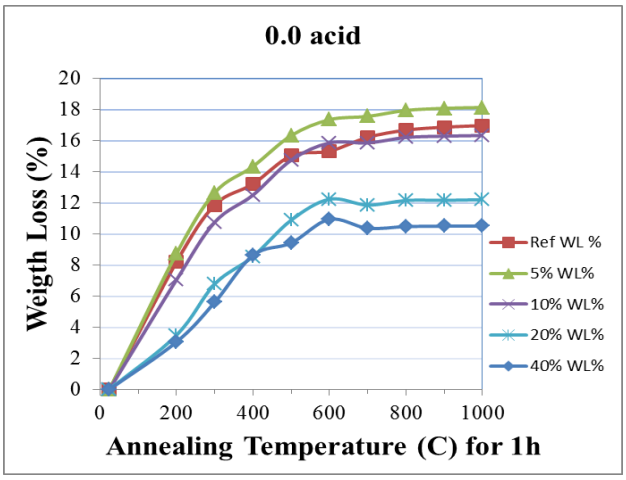

c

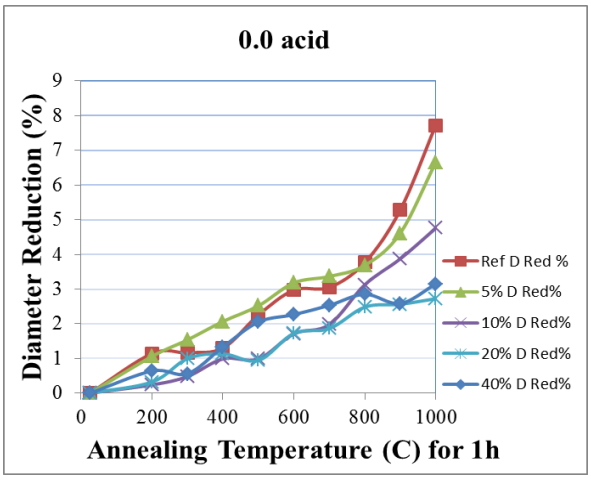

d

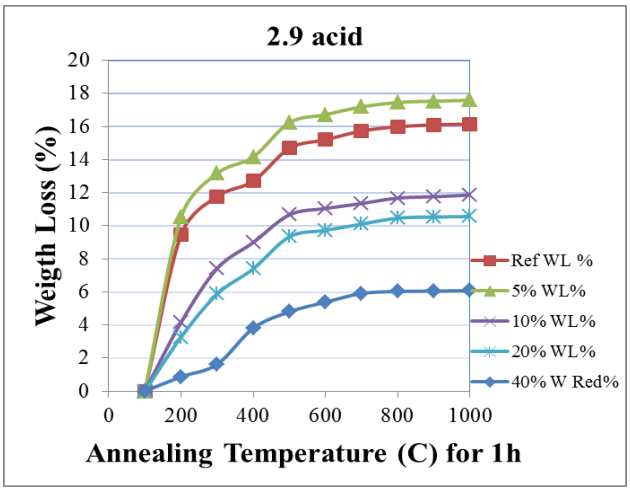

e

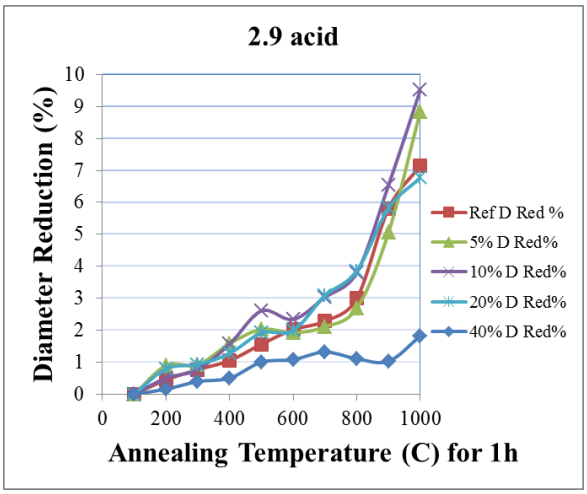

f

Figure 81 Weight loss and length reduction for samples made with the 5.0 (reference), 0.0 and 2.9wt% of borax.

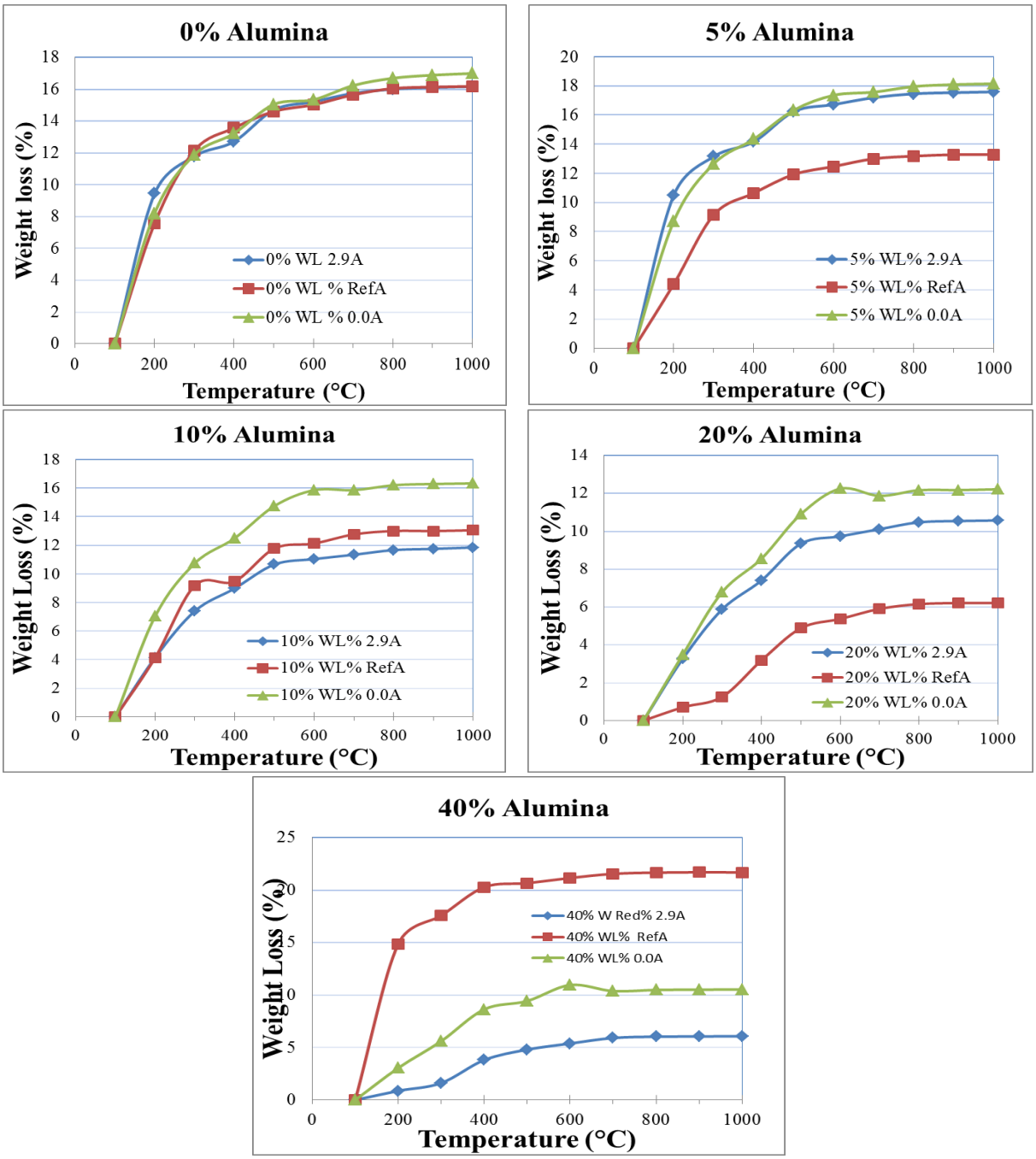

Figure 82 Weight loss % after different thermal exposure treatments for 1h for PC samples with different alumina content

For 5wt% of alumina added, the acid with 2.9wt% of borax has the best values since it has the lowest weight loss after the thermal exposure. The acids with 0.0 and 2.9wt% of borax have

basically the same values, and they have higher weight loss than the regular acid. This means that at 5% additions, the resulting sample can be worst than the sample without alumina. This suggest the structure is significantly affected by the "Ca" ions. Since damage appears as shown in Figure 79, the binding phase is a combination of moslty calcium phosphates and minor contents of aluminum phosphates. This will be shown later in this chapter with XRD data.

When 10wt% of alumina was added, using regular acid exhibited the lowest weight loss after the thermal exposure. The acid with 0.0wt% of borax has the worst weight loss data. Similar trend is observed for 20 wt% sample. However, when 40wt% of alumina added, the acid with 2.9wt% of acid has the best values while the regular acid has the worst weight loss data. The XRD of the raw powders wollastonite and alumina is shown in Figure 83. The following characterization for this alumina-based PC is focused on the samples fabricated with the regular acid.

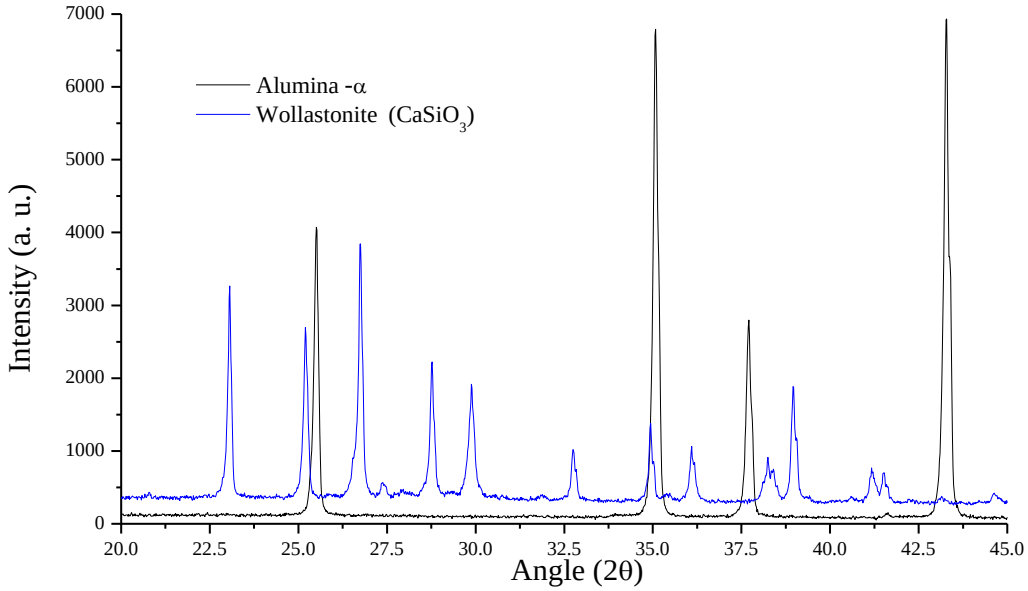

Figure 83 XRD for the raw powder.

Figure 84 shows the XRD for PCs with different alumina contents. As shown in the plot, the PC with 0.0wt% of alumina added is a multiphase composite material with wollastonite ($CaSiO_3$)

and brushite ($CaHPO_4.2H_2O$), and minor amounts of monetite ($CaHPO_4$) and quartz (SiO_2). As was explained in Chapter 4, brushite is the main binding phase and upon time transform naturally to monetite. The increase in temperature accelerates this transformation. Some amorphous peak appears near 30°, which has been related to amorphous calcium phsophates and amorphous silica, residual from the wollastonite which lost calcium while reacting with the acid.

Figure 84 shows the XRD data for PCs with different amounts of alumina. It can be seen that as the alumina content increases, new crystalline phases start to appear in the XRD. The first to appear is the residual alumina (Al_2O_3) which did not react with the acid. As the alumina added into the mixture is increased, the intensity of this residual phase increases as well as shown in the XRD. Some alumina is reacting with the acidic solition as described by equation 1. In acidic media, alumina produces aluminum cations, which in an aqueous acidic solution can react with phosphoric acid to form the aluminum phosphate ($Al\ H_3\ (PO_4)_2.H_2O$) as described by equation 2. Also, some alumina powder is reacting with this new generated aluminum phosphate and produce another aluminum phosphate, bernite ($Al\ PO_4$), as described by equation 3. From the XRD, it can be concluded that the main aluminum phosphate obtained by this route in the PC as made or with thermal drying below 200°C is $Al\ H_3\ (PO_4)_2.H_2O$.

$$AlO_{3/2} + 3H^+ \rightarrow Al^{3+}(aq) + (3/2)\ H_2O \quad (1)$$

$$Al^{3+}(aq) + H_2PO^-_4 + HPO^{2-}_4 + H_2O = Al\ H_3(PO_4)_2.H_2O \quad (2)$$

$$Al_2O_3 + 2\ Al\ H_3(PO_4)_2.H_2O \rightarrow 4\ AlPO_4 + 4H_2O \quad (3)$$

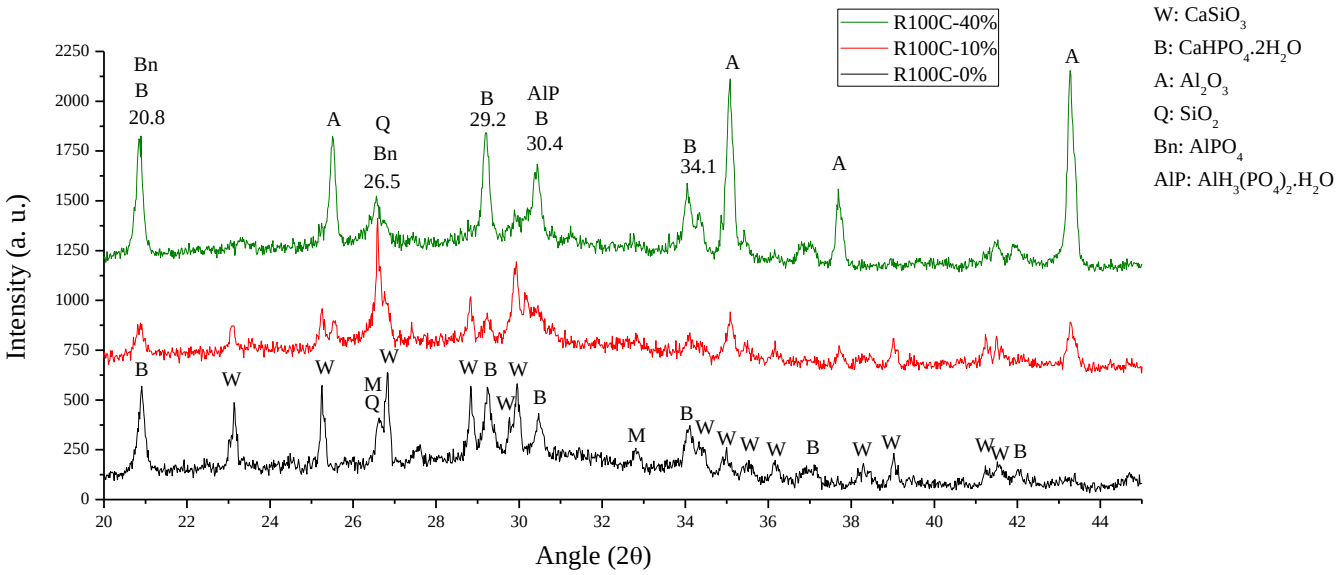

Figure 84 XRD for the PC with different alumina contents as made, after a thermal drying at 200°C.

Figure 85a shows the XRD for the PC with different alumina contents exposed to 400°C. At this temperature we can see that the main reaction is the dehydration of brushite ($2CaHPO_4.2H_2O$) into monetite ($CaHPO_4$) (see Chapter 4 for the Wo- PC, which corresponds to the 0% alumina sample as referred in this chapter). Figure 85b shows the XRD for the PC with different alumina contents exposed to 600°C. After this temperature, calcium pyrophosphate ($Ca_2P_2O_7$) appeared in the samples from the transformation of monetite. Alumina phosphate ($AlH_3(PO_4)_2.H_2O$) peaks appeared more intense after this heat exposure.

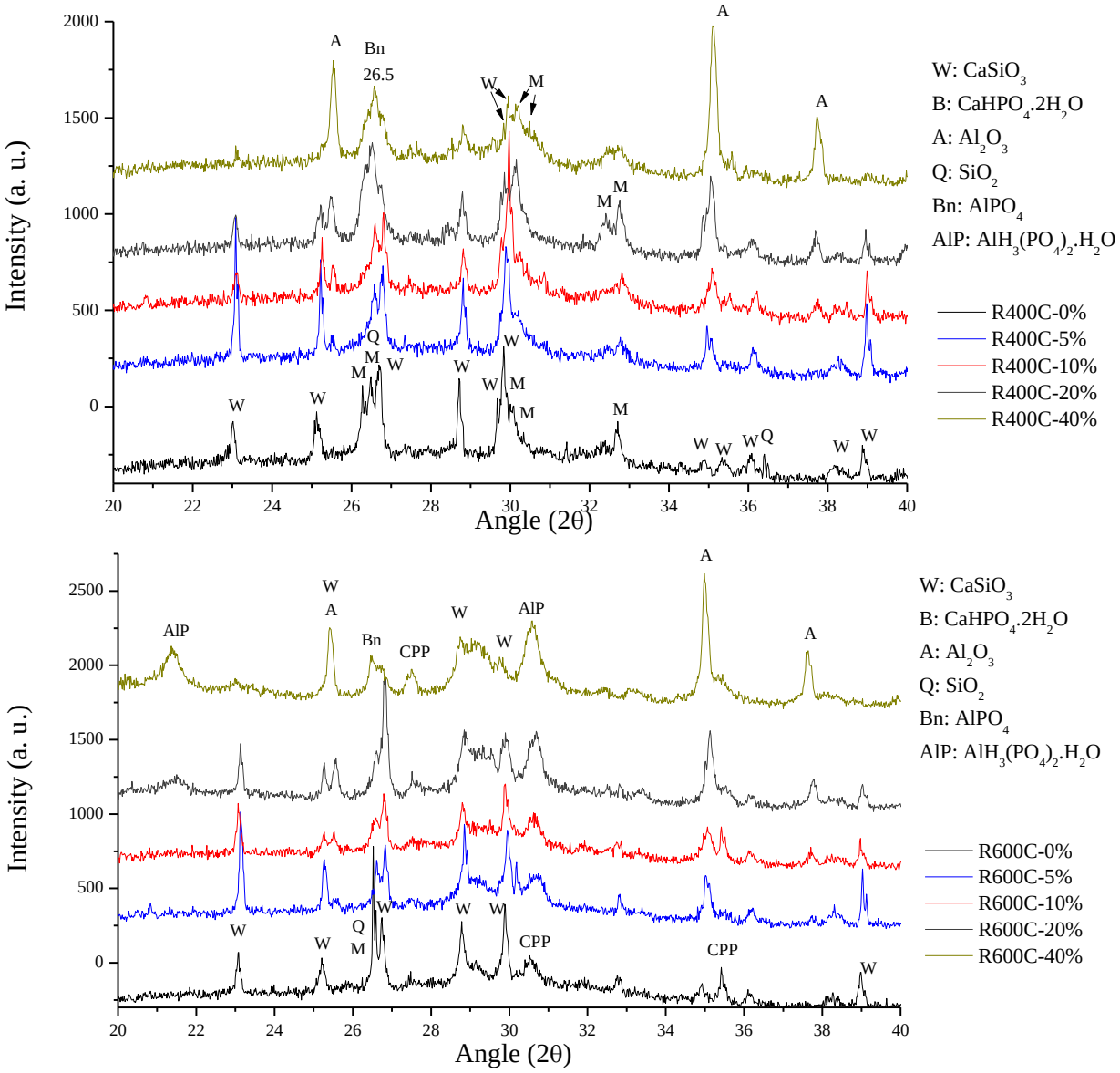

Figure 85 XRD for the new PC with different alumina contents exposed to 400 and 600°C.

Figure 86 shows the XRD for the PC with different alumina contents after the heat exposure to 1000°C. Pseudo-wollastonite is observed. The scan also shows that aluminum phosphates formed at room temperatures are still in the PC after exposed to 1000°C, which shows the aluminum phases created at room temperature by the chemical low temperature method of PC are very stable at high temperatures. These results confirm the high thermal and structural

stability found in the weight loss experiments conducted over macro samples (Figures 1, 2 and 3).

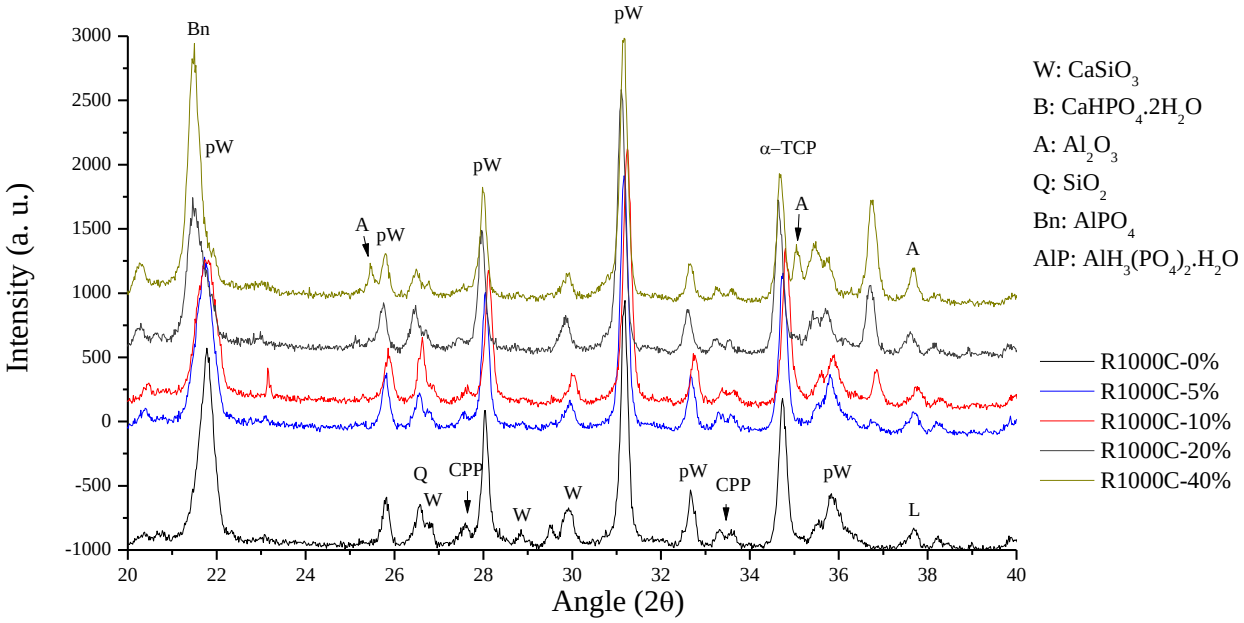

Figure 86 XRD for the PC with different alumina contents after exposed to 1000°C.

Figure 87 shows the XRD for the PC with 40wt% of alumina contents exposed to different temperatures. As temperature increases, brushite disappears and some calcium phosphate phases appear.

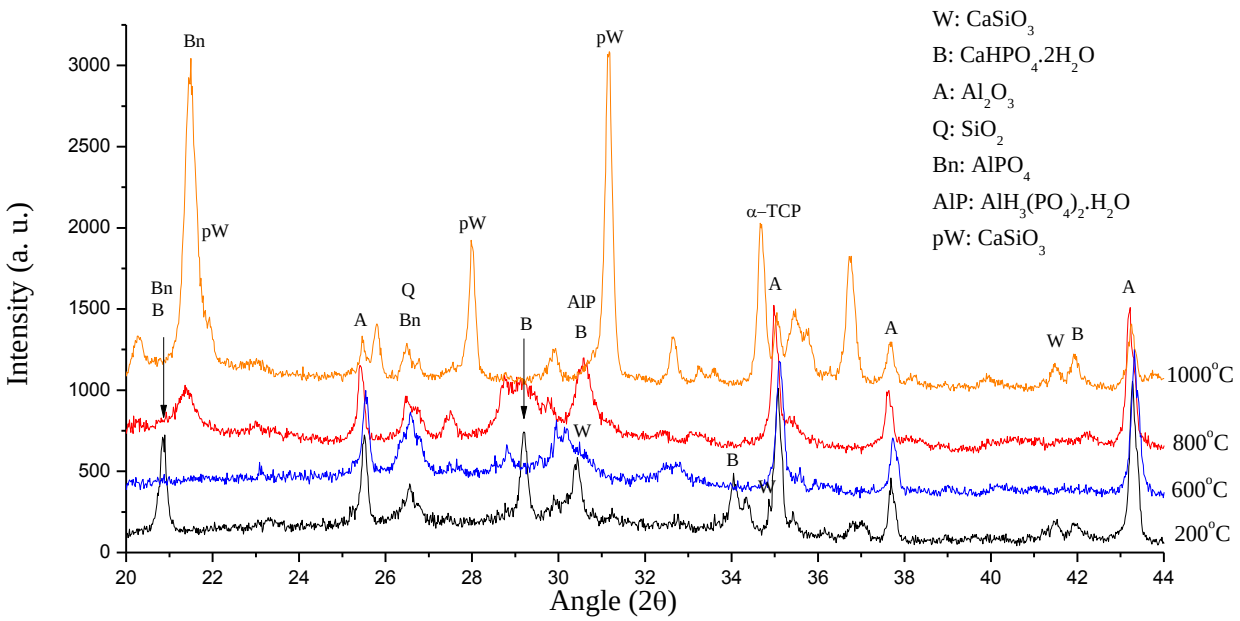

Figure 87 XRD for the PC with 40wt% of alumina contents exposed to different temperatures.

Figure 88 shows SEM images at different magnification of some grains of the raw alumina powders. These grains have a lot of micro-pores. These pores increase the contact area of alumina with the acidic solution, which accelerated the dissolution of aluminum ions into the liquid as described by the equation 1. Images of the mineral wollastonite used in this research have been showed in Chapter 4.

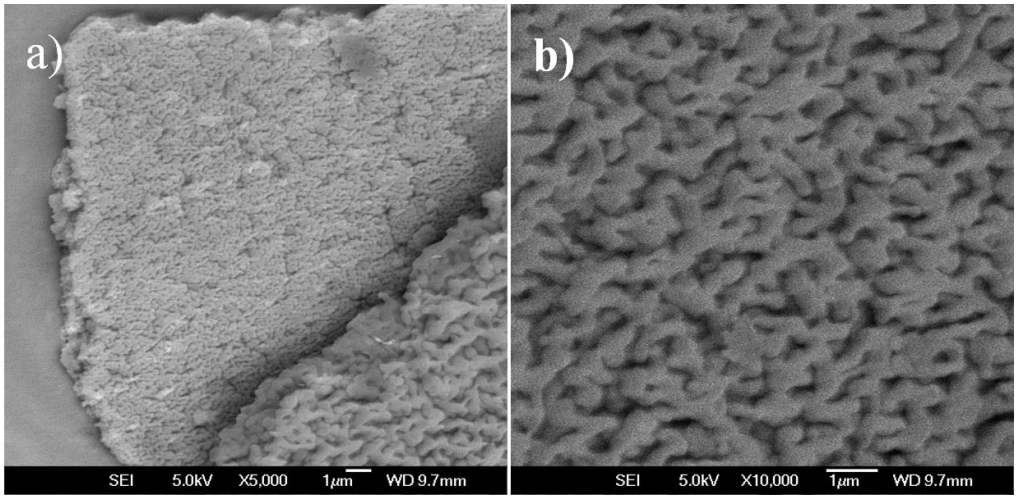

Figure 88 SEM images of the alumina powder used in the fabrication of PCs.

Figure 20 shows EDS-SEM for PC without alumina added as explained in Chapter 4. It can be seen that the Ca/P ratio in the matrix is near 1, which mostly corresponds to brushite. Inside the residual wollastonite powder grain, phosphorous has been detected which suggest an inter-diffusion of “Ca” and “P” ions through the grain-matrix interface.

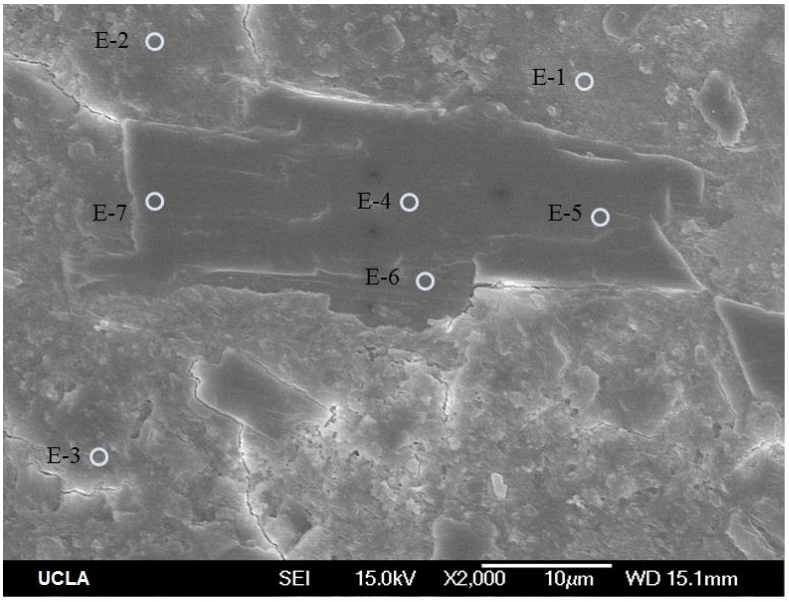

EDS Quantification of atomic percentages

Point	P	Ca	Si	Al	Ca/P	Ca/Si	Al/Ca
E1	16.22	13.45	0.43	0.47	0.83	31.28	0.03
E2	14.15	11.34	0.81	4.76	0.80	14.00	0.42
E3	7.66	4.07	0.27	23.59	0.53	15.07	5.80
E4	0.36	9.11	19.86	0.00	25.31	0.46	0.00
E5	0.70	10.01	20.73	0.00	14.30	0.48	0.00
E6	0.49	11.40	20.93	0.00	23.27	0.54	0.00
E7	0.58	9.29	18.46	0.15	16.02	0.50	0.02

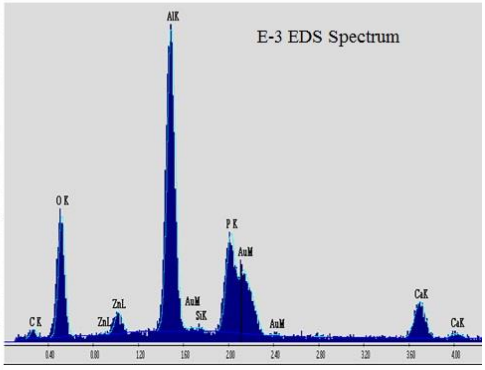

Figure 89 EDS-SEM for PC with 0% of alumina as made (without any thermal treatment).

Figure 90 shows the EDS-SEM for PC with 20% of alumina after heat exposure for 1h.different temperatures. Only high temperatures are shown where significan changes appeared.

Figure 90a shows the results for 20% of alumina after exposed for 1h to 200°C. It can be observed that “Ca” contents decreases from the center of the grain towards the interface (see E1-E2, E6-E7). Also, aluminum contents are very inhomogeneous in the matrix (see E3, E4 and E5).

Figure 90b shows the EDS-SEM for 20% of alumina after exposed for 1h to 800°C. There are more structural damages due to thermal effects. This can be due either to the weakness of the phosphate phases or to agglomeration of alumina particles.

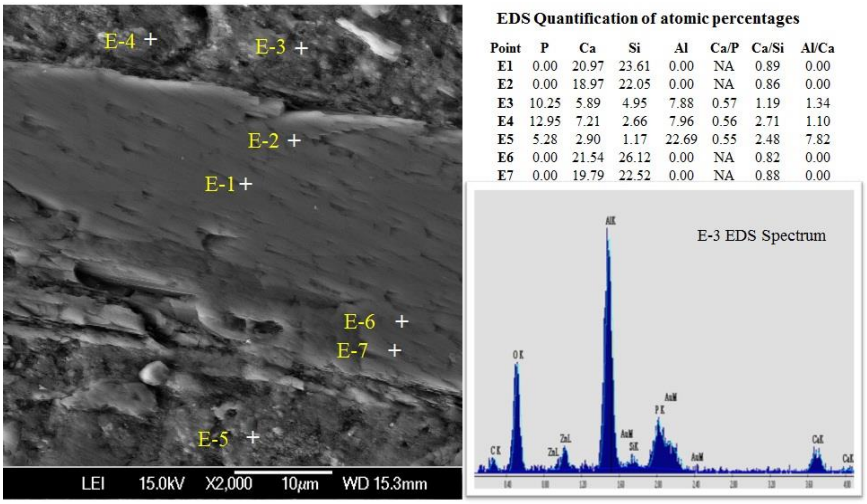

EDS Quantification of atomic percentages

Point	P	Ca	Si	Al	Ca/P	Ca/Si	Al/Ca
E1	0.00	20.97	23.61	0.00	NA	0.89	0.00
E2	0.00	18.97	22.05	0.00	NA	0.86	0.00
E3	10.25	5.89	4.95	7.88	0.57	1.19	1.34
E4	12.95	7.21	2.66	7.96	0.56	2.71	1.10
E5	5.28	2.90	1.17	22.69	0.55	2.48	7.82
E6	0.00	21.54	26.12	0.00	NA	0.82	0.00
E7	0.00	19.79	22.52	0.00	NA	0.88	0.00

a) 20% 200°C

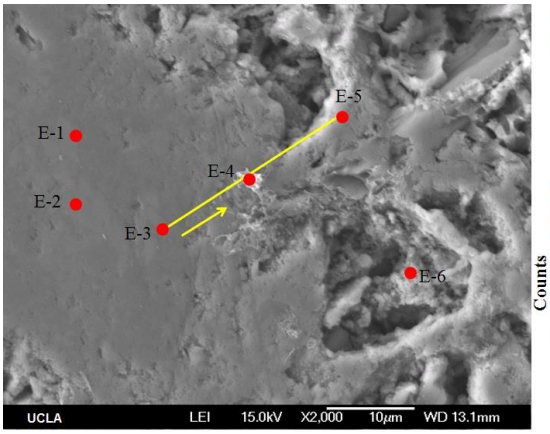

EDS Quantification of atomic percentages

Point	P	Ca	Si	Al	Ca/P	Ca/Si	Al/Ca
E1	0.00	22.87	28.52	0.00	NA	0.80	0.00
E2	0.00	24.53	27.98	0.00	NA	0.88	0.00
E3	0.00	5.36	36.46	0.00	NA	0.15	0.00
E4	11.58	8.04	2.20	11.81	0.69	3.65	1.47
E5	13.25	8.15	0.45	15.19	0.62	18.11	1.86
E6	6.84	2.60	1.33	15.41	0.38	1.95	5.93

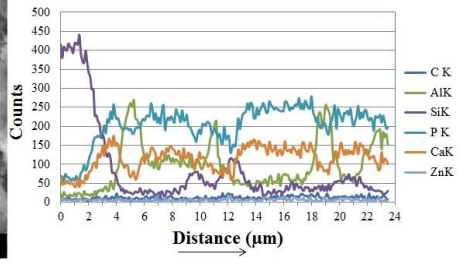

b) 20% 800°C

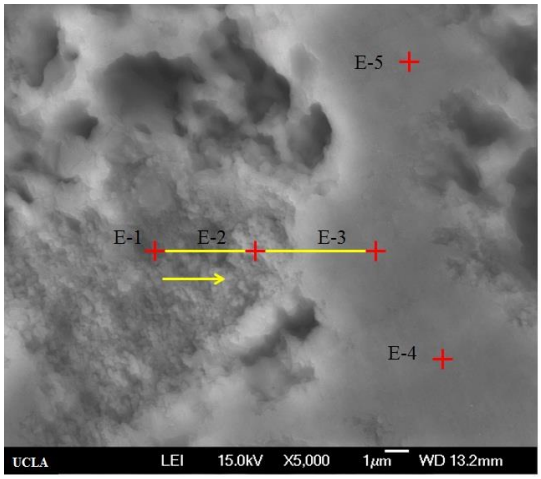

EDS Quantification of atomic percentages

Point	P	Ca	Si	Al	Ca/P	Ca/Si	Al/Ca
E1	8.78	1.76	1.96	44.37	0.20	0.90	25.21
E2	7.00	1.70	0.48	35.93	0.24	3.54	21.14
E3	18.63	11.86	0.54	16.80	0.64	21.96	1.42
E4	9.49	1.51	0.33	34.96	0.16	4.58	23.15
E5	20.84	18.49	1.68	7.45	0.89	11.01	0.40

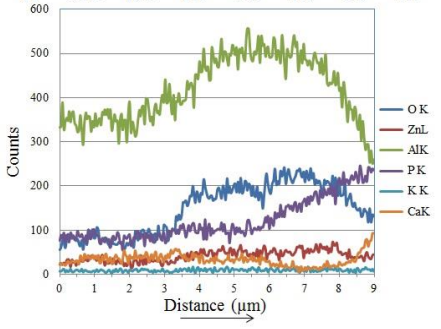

c) 20% 1000°C

Figure 90 EDS-SEM for PC with 20% of alumina after exposed for 1h to a) 200°C, b) 800°C, and c) 1000°C.

Unreacted alumina particles are poorly bonded to the matrix and hence are easily removed or dissolved during the polishing process. Figure 90c shows the EDS-SEM for 20% of alumina after exposed for 1h to 1000°C. Due to the high contents of alumina, E1 and E2 seem to be mostly aluminum and calcium phosphates and some agglomerated alumina. E4 seems to be more stable under temperature and it must be aluminum phosphate (such as $AlPO_4$). We consider that $AlH_3(PO_4)_2.H_2O$ is less possible to be present since the H_2O molecule will not survive at this temperature.

Figure 91a shows EDS-SEM for 40% of alumina after exposed for 1h to 200°C. A complex microstructure with different phases is shown. E1 and E6 correspond to mostly calcium phosphates. E7 seems to be another form of calcium phosphate. E9 seems to be aluminum phosphate. The lower part of the image is reach in wollastonite as is shown by the X-ray line.

Figure 91b shows EDS-SEM for 40% of alumina after exposed for 1h to 800°C. The microstructure shows some sub-grains (white points near E6) that are very stable under high temperatures and they have been seen in many part of the sample. Due to the information from EDAX it can be high temperature phases such as CaO or Al PO_4 obtained as a byproduct of the interdiffusion process between alimina, wollastonite and other phosphates.

Figure 91c shows EDS-SEM for 40% of alumina after exposed for 1h to 1000°C. The samples shows high structural damage when this is compared with the samples after exposed for 1h to 800°C. This corresponds mostly to phosphate deterioration since both residual wollastonite and alumina have higher melting points than 1000°C.

Figure 92 summarized the Weibull statistics for the PCs with 0, 5, 10, 20 and 40wt% of alumina. The linear fit equation, whose slope is the Weibull modulus, is included.

a) 40% 100C

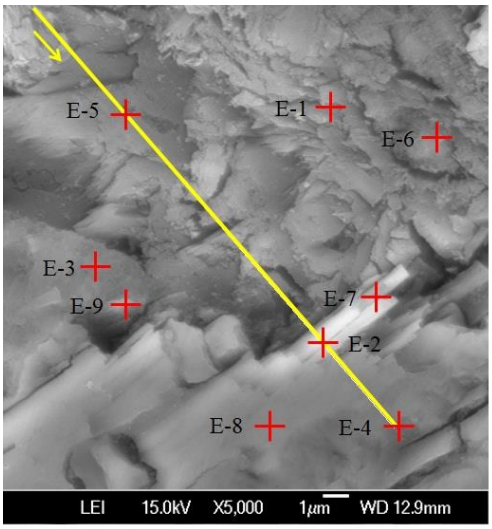

EDS Quantification of atomic percentages

Point	P	Ca	Si	Al	Ca/P	Ca/Si	Al/Ca	Si/Ca
E1	18.89	15.60	0.56	0.31	0.83	27.86	0.02	0.04
E2	1.50	14.49	18.78	0.11	9.66	0.77	0.01	1.30
E3	13.41	10.31	12.56	2.22	0.77	0.82	0.22	1.22
E4	0.00	4.35	52.28	0.07	NA	0.08	0.02	12.02
E5	17.53	14.69	0.00	1.53	0.84	NA	0.10	0.00
E6	12.43	11.62	0.00	0.53	0.93	NA	0.05	0.00
E7	4.92	14.08	0.00	0.52	2.86	NA	0.04	0.00
E8	0.00	22.61	27.48	0.00	NA	0.82	0.00	1.22
E9	10.93	13.23	16.27	3.76	1.21	0.81	0.28	1.23

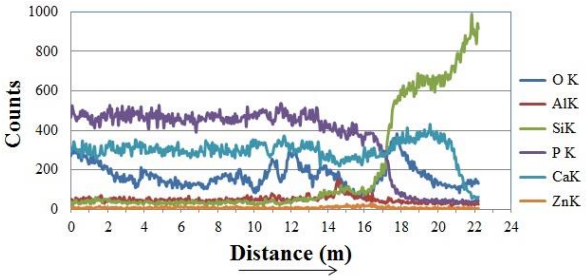

b) 40% 800

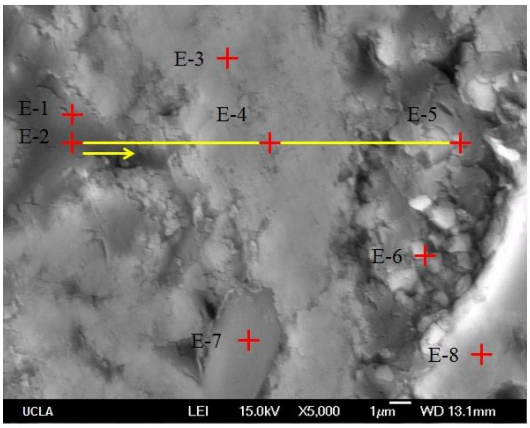

EDS Quantification of atomic percentages

Point	P	Ca	Si	Al	Ca/P	Ca/Si	Al/Ca
E1	2.01	0.88	0.00	3.41	0.44	NA	3.88
E2	1.66	0.73	0.00	1.99	0.44	NA	2.73
E3	13.07	8.67	0.00	15.49	0.66	NA	1.79
E4	16.34	12.20	0.00	9.18	0.75	NA	0.75
E5	0.00	0.00	20.59	0.00	NA	0.00	NA
E6	3.53	2.07	2.33	1.84	0.59	0.89	0.89
E7	1.63	0.50	29.04	1.03	0.31	0.02	2.06
E8	10.14	1.74	0.46	18.29	0.17	3.78	10.51

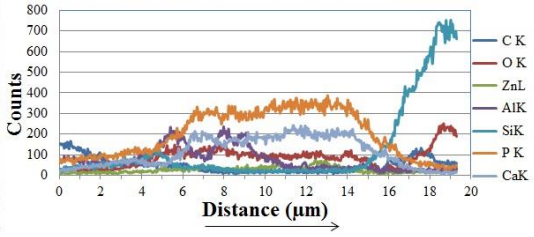

c) 40% 1000C

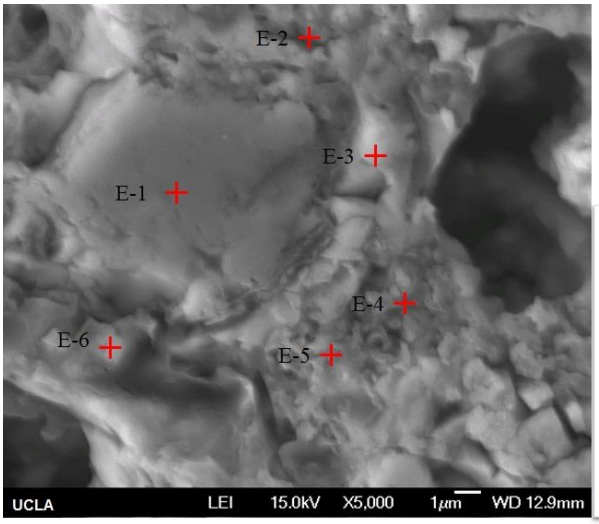

EDS Quantification of atomic percentages

Point	P	Ca	Si	Al	Ca/P	Ca/Si	Al/Ca
E1	1.79	1.55	28.66	0.83	0.87	0.05	0.54
E2	6.92	4.42	1.36	11.87	0.64	3.25	2.69
E3	12.99	14.96	0.65	1.22	1.15	23.02	0.08
E4	9.32	6.28	1.86	10.84	0.67	3.38	1.73
E5	4.36	0.89	1.96	6.89	0.20	0.45	7.74
E6	7.96	9.58	0.52	1.07	1.20	18.42	0.11

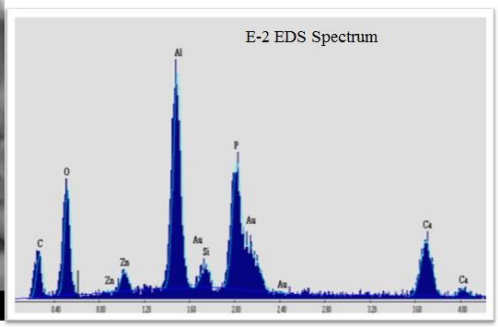

Figure 91 EDS-SEM for PC with 40% of alumina after exposed for 1h to a) 200°C, b) 800°C, and c) 1000°C.

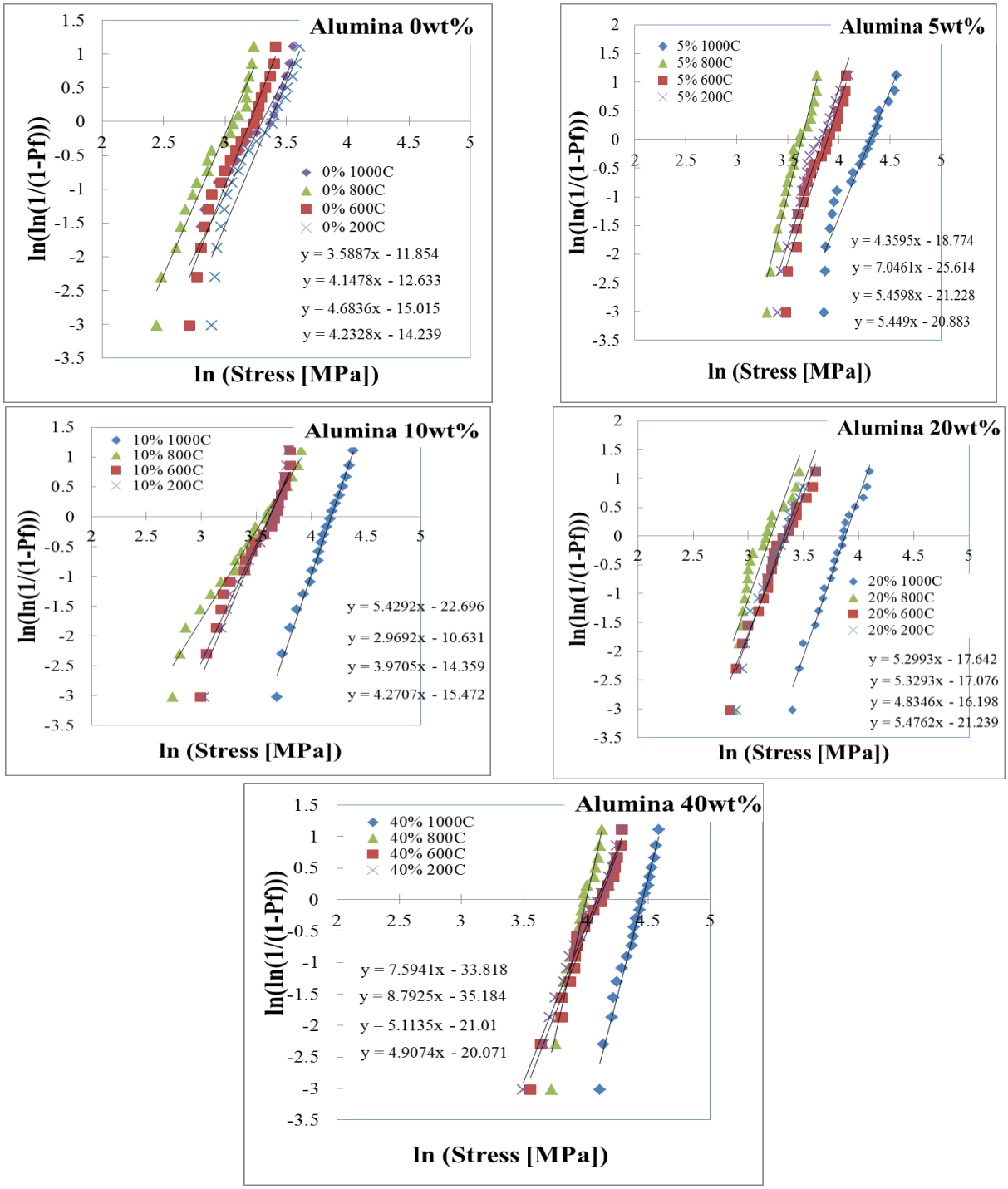

Figure 92 Weibull distribution for PCs at different exposure temperatures for 1h, with different alumina added.

Figure 93 summarized the Weibull distribution for the PCs with 0, 5, 10, 20 and 40wt% of alumina.

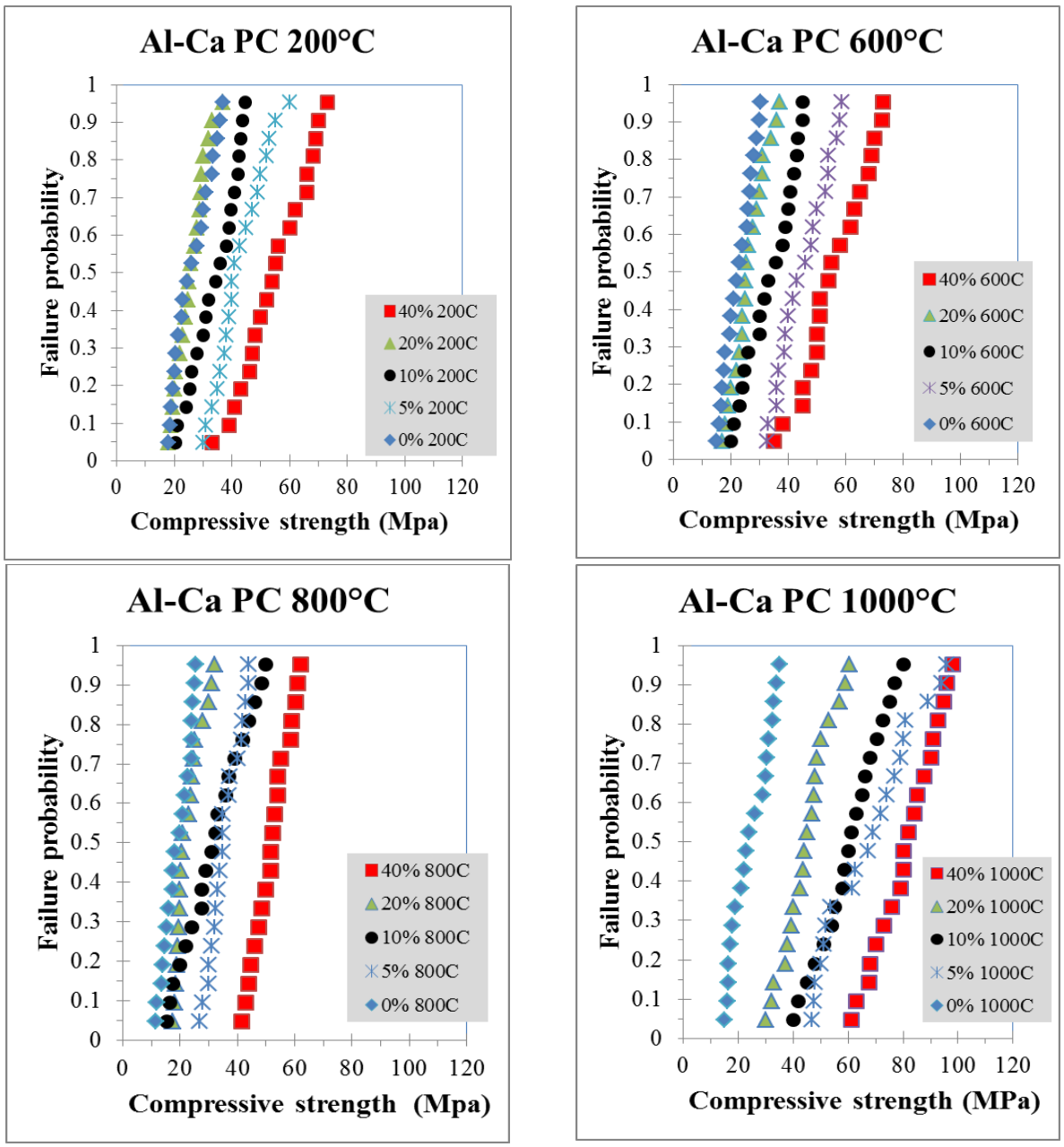

Figure 93 Weibull distribution for PCs at different exposure temperatures for 1h, with different alumina added.

Figure 94a summarizes the mean strength (for every set of 20 samples shown in Figure 93) as the temperature of the thermal treatments increases. It is observed that the mean strength is almost constant up to 600°C for all compositions. For the samples without alumina added, the strength remains almost constant even after the exposure to 1000°C, although there is a decrease (as for all other samples) after the exposure to 800°C. This decrease is mainly due to the well-known complete transformation of monetite ($CaHPO_4$) into calcium pyrophosphate (CPP, $Ca_2P_2O_7$), see Chapter 4. The most significant result of this research is the clearly improvement of strength for all samples exposed to 1000°C. This increment is due to the formation of phases stable at high temperature. These are both calcium and aluminum-phosphates.

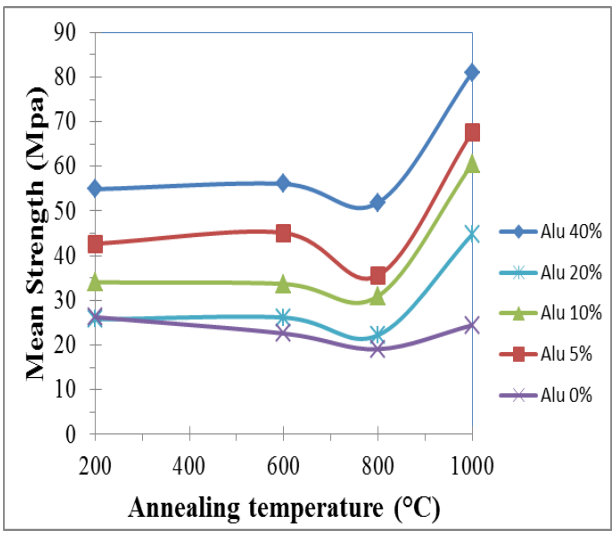

a

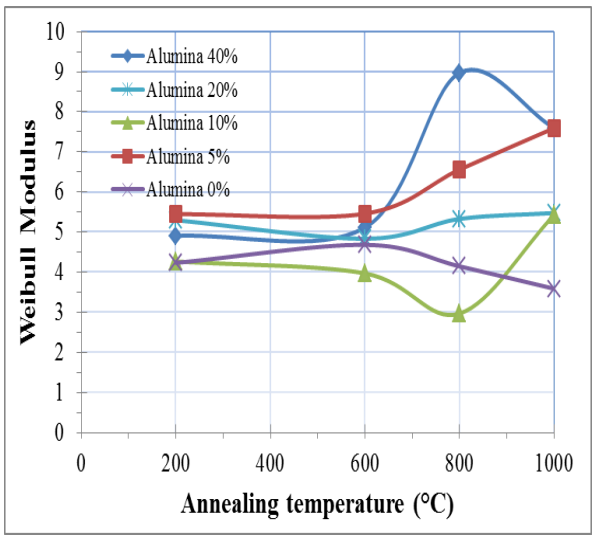

b

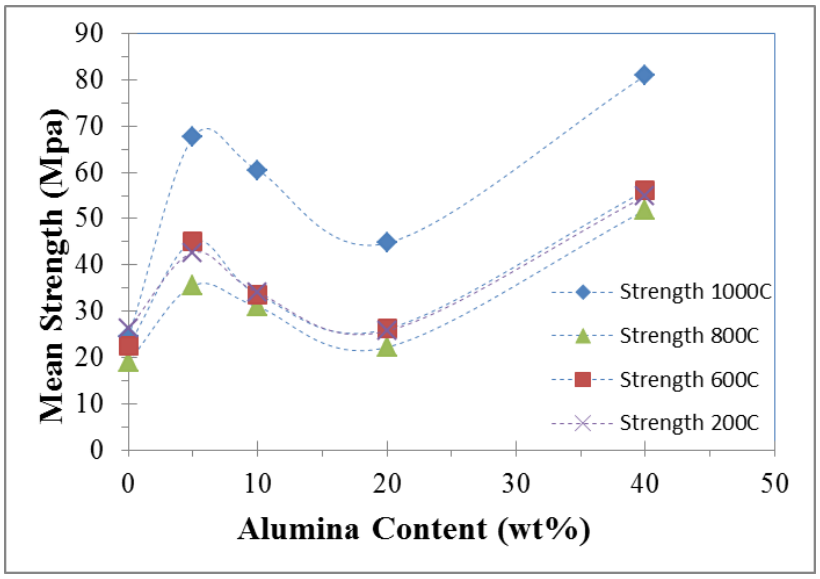

c

Figure 94 a) mean strength for different temperatures, b) Weibul modulus for different temperatures, c) mean strength different alumina contents PC. Each point was obtained from the statistics of 20 samples.

At low temperatures, some unreacted alumina acts as a filler and other reacts with the acid to form new alumina-based phosphates materials ($AlH_3(PO_4)_2.H_2O$ and $AlPO_4$) which are more stable at high temperatures than the calcium phosphates ($CaHPO_4.2H_2O$) formed at low temperatures. However, as temperature increases, wollastonite-byproducts undergo to several transformations (see Chapter 4)

generating fist monetite (CPP), and at higher temperatures calcium pyrophosphate ($Ca_2P_2O_7$) and tri-calcium phosphate (TCP: α-$Ca_3(PO_4)_2$. At high alumina contents (more than 20wt%), the aluminum phosphates and alumina dominates the properties of this new PC over the calcium phosphates. These phases create a crystalline alumina-network in the composite that reduce the cracking and shrinkage in some compositions as shown before. In fact, Figure 95a shows that as temperature increases, samples with alumina (20.0wt%) has higher compressive strengths and lower standard deviation. Also, Figure 95b shows that as exposure time is increased, all samples increased their mean strength and the samples with alumina have lower standard deviation as well.

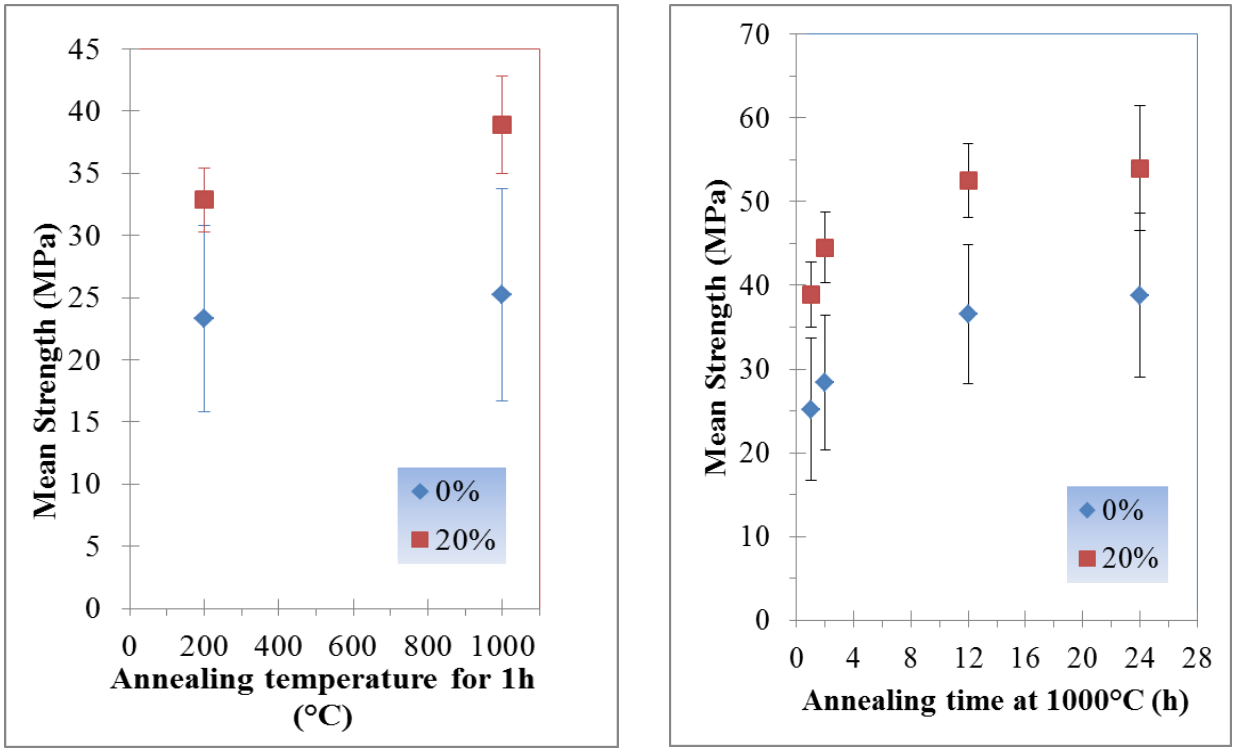

a) b)

Figure 95 a) Mean for PC samples with 0 and 20wt% of alumina exposed for 1h to 200 and 1000°C; b) mean for PC samples exposed to 1000°C exposed to different times.

Figure 96 shows the TGA for the PCs with different alumina contents. Samples from the best to the worst form the weight loss point of view are alumina 0, 40, 10, 20, and 5wt%. The weight loss at 1000°C is about 16, 15, 12, 6, and 5% respectively.

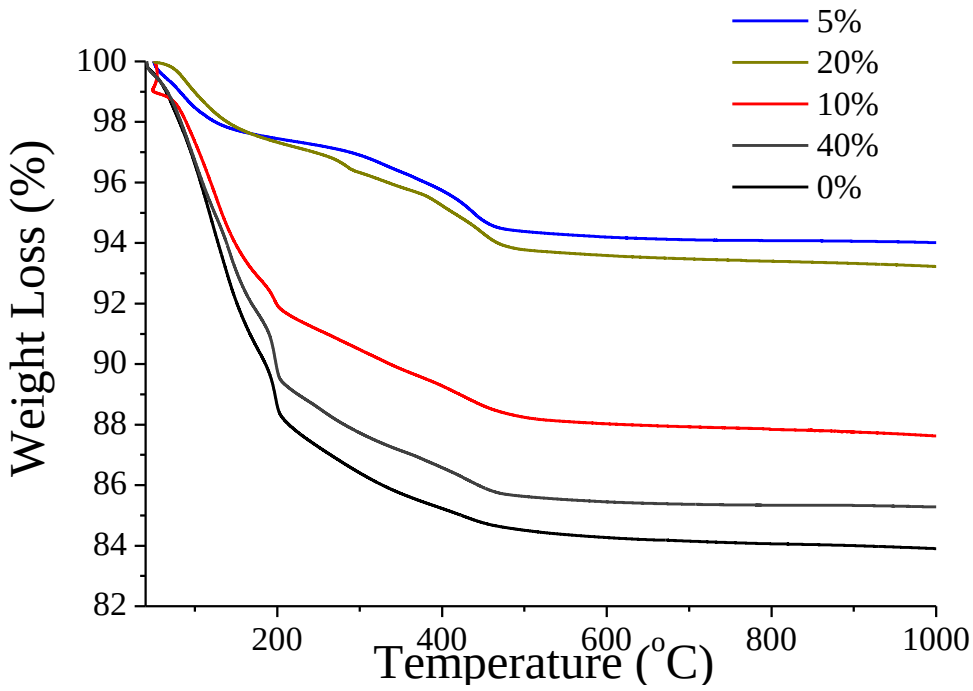

Figure 96 TGA data for PC with alumina contents.

7.4 Discussion

The Al-Ca-PC shown is a new material that is mechanically stable under temperatures up to 1000°C. This is a significant improvement over most of the phosphates developed before. Gel-timer results showed that all compositions are suitable to be used in larger scale since even with 40wt% of alumina, the setting time was 51min. This time can be easyly extended by more than twice just with precooling the raw materials in a regular refrigerator to about 5°C, or by adding the correct additives. Cracking has been reduced with the alumina content and completely eliminated for the 20 and 40wt% additions as shown in Figure 79. Figure 80b shows the significant improvement for samples with 0.0 and with 20% alumina, not only in the cracking reduction but also in the dimension stablity.

Table 14 shows data for PCs the exposure to different heat treatments. The weight loss data from the TGA (~4mg) and in a macro sample (~20g) shows a trend even though it was obtained by different treatments (continues heating vs thermal exposure at 10 different temperatures). In general, increasing alumina contents leads into a lower weight loss. However, for 40wt% of alumina added, the weight loss were basically the same as for 0.0wt% of alumina added.

Table 14 Some parameters obtained for samples made with the reference acid exposed to 1000°C.

	TGA After going from 50 to 1000°C at 10C/min		**Weigth Loss for RefA**, After 1000°C (all 10 thermal cycles)		**Compression** after 1000°C (mean)		**Shrinkage for RefA**, After 1000°C (all 10 thermal cycles)	
	Alu. %	Weight loss (%)	Alu. %	Weight (%)	Alu. %	Strength (MPa)	Alu. %	Diam. Red. (%)
WORST	**0**	16	**40**	21	**0**	24.45	**5**	11
↓	**40**	15	**0**	16	**20**	44.75	**10**	10
	10	12	**5**	12.5	**10**	60.48	**0**	8
	20	6	**10**	12.5	**5**	67.58	**20**	7
BEST	**5**	5	**20**	6	**40**	80.94	**40**	5

This result is significant and shows that the high amount of alumina content perhaps weakens the reaction with the calcium phosphates with the acid and more water is unbonded in the composite. These results are expected since alumina, wollastonite and calcium-alumino phoshates formed at this temperature are highly stable chemically. In the case of 40wt% of alumina, the weight loss increased about 4 times with respect to the 0.0wt% sample. This can be explained as part of sintering phenomena. However, in the case of 40wt% of alumina the trend is broken. This has been interpretated as a consequence of two metals ions competing to form phosphates (Al^{3+} and Ca^{+2}). We can say that at 20wt% calcium dominates, and at 40% aluminum dominates the reaction. More research to optimize this new material can optimize this ratios and get very high compressive strength values and very low shrinkage.

Another siginificant result is the increase in the compressive strength with the alumina additions exposed to 1000°C as shown in Figure 94c. This is really important, because the material instead of deteriorating is actually improving. It is well known that most of the cementitious and phosphates materials

have poorer properties in such conditions. The wollastonite-alumina PC's phases get more stable as the exposure time is increased.

Table 15 shows the shrinkage results for the different acid formulations showed before. It can be seen that after all these thermal treatments the best samples are the PCs with 20 and 40wt% of alumina added.

Table 15 Shrinkage (diameter reduction) obtained for acid formulations exposed to 1000°C.

	Shrinkage for 0.0A, After 1000°C (all 10 thermal cycles)		**Shrinkage for RefA**, After 1000°C (all 10 thermal cycles)		**Shrinkage for 2.9A**, After 1000°C (all 10 thermal cycles)	
	Alu. %	Diam. Red. (%)	Alu. %	Diam. Red. (%)	Alu. %	Diam. Red. (%)
WORST	**0**	7.8	**5**	11	**10**	9.5
	5	6.5	**10**	10	**5**	8.9
	10	4.8	**0**	8	**0**	7.2
	40	3.1	**20**	7	**20**	6.8
BEST	**20**	2.7	**40**	5	**40**	1.8

It has been shown experimentally that both wollastonite and alumina in reaction with phosphoric acid form phosphates. Moreover, all the acidic formulations used are based on aqueous phosphoric acid and consolidated solids with neutral pH. The optimization of these materials for temperatures up to 1000°C showed that combining both oxides lead into a composite that is not only stable at high temperature but also whose compressive strength increased with the exposure time at high temperature. Thus, we have two competing ions, calcium and aluminum, that contribute to the acid-base reaction. In order to understand their formation process and some of the final results that lead into all the phases shown by the XRD and described with chemical equations before, we need to understand the role of those ions in the ceramic formation. As it was presented in Chapter 4, the dissolutionn reactions and ionic concentrations $<Ca^{2+}(aq)>$ are given by the following equantions, [3] and [4]:

$$CaSiO_3 + 2H^+ = Ca^{2+}(aq) + H_2SiO_3 \qquad \text{(in the pH range 0-10)} \qquad (4a)$$

$$\log<Ca^{2+}(aq)> = 1.315 - pH \qquad (4b)$$

$$CaSiO_3 + H^+ = Ca^{2+}(aq) + H_2SiO_3^- \quad \text{(in the pH range 10-11.45)} \quad (5a)$$

$$\log\langle Ca^{2+}(aq)\rangle = -3.61 - pH \quad (5b)$$

For alumina, the dissolution reactions and ionic concentrations $\langle Al^{3+}(aq)\rangle$ are given by the following equantions, [3] and [4]:

$$AlO_{3/2} + 3H^{3+} \rightarrow Al^{3+}(aq) + (3/2)H_2O \quad \text{(in acidic conditions)} \quad (6a)$$

$$AlO_{3/2} + (3/2)H_2O \rightarrow Al(OH)_3 \rightarrow Al^{3+}(aq) + 3(OH^-) \quad \text{(in acidic conditions)} \quad (6b)$$

$$\log\langle Al^{3+}(aq)\rangle = 8.55 - 3pH \quad \text{(in acidic and neutral conditions)} \quad (6b)$$

$$AlO_{3/2} + (1/2)H_2O \rightarrow AlO_2^-(aq) + H^+ \quad \text{(in alkaline conditions)} \quad (7a)$$

$$\log\langle Al^{3+}(aq)\rangle = -11.76 + pH \quad \text{(in alkaline region)} \quad (7b)$$

Figure 13 shows the ionic concentrations (from equations 4b, 5b, 6b and 7b) for wollastonite and alumina as a funciton of pH. At low pH the dissolution of Al^{3+} is higher than for Ca^{2+}. Thus, when both oxides are in the acidic solution, they both are released (as described in Chapter 4) from the wollastonite and alumina grains at different rates. Alumina has been found to delay the setting and decrease the exothermic reaction. Alumina pH was found to be 9, wollastonite was 10, and phosphoric acid formulation to be 1.

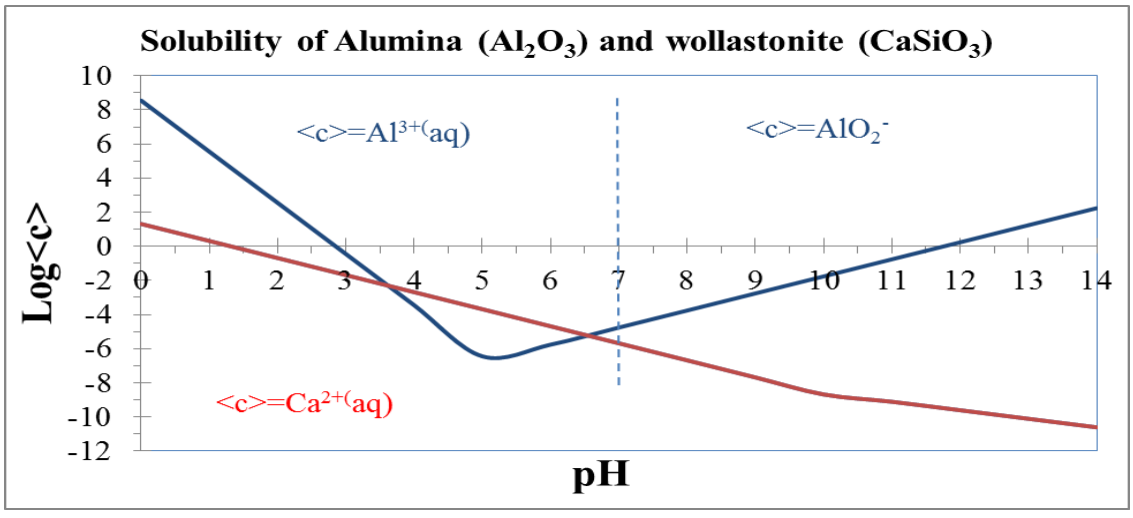

Figure 97 Solubility curves of alumina and wollastonite as a function of pH.

Therefore, when both powders are initially put into the phosphoric acid formulation pH of 1, the wollastonite reaction is slower (see Figure 13). Aluminun cations mainly react with water by hydrolysis. As time is goes on, the pH of the mixture increases, and the calcium ions are realeased and react with water by hydrolysis. Therefore, aluminum cations decrease the acid reactivity and may lead into a better microstructure. Up to a pH of 3, the aluminun cations are more prevalent. This is very significant when the alumina content is high because we can expect an interconnected network of alumino-phosphates rather than calcium phosphates. At higher pH, between 3.5 and 7, the calcium dominates but now the release rate from the oxide is slower. Samples with higher pH were not fabricated in this thesis because we focus in applications with neutral pH. However, it is possible to make these materials with a low pH to endure an extreme acidic environment.

From results presented in Chapter 4, it has been found that is the very surface (about 1μm depth) which lose the ions. In case of wollastonite ($CaSiO_3$), the by products are silica or calcium hydroxides. In case of alumina it dissolves completely depending of the size. Therefore, we always have residual wollastonite and alumina, and the grain tranform completely in case they are very small (about 1μm size). Thus, we have wollastonite grains covered with a thin layer SiO_2 due to the dissolution of calcium, and the most external layer made of calcium phosphates (brushiste, $CaHPO_4.2H_2O$; and very few monetite, $CaHPO_4$). On the other hand, we will have residual alumina surrounded by mainly aluminum phosphates (bernite, $AlPO_4$; and alumino-phosphate, $Al\ H_3(PO_4)_2.H_2O$).

From results we obteined there are two critical compositions, 20wt% alumina-80wt% wollastonite, and 40wt% alumina-60wt% wollastonite we found thery both with advantages (see Table 14 and Figure 94 where 40% alumina was better in compressive strength ans shrinkage over the macro samples, while 20% has lower weigth loss when TGA was used. From XRD, we can see that structure is due to the alumino phosphates. But wollastonite and the calcium phosphates also can play important roles in the composite.

They act as reinforcements and reduce the costs since wollastonite is cheaper than alumina powders. Moreover, if alumina is higher than 40wt% it has been found that samples sometimes do not set unless a drying process is employed (usually at more than 100ºC). However, it has been obersed that if a more reactive alumina is used (it could be a higher pH or a new powder to avoid water absorption effects), up to 80% of alumina can be added to consolidate a PC based on the reaction wollastonite-alumina-phosphoric acid. Also, in general, the higher the residual alumina content, the better the stability at temperatures higher than 1000ºC. This surely will improve as exposure time increases (this needs to be optimized in a manufacturing process) for reason including sintering of residual particles. However, tha main advantage of this composite is that it is completely cured at room temperature. Additionally, with reasonable amounts of alumina we can create a stable structure at 1000ºC.

Figure 98 shows a representation of the PC material developed in this research when more than 20wt% of alumina is added. Figure 98a) shows the formation of phosphates from wollastonite and alumina powders in an early stage where new phosphate crystals are in formation. Figure 98b shows the same area after the PC is complete solidified. Figure 98 shows the same PC but only emphasizing the interconnected matrix, an aluminum-phosphates dominant structure. In case alumina added is low, the matrix will be dominated by the calcium phosphates as was described in chapters before.

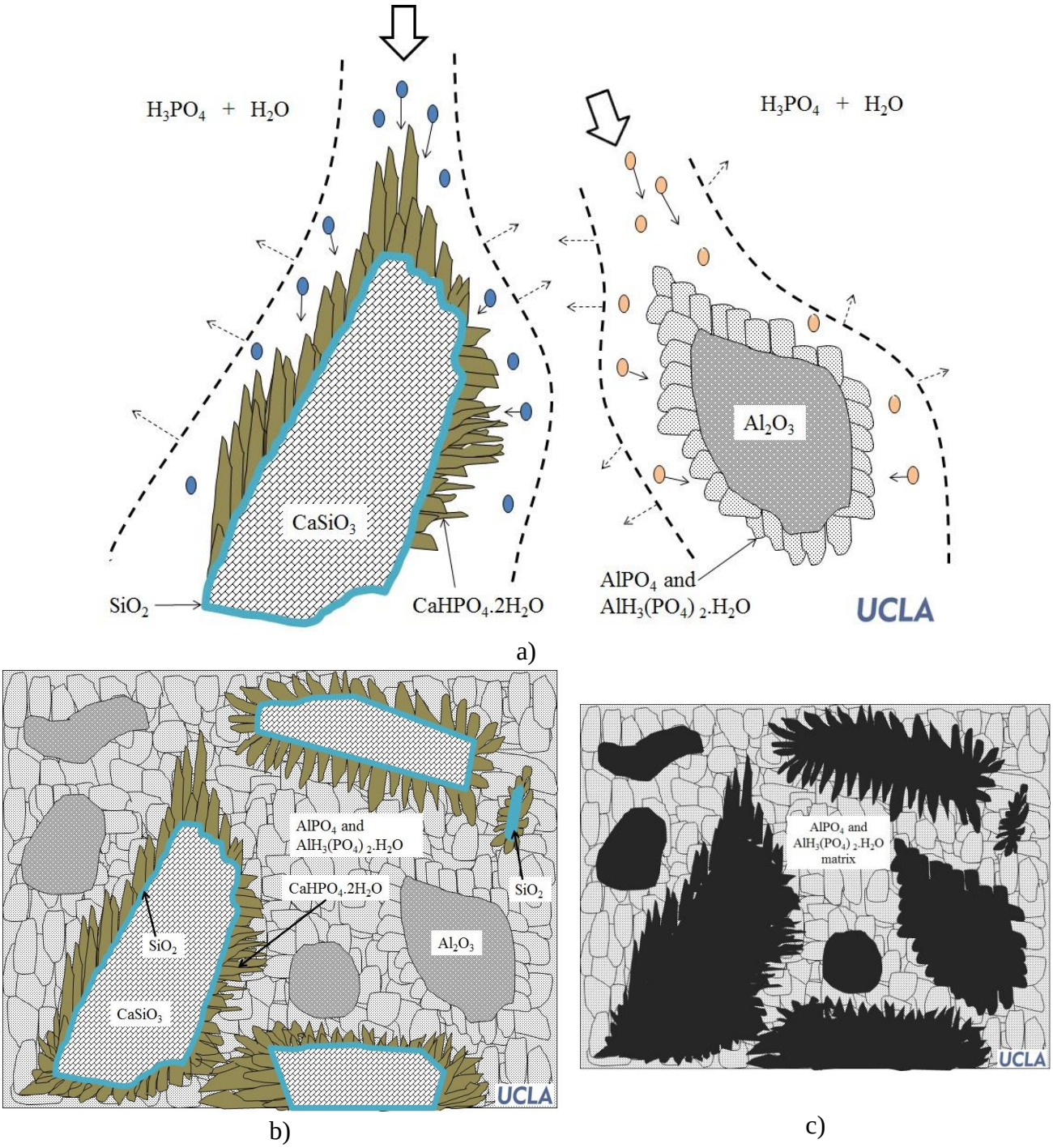

Figure 98 Representation of the material developed in this research when the alumina concentration is high (more than 20wt%): a) formation of phosphates from wollastonite and alumina powders; b) final composite after complete solidification; aluminum-phosphates dominant structure as the ceramic interconnected matrix.

Finally, Figure 99 summarizes the effect of the heat exposure on the Al-Ca PC. For the reference sample made with 5.0wt% of borax (A5.0), Figure 99a, the cracking desapeared when 5wt% of alumina or more is added. For the sample made with 0.0wt% of borax (A0.0), the cracking appeared for samples with less than 20wt% of alumina. Therefore, the borax content not only has a significant impact on the manufacturing with the optimization of the setting time (see Figure 23), but also the borax contributes to reduce the damages in the sample. This cracking reduction is the result of the weakening of the phosphoric acid, which allows the enough time for cations to dissolve and slowly to a more relaxed crystalline matrix structure.

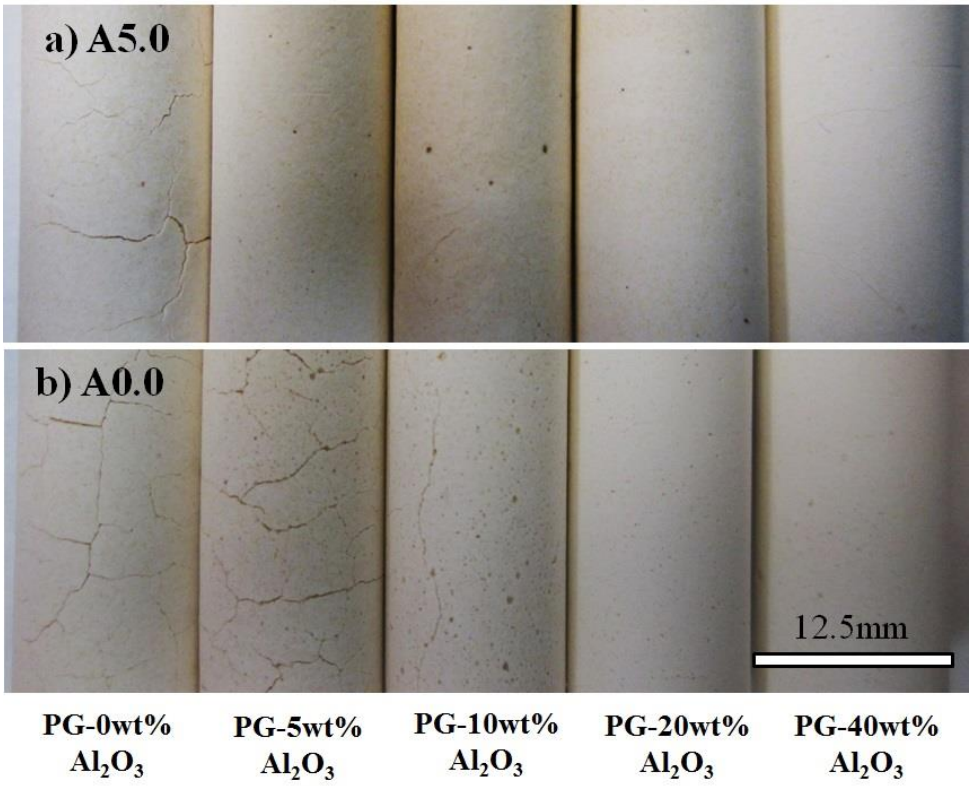

Figure 99 Samples after the exposure to different exposure temperatures for 1h, a) sample made with the acid formulation with 5.0wt% borax (A5.0 or RefA); b) sample made with the acid formulation with 0.0wt% borax. The scale bar is the same in both images.

7.5 Conclusion

Materials that give an alternative solution to high performance cements have been presented in this thesis. The composite material is suitable to be used in high temperatures. The main advantages include that it is a green material completely made at room temperature and do not require any further processing. This is because the process is fully made at room tempeature since there is no need to do any thermal process or syntering during the manufacturing. It has very fast setting time, curing in minutes to a couple of hours before reaching its final compressive strength (instead of days for cements). Also, it is pH is neutral, which is important when fibers are used to avoid corrosion or other damage. Perhaps the most important achievement with this material is discovery that compressive strength increases under 1000°C due to the combination of calcium and alumino phosphates that aids stable at high temperatures.

Future work to further improve the properties of this material will be further processing which may include the use of nano particles, alumina plateles and fibers.

7.6 References

[1] Colorado H., Hiel C., Hahn H.T. and Yang J.M.: Chemically Bonded Phosphate Ceramic Composites, Metal, Ceramic and Polymeric Composites for Various Uses. InTech, 2011. p. 265-282 (2011).

[2] Composite Support & Solutions Inc., PC manufacturers. Website: http://www.intellifirewall.com/?link=company.

[3] Provis, John L., and Jan Stephanus Jakob Van Deventer, eds. Geopolymers: Structure, processing, properties and industrial applications. Cambridge, UK: Woodhead, 2009.

[4] Scrivener, Karen L., Jean-Louis Cabiron, and Roger Letourneux. "High-performance concretes from calcium aluminate cements." Cement and concrete research 29.8 (1999): 1215-1223.

[5] Sakai, Etsuo, et al. "Mechanical properties and micro-structures of calcium aluminate based ultra-high strength cement." Cement and Concrete Research40.6 (2010): 966-970.

[6] Popoola, Oludele O., Waltraud M. Kriven, and J. Francis Young. "Microstructural and Microchemical Characterization of a Calcium Aluminate-Polymer Composite (MDF Cement)." Journal of the American Ceramic Society74.8 (1991): 1928-1933.
[7] Ukrainczyk, Neven, and Tomislav Matusinović. "Thermal properties of hydrating calcium aluminate cement pastes." Cement and Concrete Research 40.1 (2010): 128-136.
[8] Nilforoushan, Mohammad Reza; Talebian, Nasrien. The Hydration Products of a Refractory Calcium Aluminate Cement at Intermediate Temperatures. Iran. J. Chem. Eng.Vol. 26 No. 2, 71-76.
[9] Pourbaix, M. Atlas of electrochemical equilibria in aqueous solutions. Pergamon Press, New York, 1974.
[10] Wagh, Arun S. Chemically bonded phosphate ceramics: Twenty-first century materials with diverse applications. Elsevier Science, 2004.

8 General overview of other PCs developed and its current or potential applications

8.1 Introduction

This Chapter presents three different applications of chemically bonded ceramics (PC) method. The first application is a PC material based on boron oxide for neutron shielding applications [1]. The shielding application is possible because of the high neutron's boron cross section (which is used to express the likelihood of interaction between an incident neutron and a target nucleus). The second application is a PC material based on fly ash for structural applications that could be used for the stabilization and encapsulation of high contents of waste stream products [2]. Both the boron- and the fly ash-based mixture components can tailor the properties PC material (i.e. pH and process parameters) [3]. The third application is the Wo-PC (see Chapter 4) used as a ceramic matrix composite for firewalls, [4] [35].

8.2 New material based for nuclear waste and radiation shielding applications

PCs are formed in low temperature conditions by mixing a base powder with phosphoric acid. The compound that forms from the cement like processing has the properties of an engineering ceramic with the advantage of being able to be formed with relative ease and low expense [1], [4] and [10]196. PCs' properties can also be enhanced without a major degradation of the structural properties through formulated additives. The high melting temperatures and the good thermal resistance allow this ceramic to be used as a firewall to prevent transformer explosions [7]. Based upon these principles the ceramic was examined with several different additives to determine the improvement of the linear attenuation coefficient for dry cask spent fuel storage and/or transportation cask for spent nuclear fuel.

Dry cask spent fuel storage involves storing spent nuclear fuel above ground and/or transporting it in casks that are lined with gamma and neutron shields [8], [1]. Though these casks are

designed to withstand high temperatures for short periods of time, there have been examples of traffic accidents[9],[10] that have resulted in temperatures and times exceeding the current safety design parameters. This research examines PCs with regards to neutron shielding in order to obtain preliminary data for an improved design of nuclear casks that can survive a traffic accident of similar nature to the new scenarios considered.

PC samples were fabricated by mixing an aqueous phosphoric acid formulation and natural wollastonite powder ($CaSiO_3$) M200 (from Minera Nyco). Also, boron oxide (from Alfa Aesar) was added to the mixture. For all samples, the 1.2 ratio liquid (phosphoric acid formulation) to powders (wollastonite + B_2O_3) was maintained constant. The mixing process of the components was conducted in a Planetary Centrifugal Mixer (Thinky Mixer® AR-250, TM). First, wollastonite was mixed with the acidic liquid for 1 min, then, boron oxide was added and mixed for 1 min. All samples were dried for 2 days at 100°C in order to stabilize the weight. The fabrication and characterization details have already been reviewed [1].

In order to determine the shielding effect of PCs, a method for measuring the attenuation of neutrons was implemented. In order to allow for quick measuring of the attenuation coefficients a He-3 neutron detector was used. The He-3 detector gives a count of thermal neutrons over a set time period. This detector was connected to a lower level discriminator to reduce noise and a scaler to obtain counts. A PuBe neutron source was used at the Missouri University of Science and Technology Research Reactor (MSTR). The production of neutrons from the PuBe sources occurs when the alpha particle released from the plutonium reacts with beryllium in the source producing neutrons according to the reaction shown in equation 1.

$$ {}^{4}_{2}He + {}^{9}_{4}Be \rightarrow {}^{12}_{6}C + {}^{1}_{0}n \quad (1) $$

This produces neutrons with a wide energy range; the neutron energy spectrum for PuBe can be seen in Figure 1a.

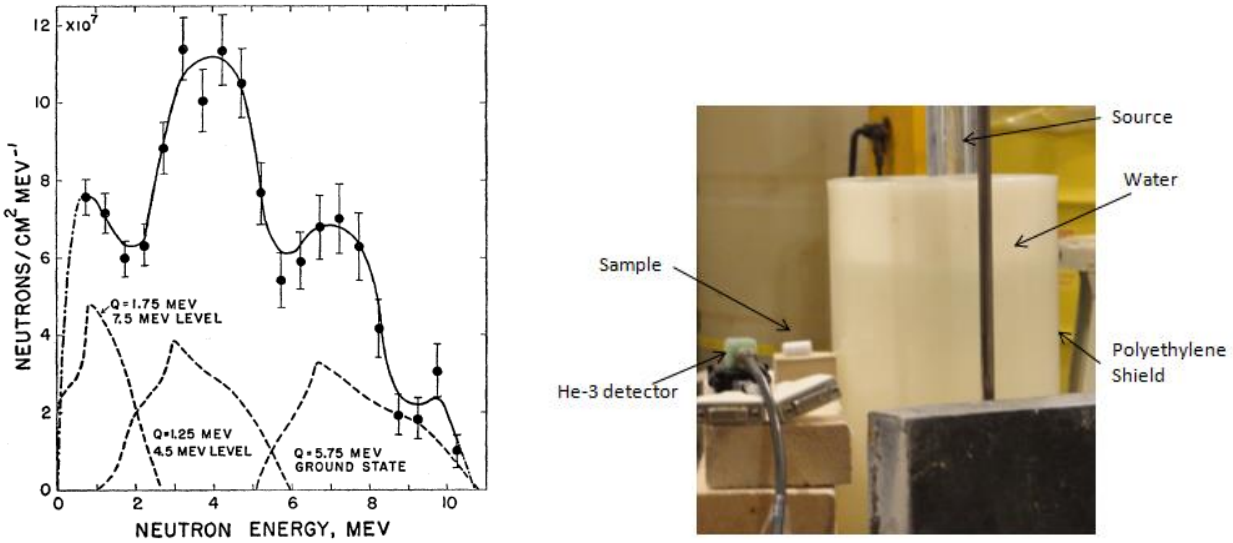

a) b)

Figure 100 a) PuBe neutron energy spectrum [11], and b) neutron attenuation setup

Since the spectrum of the PuBe source contains more fast neutrons then thermal neutrons a method for thermalizing the neutrons was used. The average distance for thermalizing a fast neutron in water is about 12.7 cm (estimated from the neutron age for fast neutrons ~27 cm^2) [12]. The source was suspended in water in a container of low density polyethylene (borosilicate glass must be avoided) with a distance to the wall of 9 cm. The sample was placed on a platform with the edge of the sample 1 to 2 cm away from the polyethylene wall. The samples (what was counted) were then counted using a He-3 detector with 10 minute count rates with and without a 0.6 mm cadmium shield placed over it. When present, the cadmium shield absorbs all the thermalized neutrons traveling through the sample, and the difference measured with and without the Cd shield gives the neutron difference used to calculate the attenuation for the samples. A picture of the setup is shown in Figure 1b.

Results

Figure 2 shows SEM images for the PCs fabricated. $CaSiO_3$, $CaHPO_4.2H_2O$, BPO_4 and B_2O_3 have been identified in the images. These results were confirmed by the XRD data as shown in Figure 102.

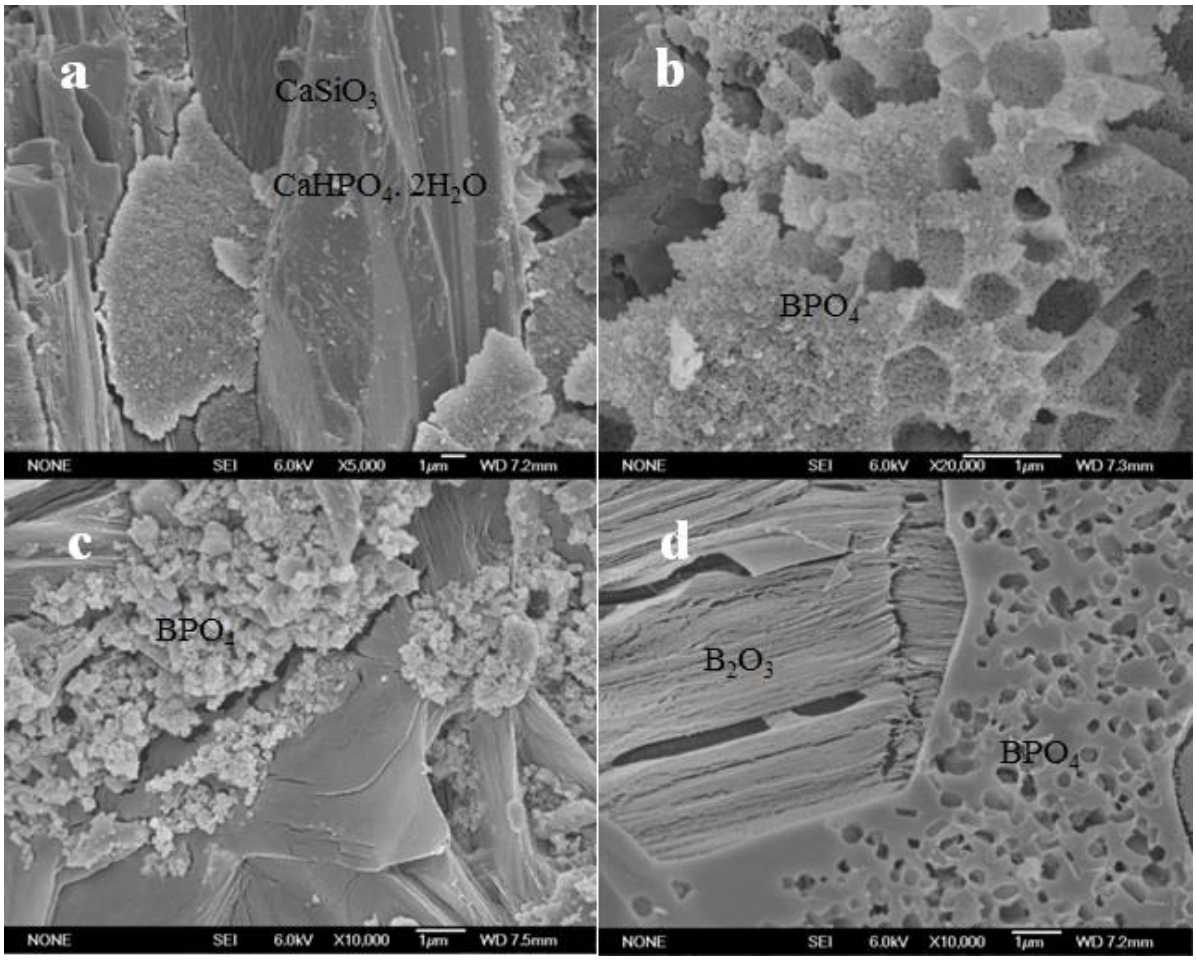

Figure 101 SEM images for the boron-based PC.

Figure 102 shows the XRD for the materials used (raw powders) and fabricated in this research. $CaSiO_3$, $CaHPO_4.2H_2O$, BPO_4, and B_2O_3 are shown. B_2O_3 is mostly amorphous. Brusite ($CaHPO_4.2H_2O$) is the result of the reaction between $CaSiO_3$ and H_3PO_4. Brusite and boron phosphate are the binding phases.

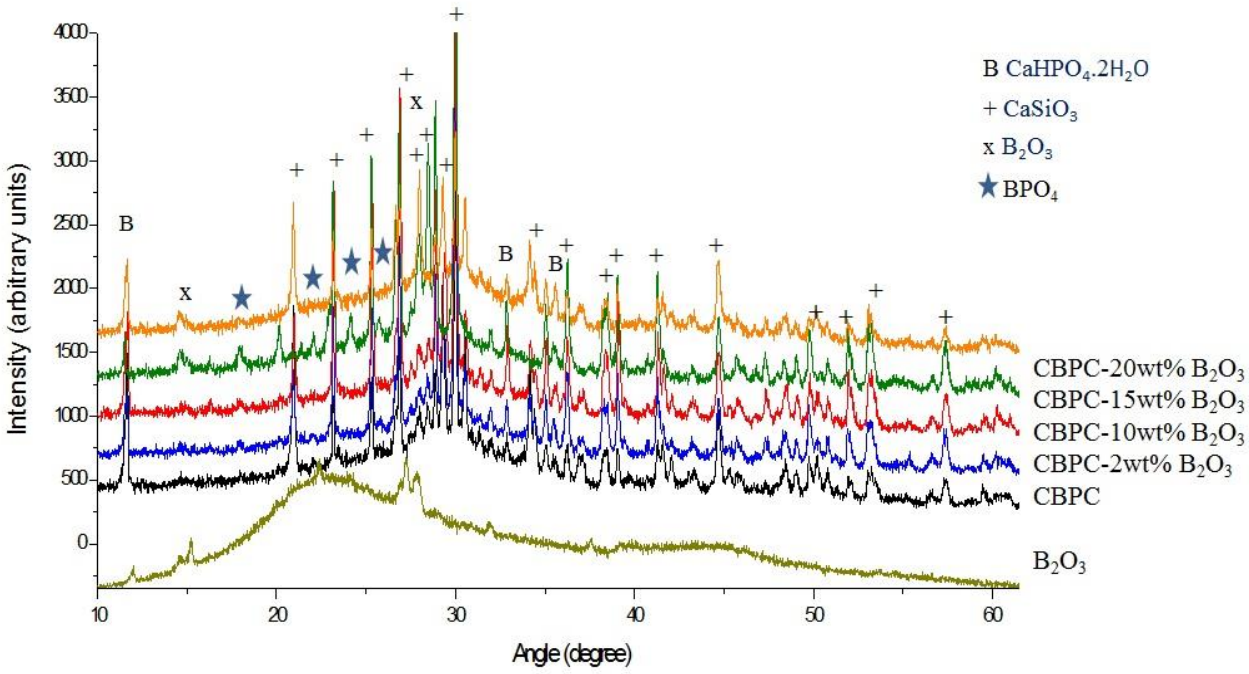

Figure 102 XRD for the raw powders and ceramics fabricated.

Figure 103 shows the compressive strength for the PCs with B_2O_3 contents. The standard deviation was bigger for the sample with 10% B_2O_3. As the B_2O_3 contents increases, the compressive strength decreases.

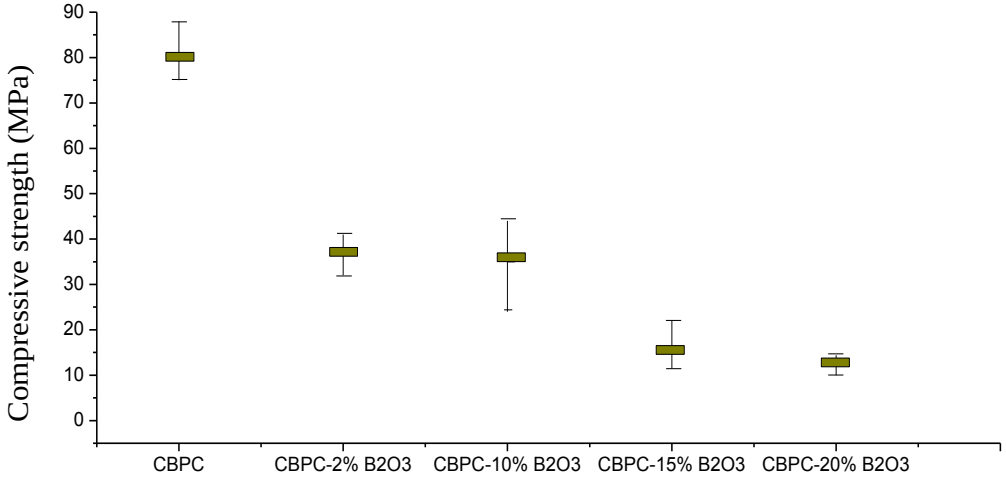

Figure 103 Compressive strength for the boron-based PC (PC) fabricated.

Results for the neutron attenuation experiment for several different PCs are summarized in Table 16.

Table 16 Thermal Neutron Attenuation Values for PCs

Component	Thickness (cm)	Linear Attenuation (cm^{-1})	Error
20% Boron	2.774	0.089	0.017
0%	1.664	0.060	0.018
50% PbO	1.284	0.045	0.023
Boron oxide	1.308	0.068	-

From the results the addition of boron improved the attenuation of PCs by 48% for thermal neutrons. However the addition of PbO caused a decrease in attenuation by 25%. The PCs compared well to boron oxide during the testing being only 11% lower. The PC also compares favorably when it was combined with boron oxide showing a definite increase in thermal neutron attenuation for both materials. However, these results still have large error values and further testing on neutron attenuation with a more intense source is recommended.

One of the reasons for the relatively large errors is due to the continued thermalization of neutrons within the sample, i.e. the sample is not only blocking neutrons but is still thermalizing them. Another possible error is that the source location has small variations in its position. This happens because the source had to be repositioned several times over the course of the experiment to guarantee a safe working environment for the experimenter (i.e. ALARA). Missouri S&T has a new neutron generator in the process of being licensed. Utilizing a neutron generator as a source of neutrons will alleviate the safety problems, since the generator can be started and stopped at will as opposed to the PuBe neutron source.

The reaction generating brushite is shown in equation 2. $CaHPO_4$. $2H_2O$ is a calcium phosphate that under time and temperature can lose the bonded water molecule and transform to a more stable phase, monetite, $CaHPO_4$.

In the acidic formulation used, boron oxide is dissolved and boric acid (H_3BO_3) is generated. Then, the reaction of boric acid and phosphoric acid can generate boron phosphate (BPO_4) as found experimentally.We suggest the reaction generating BPO_4 in equation 3.

$$CaSiO_3 + H_3PO_4 + 2H_2O = SiO_2.H_2O + CaHPO_4.\ 2H_2O \quad (2)$$

$$H_3PO_4 + H_3BO_3 = BPO_4 + 3\ H_2O \quad (3)$$

As B_2O_3 presence increases, the compressive strength is decreased. This can be associated with two factors. The first one is likely due to a weak reaction of saturation of boron ions in the acidic solution. The second one is that when the residual boron oxide content increases, there is more possibility to have agglomeration of these particles. The agglomeration produces a poor liquid impregnation, which decreases the compressive strength.

Summarizing, the addition of boron oxide to PC shows significant improvement in neutron attenuation for the ceramic. A previously prepared sample with PbO however, demonstrated a significant drop in neutron attenuation. For applications of this ceramic as a shielding material, a balance between boron oxide and lead oxide needs to be determined in order to function as an effective radiation shield. In this regard further testing on the ceramic with more variation in regards to boron content will be performed.

8.3 Materials based on Fly-ash for structural applications

High temperature manufacturing processes contribute to global warming especially from the processing of cementitious and ceramic materials. Each year, coal-burning power plants, steel factories and similar facilities in the United States produce more than 125 million tons of waste. A large portion of this waste from combustion is fly and bottom ash. This quantity depends on the fuel type, raw ingredients used and the energy efficiency of the cement plant [13]

In this chapter, fly ash was used as the source of the ceramic composite itself. This signified an enormous decrease in costs and weight with respect to not only conventional ceramics and cement, but also to previous formulations of PCs. This new material uses more waste ashes than normal PCs, which themselves used to be a big source of contamination, thus reducing their impact in the environment. On the other hand, this fly ash-based PC has shown good compression strength, which enables this new material as a substitute for cementitious materials.

The manufacturing of PC samples was conducted by mixing phosphoric acid, fly ash and in some cases natural wollastonite as reinforcement. The pH of the PC after curing was near neutral in all cases. Fly ash was obtained from Diversified Minerals Inc and wollastonite was obtained from Minera Nyco. In all cases after the liquid mixture completed to set, the pH was about 7. Figure 7 (a, b and c) show SEM images of fly ash class C, fly ash class F and $CaSiO_3$, which correspond to the solid raw materials (as received) used in this research. Figure 7 (d) shows a cross section view image of a fabricated PC with fly ash. More details regarding the fabrication and characterization details were communicated before [2].

XRD data, presented in Figure 105, shows that the binding phase is brushite. This phase was obtained from the reaction of CaO and phosphoric acid, given by the equations 4 and 5. These

phases are calcium, iron and aluminum phosphates and combinations of them (where is the aluminum and iron). Amorphous phases of those are also present. The role of all these phases on the composite need to be further investigated.

$$3\ CaO(s) + 2\ H_3PO_4\ \ (aq) \rightarrow Ca_3\,(PO_4)_2(aq) + 3\ H_2O(l) \quad (4)$$

$$Ca_{23}(PO_4)_2 + 6\ H_2O \rightarrow\ 2CaHPO_4.2H_2O + Ca(OH)_2 \quad (5)$$

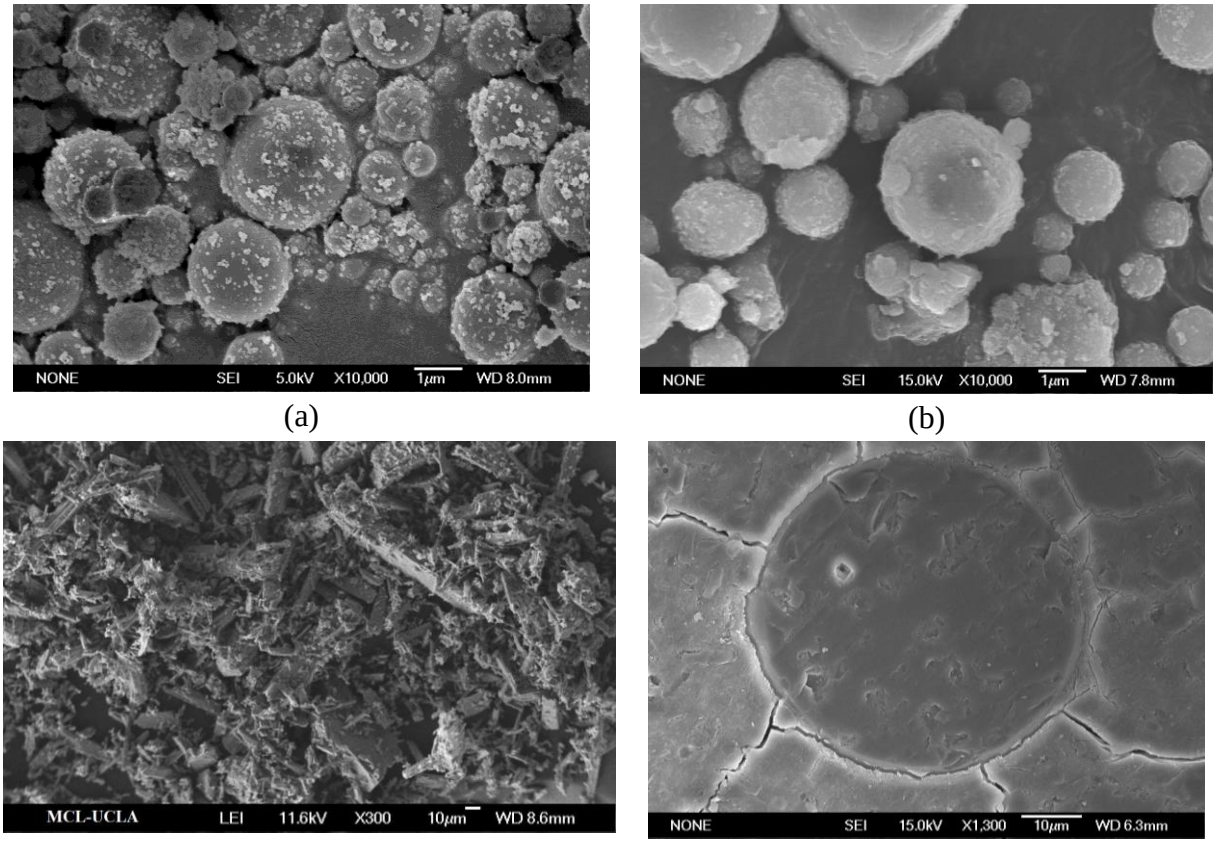

(a) (b)

(c) (d)

Figure 104. Fly ash class C (a), fly ash class F (b), $CaSiO_3$ (c), and PC with fly ash (d).

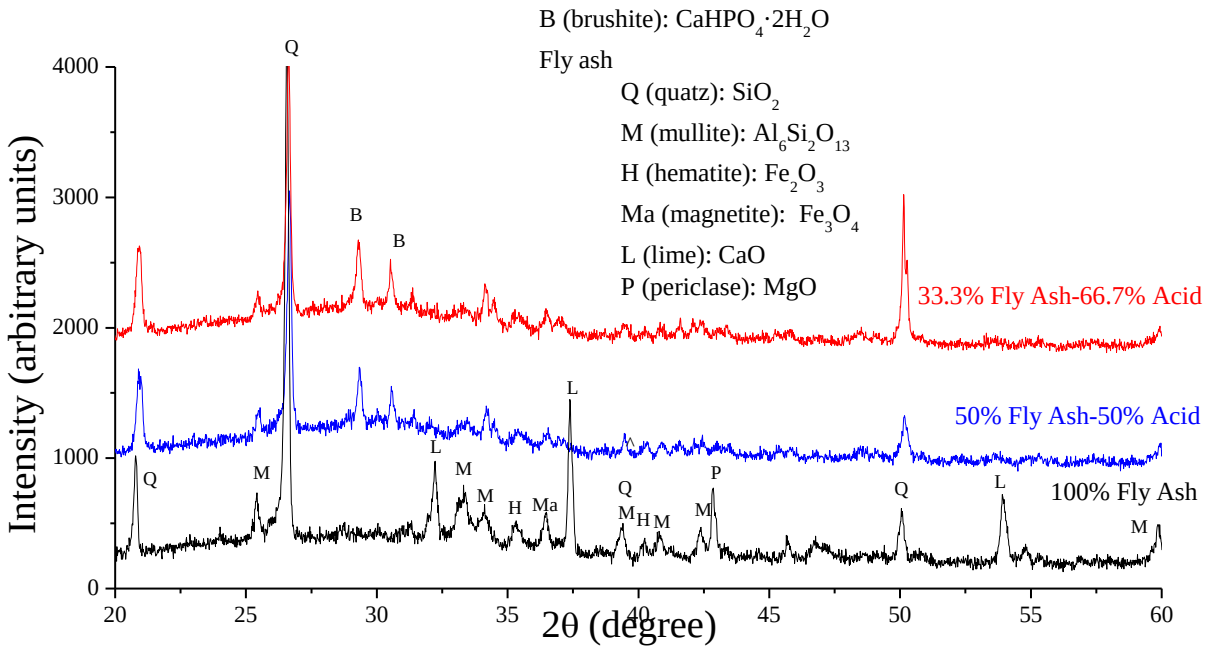

Figure 105. XRD spectra for different materials fabricated based only in fly ash.

Figure 106 shows diverse microstructures for the fly ash-based PC with two compositions: 33.3% Fly Ash-66.7% Acid and 50% Fly Ash-50% Acid. Images were obtained from fractured surfaces or from the sample' surfaces as made.

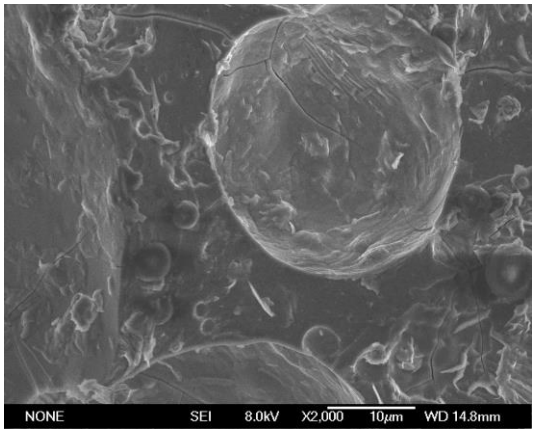

(a) 33.3% Fly Ash-66.7% Acid

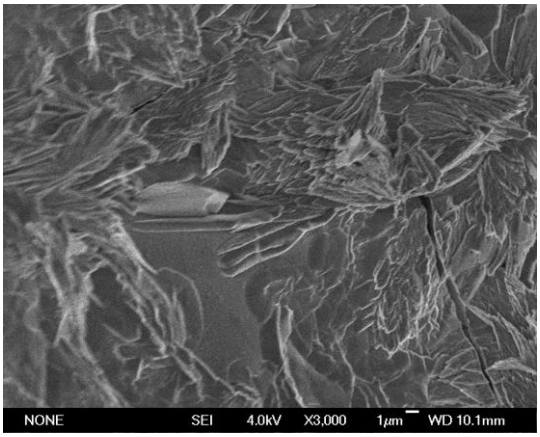

(b) 33.3% Fly Ash-66.7% Acid

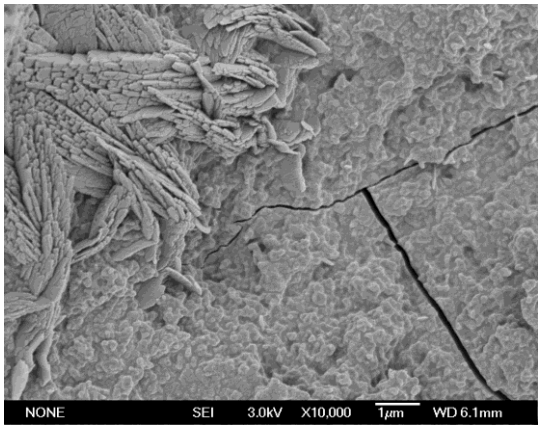

(c) 50% Fly Ash-50% Acid

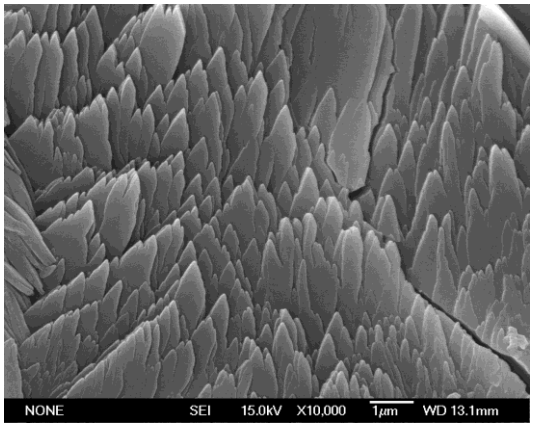

(d) 50% Fly Ash-50% Acid

Figure 106 SEM images showing the glassy amorphous phases and some new crystals grown during the chemical reaction at low temperature for this fly ash-based material. The acidic formulation to fly ash is indicated.

Some properties of the material presented above are summarized on Table 17. As the acidic formulation to fly ash ratio increases, current values for compressive strength and density were found to increase. The compressive strength is under improvement and some manufacturing procedures followed Chapter 4 will be applied.

Table 17 Properties for the PC made completely from fly ash

Acidic formulation to fly ash ratio	Compressive strength [MPa]	Density [g/cm^3]
2.0	12.6	2.2
1.5	7.0	1.9
1.0	12.0	1.9
0.5	3.0	1.4

Figure 107 shows the Weibull distributions for these fly ash-base materials with $CaSiO_3$ as reinforcement. The largest values were obtained for the PC with no filler.

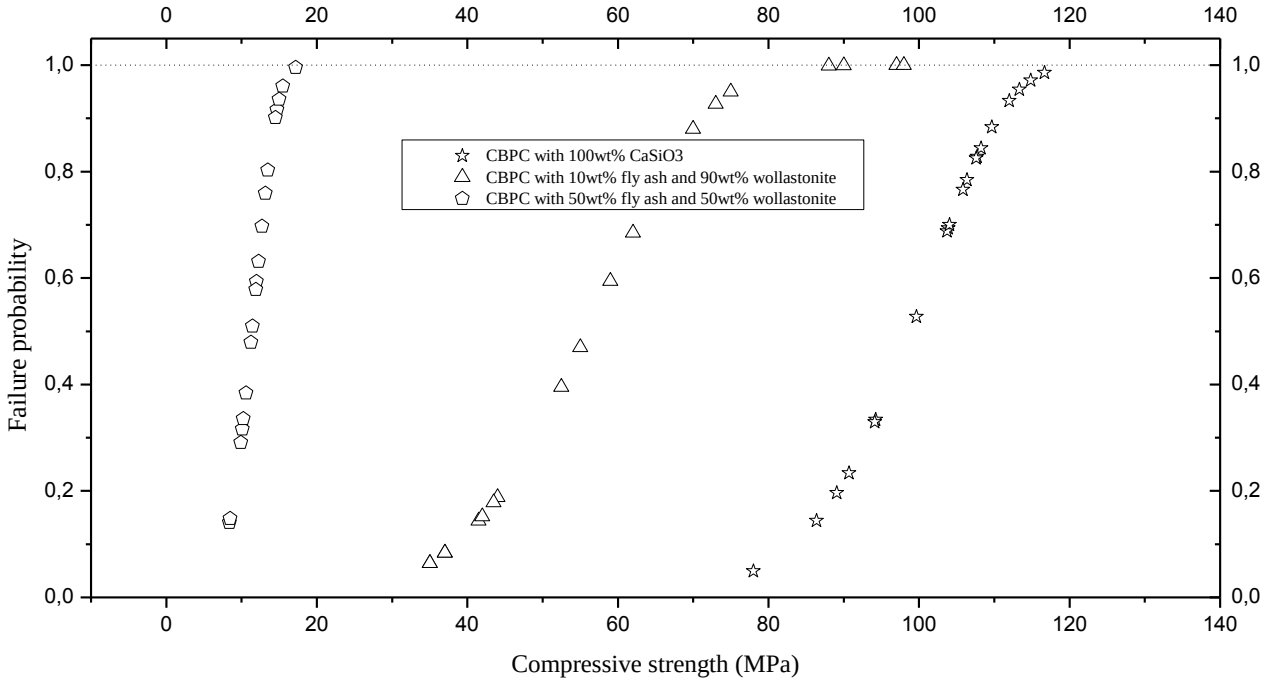

Figure 107 Weibull distributions for PCs fabricated with wollastonite powder M200 and with fly ash.

Summarizing, fly ash was used as the source of the ceramic composite itself, which represents an enormous decrease in cost and weight with respect to conventional ceramics and cements as well as previous formulations of PCs. Because of the mechanical properties presented above, we are proposing there should be further investigation into this material. The results can produce not

only a good solution for replacing high performance cement concrete (not needed of aggregates or reinforcements) but also a high performance material to be used in firewalls and aerospace applications.

This material is fabricated at room temperature with very little processing in order to replace high performance concrete cement. Since we are using fly ash contaminants as the main component and very little amount of phosphoric acid in a very inexpensive acidic solution, we are not only proposing a competitive inexpensive material but also a good solution for the environment.

8.4 Wo-PCs composite panels for firewalls

One structural application involving high temperatures is the firewall structure, fabricated from Wo-PCs reinforced with different fibers. These are shown in Figure 108. Electrical transformers are expensive equipment, usually installed in groups with little space in between them. If fire ignites in one transformer, the flame can be easily transferred to neighbouring transformer like a chain reaction. Wo-PCs have been successfully applied as firewalls to help protect transformers from fire. In addition, since these are versatile cements, the curing can be easily reduced to short periods for feasible in situ fabrication and repair.

a

b

Figure 108 Composites fabricated from Wo-PCs, a) firewalls made of PCs composite panels reinforced with fibers for protection of electric transformers, b) detail of the panels installation.

8.5 References

[1] H.A. Colorado, J. Pleitt, C. Hiel, J.M. Yang, H.T. Hahn, C.H. Castano. Wollastonite based-Chemically Bonded Phosphate Ceramics with lead oxide contents under gamma irradiation. *Journal* of Nuclear Materials, 425, 197–204 (2012).

[2] Colorado, Henry A., and Jenn-Ming Yang. "Ceramicash: A New Ultra Low Cost Chemically Bonded Ceramic Material." Developments in Strategic Materials and Computational Design III: Ceramic Engineering and Science Proceedings(2012): 43.

[3] Colorado, H. A., Roopa Ganga, and Dileep Singh. "Chemically Bonded Phosphate Ceramics for Stabilization of High-Sodium Containing Waste Streams." Developments in Strategic Materials and Computational Design III(2013): 55-68.

[4] Colorado, H. A., C. Hiel, and H. T. Hahn. "Pultrusion of glass and carbon fibers reinforced Chemically Bonded Phosphate Ceramics." Journal of Composites Materials (2010).

[5] Colorado, H. A., Hiel C., Hahn H. T. and Yang J. M.. "Wollastonite-Based Chemically Bonded Phosphate Ceramic Composites." Intech (2011).

[6] Henry Colorado, Clem Hiel, H. Thomas Hahn and Jenn-Ming Yang Chemically Bonded Phosphate Ceramic Composites, Metal, Ceramic and Polymeric Composites for Various Uses, John Cuppoletti (Ed.), ISBN: 978-953-307-353-8, InTech, 265-282 (2011).

[7] H. A. Colorado, C. Hiel and H. T. Hahn. Chemically bonded phosphate ceramic composites under thermal shock and high temperature conditions. Society for the Advancement of Material and Process Engineering (SAMPE), May 17-20, 2010. Seattle, Washington USA (2010).

[8] Jason Pleitt, Henry A. Colorado, Carlos H Castano. Materials Science & Technology 2011 Conference. Materials for Nuclear Waste Disposal and Environmental Cleanup Symposium. Radiation Shielding Simulation for Wollastonite-Based Chemically Bonded Phosphate Ceramics. Columbus, Ohio (2011).

[9] H.E. Adkins, B.J. Koeppel, J.M. Cuta, A.D. Guzman, C. S. Bajwa. Spent Fuel Transportation Package Response to the Caldecott Tunnel Fire Scenario. NUREG/CR-6894, Rev. 1. PNNL-15346 (2006).

[10] R. J. Halstead and F. Dilger. Implications of the Baltimore rail tunnel fire for full-scale testing of shipping casks. Waste Management Conference 2003. February 23-27, Tucson, AZ (2003).

[11] Stewart, L. Neutron Spectrum and Absolute Yield of a Plutonium-Beryllium Source. Physical Review, 740-743 (1954).

[12] John R. Lamarsh, A. J. Introduction to Nuclear Engineering. New Jersey: Prentice-Hall, Inc. (2001).

[13] Environmental Protection Agency AP 42 - Compilation of Air Pollutant Emission Factors, Volume I Stationary Point and Area Sources, Arunington, DC, 2005.